



**UNIVERSITÀ DEGLI STUDI DI ROMA
“LA SAPIENZA”**

**DIPARTIMENTO DI INGEGNERIA STRUTTURALE E
GEOTECNICA**

**DOTTORATO DI RICERCA IN
INGEGNERIA GEOTECNICA**

FABIANA MACCARINI

*“Behaviour of vertical caisson breakwaters under
wave-induced cyclic loading”*

Tutor Prof. Renato Ribacchi, Università degli Studi di Roma “La Sapienza”
Co-Tutors Prof. Giovanni Calabresi, Università degli Studi di Roma “La Sapienza”
Prof. Stefano Aversa, Università di Napoli “Parthenope”
Prof. Giuseppe Scarpelli, Università Politecnica delle Marche

International Collaboration with

Prof. Han J.K. Vrijling, Delft University of Technology, Hydraulic Section, The Netherlands
Dr. Ing. Stefan van Baars, Delft University of Technology, Geotechnical Department, The Netherlands
Maarten de Groot, Senior Engineer, GeoDelft, The Netherlands

Committee

Prof. Leonardo Cascini, Università di Salerno
Prof.ssa Cristina Jommi, Politecnico di Milano
Prof. Renato Lancellotta, Politecnico di Torino

*Behaviour of vertical caisson breakwaters under
wave-induced cyclic loading*

Fabiana Maccarini

University of Rome “La Sapienza”

Dept. of Structural and Geotechnical Engineering

Via di Monte d’Oro 28, 00186

Rome, Italy

fabiana.maccarini@uniroma1.it

Contents

Summary	x
Sommario	xiv
Chapter 1: Introduction	1
1.1 <i>Aims and scopes</i>	1
1.2 <i>Contents</i>	3
Chapter 2: General background and literature review	5
2.1 <i>Introduction</i>	5
2.2 <i>Hydraulic aspects</i>	11
2.2.1 Introduction	11
2.2.2 Pulsating wave loads	14
2.2.3 Wave impact loads	15
2.2.4 Proposal of universal wave pressure formulae	19
2.2.5 General conclusions	23
2.3 <i>Geotechnical aspects</i>	24
2.3.1 Introduction	24
2.3.2 Soil investigations and soil parameters	27
2.3.3 Relevant phenomena in the structure-foundation interaction	28
2.3.4 Possibilities for design improvements	43
2.3.5 General conclusions	43

<i>2.4 Structural aspects</i>	44
2.4.1 Types of reinforced concrete caissons	44
2.4.2 Geomechanical and hydraulic aspects relevant to the structural response	46
2.4.3 Loads acting on the caisson	47
2.4.4 Failure structural modes	47
2.4.5 Design codes	49
<i>2.5 Probabilistic aspects</i>	50
Chapter 3: Mechanical behaviour of cohesionless soils: experimental observations and constitutive modelling	53
3.1 <i>Introduction</i>	53
3.2 <i>Experimental observations</i>	56
3.2.1 Monotonic loading: drained conditions	56
3.2.2 Monotonic loading: undrained conditions	58
3.2.3 Cyclic loading: drained conditions	64
3.2.4 Cyclic loading in undrained conditions: liquefaction and cyclic mobility	64
3.3 <i>Constitutive modelling</i>	74
3.3.1 A generalised plasticity model for sands	75
3.4 <i>General conclusions</i>	83
Chapter 4: Laboratory experiments: dynamic centrifuge tests	85
4.1 <i>Introduction</i>	85
4.2 <i>General considerations and scaling for dynamic problems</i>	86
4.3 <i>Scope of the centrifuge tests</i>	88

4.4 <i>Model structure and model set-up</i>	89
4.5 <i>Loading scheme</i>	92
4.6 <i>Model soil</i>	98
4.7 <i>Measurements and test results</i>	103
4.7.1 Test n. 1: two irregular storms	103
4.7.2 Test 2: regular/ irregular storms and regular storms	109
4.8 <i>Failure mechanism: role of instantaneous pore pressures and cyclic mobility</i>	121
4.9 <i>General conclusions</i>	125
4.10 <i>Additional research and numerical approach</i>	127
Chapter 5: Conclusions and Future Needs	129
APPENDIX I: Results of centrifuge tests	134
<i>Figure A1</i> – First Test : Applied force versus time	135
<i>Figure A2</i> – First Test: Horizontal displacements versus time	136
<i>Figure A3</i> – First Test: Vertical displacements (front) versus time	137
<i>Figure A4</i> - First Test: Vertical displacements (back) versus time	138
<i>Figure A5</i> - First Test: Rotation versus time	139
<i>Figure A6</i> - First Test: Pore pressure versus time, transducer UM1	140
<i>Figure A7</i> - First Test: Pore pressure versus time, transducer UM2	141
<i>Figure A8</i> - First Test: Pore pressure versus time, transducer UM3	142
<i>Figure A9</i> - First Test: Pore pressure versus time, transducer UM4	143
<i>Figure A10</i> - First Test: Pore pressure versus time, transducer UM5	144
<i>Figure A11</i> - First Test: Pore pressure versus time, transducer US1	145

<i>Figure A12</i> - First Test: Pore pressure versus time, transducer US2	146
<i>Figure A13</i> - First Test: Pore pressure versus time, transducer US3	147
<i>Figure A14</i> - First Test: Pore pressure versus time, transducer US4	148
<i>Figure A15</i> - First Test: Pore pressure versus time, transducer US5	149
<i>Figure A16</i> – Second Test : Applied force versus time	150
<i>Figure A17</i> – Second Test: Horizontal displacements versus time	151
<i>Figure A18</i> – Second Test: Vertical displacements (front) versus time	152
<i>Figure A19</i> – Second Test: Vertical displacements (back) versus time	153
<i>Figure A20</i> - Second Test: Rotation versus time	154
<i>Figure A21</i> – Second Test: Pore pressure versus time, transducer UM1	155
<i>Figure A22</i> – Second Test: Pore pressure versus time, transducer UM2	156
<i>Figure A23</i> – Second Test: Pore pressure versus time, transducer UM3	157
<i>Figure A24</i> – Second Test: Pore pressure versus time, transducer UM4	158
<i>Figure A25</i> – Second Test: Pore pressure versus time, transducer UM5	159
<i>Figure A26</i> - Second Test: Pore pressure versus time, transducer US1	160
<i>Figure A27</i> - Second Test: Pore pressure versus time, transducer US2	161
<i>Figure A28</i> - Second Test: Pore pressure versus time, transducer US3	162
<i>Figure A29</i> - Second Test: Pore pressure versus time, transducer US4	163
<i>Figure A30</i> - Second Test: Pore pressure versus time, transducer US5	164
APPENDIX II: Settlements of a real vertical caisson breakwater under wave induced cyclic loading	165
1. <i>Introduction</i>	165
2. <i>Ground profile and geotechnical characterisation</i>	168
3. <i>Recorded settlements</i>	173

3.1 Total settlements	173
3.2 Settlements due to the filling of the caissons	179
3.3 Settlements due to the sea wave action	181
3.4 Effect of important storms	184
4. <i>Final remarks</i>	188
References	190
Acknowledgements	
About the Author	
Publications	

Summary

The continuous increase of human activities along coastal zones has encouraged coastal and maritime engineering to realise even more structures, as breakwaters, to reduce the wave action in harbours and on the shores.

Monolithic structures, especially for breakwaters at great depth, constitute a particularly competitive structure in term of total costs, construction time, maintenance and environmental aspects because of their flexibility to adapt to any requirements related to their shape, size and multi-purpose use. On the other hand, the design of vertical caisson breakwaters is particularly complex due to the transient phenomena involving the soil-fluid-structure interaction and the wave loads may cause failure of the foundation of a gravity structure in several ways.

The interest to this research comes from observing that many vertical breakwaters, apparently properly designed, have collapsed or experienced bleak damage that could not be predicted at the design stage and cannot be explained by stationary design methods and analyses.

Until 1990's limited attention has been paid by the traditional design methods to the soil mechanical aspects involved in the breakwaters, favouring the understanding of the hydraulic and structural aspects. For vertical breakwaters numerous failures were recorded in the 1930s and, consequently, they were almost abandoned in favour of the rubble mound breakwater type (Oumeraci, 1994). After a series of catastrophic failures experienced also by large rubble mound breakwaters at the end of the 1970s and the beginning of 1980s, a number of actions were started to promote the revival of vertical breakwaters.

Hence, important research activities were undertaken aimed at better understanding the short duration loads by wave impacts and the actual foundation response to impact and cyclic loading. Nowadays, new knowledge and considerable improvements have been achieved with respect to the mechanism responsible for geotechnical failures, their prediction and the associated uncertainties.

Research results show that most of the failure modes are associated with the dynamic nature of the wave loads and the transient phenomena involved in the structure-foundation interaction. Consequently, several studies should be aimed at improving an integrated design of vertical coastal structures, embracing hydraulic, structural and geotechnical aspects. In this framework, several European Research Projects have been developed.

The problem of the stability of monolithic breakwaters has not yet been solved in a commonly accepted way and designers generally use practical formulae rather than a theoretical approach. The traditional foundation design is based on stationary equilibrium equations for sliding and overturning of the wave loaded structure. The bearing capacity is accounted for by comparing the stresses transmitted into the foundation, by the wave load, to a threshold value associated with the characteristic of the foundation material. The wave load is derived from equations such as the well-known Goda's formula (Goda, 1985).

This simplistic approach completely ignores the processes induced in the foundation like, for instance, the irregular pore pressure distribution in the bedding layer, the instantaneous and residual excess pore pressures effects, the soil degradation due to repetitive wave loading and other phenomena. Consequently, many forms of unexpected failures can occur and sometimes no clear boundary between failure and non-failure is evident, but small residual deformations under repetitive high loads are present.

This *Doctorate Research* concerns the behaviour of vertical caisson breakwaters under cyclic loading induced by the wave action. More specifically, we mainly focus on the geotechnical aspects, with particular reference to sandy subsoils.

Some mechanisms of failure taking place in sandy soils foundations have been studied, paying attention to the mechanical behaviour of sands cyclically loaded.

During the storms the action of the waves on the sand foundation generated shear stress and strains that are cyclic in nature. Many studies have been carried out on the effect of the direct sea-wave action on the seabed but many uncertainties characterise the dynamic wave-structure-foundation interaction, not yet well investigated.

The study of the mechanical behaviour of granular soils under cyclic loading, based on standard laboratory tests, has evidenced that wave-induced cyclic action may induce phenomena of partial liquefaction and cyclic mobility of sandy soils. Liquefaction and cyclic mobility have been object of a continuing discussion within the geotechnical engineering, commonly associated to ground failures due to the earthquakes. Although liquefaction is commonly used to describe all failure mechanisms resulting from the build-up of pore pressures during undrained cyclic shear of saturated soils, several researchers have argued that liquefaction and cyclic mobility should be carefully distinguished.

The constitutive modelling of granular soils under transient and cyclic loading is also quite complex. In the last decades extensive research enabled to develop advanced models in order to take into account several aspects of granular soil behaviour under loading, unloading and reloading. Progressively, more sophisticated studies have helped to develop constitutive models of increasing complexity, arriving to describe phenomena as liquefaction and cyclic mobility (e.g. the generalised plasticity model developed by Pastor-Zienkiewicz, 1990).

A significant part of this research deals with the analysis of some laboratory test results performed in the framework of a European Research Project (PRObabilistic Design Tools for VERtical BreakwaterS, Oumeraci et al., 2001).

In this project, sandy foundation of vertical caisson breakwaters has been studied with dynamic centrifuge tests performed at the laboratory of GeoDelft (Delft, The Netherlands) (Van der Poel and De Groot, 1998).

The modelled structure was subjected to cyclic horizontal loading simulating regular and irregular wave loading, until failure occurred. The critical failure mechanism has been studied by analysing caisson displacements and rocking motion. The influence of the loading scheme on the structure's response and pore pressure distribution along the caisson has been analysed.

Test results show that failure occurs according to a more complex mode than the mechanism expected (liquefaction flow failure). The induced collapse is not a consequence of a specified wave load but it occurs according to a progressive mechanism under repetitive high loads. The wave action leads to oscillatory motions

and residual permanent deformations of the structure, causing a “stepwise” bearing capacity failure in the subsoil.

The dilative nature of sand and the instantaneous undrained conditions, with drainage characteristic time larger than load application time, lead to think that phenomena of “instantaneous liquefaction” and “cyclic mobility” were probable responsible of failure process.

In conclusions, the research has resulted in increased insight into the interpretation of foundation failures of vertical coastal structures. It increased understanding of the mechanical behaviour of sandy soils cyclically loaded by the wave action and the transient phenomena involved in the structure-foundation interaction.

The study, based on the interpretation of centrifuge tests, has evidenced that complicated phenomena, not taken into account by the traditional design approach, may play a significant role in the failure mode. On the other hand, it could significantly be important to study the mechanical response of sand underneath the caisson in terms of effective and total stress paths. This could prove that the soil follows the typical path of cyclic mobility. Then, it would be important to carefully investigate the cinematic aspects in the structure-foundation interaction, especially as regards the deformation field characterising the subsoil.

The research provides the basic tools useful to develop a numerical modelling activity based on experimental results.

Finally, the monitoring a real vertical caisson breakwater cyclically loaded for a long period (Appendix II) showed the importance, in the practical design, to observe real structures under wave action, in order to make a good prediction of their behaviour.

Chapter 1

Introduction

1.1 Aims and scope

The continuous increase of human activities along coastal zones has encouraged maritime engineering to realise an increasing number of structures, as breakwaters, to reduce the wave action in harbours and on the shores. Until 1990's limited attention has been paid by the traditional design methods to the soil mechanical aspects involved in the breakwaters, favouring the understanding of the hydraulic and structural aspects.

With respect to monolithic breakwaters, as vertical wall breakwaters or caisson breakwaters, the problem of the stability has not yet been solved in a commonly accepted way and designers generally use practical formulae rather than a theoretical approach. The traditional foundation design is based on stationary equilibrium equations for sliding and overturning of the wave loaded structure. The bearing capacity is accounted for by comparing the stresses transmitted into the foundation, by the wave load, to a threshold value associated with the characteristic of the foundation material. The wave load is derived from equations such as the well-known Goda's formula (Goda, 1985).

Many good designs have been made in this way. Nevertheless, observed case-histories and a literature survey have revealed that many vertical breakwaters, apparently properly designed, have collapsed or experienced bleak damage that could not be predicted at the design stage and cannot be explained by the current stationary design methods and analyses. Most of the failure modes, in fact, are associated with the dynamic nature of the wave loads, with the subsoil resistance and with the transient phenomena involved in the structure-foundation interaction. The traditional procedure to analyse the stability of vertical monolithic breakwater completely ignores the processes induced in the foundation like, for instance, the irregular pore

pressure distribution in the bedding layer, the instantaneous and residual excess pore pressures effects, the soil response due to repetitive wave loading and other phenomena. Consequently, many forms of failures may occur and sometimes no clear boundary between failure and non-failure is evident, but residual deformations under repetitive high loads are present.

In the last thirties, as a consequence of several catastrophic failures, vertical structures were almost abandoned for a long period (Oumeraci, 1994). Conversely, monolithic structures, especially for breakwaters at great depth, represent a good solution in term of total costs, construction time, maintenance and environmental aspects. These aspects justified a renovate interest for vertical structures and induced important research activities, aimed at achieving a more exhaustive knowledge of main involved phenomena and at investigating simultaneously dynamic, hydraulic and geotechnical aspects. Hence, new knowledge and considerable improvements have been achieved with respect to the mechanisms responsible for geotechnical failures, their prediction and the associated uncertainties. Nevertheless, the research is still at the beginning and important further developments are needed in the future.

This Doctorate research concerns the behaviour of vertical caisson breakwaters under cyclic loading induced by the wave action. More specifically, we mainly focus on the geotechnical aspects, with particular reference to sandy subsoils, paying attention to the dynamic aspects involved in the problem. The study is aimed at analysing the action of the short duration loads by wave impacts and the actual foundation response to impact and cyclic loading. For failure cases with sandy subsoils we discuss the question whether “liquefaction”, at least “pore pressure build-up after each load cycle” may play a role or rather an accumulation of small irreversible strains at repetitive peak stresses.

In the research an experimental approach is followed. This is based on the interpretation of laboratory tests executed in the framework of an important European Research Project, performed by Oumeraci et al. (2001) and called “PROVERBS” (PRObabilistic Design Tools for VERTical BreakwaterS). This project is a large EU-funded research project involving 23 institutes from 8 European countries and different disciplines like fluid mechanics, applied mathematics, soil mechanics, structural dynamics, hydraulic and coastal engineering. It started in 1996

and finished in 1999 and had intended to develop new probabilistic design/analysis methods for monolithic coastal structures and breakwaters subjected to the wave attacks. Within the framework of this project, sandy foundation of vertical caisson breakwaters has been studied with dynamic centrifuge tests, performed at GeoDelft (Delft, The Netherlands) (Van der Poel and De Groot, 1998). A significant part of the thesis deals with the results obtained by these tests and an interpretation of the observed failure behaviour is proposed. The failure process has been analysed by examining the effects of the cyclic wave action on the mechanical behaviour of sandy soil foundation. The outcome of this study is that the failure occurred according to a more complex mode than the mechanism expected when the tests were designed, that was a “liquefaction flow failure” involving the structure. Conversely, phenomena of “instantaneous liquefaction”, “residual liquefaction” and “cyclic mobility” have been considered responsible of failure process.

We conclude that such a phenomena, not taken into account by the traditional design approach, may have played a significant role in the failure mode.

Since July 2003 to July 2004 the PhD research has been performed in Delft (The Netherlands), under the leadership of Prof. H. Vrijling (Delft University of Technology, Hydraulic Section), Stefan van Baars (Geotechnical Department) and M. B. De Groot (GeoDelft).

It is finally important to remark that the present research has been partially financially supported by “Impresa Pietro Cidonio” S.p.A., specialised Company for civil and maritime works.

1.2 Contents

The structure of the thesis can be summarised as follows:

- *Chapter 2* presents a general background and an extensive literature review of the main design tools for vertical breakwaters, with particular regard to the research explicated within the framework of PROVERBS Project;
- *Chapter 3* describes the mechanical behaviour of granular soils under static and cyclic loading conditions, deduced by the standard laboratory experimental tests;

then, the constitutive modelling of cyclically loaded sand is analysed and an advanced material constitutive model is presented;

- *Chapter 4* shows the results of the centrifuge tests performed in GeoDelft and proposes a key of interpretation of the observed failure's behaviour;
- *Chapter 5* summarises the general conclusions and presents some suggestions on the future improvements and developments of the research.

Finally, the thesis comprises two Annexes.

In *Annex I* all the results of the centrifuge tests have been collected.

In *Annex II* a study of a real vertical caisson breakwater sited in the Port of Civitavecchia (West Coast of Italy) is presented. Measurements of settlements of the breakwater, recorded during the different stages of the structure's construction, enabled to increase the understanding of the breakwater's behaviour under static and wave-induced cyclic loading.

Chapter 2

General background and literature review

2.1 Introduction

A breakwater is a coastal structure that provides sufficient protection of the area behind it from the wave action. Its main function is to reduce the wave transmission around, trough and over the breakwater itself, but also the wave reflection (important, for instance, for ship manoeuvres) and wave overtopping (important, for instance, for installations/operations on and behind the breakwater).

Two main different types of breakwaters can be distinguished, according to their structural features: *rubble-mound breakwater* type and *vertical breakwater* type.

When the rock is available conveniently for quarrying, the *rubble-mound breakwater* is generally the most economical structure for protection. It is characterised by a core of quarry-run (“tout-venant”), containing a limited percentage of fines (to minimise settlements due to washing out), covered with layers of stones of increasing size and by a final, larger, two-layer armouring on the seaward face, in order to absorb the wave energy by breaking, friction and percolation. It can dissipate steep storm waves by turbulence, as water penetrates the voids between the rocks. Armour layers should then have a high porosity in order to reduce wave runup and overtopping. A wide, shallow toe berm can also reduce overtopping by forcing the wave to break against the main armoured layer.

A *vertical breakwater* consists of a wall and a foundation. It is characterised by a high wave reflection. The wall may be realised with cellular caissons, crowned by a concrete superstructure, or with a block-structure. Cellular caisson is a pre-fabricated rectangular structure sunk trough water to the prescribed founding depth, filled with sand, rock or concrete. In both cases (caissons or block-structure) the wall may be considered for the foundation as a stiff monolithic structure. The foundation of a vertical breakwater consists of two parts, a rubble foundation (usually constituted of

granular material, no more than gravel) and the subsoil (often original seabed). In some cases part of the original seabed material is removed and replaced by sand or fine gravel, that becomes part of the subsoil. Caisson breakwaters are very popular in Mediterranean countries due to a number of different factors: monolithicity; low cost and good quality of the concrete; small variation of water levels; rapidity of placement on site; reduced maintenance; environmental constraints related to the use of rock quarries and to rock transport and dumping pollution.

The main difference between the mound type and the monolithic type of breakwater is due to the interaction between the structure and the subsoil and to the behaviour at failure. The mound-type structures can follow uneven settlement of the foundation layers, whereas the monolithic structures require a solid foundation that can cope with high and often dynamic loads. The behaviour of the structures close to failure is also quite different. When a critical load value is exceeded, a monolithic structure will lose stability at once, whereas a mound-type of structure will fail more gradually as elements from the armour layer disappear one after another.

Finally, *composite breakwaters* are sometimes used in order to save material and reduce the width of the section. They consist of vertical caissons protected by a conventional rubble-mound on the seaside, which ensures their stability by reducing the hydrodynamic force of breaking waves. This solution is sometimes adopted to rehabilitate a damaged vertical structure, combining a rigid element with a flexible structure.

In Figures 2.1, 2.2, 2.3 and 2.4 some examples of the described breakwaters types have been reported.

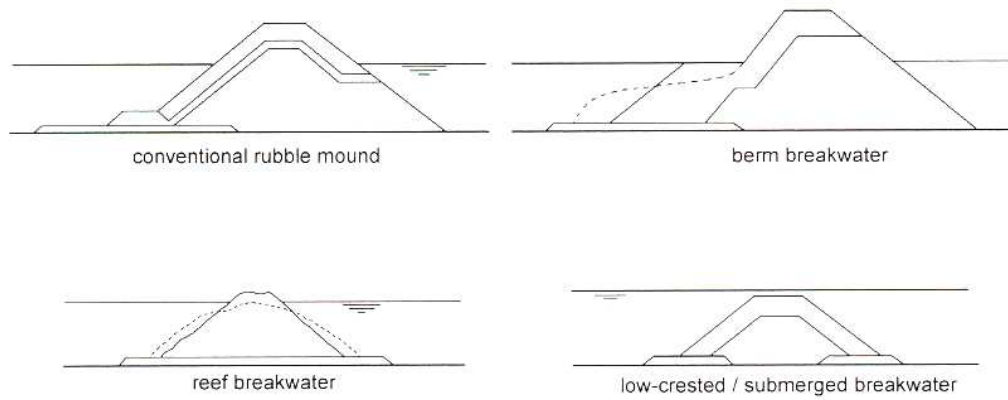


Figure 2.1 – Mound breakwaters types

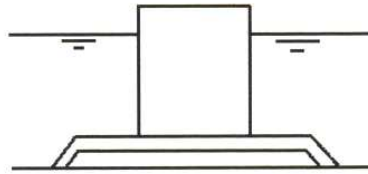


Figure 2.2 – Monolithic breakwaters type

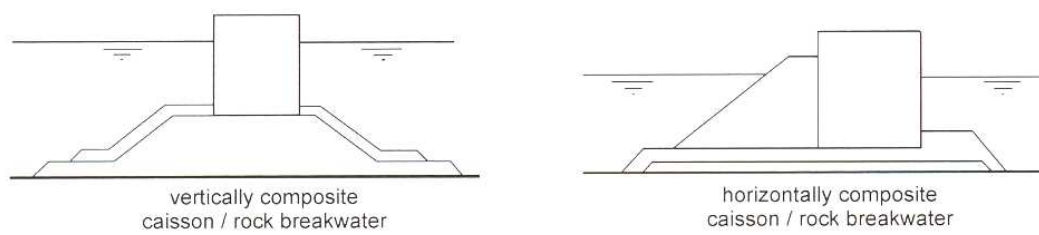


Figure 2.3 – Composite breakwaters types

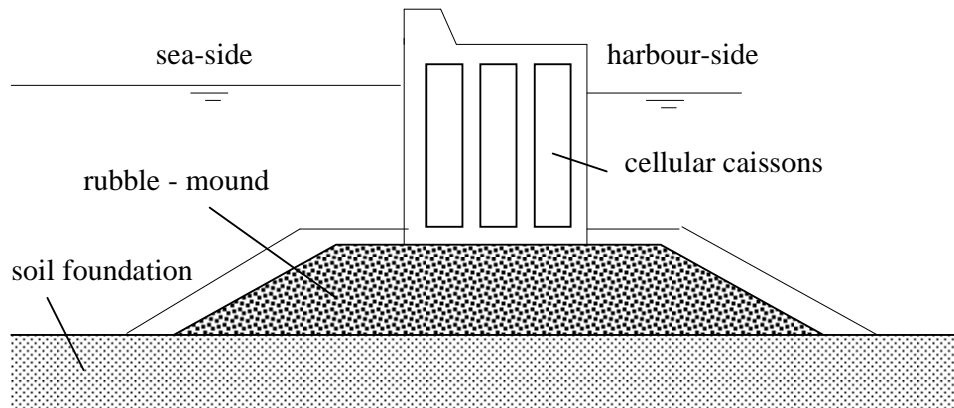
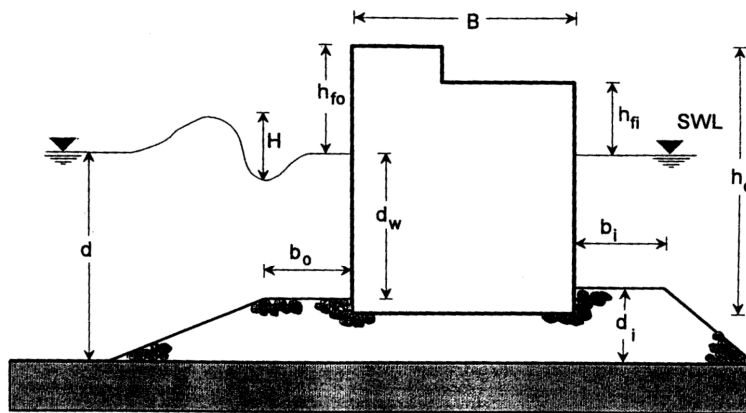


Figure 2.4 – Vertical caisson breakwater

Analysing the “history” of the breakwaters we discover that the first breakwaters date back to the ancient Egyptian, Phoenician, Greek and Roman cultures. As early as 2000 BC, mention was made of a stone masonry breakwater in Alexandria, Egypt (Takahashi, 1996). The Romans also constructed true monolithic breakwaters, since they had mastered the technique of making concrete. The Roman Emperor Traiano (A.D. 53-117) initiated the construction of a rubble mound breakwater in Civitavecchia, which still exists today. The very flat seaward slope and the complicated superstructure are proof of a history of trial and error, damage and repair (Vitruvius, 27 BC; Shaw, 1974; Blackman, 1982; De la Pena, Prada and Redondo, 1994; Franco, 1996). The rapidly increasing sea-borne trade in the 19th century led to a large number of breakwaters being built in Europe and in the emerging colonies. In order to avoid the problems of construction in deep water, rubble mound berms were used for the foundation of a monolithic superstructure and thus the first real composite breakwaters came into existence. The composite breakwater became the most widely used type in the early 20th century, especially in Italy, where a lot of breakwaters were constructed in relatively deep water along Mediterranean coast. In the meantime, the Japanese continued to build and develop the monolithic breakwater. An important contribution was given by a French engineer, G.E. Jarlan (1961), who introduced the perforated front wall to reduce reflection and wave impact forces.

Both the rubble-mound breakwater type and the vertical breakwater type experienced several catastrophic failures in the past. For vertical breakwaters numerous failures were recorded in the 1930s and the cost to re-build was 2÷3 times more than the original cost. An interesting review of catastrophic failures experienced by vertical breakwater is reported in Oumeraci (1994). He distinguishes three reasons for failures: a) reasons inherent to the structure itself (non-monolithicity of the structure, weakness of the concrete, etc.); b) reasons inherent to the hydraulic forcing and loads conditions (excess of design wave conditions, occurrence of breaking waves and wave impact loads, wave overtopping etc.); c) reasons inherent to the foundation and seabed morphology (unfavourable configuration of the seabed, seabed scour and erosion, settlements of the structure and shear failure of the foundation). These aspects are systematically discussed for different cases occurred in different countries (Figure 2.5 and Table 2.1). Oumeraci concludes that the traditional design approaches cannot explain most of the failure modes analysed and that the stability of vertical breakwaters is an integrated and complex problem, which can satisfactorily be solved only by dynamic analyses and probabilistic design approaches.



Notations in Tab. 1

T	= Wave Period	UCY	= Cyclopean Block Type (unbounded) ¹⁾
RMF	= Rubble Mound Foundation	CEL	= Cellular Block Type ¹⁾
CA	= Caisson Type	WEL	= Well Block Type ¹⁾
BCY	= Cyclopean Block Type (bounded) ¹⁾		

Figure 2.5 – Vertical Breakwater – definition sketch for Table 2.1

(adapted from Oumeraci, 1994)

Breakwater	H (m)/T(sec)		Nature of seabed	B (m)	D (m)	h _{r0} (m)	h _{m0} (m)	d _i (m)	Reasons for failure
	Design	Actual		h _c	d _w	h _{fi}	b _j	l/m	
Bizerta (Tunisia, 1915)	-	-	-	8	17	5	10	10	Breaking waves Overtopping Erosion of rubble mound foundation
				13	8	3	5	4/5	
Genova (Italy, 1955)	5.5/7	7/12	Fine-grained sand	12	17.5	7.4	6.0	8/7	Exceedance design wave Non-monolithicity Breaking waves Wave overtopping (sliding)
				17.9	10.5	3.0	12	1/1	
Nigata (Japan, 1976)	7/13	7/13.5	Silty-sand	15	17	4.5	9.0	4.0	Breaking waves Overtopping Differential settlement
				-	10	4.5	7.0	1/3	
Naples (Italy, 1987)	-	5	-	13	19	7.5	10	-	Wave breaking (sliding and overturning)
				18	12.5	2.0	3.5	1/1.5	
Mashike (Japan)	5.5/10	6.6/12	-	14.5	7	1.0	6.9	2.8	Exceedance design wave Wave breaking Overtopping (sliding = 2.9 m)
				6.0	3.9	1.0	6	1/3	
Fukaure (Japan)	7.6/11	6.3/13	-	20.5	15	2.5	17	4.3	Wave breaking Overtopping Erosion of rubble mound foundation
				12.5	11	2.5	12	1/3	
Sakata (Japan)	3.3/8.8	5.5/13	-	6.5	7.0	5.5	10	2.5	Exceedance design wave Wave breaking Differential settlement (sliding and shoreward tilt)
				10	2.9	2.5	4.5	1/1.5	

Table 2.1 - Review and analysis of vertical breakwater failures – lessons learned
Coastal engineering, 22 (1994) 3-29. Adapted from Oumeraci, 1994

Consequently to these failures, vertical structures were almost abandoned in favour of the rubble mound breakwater type. After a series of catastrophic failures experienced also by large rubble mound breakwaters at the end of the 1970s and the beginning of 1980s, a number of actions were started to promote the revival of vertical breakwaters and the development of new breakwater concepts (Oumeraci et al., 1991). In this sense, monolithic caisson type structures constitute a particularly competitive structure, especially at greater depth, because of their flexibility to adapt to any requirements related to their shape, size and multi-purpose use. Example from Japan (Tanimoto and Takahashi, 1994), Monaco (Bouchet et al., 1994) and Korea (Lee and Hong, 1994) have already shown that the potential of adapting caissons type structures to meet any requirement of technical, social and ecological nature is higher than any other traditional type of structure. This however, requires a high level of knowledge and technology.

Consequently, several studies have been performed in order to improve an integrated design of vertical coastal structures, that comprehends hydraulic, structural and geotechnical aspects.

In the following sections these different aspects are briefly discussed, especially with reference to the research performed in the framework of PROVERBS Project (Oumeraci et al., 2001).

2.2 Hydraulics aspects

2.2.1 Introduction

The interaction between the waves and the structures plays a significant role in the design of marine structures. A good design has to dimension the vertical breakwater, its structural elements and its foundation to resist wave action and its effects, and to deliver required hydraulic performance. On the other hand, the prediction of waves forces and distributed pressures on structures is complicated and characterised by high uncertainties.

Waves are generated by wind fields over the sea offshore from the coast of interest. In general, a wave field is characterised by a significant wave height, H_s , and a peak

period, T_p . H_s is defined as the average height of the highest third part of the waves in a wave field, while T_p is the peak period of the wave spectrum, the period with the maximum energy density. H_s , in a combination with the Rayleigh distribution, characterises the state of the sea at a certain moment. The state of the sea can change every hour, giving different values for H_s , which also has a different distribution in time, the so-called “long-term distribution”. For maintenance and design considerations, the long-term distribution is important in the choice of representative loading conditions.

Wave loads on structures are traditionally classified into *pulsating wave loads* (or *non-breaking wave loads* or *standing wave loads*) and *impact wave loads* (or *breaking wave loads*).

For *pulsating wave loads* the load duration is larger than expected dynamic response of the structure and a “quasi-static” approach can be applied. The loads defined so far are called quasi-static forces, because they fluctuate with the wave period of several seconds and do not cause any dynamic effects. Inertial effects need not to be taken into account.

When the wave collides with the surface, a very short impact pressure (*impact wave loads*) characterised by a very large local magnitude will occur. The quasi-static pressures are always in the order of $\rho g H$, but the impact pressures can be 5 or 10 times higher, reaching values between 50 and 150 *mwc* (meters water column). In this case the load duration is most relevant for the dynamic response of the structure and a dynamic analysis is necessary.

Many researchers have studied the phenomenon in the laboratory and none have found a satisfactory explanation that can predict the occurrence and the magnitude of a wave impact as a function of external parameters. Apparently, the deceleration of the mass of the water in the wave crest, combined with the magnifying effect of the air cushion, causes the high pressure.

Depending on the purpose and the failure modes for which they are used, a further classification of the wave loads is suggested: *quasi-static loading* (which may induce an overall failure of the structure), *impact loading* (causing local overall failure and structural failure modes) and *cyclic loading* (causing fatigue and stepwise failure).

In Figure 2.6 the different types of wave loading for monolithic structures are represented.

A parameter response map for prediction of the type of wave loading on vertical and vertically composite breakwaters based on structure geometry and wave conditions has developed in the framework of PROVERBS Project. The parameter map, reported in Figure 2.7, has been validate against a number of model data sets from several Researches Institutes and Universities.

In the next Sections the methods to calculate the pressure on vertical structures induced by wave loading are briefly presented. This is done both for pulsating and impact loads.

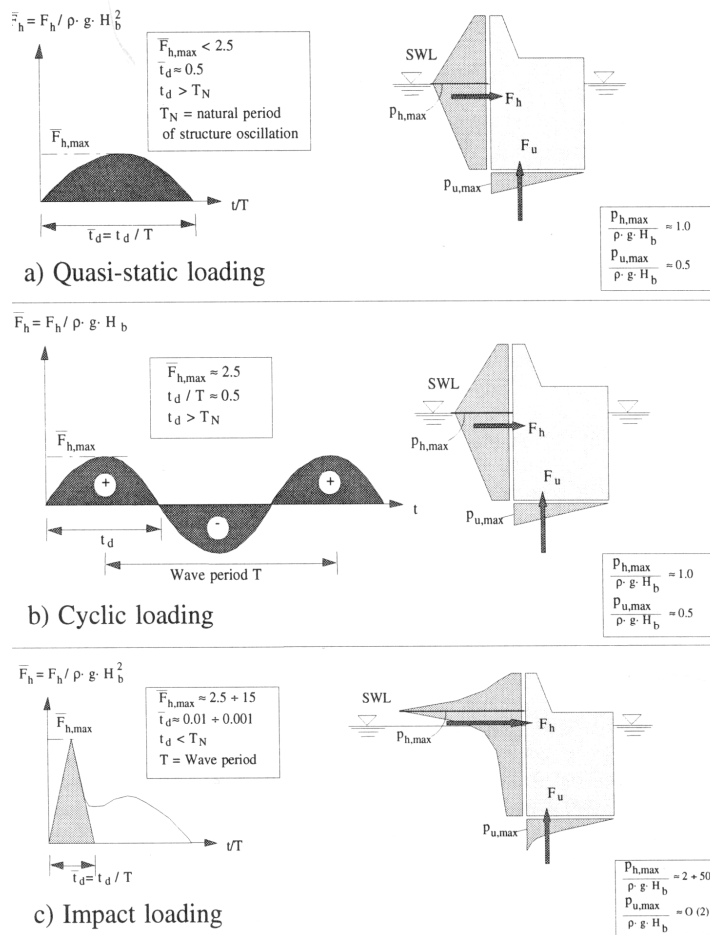


Figure 2.6 – Wave loading for monolithic structures

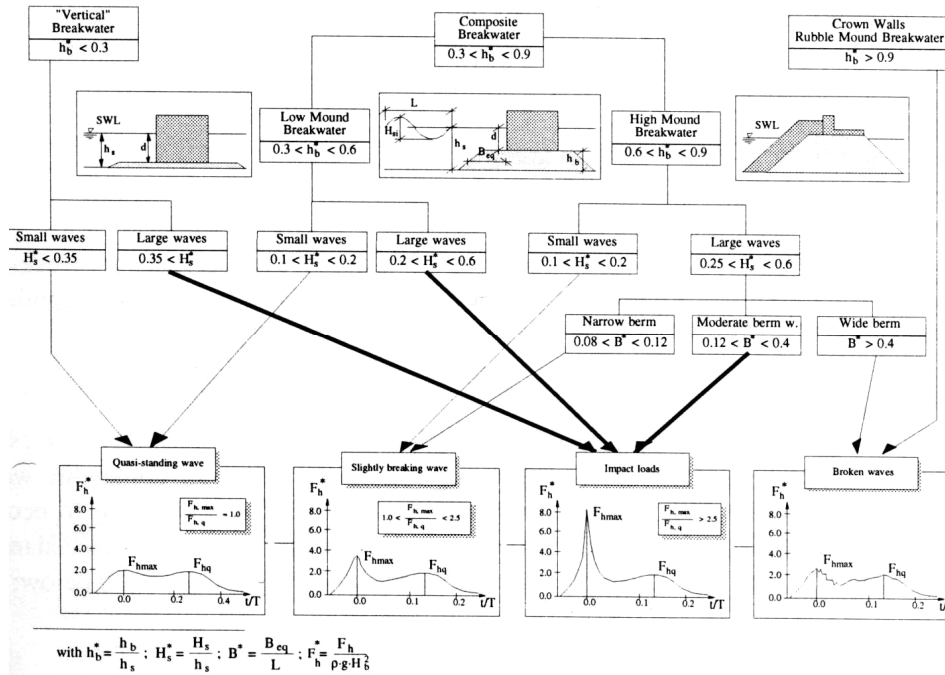


Figure 2.7 – Parameter map

2.2.2 Pulsating wave loads

The first method to calculate pressures exerted on a vertical wall by standing waves was developed by Sainflou in 1928, on the basis of the formula for the pressure distribution under a wave according to the linear wave theory. Sainflou published a theory of trochoidal waves in front of a vertical wall and presented a simplified formula for pressure estimation. The pressure distribution is sketched as in Figure 2.8.

The pressure intensities and the quantity of water level rise δ_0 are given as:

$$p_1 = (p_2 + w_0 h)(H + \delta_0)/(h + H + \delta_0) \quad (1)$$

$$p_2 = w_0 H / \cosh kh \quad (2)$$

$$\delta_0 = (\pi H^2 / L) \coth kh \quad (3)$$

where L is the wavelength and k is the wave number of $2\pi/L$. It is important to observe that the formula was derived when the concept of wave irregularity was unknown.

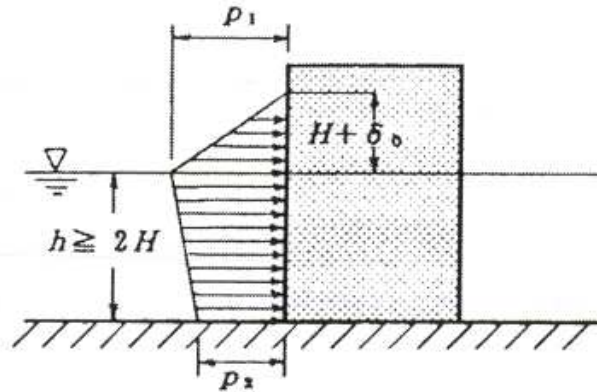


Figure 2.8 – Wave pressure distribution by Sainflou's formula

In 1958 Rundgren carried out a series of model experiments and concluded that Sainflou's method gives good results for long and less steep waves, but it overestimates the wave force for steep-waves. Rundgren then used and modified the approach proposed by Miche (1944) and they developed a method (Miche- Rundgren method) that gives satisfactory results for steep waves. The main and most important aspect of the Miche- Rundgren approach is the definition of parameter h_0 , which is a measure for the asymmetry of the standing wave around SWL.

2.2.3 Wave impact loads

Because of vertical breakwaters are massive structures, they do not seem to respond to very short duration impacts so that the incidence of failure appears to be relatively low. Recent failures of vertical breakwaters in UK, Japan and Italy have demonstrated that wave impacts may have considerable influence on loading and caused catastrophic failures of several vertical breakwaters. Hence, a good prediction of the effect of impact loads is particularly important in the design of coastal structures.

The first wave pressure formula for breakwater design was published by Hiroi in 1919. The formula calculates the uniform pressure distribution in the following way:

$$p = 1.5w_0H \quad (4)$$

where w_0 denotes the specific weight of the sea water and H the incident wave height. This pressure distribution extends to the elevation of $1.25H$ above the design water level or the crest of breakwater if the latter is lower (Figure 2.9). Hiroi's wave pressure formula was intended for use in relatively shallow water where breaking waves are the governing factor. It was accepted by harbour engineers in Japan and almost all breakwaters had been designed by this formula until the mid 1980s. Although this formula had been changed several times in order to take into account different aspects (application for standing wave pressures, introduction of the concept of significant height, variations in wave period and others factors), the total wave force thus estimated was quite reliable on the average.

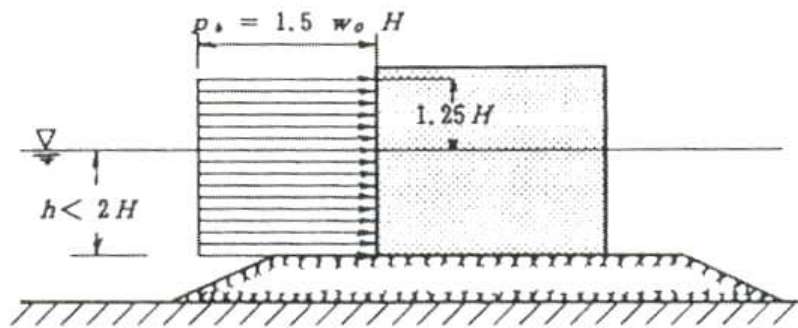


Figure 2.9 – Wave pressure distribution by Hiroi's formula

In 1950, Minikin proposed a formula for breaking wave pressure, which consisted of the dynamic pressure p_m and the hydrostatic pressure p_s . This formula was the first known one and then the most used, in Europe and USA, but, in the light of the present knowledge of the nature of the impact wave, it has several contradictions and it has been definitely denied.

Presently, there are few design formulae for wave impact loads (Goda, 1985; Takahashi et al. 1994). Recent several researches have shown that some methods are limited and may over- or under- predict loadings under important conditions. In PROVERBS Project a new procedure has been proposed to predict impact loading and associated load duration, including the effect of air content. Based on statistical distribution of forces and theoretical considerations derived from solitary wave theory (Oumeraci and Kortenhaus, 1997), this procedure enables to predict horizontal impact wave force as a function of the relative rise time t_r . The effective impact force transmitted to the foundation is dependent on the dynamic response characteristics of the structure and its foundation, then the applied force must be corrected by these dynamic response characteristics. Based on the analysis of almost 1000 breakers of different types hitting a vertical wall, the simplified distribution of impact pressure at the time where the maximum impact force occurs is calculated by means of four parameters:

- 1) the elevation of pore pressure distribution η^* above design water level;
- 2) the bottom pressure p_3 ;
- 3) the maximum impact pressure p_1 which is considered to occur at the design water level;
- 4) the pressure at the crest of the structure p_4 if overtopping occurs.

The vertical pore pressure distribution induced by impact loading at the caisson front wall is reported in Figure 2.10. The same statistical procedure enables to calculate also the uplift force and the uplift pore pressure distribution calculated as follows:

$$p_u = \frac{2F_{u,max}}{B_c} - p_{ru} \quad (5)$$

where B_c is the caisson width, $F_{u,max}$ is the maximum uplift force calculated for impact conditions and p_{ru} is the pressure at the shoreward side of the structure. The pressure p_u calculated in this way represents an upper bound. Another upper bound is $p_u = p_3$.

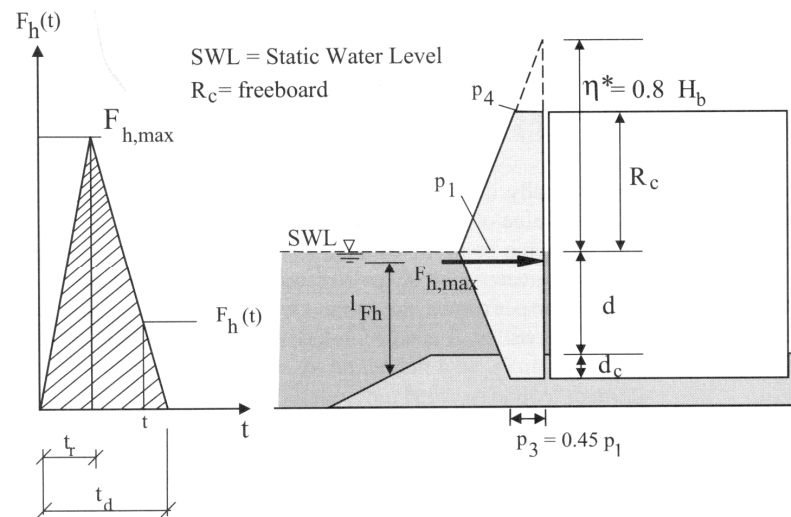


Figure 2.10 – Simplified vertical pressure distribution at the caisson front wall
(Oumeraci et al. 2001)

Many breakwaters may experience significant static and dynamic loading on both seaward and rear faces and many failures may occur involving a seaward motion. The most likely mechanism for the generation of large dynamics loads from the harbour side is the overtopping waves plunging into the harbour basin behind the breakwater. This mechanism has been proved by wave flume tests and numerical modelling based on pressure impulse theory. The improved physical understanding of the generation mechanisms achieved by these results is particular important in the design to avoid the seaward tilting failures due to excessive wave overtopping.

Numerical models represent a useful tool to study the pressure impulse of a wave impacting on a vertical wall. Neural networks can also predict wave forces (Van Gent and Van den Boogaard, 1998).

However, the maximum force and the duration of impacts are still a matter of discussion. In the meantime a designer should try to avoid creating impact conditions in front of the vertical breakwater. A study of the parameter map shows that impact can be avoided by choosing the appropriate geometry for the caisson and the mound on which it is founded.

2.2.4 Proposal of universal wave pressure formulae

According to Goda (1992), the difference between the magnitudes of breaking and non breaking wave pressures is a misleading one. The absolute magnitude of breaking wave pressures is much larger than of non-breaking one but the height of the waves breaking in front of a vertical wall is also much greater than that of non-breaking waves. The dimensionless pressure intensity, p/w_0H , therefore, increases gradually with the increase of incident wave height beyond the wave breaking limit.

The first proposal of universal wave pressure formula for upright breakwater was made by Ito et al. (1966), based on the sliding test of a model section of breakwaters under irregular wave actions. Then Goda (1973, 1974) presented another series of formulas that, critically analysed and reviewed, were finally adopted as the recommended formulas for upright breakwater design in Japan in 1980, instead of the previous dual formulas of Hiroi's and Sainflou's.

Goda analysed many of successful and unsuccessful structures realised in Japan and came up with a practical formula that can be used to analyse the stability of a monolithic breakwater. With his method Goda (1985) established for all wave conditions (standing and breaking waves, crest wave and trough wave) the horizontal force distribution along vertical structures as well as the uplift pressure induced by the wave action along the caisson bottom. The basis of the Goda's model is to assume pressure distributions over the height and width of the caisson which, integrated over the front face and underside, give equivalent sliding forces.

The Goda's formulae are written as (see Figure 2.11):

$$\eta^* = 0.75(1 + \cos \beta)\lambda_1 H \quad (6)$$

$$p_1 = 0.5(1 + \cos \beta)(\lambda_1 \alpha_1 + \lambda_2 \alpha_2 \cos^2 \beta) \rho g H \quad (7)$$

$$p_3 = \alpha_3 p_1 \quad (8)$$

$$p_4 = \alpha_4 p_1 \quad (9)$$

$$p_u = 0.5(1 + \cos \beta)\lambda_3 \alpha_1 \alpha_3 \rho g H \quad (10)$$

where η is the water elevation above the still water level to which the wave pressure is exerted, H is the incident wave height in front of the structure, β is the obliquity of wave attack relative to normal to the structure, $\lambda_1, \lambda_2, \lambda_3$, are multiplication factors dependent on the geometry of the structure and $\alpha_1, \alpha_2, \alpha_3, \alpha_4$, are multiplication factors dependent on the wave conditions and the water depth given by:

$$\alpha_1 = 0.6 + 0.5 \left(\frac{4\pi h_s / L_p}{\sinh(4\pi h_s / L_p)} \right)^2 \quad (11)$$

$$\alpha_2 = \min \left(\frac{\left(\left(1 - \frac{d}{h} \right) \left(\frac{H}{d} \right)^2 \right)}{3}, \frac{2d}{H} \right) \quad (12)$$

$$\alpha_3 = 1 - \left(\frac{d + d_c}{h} \right) \left(1 - \frac{1}{\cosh(2\pi h / L_p)} \right) \quad (13)$$

$$\alpha_4 = 1 - \frac{R_c^*}{\eta^*} \quad (14)$$

In the above formula, h_s is the water depth in front of the structure, L_p is the wave length, d is the depth in front of the caisson, d_c is the height over which the caisson protrudes in the rubble foundation and R_c^* is the minimum of the freeboard R_c and the notional run-up elevation η^* .

When the wave pressures are known, the wave forces are given by:

$$F_{h,Godal} = \frac{1}{2} (p_1 + p_4) R_c^* + \frac{1}{2} (p_1 + p_3) (d + d_c) \quad (15)$$

$$F_{v,Godal} = \frac{1}{2} p_u B_c \quad (16)$$

in which B_c is the width of the caisson bottom. The uplift force p_u may need some corrections depending on the geometry and the grain sizes of the rubble foundation.

The lever arms of the wave forces with respect to the centre of the caisson bottom are given by:

$$l_{h,Goda} = d + d_c + \frac{R_c^{*2} (p_1 + 2p_4) - (d + d_c)^2 (p_1 + 2p_3)}{3R_c^* (p_1 + p_4) + 3(d + d_c)(p_1 + p_3)} \quad (17)$$

$$l_{v,Goda} = \frac{1}{6} B_c \quad (18)$$

With respect to the heel of the caisson, half of the caisson width B_c has to be added to $l_{v,Goda}$ resulting in $l_{v,Goda} = 2/3 B_c$. Using the expressions for the wave forces and the lever arms, the total moment due to the wave forces can be calculated by:

$$M_{Goda} = l_{h,Goda} \cdot F_{h,Goda} + l_{v,Goda} \cdot F_{v,Goda} \quad (19)$$

These calculated forces and moment serve as input in several limit state equations describing the stability of the breakwater, that will be discussed in the next section.

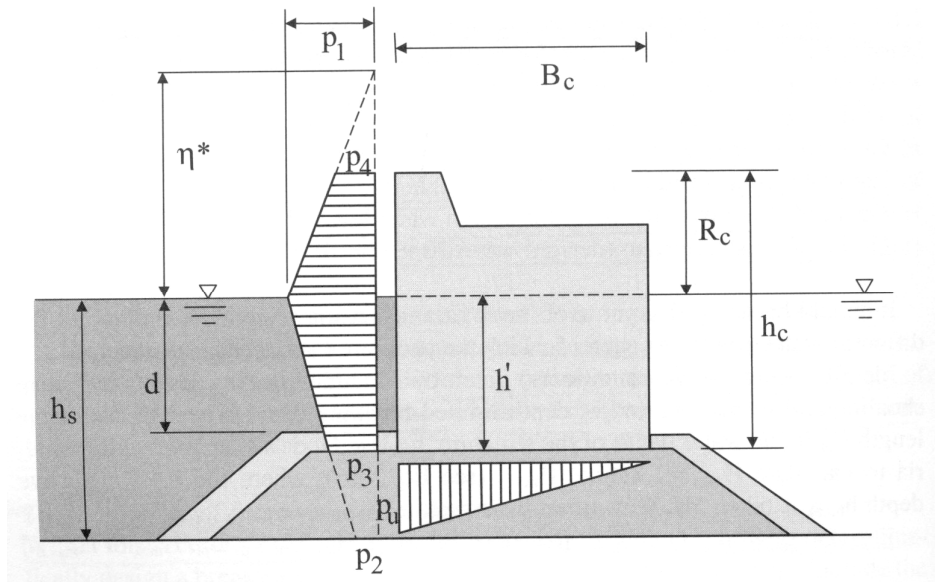


Figure 2.11 – Distribution of wave pressure on an upright section of a vertical breakwater (Goda, 1985)

From a theoretical point of view, the safety factor that Goda proposes is apparently adequate, as long as one realises that conditions with breaking waves should be avoided as much as possible. If this is not possible, extensive model investigations must be carried out, followed by a dynamic analysis of the structure and the foundation, taking into account all inertial terms.

Although the Goda's method is a valuable design method, field measurements of wave pressures and hydraulic model tests (Oumeraci et al., 1991) showed that wave forces under pulsating waves conditions on many structures were often larger than the ones predicted by simple prediction methods. This can be ascribed to several uncertainties generated from two main sources:

- the uncertainty of the maximum individual wave height in a wave field;
- the model uncertainty in the Goda wave force model.

The distribution of individual wave heights in a wave field can generally be assumed to follow a Rayleigh distribution, in which there is only one parameter, the significant wave height H_s . Consequently, F_H can be calculated as follows:

$$F_H(H) = 1 - e^{-2\left(\frac{H}{H_s}\right)^2} \quad (20)$$

By considering the maximum wave height in a wave field, the maximum horizontal force is given by the following equation:

$$F_{H_{max}}(H) = \left(1 - e^{-2\left(\frac{H}{H_s}\right)^2}\right)^N \quad (21)$$

where N denotes the number of individual waves in the wave field. For given values of H_s and N it is now possible to derive the ratio between the significant wave height and the maximum individual wave height. The multiplication factor present in the Goda's model appears to correspond to a wave field with 250 individual waves.

As concerns the model uncertainties of the Goda wave force model, comparison with model tests showed that the Goda's model provides an overestimation of the wave forces (Van der Meer et al., 1994).

Finally, in the Goda's model, no detailed information on flows and pressures under wave conditions can be obtained, nor can the influence of certain parameters such, for instance, the rock size of the rubble mound foundation be quantified.

Numerical models that can simulate the flow pattern in front of vertical structures and flows/pressures inside the rubble-mound foundation might be able to overcome such problems, although the development of a numerical model covering all relevant aspects in detail is very complex.

In PROVERBS Project, two types of models have been applied for simulating relevant processes for vertical breakwaters. In addition to numerical models other methods exist to predict wave forces which make direct use of results from physical model tests.

2.2.5 General conclusions

Stationary and impact loads may cause damage or failure of vertical structure, so the effects of these loads must be considered. In this section a brief procedure is given on how to deterministically design a breakwater or a vertical wall structure. A number of different prediction methods for wave forces on vertical walls have been developed. Most of these were born in Japan, Korea and Taiwan, where the problem of impulsive breaking wave pressure is rather lightly dealt with. At present the site of breakwater construction is moving into the deeper water. Reliable evaluation of the extreme wave condition is becoming the most important task in harbour engineering. Despite the amount of new knowledge generated, much research work, respect to different items, has still to be done. For some response or parameter it is not yet possible to demonstrate that one particular method is more complete or more reliable than another is. For such responses it is therefore important to use engineering judgement and experience to decide which gives the most realistic result.

2.3 Geotechnical aspects

2.3.1 Introduction

Only since a few years the soil mechanics is paying more attention to the foundation problems involved in coastal structures.

The traditional foundation design of vertical (caisson) breakwaters is based on stationary equilibrium equations for sliding and overturning of the wave loaded caisson, while the bearing capacity is accounted for by comparing the stresses transmitted into the foundation by the wave load to a threshold value associated with the characteristic of the foundation material. The safety factors against sliding and overturning are defined by the following:

$$\text{- sliding: } S.F. = \mu (W-U)/P \geq 2 \quad (22)$$

$$\text{- overturning: } S.F. = (Wt-M_U)/M_P \geq 2 \quad (23)$$

where μ (usually equal to 0.6) is the coefficient of friction between the upright section and the rubble mound, W is the weight of the upright section per unit extension in still water, U is the total uplift pressure per unit extension of the upright section, P is the total thrust of wave pressure per unit extension of the upright section, t is the horizontal distance between the centre of gravity and the heel of the upright section, M_U is the moment of total uplift pressure around the heel of the upright section, M_P is the moment of total wave pressure around the heel of the upright section.

In the above formula, the wave load is derived from equations such as the Goda's formula (1985). As described in the previous section, with his method Goda established for all wave conditions the horizontal force distribution along vertical structures as well as the uplift pressure induced by the wave action along the caisson bottom.

A recent practice in Japan is to perform a further analysis of circular slips passing through the rubble mound and the foundation, by utilising the simplified Bishop method. For the rubble mound, the apparent cohesion of $c = 20$ kPa and the angle of internal friction of $\varphi' = 35^\circ$ are recommended.

Many good designs have been made in this way. Nevertheless, several foundation failures occurred that could not be explained on the basis of these conventional stationary methods. This approach, in fact, does not take into account the actual processes involved in the wave-loaded-induced dynamic structure-foundation interaction and the associated mechanical behaviour of foundation soils.

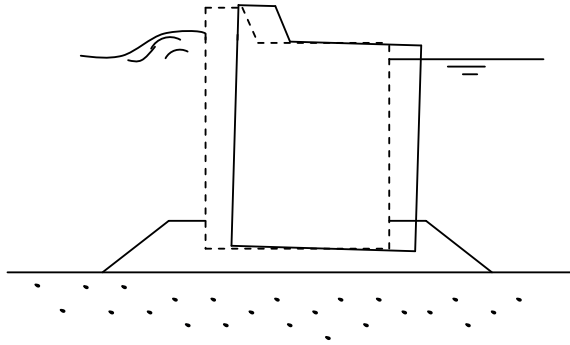
In Figure 2.12 the main geotechnical failure modes for vertical breakwaters have been reported. It is possible to distinguish four different failures:

1. sliding along the base;
2. bearing capacity failure in rubble;
3. bearing capacity failure in subsoil;
4. settlements by consolidation, creep or erosion of fine grained soil.

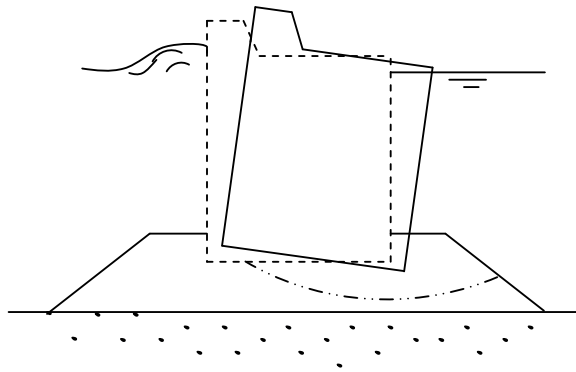
Finally, repetition of events due to wave loads and several storm may induce an unacceptable deformation so that, even though the failure is not yet the case, the breakwater loses its function. In several cases we assist to “stepwise failure” and one load, not much larger than the previous load, may induce sliding over a large distance.

In the next Section an overview of soil investigations and soil parameters for geotechnical characterisation of the seabed soil is presented. Then (Section 2.3.3) several different phenomena, relevant in the structure-foundation interaction, are discussed.

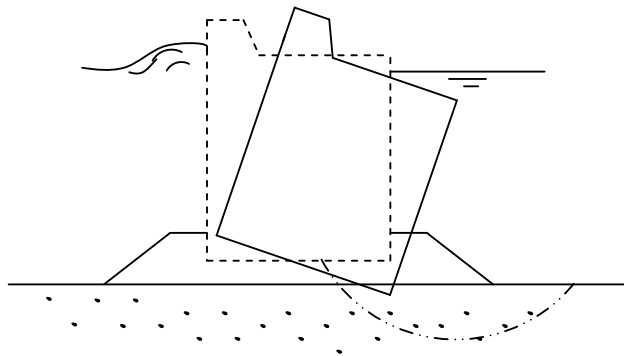
1) SLIDING ALONG THE
BASE



2) BEARING CAPACITY:
FAILURE IN RUBBLE



3) BEARING CAPACITY:
FAILURE IN SUBSOIL



4) SETTLEMENTS BY
CONSOLIDATION,
CREEP OR LOSS OF
FINE GRAINS

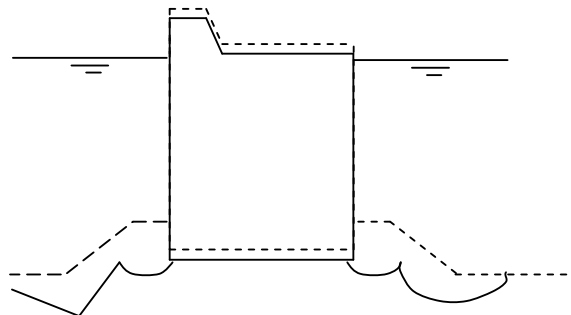


Figure 2.12 – Main geotechnical failure modes of vertical breakwater

2.3.2 *Soil investigations and soil parameters*

The collection of soil data for a new breakwater concerns information about the seabed soil where the breakwater has to be built and information about quarries capable to deliver construction material (rockfill).

After a feasibility study with the analysis of the available documents (soil investigations, geological history, etc.), a seismic survey, covering the area influenced by the structure, should be performed in order to obtain the seabed profile.

Geotechnical characterisation can be performed by means of the traditional in situ tests as CPT tests or, preferably, CPTU tests with measurements of pore pressures. In cohesion-less soils SPT's are preferred. During the design phase specific soil parameters are needed for models. So, borings with soil sampling and classification tests (determination of grain size distribution, soil density, water content, Atterberg limits, relative densities and so on) are particular important. The sampling and the in situ testing depend on factors like water depth, wave and wind conditions (Andresen and Lunne, 1986). If the water depth is less than 30-40 m and the wave and wind conditions are not too severe, the operations can be carried out as on land by using an ordinary drilling rig from an anchored barge or platform. If larger water depths or severe water and wind conditions characterise the site, "offshore" type operations may be required. More detail can be found in Lunne and Powell (1992). In general, several types of soil samplers exist and the type, which gives the least sample disturbance, should be used. Piston samplers are used in soft to stiff clays, while, in dense sand, where it is not possible to use piston samplers, hammers samplers can be useful.

The determination of the subsoils geotechnical parameters can be achieved by means of traditional laboratory tests (triaxial tests, direct simple shear tests, oedometer tests and permeability tests). A different approach has to be used for rubble mound layer. The friction angle of rubble, for instance, cannot be defined for triaxial compression but different procedures can be used (Barton and Kjaernsli, 1981; CIRIA 83/CUR 154, 1991). The Young's modulus E for the rubble layer is not always easy to evaluate; in fact, even though the material is usually very stiff, the rubble layer may be greatly compressible because of the lossy interconnection of the gravel established

during the placement of the material. For permeability of rubble in which turbulent flow may occur, Forchheimer proposes the following equation:

$$i = Av + Bv^2 \quad (24)$$

in which i is the hydraulic gradient, v is the “seepage velocity” and A and B can be estimated from a representative grain size and the porosity with the following equations (Van Gent, 1993):

$$A = \alpha \cdot \frac{(1-n)^2}{n^3} \cdot \frac{1}{gD_{EQ}^2} \quad (25)$$

$$B = \beta \frac{(1-n)}{n^3} \cdot \frac{1}{gD_{EQ}} \quad (26)$$

In (24) e (25) $\alpha \approx 1500$ and $\beta \approx 1.4$, at least for fairly uniformly distributed material, n is the kinematic viscosity of the water ($n \approx 10^{-6} \text{ m}^2/\text{s}$), $D_{EQ} = \{6 \cdot m_{50}/(\pi\rho)\}^{1/3}$ and m_{50} is the median stone mass. The permeability k can be finally obtained from the Darcy equation ($v = k \cdot i$), using a linearised k value.

2.3.3 Relevant phenomena in the structure-foundation interaction

A good design of a vertical breakwater requires a good knowledge of the main phenomena involved in the structure-foundation interaction. In the PROVERBS Project four groups of phenomena are distinguished as important in the structure-foundation interaction:

- phenomena related to the “*dynamics*”;
- phenomena related to the mechanism of “*instantaneous pore pressures*” developed in the foundation;

- phenomena related to the mechanism of “*residual pore pressures*” in foundation and consequent degradation of soil ;
- phenomena related to the “*instability*” of structure.

All the phenomena are strictly interrelated.

Dynamics phenomena have to do with the influence of the inertia of wall and added masses on the loads to the foundation. They are particularly important during the wave impacts in which the duration is rather short and may bring a significant influence of the inertia of the wall. In such a situation the soil can accelerate along with the wall and the load to the foundation differs from the load that would occur if a stationary hydraulic load, with the same peak value, would occur. In order to take into account dynamic phenomena, Oumeraci and Kortenhaus (1994) have introduced a “dynamic load factor” ν_L that multiplied by the peak of hydraulic load to the caisson wall, $F_{dyn,max}$, yields the equivalent stationary load, F_{stat} , to the foundation. This value can be estimated if the foundation is simplified to a system of linear elastic springs. In a mass-spring model isolated caissons dynamics can be represented by a mass, spring model where contributions to mass, stiffness and damping are partially due to rubble foundation, subsoil and seawater. As a rigid body every caisson has 6 degrees of freedom (3 translation and 3 rotations). If the hydraulic load $F(t)$ with peak value $F_{dyn,max}$ is known, the equations of motion can be solved. The outcome is the oscillating horizontal motion $q_1(t)$, the oscillating vertical motion $q_2(t)$ and the oscillating rotation $q_3(t)$. The maximum values of $q_1(t)$, $q_2(t)$ and $q_3(t)$ correspond to the maximum elastic load to the foundation. The dynamic load factor can then be found by calculating the stationary load F_{stat} that yields the same maximum values for q_1 . Then $F_{stat} = F_{stat,equ}$ and ν_L can be calculated.

The concept of equivalent stationary load is based on the assumption of linear elastic response of foundation and no plastic deformation. If the resulting foundation load approaches to the foundation strength, these assumptions are not realistic: the soil stiffness reduces considerably and simultaneously considerable plastic deformation takes place.

Within the PROVERBS Project a number of dynamic models have been developed and implemented based on large-scale model testing (Oumeraci and Kortenhaus,

1994; Oumeraci et al. 1995; Kortenhaus and Oumeraci, 1997a), prototype measurements (Lamberti and Martinelli, 1998a,b) and numerical modelling using more sophisticated FE-Models (Hölscher et al., 1998).

Hydraulic and model testing have shown that wave impact loading induces both oscillatory motions and permanent displacements. This requires the development of models which can predict both kinds of motions. The repetitive wave impact loading, in fact, may lead to degradation and cumulative permanent displacements which induces stepwise failures before the collapse of the structure. In order to better understand such a behaviour, both elastic and plastic models have been applied to reproduce some prototype failures (Oumeraci et al., 1995) which could not be explained by existing standard design formulae and procedures. In this approach the developed plastic models can reproduce the cumulative permanent deformations related to the sliding failure over the rubble foundation as well as to the bearing capacity failure. In fact, the displacement induced by a single impact might be too small for the overall stability, but the cumulative effect resulting from repetitive impacts may yield the collapse of the structure. The elastic models are rather used to predict the dynamic amplifications effects of load transmission into the foundation and to identify the most relevant oscillation modes, including their associated natural periods.

According to Oumeraci et al. (2001), *instantaneous pore pressure* is pore pressure fluctuating during each wave cycle, caused directly by wave-induced fluctuations of the water pressures along the seabed and indirectly by the movements of the structure. Such a mechanism of pore pressure has been investigated by means of large-scale hydraulic model testing (Oumeraci et al., 1994, Kortenhaus, 1996) and an extensive program including theoretical analysis and FEM calculations with non stationary two phase flow (Hölscher et al., 1998). Field measurements at Porto Torres breakwater (Franco et al. 1998) have been analysed by means of stationary flow and FEM-simulations. Extremely high positive and negative pore pressures have been observed in the sandy subsoil during centrifuge modelling (Van der Poel and De Groot, 1997). These results are analysed in detail in Chapter 3.

Instantaneous pore pressure can be generated in rubble foundation as well as in the subsoil. In general, the drainage conditions of foundation depend on the wave load

period (T_W) and on the so-called “characteristic drainage period” of the soil ($T_{CHAR,DRAIN}$). The load duration is equal to T/π for pulsating wave loads and to t_d for wave impacts. According to De Groot et al. (2001), $T_{CHAR,DRAIN}$ is mainly determined by several physical phenomena, depending on the wave and soil characteristics:

1. spatial variation of the pore pressure induced by spatial gradients of water pressures along seabed and boundary of rubble foundation and by spatial variation of flow resistance;
2. inertia of pore fluid and skeleton;
3. elastic storage in the pores through compression and decompression of the pore water;
4. elastic storage in the pores through variation of the pore volume due to isotropic compression and decompression of the skeleton;
5. elastic storage in the pores through fluctuation of the pore volume due to contraction and dilation phenomena induced by the shear stress variations.

The first phenomenon is relevant in most cases and it is a quasi-stationary phenomenon. The others four phenomena are non-stationary and in these cases the expression for $T_{CHAR,DRAIN}$ depends on the prevalent phenomenon, amongst the four, that characterises the boundary conditions. Hence, it will be the largest of the following periods:

$$2. \quad T_{sound} [s] = A/c_p \quad \text{where} \quad c_p [m^2/s] = \text{the smallest value of } c_{p1} \text{ and } c_{p2}$$

$$c_{p1} = \sqrt{\{K_w/n + K + 4/3G\}/(n\rho_w + [1-n]\rho_s)} \quad (27)$$

$$c_{p2} = \sqrt{(K_w/\rho_w)} \quad (28)$$

$$3. \quad T_{ESP} [s] = A^2/c_{vp} \quad \text{where} \quad c_{vp} [m^2/s] = k \cdot K_w / (n \cdot \gamma_w) \quad (29)$$

$$4. \quad T_{ESS} [s] = A^2/c_{vs} \quad \text{where} \quad c_{vs} [m^2/s] = k \cdot (K + 4/3G) \gamma_w \quad (30)$$

$$5. \quad T_{ESD} [s] = A^2/c_{vd} \quad \text{where} \quad c_{vd} [m^2/s] = k \cdot G / (\tan \psi \cdot \gamma_w) \quad (31)$$

$T_{CHAR,DRAIN}$ is defined as T_{sound} if the wave pressure variation through the foundation can be described as a sound wave, which means the rubble/soil-water mixture can be considered as a one-phase material. This condition is met either if both phases move together (“no-drainage”), as occurs with fine-grained material, or if the water phase moves alone, as occurs with very coarse material (“complete drainage”). In the first case the sound propagation velocity can be expressed as c_{p1} (m^2/s), while in the second case it is expressed as c_{p2} (m^2/s). If non-stationary phenomena characterise the boundary conditions, $T_{CHAR,DRAIN}$ will depend on the values of c_{vp} , c_{vs} , c_{vd} , which are the consolidation coefficients for elastic deformation. In the above expressions K_w is the compression modulus of the pore water, K is the compression modulus of the skeleton, G is the shear modulus of the skeleton, k is the permeability, ψ is the dilation angle, n is the porosity, ρ_s is the density of the skeleton, ρ_w is the density of the water and γ_w is the water specific weight. In all the expressions A [m] is the characteristic distance (e.g. drainage distance, layer thickness or depth of rupture surface).

In the rubble foundation, because of the characteristic drainage period is very short compared to the wave period, in many cases a quasi-stationary flow can be assumed. The water pressure along the seaward slope fluctuates during any wave cycle, whereas the water pressures at the harbour side remain nearly constant. The corresponding fluctuating pressure gradients cause a fluctuating pore flow through the rubble foundation and simultaneously fluctuating pore pressure in the rubble foundation. According to the quasi-stationary approach, pressure gradients are assumed to be completely balanced by flow resistance in each phase of the wave cycle and no storage of water occurs in any part of the rubble foundation. Tests on a large-scale vertical breakwater and measurements performed underneath the breakwater in Porto Torres have shown that this stationary approach is reliable for pulsating wave loads during wave crest and wave trough, unless the rubble foundation material is very fine. As previously explained, Goda (1985) assumes a triangular pressure distribution along the bottom and hydrostatic distribution in vertical direction. However there are several phenomena that may cause deviations from this distribution:

- effects of locally varying grainsizes;

- non-flat top of the rubble foundation leaving space locally underneath the caisson bottom;
- flow concentrations around the corners and lower horizontal gradients at lower levels;
- phenomena of turbulence around the corners;
- effects induced by the apron slabs if they are placed directly adjacent to the wall and do not have large holes in it.

Consequently, often the pore pressure distribution along the base of the caisson deviates from triangular distribution (see Figure 2.13).

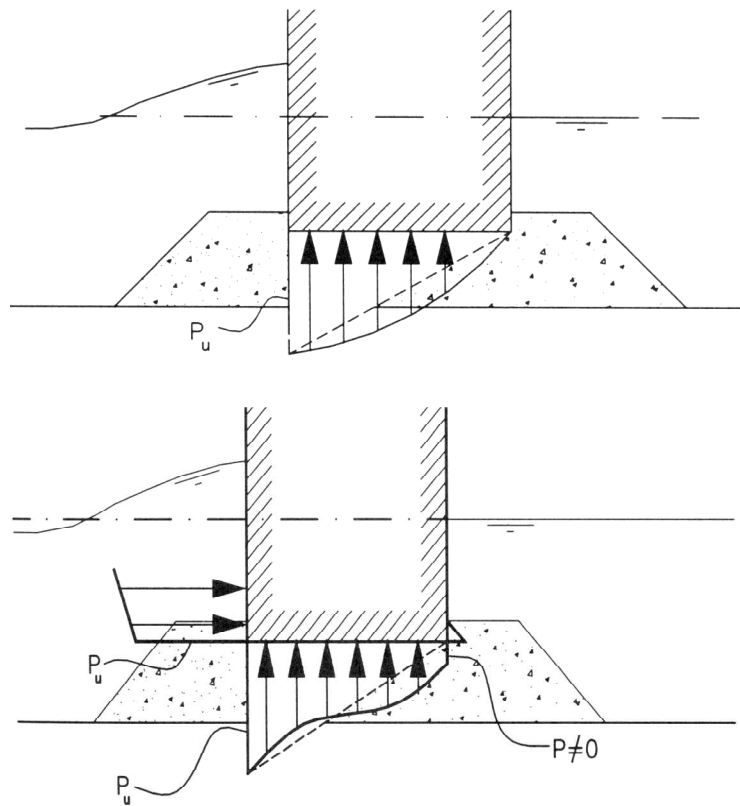


Figure 2.13 – Examples of non-linear pore pressure distribution

If the characteristic drainage period is larger than the duration of the wave load, the effects of non-stationary flow in the rubble foundation can be significant during wave impacts. Analyses and performed tests have shown that the non-stationary effects induced directly by water pressure variation at the sea side may enlarge the uplift force with up to 30% compared to the value found with stationary flow. Such effects are the largest if the impact has a very short duration, if the width of the wall is large, if the gas content in the pore water is also large and if fine grains are used for the rubble foundation. The indirect effect of non-stationary flow, due to the movements of the structure, is the reduction of pore pressures when the wall is suddenly lifted up and water is forced to flow into the additional room. In this case, the same above mentioned tests have shown that the effect is the largest if the impact has a very short duration, if the width of the wall is large, if the stiffness of the skeleton is limited and if fine grains are used for the rubble foundation. Then, more than 30% reduction of the uplift force can be found at the moment of maximum impact load.

The flow in the subsoil usually has a different character from that in the rubble foundation. In this case, in fact, $T_{CHAR,DRAIN}$ is often larger than the wave period due to the lower permeability, at least for the larger values of the characteristic distance drainage A . Hence, at great depth undrained conditions may occur. In this region the pore pressure fluctuations and the effective stress fluctuations are mainly determined by the total stress fluctuations at the boundary. Here, the instantaneous flow velocities of the pore water may be neglected and the approximation to one-phase material is justified to find the total stress distribution. The total stress fluctuations are caused by the wave passing over the seabed and the wave induced moment transferred from the wall via rubble foundation to the subsoil. These fluctuations can be found from stationary calculations with a homogeneous elastic medium. Such calculations yield two relevant results: the fluctuations of the mean total stress and the fluctuations of the shear stress. Both fluctuations are very strong with high wave attack, especially underneath both edges of the structure. The fluctuations of the isotropic total stress are partly distributed to the skeleton and partly to the water, depending on the ratio of the stiffnesses. If the pore water would not contain any gas, the pore pressure fluctuations would be practically equal to the vertical variations.

The mean total stress variations can be calculated as a function of the vertical total stress variations at the upper boundary of the subsoil. A first approximation can be found assuming the vertical total stress at the boundary varying like a sinus with wave length L . The vertical total stresses at a certain depth have the same behaviour, with an amplitude reduced according to a negative exponential function with a characteristic length $L/2\pi$. The mean stress variations cause compression or decompression of the soil inducing an increase or decrease of the mean effective stress and the pore pressure proportional to the respective stiffness: K and K_w/n . The wave load to a caisson causes a moment M , which the caisson transfers via the bedding layer to the subsoil. This moment causes an increase in the vertical stress underneath one edge of the caisson and a decrease under the other edge. The vertical total stress variations directly underneath the caisson bottom, $\Delta\sigma_v(x,0)$, are assumed to vary linearly over the caisson width, B_c , as in the following equation:

$$\Delta\sigma_v(\text{edges},0) = \pm \frac{M}{B_c^2/6} \quad (32)$$

The vertical stress variations reduce with depth as the moment transferred from higher layers to lower soil layers. The reduction with depth will be according to a negative exponential function:

$$\Delta\sigma_v(\text{edges},z) = \pm \frac{M}{B_c^2/6} \frac{1}{\exp(z\pi/B_c)} \quad (33)$$

If the horizontal total stress variation is assumed smaller than the vertical one, the mean total stress variations will be also smaller, e.g.:

$$\Delta\sigma(\text{total},z) = (\Delta\sigma_v + \Delta\sigma_{hx} + \Delta\sigma_{hy})/3 \approx 0.75\Delta\sigma_v(z) \quad (34)$$

These mean total stress variations are partly met by pore pressure variations and partly by the skeleton, depending on the ratio of the stiffnesses of pore water (K_w/n) and skeleton (K). This yields to the following equation:

$$u(\text{edges}, z) = 0.75 \frac{K_w}{K_w + nK} \Delta\sigma_v(z) = \pm 0.75 \frac{K_w}{K_w + nK} \frac{M}{B_c^2 / 6} \frac{1}{\exp(z\pi / B_c)} \quad (35)$$

A triangular region with its top at the edge of the caisson bottom is assumed in between the region right underneath the caisson and the regions adjacent to the caisson. Seaward of this region in front of the breakwater high total stresses are present at wave crest due to the wave load. A linear variation of the pore pressure in this region is assumed. An example for the case of highly incompressible pore water, $K_w/(K_w+nK) \approx 1$, is presented for wave crest in the scheme of Figure 2.14. Wave parameters, structure geometry and soil characteristics are reported in Tables 2.2 and 2.3. The meaning of the symbols in Table 2.2 has been explained in Section 2.2.

WAVE PARAMETERS	H _{1/3} (m)		H _{max} (m)		T _{1/3} (s)
	5.8		8.0		11.4
STRUCTURE GEOMETRY	B _c (m)	h (m)	h' (m)	d (m)	h _c (m)
	17.5	10.1	7.1	5.6	3.4
FORCES AND MOMENTS	F _h (kPa·m)	F _u (kPa·m)	M _h (kN/m·m)	M _u (kN/m·m)	
	1527	606	16067	7065	

Table 2.2 – Wave parameters, structure geometry and acting forces and moments

SANDY SOIL		
K	m/s	10^{-4}
K_w	MPa	1000
$K+4/3G$	MPa	100
N	(%)	40
ψ	(°)	10
$c_{vp} = k \cdot K_w / (n \cdot \gamma_w)$	m ² /s	25.00
$c_{vs} = k \cdot (K+4/3G) / \gamma_w$	m ² /s	1.00
$c_{vd} = k \cdot G / (\tan \psi \cdot \gamma_w)$	m ² /s	6.81
$T_{CHAR DRAIN} = T_{ess}$	Seconds	

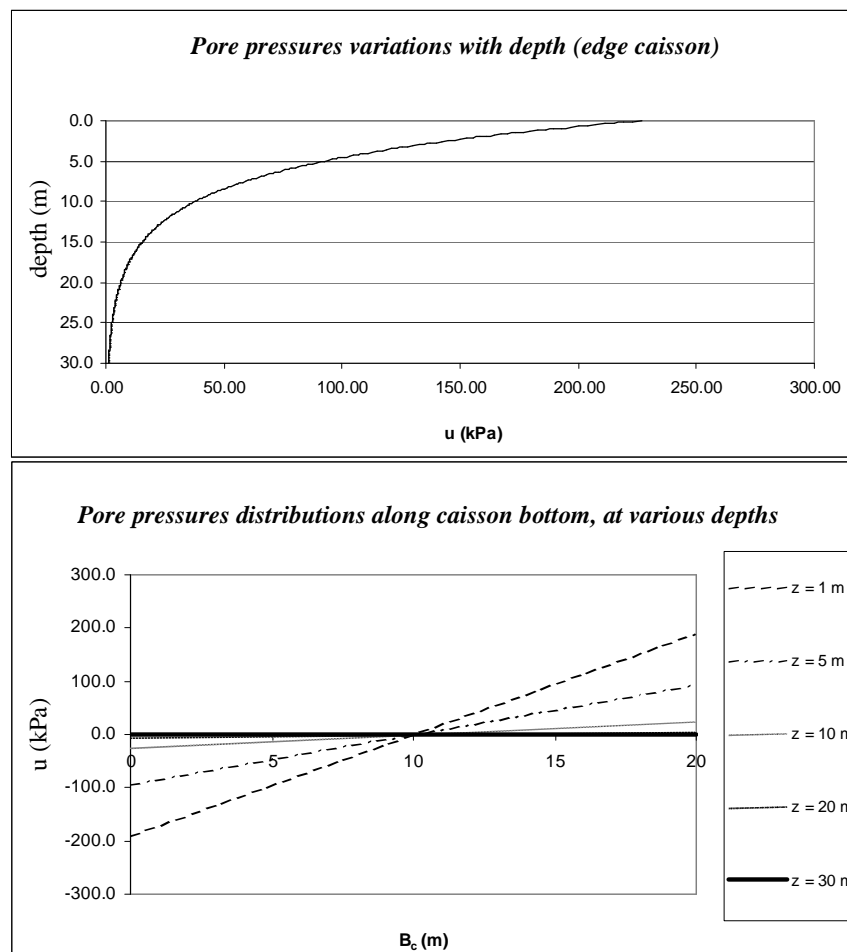
Table 2.3 – Soil characteristics and $T_{CHAR DRAIN}$ 

Figure 2.14 – Pore pressures due to mean total stress variations

The shear stress variations may cause both increasing or decreasing of instantaneous pore pressures in the subsoil. During continuous shearing of drained sand or silt usually first some contraction occurs then dilation. In undrained conditions that dilation causes negative pore pressure. Assuming a shear stress due to the wave load equal to:

$$\tau(z) \approx \frac{F_h}{B_c \cdot \exp(z\pi / B_c)} \quad (36)$$

the following negative excess pore pressure u is found:

$$u = - \frac{F_h}{B_c \exp(z\pi / B_c)} \frac{\tan \psi}{G \left(\frac{1}{K + \frac{4}{3}G} + \frac{n}{K_w} \right)} \quad (37)$$

The pore pressure reduction continues as long as shearing continues until the end of the dilation or until the absolute pore pressure is zero.

The mechanism of instantaneous pore pressures has been clearly observed during the centrifuge tests performed at GeoDelft and it will be studied in Chapter 3.

A prediction of instantaneous pore pressures in sandy or silty soils is rather complicated and affected by several uncertainties. Introduction of these pore pressures, highly varying along any potential rupture surface, is very complicated as well.

Development of *residual pore pressures* is strictly related to the cyclic loading of clay, silt and sand, causing a change of the effective shear strength and a reduction in the stiffness. In undrained conditions, if sandy or silty soils are loaded by varying shear stress induced by wave action, varying excess pore pressures are observed, caused by an elastic volume change of the skeleton. Shear stress variation may also

induce a non-elastic change in the structure of the skeleton, usually a volume decrease and hence a residual increase in excess pore pressure after unloading. This increase adds to the increase from previous shear stress variations if these excess pore pressures have not dissipated by drainage. This means that the duration of the cyclic load history is shorter than the drainage capacity of the soil. The gradual accumulation of pore water pressure resulting from the sum of instantaneous and residual pore pressures, if positive, will cause a reduction in the effective shear stresses in the soil with consequent reduction in shear strength and stiffness. The degradation effect will depend on the magnitude and number of stress reversals (wave load history) and on the drainage conditions as well (soil permeability, compressibility and drainage distance). The shear strength is further dependent on whether the soil is contractive or dilative during the shearing under the extreme loads and whether this shearing takes place under drained, partly drained or undrained conditions. If the soil is dilative and saturated and loaded in undrained conditions, a negative pore pressure will develop that will result in a higher shear strength than for drained conditions.

When the pore pressure dissipates, sandy soils experience drainage during a storm, depending on the permeability and on the drainage conditions. Laboratory tests and monitoring experiences of a real vertical caisson breakwater (see Annex II) have shown that the soil structure and the resistance to further pore pressure generation may be significantly altered when the excess pore pressure due to cyclic loading dissipates (Bjerrum, 1973; Andersen et al., 1976; Smits and al., 1978). Cycling loading with subsequent pore pressure dissipation is referred to as “precycling”. The beneficial effect of precycling phenomena occurred during smaller storms prior to the biggest storms has been observed for vertical caisson breakwater of Civitavecchia (Grisolia and Maccarini, 2004).

Clays will be undrained during a storm and also during several storms. Several experiences have shown that normally consolidated and slightly overconsolidated clays will benefit from precycling.

Significant residual pore pressures may usually occur if layers of fine, loose or medium dense sand, interrupted by silt or clayey layers, are present underneath the wall bottom. If a homogeneous sandy layer characterises the soil foundation, hardly

residual pore pressures are observed. This is clearly observed during the centrifuge tests performed at GeoDelft and discussed in Chapter 3.

Andersen (1976) developed a method to determine the residual pore pressure accumulation caused by cyclic loading. The method is based on the use of pore pressure contour diagrams. The diagrams should be site specific, but relevant test data from a developed Database (Norwegian Geotechnical Institute, 1998) may be used.

The last phenomenon considered relevant in the structure-foundation interaction in the PROVERBS Projects regards the *instability* of the structure.

When the stability analysis of a vertical breakwater is performed the equilibrium of the structure is given by the equilibrium of three elements: the wall, the part of the rubble skeleton above/to the harbour side of the rupture surface and the part of the subsoil within the rupture surface. The equilibrium follows if all the volume forces acting on these three elements are taken into account and all the surface forces acting along the boundaries of the three elements. It is often very practical to consider the equilibrium of the wall separately from the equilibrium of the soil (part of the skeleton of the rubble foundation and part of the subsoil). This means that the force acting from the wall to the skeleton of the rubble foundation must be found as resultant from the other forces acting on the wall. These forces are the weight F_g (reduced for the buoyancy), the horizontal excess water force along the front wall F_h and the vertical uplift force from the excess pore pressures in the rubble foundation F_u . Taking into account the eccentricity of the weight e_c and the level arms l_{Fh} and l_{Fu} , the resultant force acting on the skeleton of the rubble foundation can be expressed with three parameters: the horizontal component F_h , the vertical component $(F_g - F_u)$ and the distance of this force component to the harbour side edge, $B_z/2$. The value of B_z follows from the following equation:

$$B_z = 2 \frac{F_g \left(\frac{1}{2} B_c + e_c \right) - F_h l_{Fh} - F_u l_{Fu}}{F_g - F_u} \quad (38)$$

The resulting horizontal seepage force in the rubble foundation, F_{hu} , can be found with the assumptions of triangular pressure distribution in horizontal direction and hydrostatic distribution in vertical direction. This yields to the following expressions:

$$F_{hu} = \frac{h_r(2B_z - h_r / \tan \theta)}{2B_c} p_u \quad \text{for } B_z \geq h_r / \tan \theta \quad (39)$$

$$F_{hu} = \frac{B_z^2 \tan \theta}{2B_c} p_u \quad \text{for } B_z \leq h_r / \tan \theta \quad (40)$$

where θ is the angle between the bottom of the wall and the rupture surface.

A schematisation of the soil load is reported in Figure 2.15.

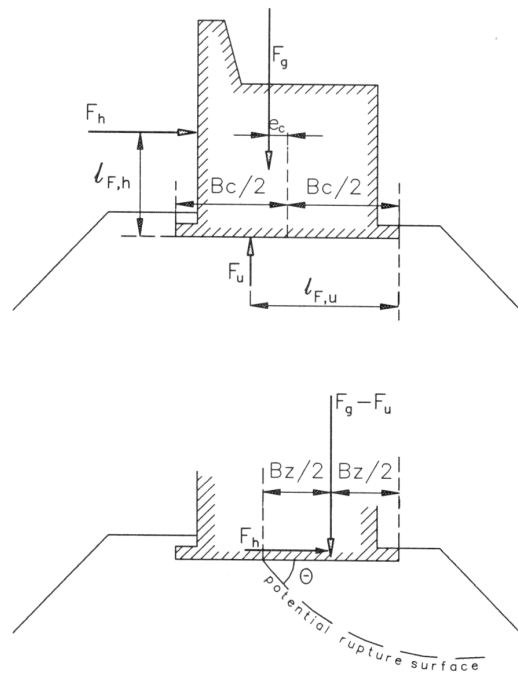


Figure 2.15 – Schematisation of soil load

For a good analysis different sub modes of failure, during wave crest, should be considered (see Figure 2.16):

- a) sliding of the wall over the foundation;
- b) rotation failure;
- c) rupture surface through rubble only;
- d) rupture surface through rubble and along top of subsoil;
- e) rupture surface through rubble and subsoil.

All the failure modes, excepted the first one, are bearing capacity failures.

Within the PROVERBS Project limit state functions (g_a , g_b , g_c , g_d and g_e) for these kinds of failures have been developed. The equation $g = 0$ describes the critical condition. The functions g_b and g_e are derived from Brinch Hansen (1968).

For seaward failure the same equations and approximations of the harbour-side failure can be used.

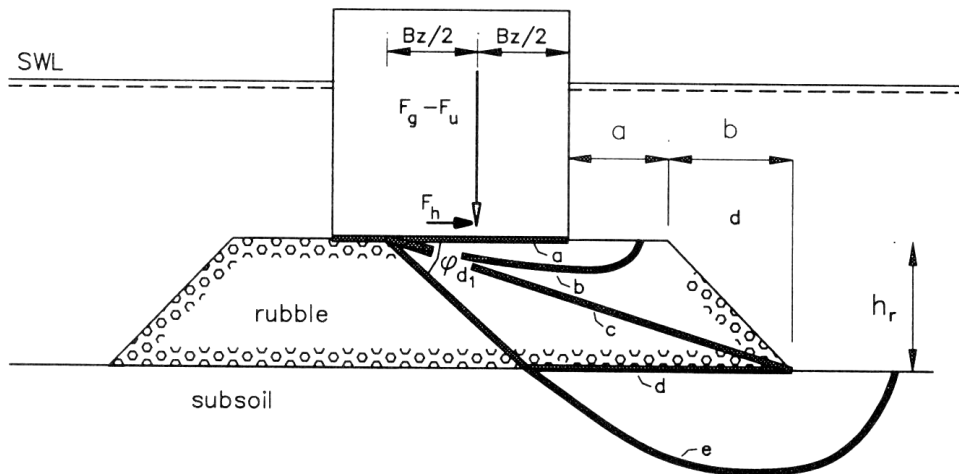


Figure 2.16 – Main failure sub-modes for which state limit equations are available

The described limited state equations, however, have many limitations: limited number of rupture surfaces, prescribed shape of these surfaces, not consideration of dilation effect. Numerical models constitute a valid alternative. One of the most common types of numerical models is that for slip circle analysis according to Bishop. They can be applied to vertical breakwaters and present several advantages as the possibility to represent complicated layering, to model complicated pore pressure distributions, to perform many calculations in a short time. On the other hand, only circular rupture surfaces can be schematised and also in this case the positive effect of dilation cannot be taken into account.

Some finite element codes also allow for the modelling of the pore flow or introduction of the pore pressure distribution. An important part of modelling regards the constitutive model of the soil that should be very sophisticated. This aspect will be discussed in Chapter 3.

2.3.4 Possibilities for design improvements

Within the PROVERBS Project several possibilities in the improvement of the design of vertical caisson breakwaters have been also analysed. They regard the variation of design parameters if rubble foundation is present or if the caissons are directly placed on sandy or clayey subsoils. Variations of the geometry and the mass of the wall in order to increase the bearing capacity of the structure have been taken into account. Soil replacement and soil improvement have been also considered if too soft clay or silty sand are present, with the risk of the generation of considerable residual pore pressures. Densification of the sand is often needed to avoid considerable settlements after construction caused by the wave-induced cyclic loading and to avoid the risk of too high residual pore pressures during extreme cyclic loading. Several soil improvement techniques (mixing with cement, stone columns, etc.) could be considered as well.

2.3.5 General conclusions

In this Section an overview of the foundation aspects of vertical caisson breakwaters has been presented. An important reference point has been the PROVERBS Project,

in which new knowledge and considerable improvements have been achieved with respect to the mechanisms responsible for geotechnical failures. However, several uncertainties still characterise the design of these structures and further research is needed. This regards, amongst several other things, the development of more advanced dynamic models, the achievement of a good prediction of the effect of extreme wave impact loading, the introduction in the design procedure of models for instantaneous pore pressures, the extension of the developed tools to the three-dimensional effects.

2.4 Structural aspects

2.4.1 Types of reinforced concrete caissons

Beside the hydraulic and the soil mechanic aspects, the coastal engineering has also to consider the structural design aspects of a vertical caisson breakwater.

Amongst the generic types of (reinforced) concrete caissons, *planar rectangular multi-celled caisson* constitutes one of the more common shapes for a vertical breakwater. A typical structural arrangement is illustrated in Figure 2.17. This form of caisson typically comprises 8 different types of load-bearing elements: 1) the front wall; 2) the rear wall; 3) the side walls; 4) the internal walls; 5) the base slab; 6) the top slab; 7) the crown wall; 8) the shear keys (not always present). The planar front wall in this class of structure reflects the incident wave. Figure 2.18 represents *perforated rectangular multi-celled caissons*. Their main peculiarity is to create a more still sea state in front of the structure, due to reduced reflections. The relative area of the perforations with respect to the total front area typically lies in the range 25 to 40%.

Circular-fronted caissons represent an interesting alternative design that do not require such large wall thickness as rectangular caissons because the external wave pressure is transmitted to the foundation by in-plane compression rather than flexure.

The general tendency in these last years is to adopt hybrid caisson forms to realise breakwater optimising the design solution. On the other hand, different aspects influence the selection of a suitable caisson type for a breakwater. Geomechanical

and hydraulic conditions will typically dictate the overall dimensions and geometric form of the structure. For example, the frictional resistance which can be mobilised at the foundation-base interface (to prevent rigid body sliding) will control the width of the base slab, the height of the structure will be influenced by the tidal range and the maximum wave height to be resisted without over-topping. Geomechanical and hydraulic factors are also significant.

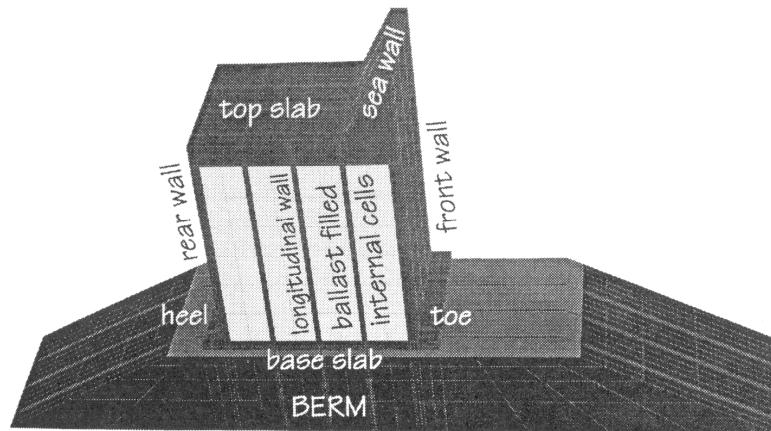


Figure 2.17 – Example of isometric view of one-half of a caisson

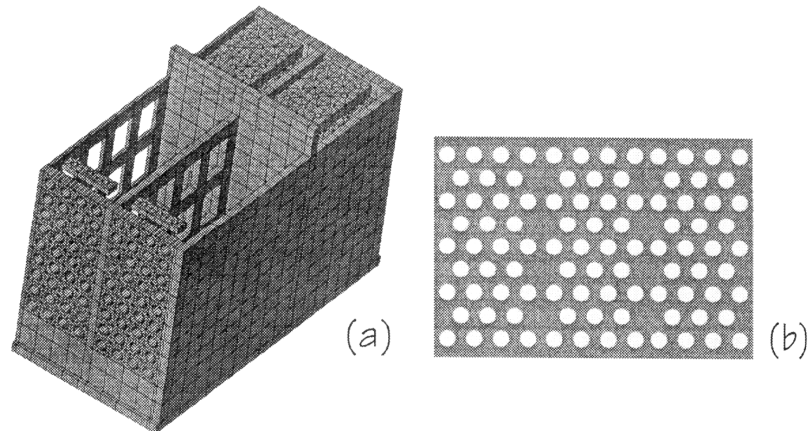


Figure 2.18 – a) Part of a perforated rectangular caisson; b) Typical perforation arrangement

2.4.2 Geomechanical and hydraulic aspects relevant to the structural response

Several *geotechnical* aspects have to be taken into account by structural engineers. These regard, for instance, the characteristics of the granular fill in the cells to calculate the internal earth pressure on the caisson walls or the elasto-plastic properties of the foundation that influence the structural dimensions and dynamic response of the front wall.

The horizontal pressure due to the granular fill in the cell is calculated as a upper limit, using the coefficient of earth pressure at rest, with the following equation:

$$\sigma_h = 0.6\rho_s \cdot g \cdot z \quad (41)$$

where ρ_s is the soil density (saturated soil density if no drainage is present in the cell), g is the gravity acceleration and z is the height of the fill.

As concerns the characteristics of rubble foundation and subsoil, actually a complete analysis of the dynamic soil-structure-fluid interaction would necessitate inclusion of a realistic elasto-plastic constitutive model for soil, able to simulate sliding and loss of contact at the caisson base-foundation interface and the transport of pore fluid within the soil skeleton. Such a detailed analysis is not normally done and a simplified approach attempts to choose reasonable values shear moduli and Poisson's ratios to enable isotropic, linear elastic soil models to be used (Wolf, 1994). Although these elastic constants are difficult to estimate, the following relationship is usually assumed for the rubble mound shear modulus:

$$G \approx G_0 \sqrt{\sigma'_v / 0.1} \text{ MPa} \quad (42)$$

where G_0 lies in the range 20-100 MPa and σ'_v in the effective vertical stress.

From an *hydraulic* point of view, in order to design the wall thickness and percentage of reinforcement required for the front face of a concrete caisson, a realistic assessment is necessary of the distribution, magnitude and duration of the pressure loading resulting from a wave impact associated with a particular return period. In the Section 2.2 the state of the art as far as wave pressures on vertical breakwaters has been described. In a preliminary analysis, the horizontal pressure should be assumed to act along the entire length of one caisson, assuming a normal wave attack on the front face. Using Goda's formulae, p_1 , p_3 and p_4 characterise the pressure intensities at the mean water level, base of the caisson and top, respectively. In the case of very short duration impact, the pressure distribution does not appear linear over the height as the peak intensity is localised over a small region. The magnitudes of pressures may be estimated from the formulae (7), (8), and (9) described in Section 2.2. Finally, another important hydraulic aspect should be considered by structural engineers regarding the overpressure on top slab and superstructure resulting from overtopping and water slamming down onto the upper surface.

2.4.3 *Loads acting on the caisson*

The main loading during the in-service life are the *permanent loads* resulting from the dead weight of the structure and the superstructure as well as the horizontal soil pressure from the fill inside the cells and from the foundation reaction; *variable loads* arising from changes in the water level, from pulsating and impact loads and overtopping wave loads as well as the harbour traffic loads; *accidental loads* resulting from vessel impacts during mooring and falling masses during cargo loading/unloading operations.

2.4.4 *Failure structural modes*

One of the most critical loading conditions to which a caisson is subjected concerns the phases of transportation and placing of the caisson itself. The act of floating and towing the caisson introduces a different set of forces on the structure. This can induce, during the pre-service state, an uncontrolled sinkage during transport, cracking or collapse of bottom slab or walls during floating stage, collapse of bottom

slab due to placement on an uneven bottom. Pre-service loading cases and failure modes might in some circumstances be even more relevant than those under in service conditions. Consequently, detailed design calculations have to take account of such pre-service limit states. This has been achieved for the first time in PROVERBS Project, within a full probabilistic framework.

Once in service, the failure of concrete caisson breakwaters may be the result of both large-scale rigid body translation of the structure (due to global sliding at the base-foundation interface or rotational collapse of the foundation) and local rupture in the structural elements. The progressive loss in structural integrity may start by chloride ingress in the splash zone of the face of the breakwater. Continued corrosion can result in a loss of bond, reduction in steel cross-sectional area and weakening of anchorage. All these mechanisms can further weaken the reinforced concrete cross-section and the wall may rupture under repeated storm loading. A regular programme of inspection, diagnosis and repair may prevent such a progressive deterioration. For the prediction of concrete degradation limit state equations have been formulated to describe chloride penetration/corrosion and cracking during pre-service and in-service conditions. This will not only help to predict possible local structural failures, but also to set up a proper strategy for monitoring, inspection and maintenance. On the other hand, local damage to the sea wall will not immediately lead to a critical failure situation and in many cases the structure may go on to provide years of active service before a collapse state is approached.

Before individual structural elements are designed, the load paths must be identified and the basic global structure action understood. Hence, particularly important is the analysis of the role of each structural member of a multi-celled caisson in order to understand the transmission of the wave forces through all these members to the foundation. These enables to use simple structural models based on the behaviour of the individual members for preliminary design and to have a first idea on the load transmission and structural behaviour before using more sophisticated FE-models for full 3D dynamic analysis. The latter demands significant computer resources and, for this reason, simplified approaches based on the assumed behaviour of individual elements are still used in the preliminary design stage.

2.4.5 Design codes

At present no single code of practice exists which explicitly covers the complete design of the reinforced concrete elements forming a caisson breakwater. Conversely, a few codes have been developed for the design of marine structures and designers are therefore forced to gather information from a variety of sources.

The following five codes constitute the more relevant codes for the European coastal engineers:

- 1) ACI 318-5 Building Code Requirements for Structural Concrete, USA
- 2) CEB-FIP 1978 *Model Code for Concrete Structures*, Comite Euro-International du Beton;
- 3) EC1 Part 1 and EC2 Parts 1 and 2 *ENV 1991, Eurocode 1, Basis of Design and Action on Structures, Part 1 Basis of Design* and *ENV 1992 Eurocode 2, Design of Concrete Structures, Part 1-1 General Rules and Rules for Buildings*, European Standardisation Committee;
- 4) BS 6349 Parts 1,2 and 7 *British Standard Code of Practice for Maritime Structure*, UK;
- 5) ROM 0.2 90 *Maritime Works Recommendations: Actions in the Design of Maritime and Harbour Works*, Ministerio de Obras Publicas, Spain.

The first three codes focus on the material and resistance parameters and offer a strategy for safely designing simplified structural components. Each code specifies different load factors, which should be used to multiply the various characteristic load intensities in order to finally arrive at the design load. None of these first three codes provide information on how to calculate the magnitude and duration of wave loads acting on a vertical breakwater.

The last two codes give very general guidance on the planning and design of maritime structures, without specific reference to the design of reinforced concrete sections or structural modelling techniques. Also in this case there is not any advice on the determination of the characteristic and design wave load.

2.5 Probabilistic aspects

From the previous sections it is evident the complexity of the problems related to breakwater stability and design and the importance of the stochastic nature of the processes involved in the wave-structure-foundation interactions, as well as the large number of possible failure mechanisms and their complex interaction. This necessarily prescribed the use of probability-based analysis methods as the more correct alternative for the design.

The most important difference of probabilistic design compared to the deterministic design is that with probabilistic design it is possible explicitly to take account of different uncertainties involved in the behaviour of the considered structure. Doubts are related to the natural boundary conditions, to the scarcity of information of the natural environment, to the quality of the structure and so on.

As described in the PROVERBS Project, in the Task of Probabilistic Aspects, the first step in a reliability analysis of any structure is defining its functions and define the ways in which failure modes of the structure can occur. In a deterministic approach the limit state equation is used to model functioning or failure of the structure. Several uncertainties are generally related to the input of the limit state equation (Vrijling and van Gelder, 1998).

With regard to vertical breakwaters, there are several ways in which a breakwater might fail to fulfil this main function, essentially related to the action of wave energy. For all limit states except wave transmission, the loading is given by the wave forces exerted at the breakwater. Within PROVERBS Project, extensive research has been directed to this aspect of breakwater design. The models used can be categorised in three types:

1. Load models describing quasi-static (pulsating) wave forces;
2. Load models describing dynamic (impact) wave forces;
3. Decision models, indicating what type of load model should be applied.

In reality, the input to these models (water levels, wave properties) is of random nature. A general vertical breakwater will therefore experience quasi-static loads as

well as impact loads during its lifetime. The distribution function of all the wave forces exerted at the breakwater is written as:

$$P(F < f) = P_{impact} \cdot P(F < f | impact) + (1 - P_{impact}) \cdot P(F < f | noimpact) \quad (43)$$

where:

- F is the wave force modelled as a stochastic variable;
- P_{impact} is the probability of occurrence of impacts;
- $P(F < f | impact)$ is the distribution function of impacts loads, conditional on the occurrence of impacts;
- $P(F < f | no impact)$ is the distribution function of pulsating wave forces, conditional on the occurrence of quasi-static loads, e.g. obtained by the model of Goda (1985).

Geotechnical failure modes have been also taken into account in the probabilistic design approach. Limit state equations for preliminary design are adopted as the standard form of modelling the foundation. Next to the stress level, the strength of the foundation is primarily decided by the properties of the soil (friction angle and cohesion, e.g.). An overview of the input for the soil models as well as the uncertainties related to the soil properties are presented. Furthermore, a comparison with other levels of modelling is discussed.

Like the modelling of foundation, also the structural limit states of vertical breakwaters can be defined on different levels of sophistication.

Within the framework of PROVERBS Project, probabilistic tools, prediction models and associated methods to quantify the uncertainties involved in the models and input parameters have been developed. Furthermore, a partial safety factor system (PSFS) has been developed on the basis of a full probabilistic approach.

Nevertheless, there are still several topics for further research. They regard, for instance, the extension of the probabilistic approach to include local morphologic changes, to develop a procedure to obtain the probability of repair/maintenance as a

function of service time, to extend the reliability tools not only to the design phase but also to other life cycles of the breakwater (construction phase, operation phase, and so on.).

On this basis, a more important goal could be achieved: the probabilistic risk analysis.

Chapter 3

Mechanical behaviour of cohesionless soils: experimental observations and constitutive modelling

3.1 Introduction

The mechanical behaviour of cohesionless soils depends mainly on their granular structure and their relative density. Experimental observations show that loose sands, monotonically or cyclically loaded, have a different response of dense sands, in like manner loaded. If the sands are fully saturated, their behaviour will be strongly influenced by the drainage conditions. In drained conditions the deviator stress will induce a volume variation ($\Delta V \neq 0$), while in undrained conditions volumetric strains are not allowed ($\Delta V = 0$) and the tendency to contract or dilate will result in pore pressure variations. Contractive and dilative properties of the granular materials, characterising the nature of the irreversible volume variations, have significant importance in the mechanical response of the material, especially in undrained conditions.

The wave action on the sand foundation generates shear stresses and strains that are cyclic in nature. In undrained conditions the wave-induced cyclic action may induce phenomena of *liquefaction* and *cyclic mobility* of sandy soils.

Liquefaction and cyclic mobility have been subject of a continuing discussion within the geotechnical engineering, commonly associated to ground failures due to the earthquakes. Because both phenomena induce increase of pore pressure and large strains, they are often confused. Although several researchers have argued that these phenomena should be carefully distinguished, liquefaction is still commonly used to describe all failure mechanisms resulting from the build-up of pore pressures during undrained cyclic shear of saturated soils. So, even though some important failures are commonly related to liquefaction, they should be ascribed more correctly to cyclic mobility, which results in limited soil deformations without liquid-like flow.

Castro (1969) and Castro and Poulos (1977) clearly distinguished the two phenomena, as follows:

“Liquefaction is a phenomenon wherein a saturated sand loses a large percentage of its shear resistance (due to monotonic or cyclic loading) and flows in a manner as a liquid until the shear stresses are as low as its reduced shear resistance”.

“Cyclic mobility is associated to cyclic shear of dilative soils that does not result in flow failure as in liquefaction phenomena, because the shear strength remains greater than the static shear stress and deformations accumulate only during cyclic loading”.

After Castro, French researchers (Schlosser, 1985; Blondeau, 1986; Canou, 1987; Canou, 1989) carried out important studies on static liquefaction phenomena, in order to give a reason of the failure in the Port of Nice in 1979.

Sladen et al. (1985) defined liquefaction as *“a phenomenon wherein a mass of soil loses a large percentage of its shear resistance, when subjected to monotonic, cyclic, or shock loading, and flows in a manner resembling a liquid until the shear stresses acting on the mass are as so low as the reduced shear resistance”.*

Phenomena of liquefaction, induced by seismic action, are particularly common in Japan, where the study of static liquefaction was started relatively recently, with the thesis of Verdugo (1992).

Casagrande in 1969 defined cyclic mobility as the *“progressive softening of a saturated sand specimen when subjected to cyclic loading at constant water content”.*

Liquefaction results from the tendency of the soils to decrease in volume when subjected to shearing stresses. When loose, saturated soils are sheared, the soil grains tend to rearrange into a more dense packing and the water in the pore spaces is forced out. If drainage of pore water is impeded, pore water pressure increases progressively with the shear load. This leads to the transfer of stress from the soils skeleton to the pore water inducing a decrease in effective stress and shear resistance of the soil. If the shear resistance of the soil becomes less than the static shear stress, the soil can experience large deformation and is said to liquefy. So, for a liquefaction flow failure to occur, a saturated soil with a tendency to contract (loose sand) must

undergo undrained shear of sufficient magnitude or sufficient number of cycles for the shear resistance to become lower than the static load.

For dense, saturated sands sheared without pore water drainage, the tendency for dilation or volume increase results in a decrease in pore water pressure and an increase in the effective stress and shear strength. For cycles of small shear strains under undrained conditions, excess pore pressure may be generated in each load cycle leading to softening and inducing the accumulation of deformations. At larger strains the tendency to dilate relieves the excess pore pressure resulting in an increased shear resistance. This property of dense sand to progressively soften is the cyclic mobility defined by Castro and Poulos (1977).

Although the different phenomena can be clearly observed in laboratory, at present, no definition or classification system appears to be entirely satisfactory for all possible failure mechanisms in situ. The National Research Council's Committee on Earthquake Engineering includes in the soil liquefaction "*all phenomena giving rise to a loss of shearing resistance or the development of excessive strains as a result of transient or repeated disturbance of saturated cohesionless soils*".

To better understand these complex phenomena, a review of some basic concepts of cohesionless behaviour is required.

In this Chapter, the different behaviour of loose and dense sand, in drained and undrained conditions, under monotonic and cyclic loading is described. The experimental results available in literature are analysed.

Finally, the constitutive modelling is briefly discussed. After a general introduction of the available constitutive models describing the behaviour of sands under monotonic and cyclic loading, the "generalised plasticity model" for sand is presented (Pastor et al. 1990). Such a model has been studied in order to start its implementation in a finite element code and to perform numerical analyses simulating the experimental behaviour observed during some centrifuge tests, which will be discussed in the next Chapter. At present, the model has been implemented and only a few simplified tests, useful to verify the correct implementation, have been performed. The numerical study, not reported in this thesis, has just been started and it is still at the beginning.

3.2 Experimental observations

3.2.1 Monotonic loading: drained conditions

In 1935 A. Casagrande, in his studies on shear strength of soils, developed the concept of the “critical void ratio”. He observed that during shear deformation, at the same confining pressure, the volume decreasing of a sand in loose state and the volume increasing in the dense state would tend to produce the same “critical density” or “critical void ratio (e_c)”. At that point, which could be reached from either loose or dense state, a “cohesionless soil can undergo any amount of deformation or actual flow without volume change”.

In order to develop a method to measure the critical void ratio of sands, in 1936 Casagrande performed a series of drained, strain-controlled triaxial tests, drawing the following conclusions (see Figure 3.1):

- all specimens tested at the same confining pressure approach the same density when sheared to large strains and continued to shear with constant shearing resistance;
- loose sand specimens show a volume reduction throughout the test, reducing the initial void ratio until reaching the critical value e_c , where residual conditions take place and plastic flow arises at constant volume. Only a small increase in volume occurs at large strains toward the end of the test;
- dense specimens show a small volume decrease at the start of the test (reaching a minimum void ratio), but as the peak compressive stress is approached they strongly dilate and the volume increase continues to the end of the test;
- stress-strain curve for dense sand develops a definite peak, after which a shear failure plane is observed, and with the increasing in strain a steady decreasing in resistance takes place approaching the strength of the loose specimen (*softening behaviour*);
- stress-strain curve for loose sand does not develop a peak and the residual conditions are reached according to an *hardening behaviour*.

By performing tests at different effective confining pressures, Casagrande found that the critical void ratio was uniquely related to the effective confining pressure (decreasing with it) and called the locus the *critical void ratio line (CVR)*.

Therefore a critical state exists for sands and the *CVR* line constitutes the boundary between dilative and contractive behaviour in drained triaxial compression. A soil in a state above the *CVR* line exhibits contractive behaviour and vice versa (see Figure 3.2).

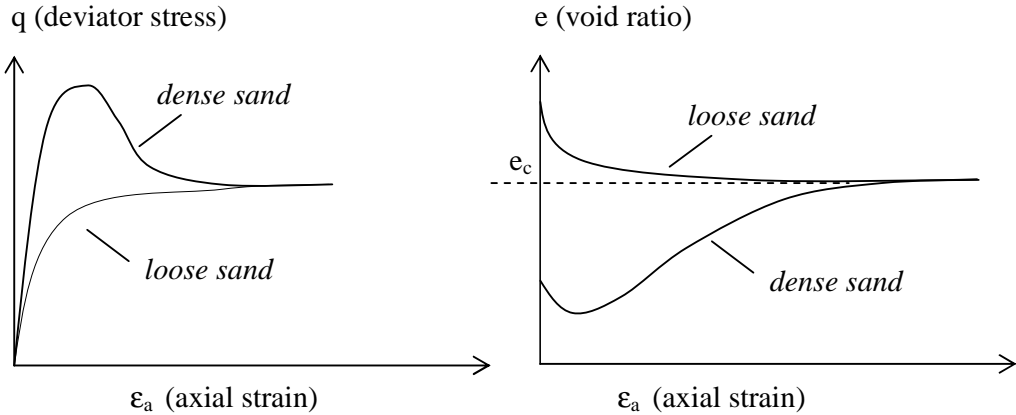


Figure 3.1 – Behaviour of dense and loose soils in monotonic strain – controlled triaxial tests

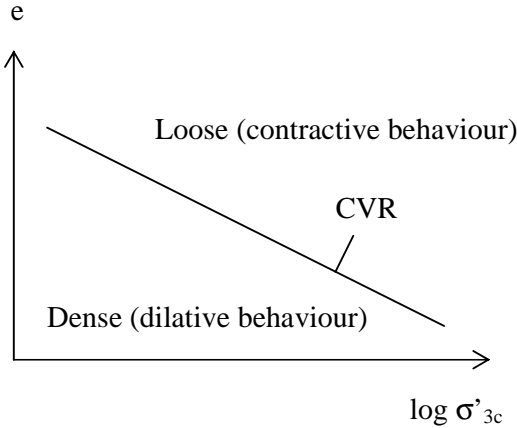


Figure 3.2 – CVR-line for logarithmic confining pressure

3.2.2 *Monotonic loading: undrained conditions*

From his studies, Casagrande deduced that if a saturated sand is not allowed to change its volume then the tendencies to volume changes will result in changes in the pore water pressure. Hence, strain-controlled undrained triaxial tests would produce positive excess pore pressure in specimens in a state looser than that of the critical void ratio and negative excess pore pressure in dense specimens, with void ratio higher than the critical void ratio.

In 1969 Castro, a Ph.D. student of Casagrande, performed a series of undrained, stress-controlled triaxial tests, on specimens of sand with different relative densities. From this study three different types of stress-strain behaviour, depending on the soil state, were observed (see Figures 3.3, 3.4 and 3.5).

Very loose samples (case *a* in the Figures), with $D_r = 27\%$, showed the development of a peak strength at a small strain level (Figure 3.3). After application of the last load increment, the rate of strain gradually increased. Then, suddenly, the specimen collapsed and failed rapidly with large strains. The great speed of deformation during the failure was caused by the sudden increase in pore pressure (see Figure 3.4), which induced a substantial change in the arrangement of the sand grains. Castro indicated the correspondent reduction of strength and the induced large strains as the basic characteristic of “liquefaction”, now commonly referred to as “flow liquefaction”. In the specimen exhibiting flow liquefaction behaviour the static shear stresses required for equilibrium (point A) were greater than the available shear strength (point B).

The hypothesis that a flowing liquefied sand has a “*flow structure*” in which grains continuously rotate to orient themselves in a structure of minimum frictional resistance was developed by Casagrande in 1976.

A different behaviour was observed for dense sands (case *b* in the Figures). Dense specimens ($D_r = 47\%$) initially tended to contract and then to dilate until a relatively high constant effective confining pressure and large-strain strength was reached. These tendencies resulted respectively in increase and decrease of pore pressure. In Figure 3.5 a quasi-linear increase in resistance is evident as the pore pressure decreases. This behaviour is typical of a dilative specimen.

The test on a medium dense specimen (case *c* in the Figures) with $D_r = 44\%$, slightly looser than the sample *b*, represent a case intermediate between the liquefaction failure and dilative behaviour. It initially showed the same behaviour as the loose samples but, after initially contractive behaviour, the soil "transformed" and exhibited dilative behaviour. Castro referred to this type of behaviour as "limited liquefaction".

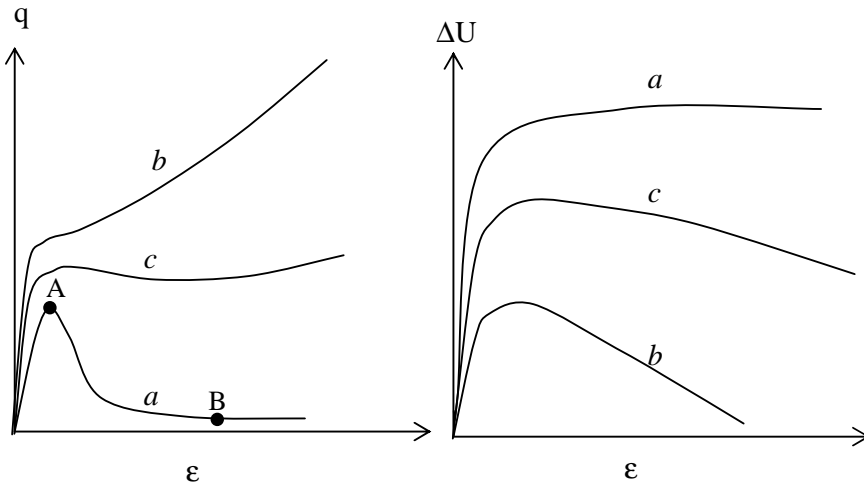


Figure 3.3 – Stress – strain curves

Figure 3.4 – Pore pressures – axial strain

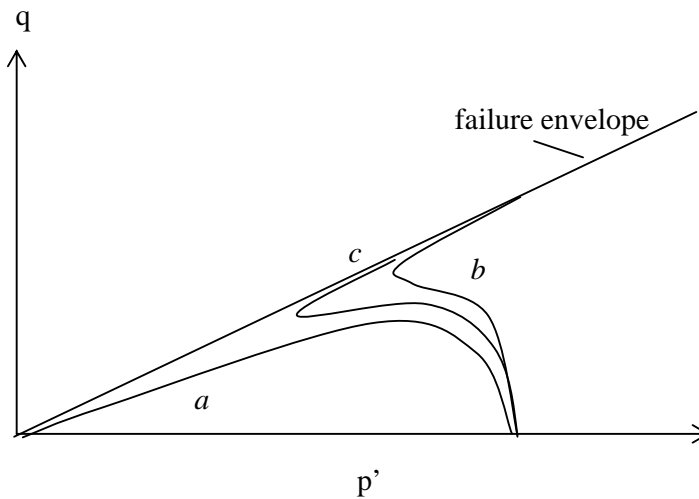


Figure 3.5 – Stress-paths

(Adapted from Castro, 1969)

specimen "a": loose sand with $D_r = 27\%$

specimen "b": dense sand with $D_r = 47\%$

specimen "c": medium-dense sand with $D_r = 44\%$

Castro and Poulos (1977) and Poulos (1981), in order to explain the behaviour of sands at very large shear strains, introduced the concept of *steady state condition*.

A soil in a *steady state* is a soil for which the deformations are occurring at constant volume or void ratio, constant effective stress, constant shear stress or resistance, and constant rate of shear strain. In this condition the original structure of the soil has been reworked at very high strains into a statistically constant particle orientation that Casagrande had defined as “flow structure”. A soil can reach the steady-state condition only after experienced sufficient remolding such that further deformations are not affected by particle orientation. If deformations cease, the soil is no longer considered to be in the steady-state condition. Steady-state flow can be achieved through monotonic or cyclic loading.

The relationship between effective confining pressure and void ratio at large strains is represented by the Steady State Line (*SSL*), which is actually a 3-D curve in $e-\sigma'-\tau$ plane, defined as the *CVR* line for undrained stress-controlled tests. In Figure 3.6 a projection of the *SSL* on the $e-\sigma'$ plane is represented. Soils in an initial state that are below the *SSL* are not susceptible to flow liquefaction whereas soils plotting above the *SSL* are susceptible to flow liquefaction if the static shear stress exceeds their steady state or residual strength of the soil.

Using concepts of critical-state soil mechanics, the behaviour of a cohesionless soil should be more closely related to the proximity of its initial state to the steady state line than to absolute measures of density (Roscoe and Pooroshasb, 1963). This means that soils in states located at the same distance from the steady-state line should exhibit similar behaviour. With this approach a *state parameter* (Been and Jeffries, 1985) can be defined as:

$$\psi = e - e_{ss}$$

where e_{ss} is the void ratio of the steady-state line at the effective confining pressure of interest (Figure 3.7). When the state parameter is positive, the soil exhibits contractive behaviour and may be susceptible to flow liquefaction. When it is negative, dilative behaviour will occur and the soil is not susceptible to flow liquefaction.

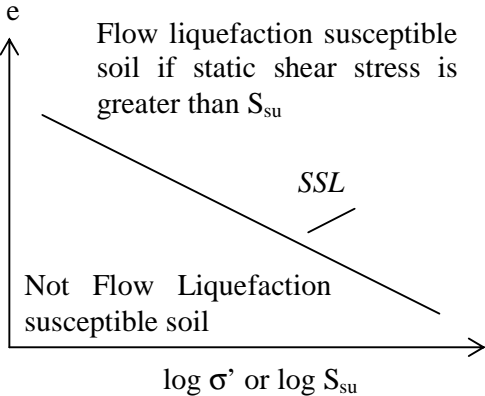


Figure 3.6 – 2-D projection of SSL for logarithmic confining pressure

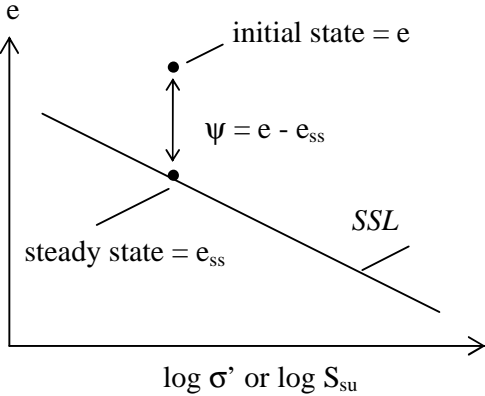


Figure 3.7 – State parameters

In 1975 Ishihara introduced an important concept similar to the one expressed by the *CVR* and *SSL* lines, but in the $q-p'$ plane. It is identified as the “Phase Transformation Line” (*PTL*) and represents a plot of the stress path points at which the transformation from contractive to dilative behaviour takes place. This line is not the critical state line, which will be reached at residual conditions, and during the test it can be crossed a first time, with the specimen still far from the residual state. If shearing continues, the stress path will finally approach the critical state line. Before

the critical state line, in the contractive region, an undrained stress path will tend to move to the left as the tendency for contraction causes pore pressure to increase and p' to decrease. As the stress path approaches the *PTL*, the tendency for contraction reduces and the stress path becomes more vertical. When the stress path reaches the *PTL*, there is no tendency for contraction or dilation, hence p' is constant and the stress path is vertical. After the stress path crosses the *PTL*, the tendency for dilation causes the pore pressure to decrease and p' to increase, and the stress path moves to the right. The described behaviour is illustrated in Figure 3.8.

Because the stiffness of the soil depends on p' , the stiffness decreases (while the stress path is below the *PTL*) but then increases (when the stress path moves above the *PTL*). This change in stiffness produces the "limited liquefaction" behaviour originally noted by Castro.

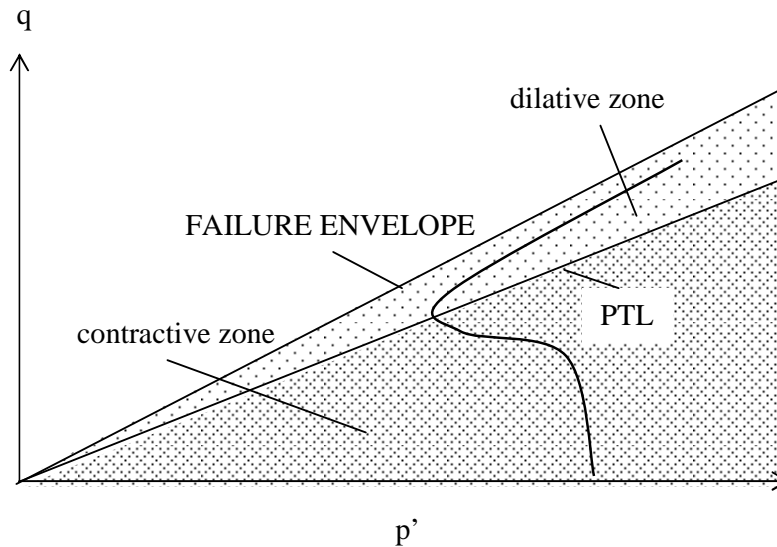


Figure 3.8 – Stress-path example in a q - p' plane

In Figure 3.9 is shown the response under monotonic loading of a series of triaxial specimens initially consolidated to the same void ratio at different effective confining pressures. At the same void ratio, they will reach the same effective stress conditions at the steady state but by different stress-paths. The initial state of specimens A e B is below the *SSL* so, during the shearing, they will exhibit dilative behaviour.

Conversely, the initial state of specimens C, D and E is above the *SSL* and during the loading they will exhibit a contractive behaviour, reaching a peak undrained strength and straining rapidly toward the steady state. For these specimens, flow liquefaction initiates at the peak of each stress path.

The locus of points describing the effective stress conditions at the initiation of flow liquefaction is a straight line and, in the stress path space, it defines the *flow liquefaction surface (FSL)*. This form of *FSL* was first proposed by Vaid and Chern in 1985. Since flow liquefaction cannot occur below the steady-state point, the *FSL* is truncated at that level (Figure 3.10).

The *FSL* marks the boundary between stable and unstable states in undrained conditions. When the stress conditions of soils reach the *FSL* under undrained conditions, whether by monotonic or cyclic loading, flow liquefaction will be triggered and the shearing resistance is reduced to the steady-state strength. Therefore the *FSL* describes the conditions at which flow liquefaction is initiated.

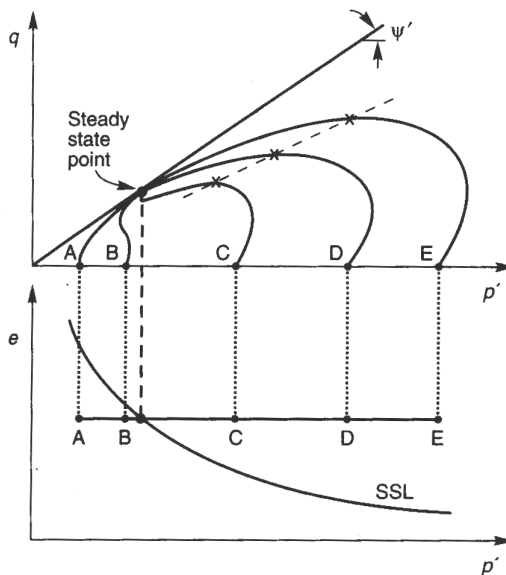


Figure 3.9 – Response of five specimens isotropically consolidated to the same void ratio at different effective confining pressures (from Kramer, 1996)

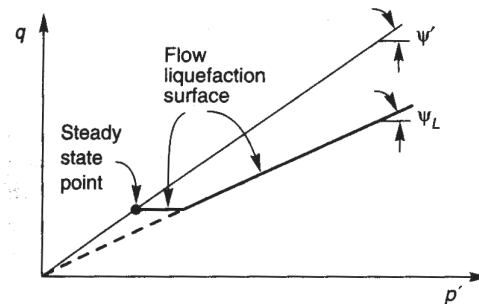


Figure 3.10 – Orientation of the flow liquefaction surface in stress path space (from Kramer, 1996)

3.2.3 *Cyclic loading: drained conditions*

Under cyclic loading, the sand behaviour becomes even more complex. Sands tends usually to densify under consecutive cyclic loads and the mechanism to become denser depends on contractive and dilative properties of material, function of its initial state rather than the characteristic of cyclic load.

Remembering that the failure envelope and *PTL* exist for negative shear stresses as well as positive, it is easy to see that a cyclically loaded soil can undergo the contraction/dilation transformation in two different directions.

If loose sand is cyclically loaded in drained condition it tends to become denser, per each cycle applied. As long as the stress-path developed during the cyclic loading crosses the *PTL*, the specimen contracts and a continuous volume reduction is evident per each cycle, with progressive hardening of the material. If the stress-path crosses the *PTL* (dense sand), during loading phase (both in compression and in extension) the sand dilates and the dilating phase is succeeded, during the following unloading, by an incremented contraction. This behaviour makes the “densification process” faster. The densification mechanism during to the unloading phase, which starts when the stress-path is above the *PTL*, can be related to the rearrangement of the grains and the “structure” of skeleton, in accordance with an irreversible mechanism (conversely, an elastic response during the unloading phase would be expected by the classic elastoplasticity) (Canou et al., 2002).

For a loose sand only a contractive behaviour is observed.

De Gennaro et al., (1996) and Benhamed (2001) observe that compression and extension phases have a different effect on the mechanical response of medium dense sand, with dilative behaviour in compression and contractive behaviour in extension. On this hypothesis, during cyclic alternate loading, the instability and failure will start during the extension phase.

3.2.4 *Cyclic loading in undrained conditions: liquefaction and cyclic mobility*

Also for cyclic loading, in undrained conditions the tendency to contract and dilate will be transferred in increase and decrease of pore pressure.

A comprehensive investigation of the effects of controlled cyclic stresses on the deformation and build-up of pore pressure on saturated sands was carried out by Seed (1966, 1967), Lee (1967) and Peacock (1968) at the University of California between 1966-1968. Particularly interesting are some undrained triaxial tests during which a cyclic deviator stress, of equal magnitude in compression and extension, was applied to specimens of saturated sand initially consolidated under an all around confining pressure. The range of relative density used was from 38 to 100%.

Several interesting observations could be drawn from these tests:

- up to a certain number of cycles the strains developing during each cycle were very small (less than 1%), but the cyclic pore pressure showed a cumulative increase;
- a moment was reached after which the value of the pore pressure at zero deviator stress became equal to the confining pressure; this means that the effective stresses dropped to zero. This event was called “initial liquefaction” from Seed and Lee (1966, 1967). The number of the cycles required to reach this condition was found to be a function of the void ratio of the specimen and of the magnitude of the cyclic deviator stress and confining pressure;
- after “initial liquefaction”, the strains during each subsequent cycle became progressively larger as more cycles of load were applied. The pore pressure was equal to the confining pressure at zero deviator stress and dropped substantially when either the axial extension or axial compression load was applied;
- when the cyclic strain reached an amplitude of 20% the sand was said to have developed “complete liquefaction”. Intermediate stages between “initial” and “complete” liquefaction were called “partial” liquefaction.

After initial liquefaction for loose specimens the strains rapidly increased, but only slowly for dense specimen and, in the last case, the required cycles to achieve complete liquefaction were much more than the required cycles for loose specimen. In both tests “initial” liquefaction developed during the same cycle. In all tests “partial” and “complete” liquefaction always ended in dilative behaviour.

The above mentioned observations and, more generally, the behaviour of loose (contractive) or dense (dilative) sand under cyclic loading can be understood with the help of the *PTL* line.

In the early stages of loading (before the stress-path has reached the *PTL*) the soil tends to contract and, in undrained conditions, a reduction of p' is experienced. If the stress-path of the sand lies for all the time under the *PTL* (loose sand) then the failure is reached through the same mechanism developed during monotonic load (“true static liquefaction”), due to a continuous pore pressure build-up, until “true cyclic liquefaction”. As long as the stress- path is below the *PTL*, the unloading phase is in elastic regime.

When at certain point of the cyclic loading the stress-path crosses for the first time the *PTL* line (usually during the extension phase in triaxial tests, according to Canou et al., 2002), the sand tends to dilate with consequent increase of p' . The developed negative pore pressure limits further straining in additional cycles. From this point the unloading phase, both in compression and in extension, induces the tendency of the soil to become denser and, in undrained condition, the pore pressure to increase. Such as mechanism causes a great decrease of p' . In the final state the observed stress-path is the distinctive "butterfly" profile, arising from the alternate phases of dilation and densification. The stress path will pass the point of zero, or close to zero, effective stress twice per cycle. Consequently, alternate hardening and softening phases characterise the stress-strain curve.

While significant strains can occur during cyclic loading, the very large deformations associated with a flow failure do not develop in dense, dilative soils. In this case the shear strength remains greater than the static shear stress and the failure occurs for the phenomenon called “cyclic mobility” (Castro and Poulos, 1977).

The initiation and development of both cyclic true liquefaction and cyclic mobility will depend on several parameters characterising the cyclic load as amplitude, alternate character or not of cycles, number of cycles, symmetry etc.

True cyclic liquefaction and cyclic mobility have been observed during alternated symmetrical undrained triaxial tests, respectively on loose and dense specimens of Hostun sand (Benhamed, 2001).

In the case of loose sand (Figure 3.11), until a certain number of cycles ($N=60$), a “regular” increase of pore pressure and decrease of effective stress p' are observed. During this phase small axial deformations are developed. When the load reaches a specific number of cycles ($N>60$) a sudden loss of shearing resistance and rapid increment of deformations, coupled to high values of pore pressure, are observed. The stress-path in the q - p' plane shows a behaviour quite similar to the one observed for the static liquefaction.

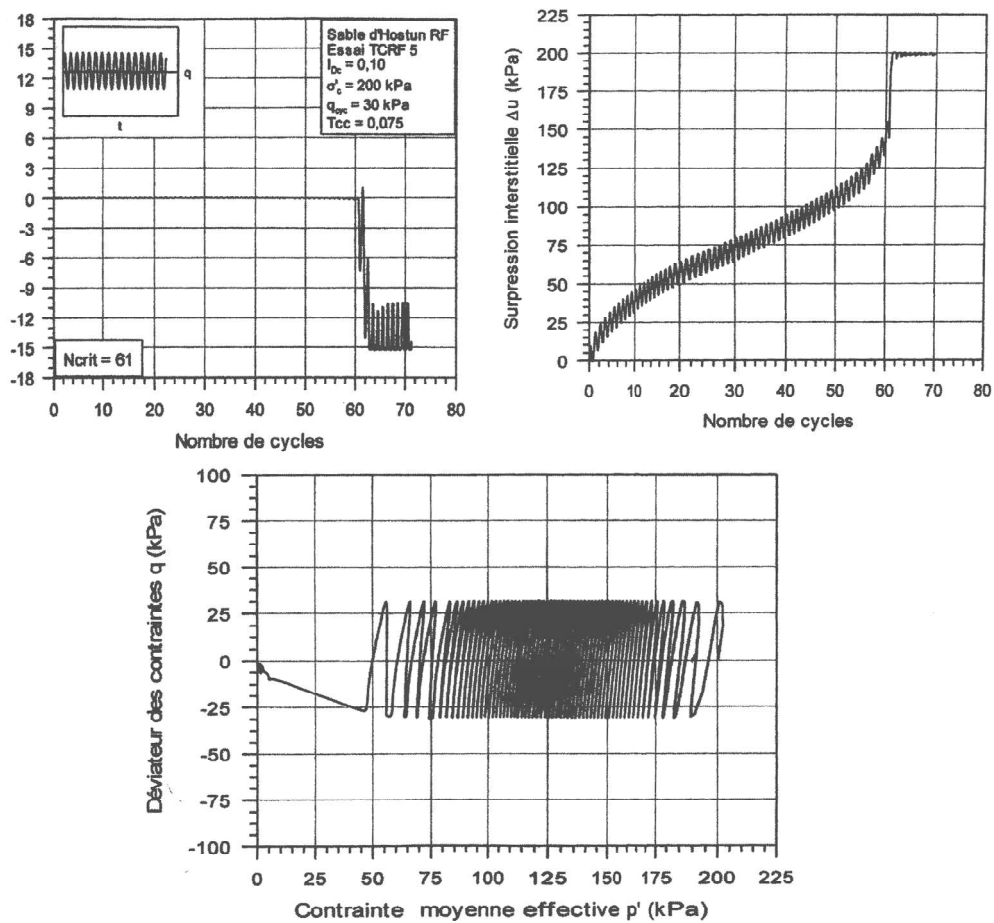


Figure 3.11 – Typical true cyclic liquefaction behaviour as observed in an alternated symmetrical triaxial test (Benhamed, 2001)

In the case of dense sand (Figure 3.12) two different types of behaviour are evidenced. In a first phase a continuous increase of pore pressure, with “one peak” build-up per cycle, and the occurrence of very small deformations are observed. In the q - p' plane p' decreases regularly as long as the cycles are applied. This behaviour can be related to the tendency of the sand to contract in the initial phase of the test. At certain point of the test an abrupt variation of the “process” is evident: the pore pressure increases with a mechanism of two peaks build-up per cycle and a fast accumulation of larger amplitude deformations appears. The stress-path also changes, with the tendency of p' to increase during the loading phase and to decrease during the unloading (both in compression and extension).

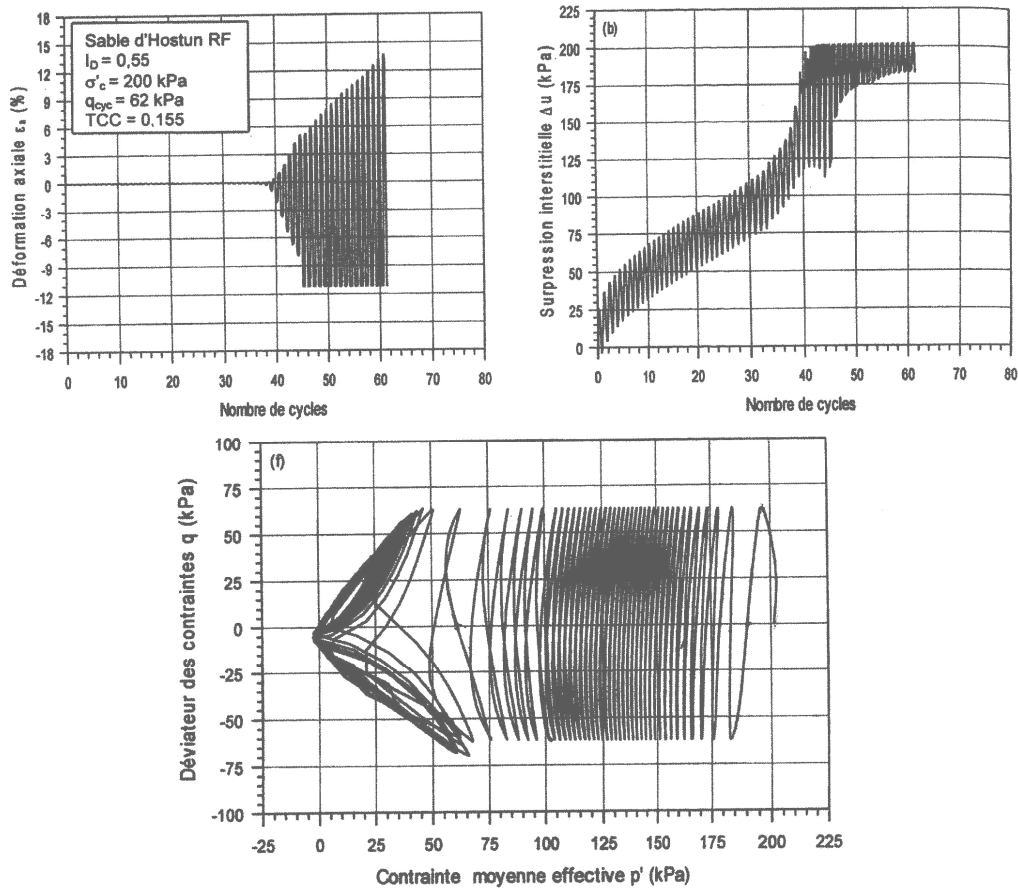


Figure 3.12 – Typical cyclic mobility behaviour as observed in an alternated symmetrical triaxial test (Benhamed, 2001)

The difference between liquefaction and cyclic mobility may be also illustrated by using the state diagram, reported in Figure 3.13 (Castro and Poulos, 1977). In the graph, with axes effective minor principal stress and void ratio, the steady state line is reported.

If the specimen lies above the *SSL* and it is loaded by monotonic or cyclic undrained loading, it starts to contract and, in undrained conditions, a significant rise in pore pressure is observed. If the load applied is large enough, liquefaction can be triggered. In the state diagram, liquefaction is the result of undrained failure of a fully saturated, highly contractive (loose) sand, starting at point C and ending with steady state flow at constant volume and constant σ'_3 at point A. During undrained flow, the soil remains at Point A in the state diagram. The further to the right of the *SSL* that the starting point is, the greater will be the deformations associated with the liquefaction. The condition in which the specimen has zero effective stress and void ratio higher than Q represents the “quicksand condition”. In this state, sand has zero strength and is neither dilative nor contractive. If the initial condition is above Q, the strength after liquefaction will be zero. If it is below Q, the strength after liquefaction will be small but finite. Liquefaction can occur only in specimens that are highly loose and contractive.

When a fully saturated dilative sand (point D in the state diagram) is loaded monotonically (“statically”) in undrained condition, the point on the state diagram may move slightly to the left of point D but then it will move horizontally toward the steady state line as load is applied (it tends to dilate and, in undrained conditions, pore pressure decreases). If now a new test is started and cycling loading is applied the state point move horizontally to the left, because the average void ratio is held constant and the pore pressure rises due to cyclic loading. So, saturated sands starting at points on or below the steady state line, will be dilative during undrained monotonic loading and the state point will move to the right. If cyclically loaded the state points will shift to the left as strains occur and the specimen softens. If these strains are large enough specimen develops cyclic mobility. If enough cycles are applied, if they are large enough, and if the hydrostatic stress condition is passed during each cycle, then the zero effective stress condition can be reached. The magnitude of pore pressure build-up in cyclic test will depend on magnitude of the

cyclic load, the number of cycles, the type of test and the soil type. Cyclic mobility can occur in the laboratory in a specimen for any initial state, but, without stress reversal, the larger strains do not occur.

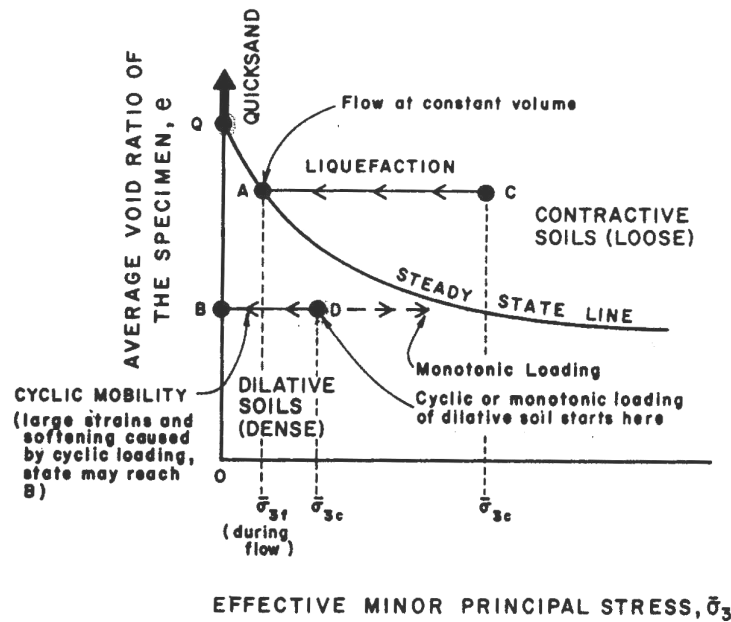


Figure 3.13 – Undrained Test on Fully Saturated Sands Depicted on State Diagram (Castro and Poulos, 1977)

In Figure 3.14 the response of two identical specimens of loose, saturated sand, respectively monotonically and cyclically loaded, in undrained condition, is reported. Initially (point A) the specimens are in drained equilibrium under a static shear stress, τ_{static} , that is greater than the steady-state strength, S_{su} . During the loading, both monotonic and cyclic, the shear resistance increases until the stress path approaches the *FSL* (point B and D). Then strains rapidly increase until point C, approaching the steady state of deformation. The effective stress path moves to the left as positive excess pore pressures develop and permanent strains accumulate.

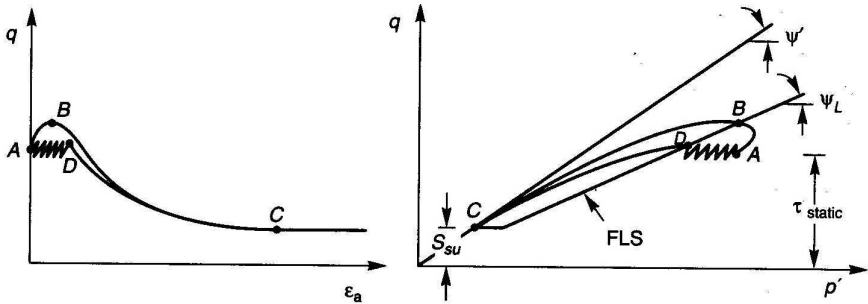


Figure 3.14 – Flow Failure induced by cyclic and monotonic loading (by Kramer, 1996)

The *FLS* marks the onset of the instability that produces liquefaction and flow liquefaction can be initiated by cyclic loading only when the shear stress required for static equilibrium is greater than the steady-state strength (see Figure 3.15).

Conversely, cyclic mobility can develop when the static shear stress is smaller than the steady-state shear strength. (Figure 3.16).

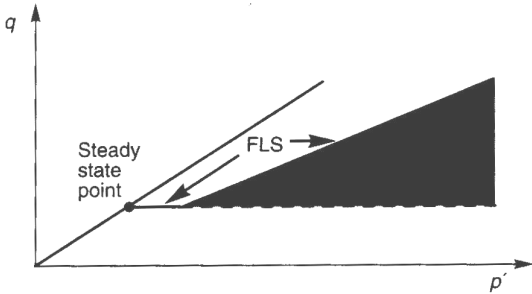


Figure 3.15 – Zone of Flow Liquefaction susceptibility (adapted from Kramer, 1996)

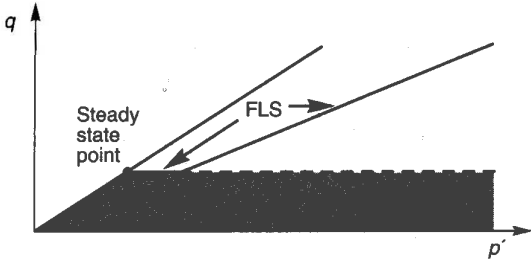


Figure 3.16 – Zone of Cyclic Mobility susceptibility (adapted from Kramer, 1996)

Kramer (1996) distinguishes three combinations of initial conditions and cyclic loading conditions that generally produce cyclic mobility.

In Figure 3.17 these three cases are represented:

- a) In the first case $\tau_{\text{stat}} - \tau_{\text{cyc}} > 0$ (this means that there is no shear stress reversal) and $\tau_{\text{stat}} + \tau_{\text{cyc}} < S_{\text{su}}$.

During the loading the effective stress path moves to the left until it reaches the drained failure envelope. Additional loading cycles cause it to move along the envelope, resulting in a final stabilisation of the effective stress. Flow liquefaction cannot develop because any unidirectional straining would produce dilation. The effective confining pressure has decreased and the resulting low stiffness can allow significant permanent strains to develop within each loading cycle.

- b) In the second case $\tau_{\text{stat}} - \tau_{\text{cyc}} > 0$ (this means that there is no shear stress reversal) and $\tau_{\text{stat}} + \tau_{\text{cyc}} > S_{\text{su}}$.

Also in this case the effective stress path moves to the left during the loading until to reach the *FSL*, where momentary instability will occur. Significant permanent strains may develop during these periods that generally will stop at the end of the cyclic loading when the shear stress returns to the τ_{stat} .

- c) In the last case $\tau_{\text{stat}} - \tau_{\text{cyc}} < 0$ (this means that shear stress reversal occurs) and $\tau_{\text{stat}} + \tau_{\text{cyc}} < S_{\text{su}}$.

In this case the direction of the shear stress is characterised by compression and extension. Because the pore pressures generation rapidly increases with increasing degree of stress reversal (Dobry et al., 1982; Mohamad and Dobry, 1986), the effective stress path moves very quickly to the left and oscillates along the compression and extension failure envelope. In this way, the effective stress path passes twice per cycle through the origin and, in this point, the effective stresses are instantaneous equal to zero. This state of zero effective stresses is referred as *initial liquefaction* (See and Lee, 1966). Significant permanent strains may accumulate during cyclic loading but flow failure cannot occur because the

loading phase (in both directions) will induce dilation and recover of shear strength.

Conversely to the liquefaction, for cyclic mobility there is not a clear point in which the phenomenon initiates.

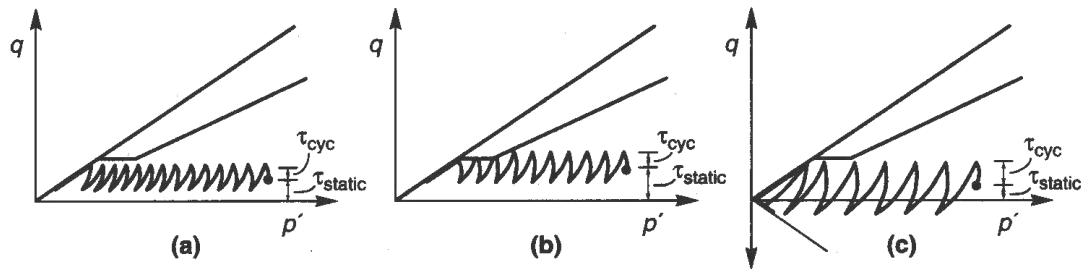


Figure 3.17 - Combinations of initial conditions and cyclic loading conditions producing cyclic mobility
(from Kramer, 1996)

3.3 Constitutive modelling

The constitutive behaviour of soils, as it has been observed in the previous Sections, is characterised by irreversibility and non-linearity. The modelling of the behaviour of granular soils under transient and cyclic loading is quite complex because of the number of factors influencing it. In the last decades extensive research enabled to develop advanced models in order to take into account several aspects of granular soil behaviour under loading, unloading and reloading. Progressively more sophisticated studies have helped to develop constitutive models of increasing complexity, arriving to describe phenomena as liquefaction and cyclic mobility.

In order to describe the mechanical behaviour of granular soil under static loading, classical plasticity models was extended to the sands considering that the behaviour of granular soils depends mainly on the density. The traditional Critical State Models can describe the behaviour of loose and dense sands, in drained and undrained conditions considering three fundamentals facts: 1) hardening laws depending on deviator and volumetric plastic strain; 2) non-associative plastic flow rules; 3) plastic deformations existing throughout the process. The critical state models are based on the knowledge of the yield surface and the plastic potential. The yield surface will expand or contract depending on whether the material is hardening or softening.

These models are quite good for monotonic loading but they cannot reproduce the behaviour of the soil during cyclic loading and the related phenomena as pore pressure generation in fast processes or densification. In fact, the material remained elastic within the yield surface, where no plastic deformation can develop.

Within the framework of elastoplasticity, *plastic advanced models* represent one of the most important theoretical approaches usually followed to simulate the mechanical behaviour of soils subject to cyclic loading. In this framework we can distinguish three different classes: a) the bounding surface models, b) the generalised plasticity and c) the multiple mechanism plastic models. Class a) is characterised by two surfaces, an outer ‘consolidation’ surface, and an inner loading locus, and provides a rule for the definition of the hardening modulus in the space between them. In the generalised plasticity (class b) the concept of loading and unloading, as well as of flow rule, are extended. In these models no yield surface needs to be

defined and plastic deformations can be evolve during stress reversals. Finally, the natural extension of single mechanism plasticity is provided by multiple mechanism plasticity, in which two or more yield surfaces and plastic potentials are defined.

As an alternative to elastoplasticity, soil behaviour can be modelled with hypoplasticity. In this constitutive theory the strain rate is not a priori decomposed into a elastic and plastic part, as in the elastoplasticity theory. Yield functions, potential functions and flow rules are not necessarily needed, giving hypoplasticity a simple structure. Hypoplasticity may be applied to loading and unloading problems, but not yet to cyclic loading problems (Heeres, 2001).

As follows a generalised plasticity model (Pastor et al. 1990), describing the behaviour of sands under monotonic and cyclic loading, is presented.

3.3.1 A generalised plasticity model for sands

The model here proposed is an extension of generalised plasticity theory, to model sand behaviour under monotonic and cyclic loading. The generalised plasticity theory belongs to the elastoplasticity theory, so first some general aspects of standard elastoplasticity will be reported and, next, the singularity of the generalised plasticity will be described.

Concerning the adopted symbols, underlined lower-case characters represent first-order tensors, second-order tensors and vectors; underlined upper-case characters represent fourth-order tensors and matrices. Regular symbols and characters represent scalars.

In standard elastoplasticity the total strain rate is decomposed into an elastic reversible component and into an plastic irreversible component:

$$\underline{\underline{\dot{\epsilon}}} = \underline{\underline{\dot{\epsilon}}^{\text{el}}} + \underline{\underline{\dot{\epsilon}}^{\text{pl}}}$$

The elastic strain rate is connected to the stress rate $\underline{\underline{\dot{\sigma}}}$ by the constitutive relation

$$\underline{\underline{\dot{\epsilon}}^{\text{el}}} = (\underline{\underline{D}}_t^{\text{el}})^{-1} : \underline{\underline{\dot{\sigma}}}$$

with $\underline{\underline{D}}_t^{el}$ the fourth-order tangent elastic stiffness tensor. If elasticity is assumed isotropic, $\underline{\underline{D}}_t^{el}$ is defined by two independent coefficients, tangent elastic bulk modulus K_t^{el} and tangent elastic shear modulus G_t^{el} .

The plastic strain rate is so defined (flow rule):

$$\underline{\underline{\dot{\epsilon}}}^p = \mathcal{K} \underline{\underline{m}}(\underline{\underline{\sigma}}, \underline{\underline{\phi}})$$

in which \mathcal{K} is a non-negative scalar which specifies the magnitude of the plastic strain rate and it is called consistency parameter or plastic multiplier. The second-order tensor $\underline{\underline{m}}$ specifies the direction of plastic strain and, in the standard elastoplasticity, it depends on the current stress $\underline{\underline{\sigma}}$ and on a finite set of variables $\underline{\underline{\Phi}}$ (this parameters takes into account of history effects and its evolution is proportional to the consistency parameter). Tensor $\underline{\underline{m}}$ follows from differentiation of a plastic potential function $g(\underline{\underline{\sigma}}, \underline{\underline{\Phi}})$ with respect to the stress. In standard elastoplasticity there exists a yield function f , which is usually a comparison between a stress intensity (through the tensorial invariants p and q) and strength, depending on the current stress $\underline{\underline{\sigma}}$ and on the internal variables $\underline{\underline{\Phi}}$. If $f(\underline{\underline{\sigma}}, \underline{\underline{\Phi}}) < 0$ the stress intensity is smaller than strength and the behaviour of the material is elastic (which means that plastic strain rate is null). The maximum value that can be reached by the yield function is $f(\underline{\underline{\sigma}}, \underline{\underline{\Phi}}) = 0$, because stress intensity cannot exceed the material strength. In such a situation both the stress intensity and the strength change in the same amount (consistency condition):

$$\mathcal{K}(\underline{\underline{\sigma}}, \underline{\underline{\phi}} = 0)$$

Usually, the yield function f and the plastic potential function g are identical and *associative plasticity* is obtained. In a cyclic behaviour it is needed to take into account of the dilative-contractive behaviour of the material, so a *non-associative plasticity* has to be adopted, with $f \neq g$.

Combining the consistency condition with the expression of $\underline{\dot{\epsilon}} = \underline{p}(\underline{\sigma}, \underline{\phi})\underline{\dot{\lambda}}$, where \underline{p} is a vector, an expression for $\underline{\dot{\lambda}}$ is obtained:

$$\underline{\dot{\lambda}} = \frac{\frac{\partial f}{\partial \underline{\sigma}} : \underline{D}_t^{el} : \underline{\dot{\epsilon}}}{h + \frac{\partial f}{\partial \underline{\sigma}} : \underline{D}_t^{el} : \frac{\partial g}{\partial \underline{\sigma}}}$$

In the above expression the *hardening modulus* h has been introduced, so defined:

$$h = -\frac{\partial f}{\partial \underline{\phi}} \cdot \underline{p}(\underline{\sigma}, \underline{\phi})$$

In the generalised plasticity theory the incremental non-linear elastoplastic relations between increments of strain and stress can be defined as:

$$\underline{\dot{\epsilon}} = \left(\underline{D}_t \right)^{-1} : \underline{\dot{\sigma}}$$

where $\underline{\dot{\epsilon}}$, $\underline{\dot{\sigma}}$ and \underline{D}_t are Cartesian tensors of orders two and four.

The deformation of the material can be considered as the result of deformations produced by M separated mechanism, all of these subject to the same state of stress:

$$\underline{\dot{\epsilon}} = \sum_{m=1}^M \underline{\dot{\epsilon}}^m$$

In order to simplify the dependency of \underline{D}_t on the direction of the stress rate, a vector of direction $\underline{n}^{(m)}$ is defined, discriminating between loading and unloading for each mechanism:

$$\underline{n}(\underline{\sigma}, \underline{\phi}) : \underline{\dot{\sigma}} > 0 \rightarrow \text{loading}$$

$$\underline{n}(\underline{\sigma}, \underline{\phi}) : \underline{\dot{\sigma}} < 0 \rightarrow \text{unloading}$$

In the classical plasticity theory:

$$\underline{n} = \frac{\frac{\partial f}{\partial \underline{\sigma}}}{\left| \frac{\partial f}{\partial \underline{\sigma}} \right|}$$

Incremental stress-strain relations for a single mechanism (m) have the form:

$$\underline{\underline{e}}^m = \underline{\underline{C}}^{L(m)} : \underline{\underline{e}}$$

$$\underline{\underline{e}}^m = \underline{\underline{C}}^{U(m)} : \underline{\underline{e}}$$

where $\underline{\underline{C}}$ is the inverse of the stiffness matrix $\underline{\underline{D}}_t$ and L and U are for loading and unloading directions, respectively.

The constitutive tensors $\underline{\underline{C}}^{L(m)}$ and $\underline{\underline{C}}^{U(m)}$ are so defined:

$$\underline{\underline{C}}^{L(m)} = \underline{\underline{C}}^{e(m)} + \frac{1}{H_L} \underline{n}_{gL} \otimes \underline{n}^{(m)}$$

$$\underline{\underline{C}}^{U(m)} = \underline{\underline{C}}^{e(m)} + \frac{1}{H_U} \underline{n}_{gU} \otimes \underline{n}^{(m)}$$

where H is the hardening modulus and $\underline{n}_g^{(m)}$ is the direction of plastic flow (the second-order tensor $\underline{\underline{m}}$ in the standard elastoplasticity); it follows from differentiation of a plastic potential function :

$$\underline{n} = \frac{\frac{\partial g}{\partial \underline{\sigma}}}{\left| \frac{\partial g}{\partial \underline{\sigma}} \right|}$$

Total increment of strain is given by the summation of all mechanisms:

$$\underline{\underline{\epsilon}} = \sum_{m=1}^M \underline{\underline{C}}^{e(m)} : \underline{\underline{\epsilon}} + \sum_{m=1}^M \frac{1}{H_{L/U}^{(m)}} \left[\underline{\underline{n}}_{gL/U} \otimes \underline{\underline{n}}^{(m)} \right] : \underline{\underline{\epsilon}}$$

that can be also so expressed:

$$\underline{\underline{\epsilon}} = \underline{\underline{C}}^e : \underline{\underline{\epsilon}} + \sum_{m=1}^M \frac{1}{H_{L/U}^{(m)}} \left[\underline{\underline{n}}_{gL/U} \otimes \underline{\underline{n}}^{(m)} \right] : \underline{\underline{\epsilon}}$$

The first member of the sum represents the elastic component of the strain increment and the second one is the plastic component.

The above equation can also be written as:

$$\underline{\underline{\epsilon}} = \underline{\underline{C}}_{L/U}^{ep} : \underline{\underline{\epsilon}}$$

Inversion of $\underline{\underline{C}}^{ep}$ will give the equivalent $\underline{\underline{D}}_{t, L/U}$.

The main advantage in the proposed model is that irreversible plastic deformations are introduced without the need to explicitly define plastic potential or yield surfaces, no hardening rules. Indeed, the model is fully determined by specifying three directions ($\underline{\underline{n}}_{gL/U}^{(m)}$ and $\underline{\underline{n}}^{(m)}$) and two scalar functions of hardening moduli ($H_{L/U}^{(m)}$). Different expressions can be selected for loading and unloading and, consequently, the generalised plasticity model is particularly suitable in cyclic loading conditions.

In the derived generalised plasticity model for sands presented in Pastor et al. (1990), the elastic behaviour and elastoplastic behaviour are assumed isotropic.

In the monotonic loading the direction $\underline{\underline{n}}$ is so defined:

$$\underline{\underline{n}}^T = (n_v, n_s) = \left(\frac{d_f}{\sqrt{1+d_f^2}}, \frac{1}{\sqrt{1+d_f^2}} \right)$$

where the first component refers to hydrostatic effects and the second component refers to deviator effects. In the equation d_f is a dilatancy, so expressed:

$$d_f = (1 + \alpha) \cdot (M_f - \eta)$$

where M_f and α are constitutive parameters and η is the stress ratio q/p' .

Because of the flow-rule is non-associative (in order to model the unstable behaviour within the hardening region) the direction \underline{n} is different from \underline{n}_{gL} .

The direction of plastic flow \underline{n}_{gL} in the triaxial space is given by:

$$\underline{n}_g^T = \left(\frac{d_g}{\sqrt{1+d_g^2}}, \frac{1}{\sqrt{1+d_g^2}} \right)$$

where the dilatancy d_g can be approximated by a linear function of stress ratio $\eta(\frac{q}{p'})$

so defined:

$$d_g = (1 + \alpha) \cdot (M_g - \eta)$$

In this expression M_g is an additional parameter of the model. Both M_f and M_g depend on Lode's angle. We note that a yield surface and a plastic potential can be found by integrating respectively the expressions for \underline{n} and \underline{n}_g . From Pastor, Zienkiewicz and Leung (1985) the ratio M_f/M_g can be assumed to be the same as relative density D_r .

A convenient law for the plastic modulus H_L can be so defined:

$$H_L = H_0 p' H_f \{H_v + H_s\}$$

This expression takes into account several important aspects, as:

- residual conditions take place at the critical state line ($q/p' = M_g$);
- failure does not necessarily occur when this line is first crossed;

- the frictional nature of material response requires the establishment of a boundary separating impossible states from those which are permissible.

With the above expression the critical state line $q/p' = M_f$ can be passed with a positive hardening modulus, allowing for a peak strength during shearing.

In the equation

- H_0 is a material constant and it can be found as a function of λ, κ and e :

$$H_0 = \frac{1+e}{(\lambda-\kappa)}$$

where λ and κ are the slopes of normal consolidation and elastic unloading lines in the $(e, \ln p')$ plane; e is the void ratio;

- H_f limits the possible states and is so defined:

$$H_f = \left(1 - \frac{\eta}{\eta_f}\right)^4$$

$$\eta_f = \left(1 + \frac{1}{\alpha}\right) M_f$$

- H_v is so defined:

$$H_v = \left(1 - \frac{\eta}{M_g}\right)$$

- $H_s = \beta_0 \beta_1 \exp(-\beta_0 \xi)$

- $\xi = \int \underline{\underline{\epsilon}}_d^{pl} dt = \int (d\underline{\underline{e}}^{pT} \cdot d\underline{\underline{e}}^p)^{1/2}$ is the accumulated deviator plastic strain.

The model of generalised plasticity here analysed to simulate the soil behaviour under monotonic loading has 8 parameters:

- two elastic constants K_0 and G_0 that can be determined from unloading-reloading tests; it is so possible to calculate $K_i^{el} = K_0 \frac{P}{p_0}$ and $G_i^{el} = \frac{G_0}{3K_0} K_i^{el}$
- a parameter α that controls dilatancy;
- the slope M_g of the critical state line on the $(p' - q)$ plane (found from drained or undrained tests);
- the slope M_f that can be found from the relation between M_g and D_r ;
- the constant H_0 ;
- β_0 and β_t .

The proposed model for monotonic loading can be extended to simulate the unloading, introducing a new expression for the plastic modulus, because of during unloading plastic strains of contractive nature are developed:

$$H_u = H_{u0} \left(\frac{M_g}{\eta_u} \right) \rightarrow \text{for } \left| \frac{M_g}{\eta_u} \right| > 1$$

$$H_u = H_{u0} \rightarrow \text{for } \left| \frac{M_g}{\eta_u} \right| \leq 1$$

where $\eta_u = (q/p')_u$. Two new parameters are introduced: H_{u0} , and γ

The direction of plastic flow produced upon unloading will be so defined:

$$\underline{n}_{gU} = \left(-abs \left(\frac{d_g}{\sqrt{1+d_g^2}} \right), + \frac{1}{\sqrt{1+d_g^2}} \right)^T$$

Cyclic loading under undrained conditions causes progressive pore pressure build-up leading to failure. In the case of very loose sands liquefaction takes place following a series of cycles in which the stress path migrates towards lower confining pressures. As it has been observed, denser sands do not exhibit liquefaction but cyclic mobility: failure is progressive since the stress path approaches the *CSL* by its shift caused by the pore pressure build-up. Deformations during unloading cause the stress path to

turn towards the origin, and strains produced during the next loading branch are of higher amplitude. In order to take into account the cyclic loading phenomena, a new memory factor multiplying the plastic modulus is needed. The new plastic modulus is so defined:

$$H_L = H_0 p' H_f (H_v + H_s) H_{Dm}$$

Where H_{Dm} is given by:

$$H_{Dm} = \left(\frac{\zeta_{\max}}{\zeta} \right)^\gamma$$

$$\zeta = p' \left\{ 1 - \left(\frac{1 + \alpha}{\alpha} \right) \frac{\eta}{M} \right\}^{1/\alpha}$$

It is possible now to model cyclic phenomena as liquefaction and cyclic mobility in loose and medium sands under cyclic loading.

3.4 General conclusions

In this Chapter the mechanic response of sand under monotonic and cyclic loading, in drained and undrained conditions, has been treated. Concepts of liquefaction and cyclic mobility deduced by the literature experimental observations have been introduced. Although in situ the two phenomena are often confused they have been extensively studied in laboratory and consequently distinguished.

True liquefaction can be considered the more dangerous phenomenon since it corresponds to a particular instability characterising contractive sands (usually sand from very loose to loose), susceptible to develop very high values of pore pressure in undrained conditions. Monotonic and cyclic loading may trigger this process and it results in a flow failure with rapid drop of shear resistance until a very small value. If the shear resistance reaches the zero value the *total liquefaction* is observed.

Cyclic mobility is characteristic of dilative material (sands from medium dense to very dense) and it is developed only with cyclic loading. High values of pore

pressure are produced during contractive phases characterising the unloading (both in compression and in extension). Although the increase of shear strength during loading phases (due to the dilatancy) does not permit the development of very large deformations associated with a flow failure, significant strains can occur during cyclic loading.

It is finally important to observe that in a real situation it is not easy to distinguish failures induced by liquefaction from failures triggered by cyclic mobility. Many factors will characterise the “in situ conditions” that cannot easily be reproduced in laboratory (initial state of sand in situ, heterogeneity of material, etc.). These make the analysis of a real problem very complicated.

Chapter 4

Laboratory experiments: dynamic centrifuge tests

4.1 Introduction

In the previous Chapters it has been evidenced that marine structures and, more specifically, vertical breakwaters are not yet well studied from a geotechnical point of view and many uncertainties still characterise the design. On the other hand, the actual processes involving the soil-fluid-structure interaction are quite complicated and the wave loads may cause failure of the foundation of a gravity structure, in several ways (Oumeraci et al. 2001). The influence of the wave action on the foundation will depend on several different aspects as nature of soil, stress history experienced by the soil, relative density, drainage conditions, etc., and it is not easy to evaluate or predict.

In order to study the salient foundation aspects in the design of caisson breakwaters, dynamic centrifuge tests have been performed in the framework of the PROVERBS Project (Van der Poel and De Groot, 1998). As previously mentioned, this project has been performed by Oumeraci et al. (2001) and it has been aimed at developing a new probabilistic design/analysis method for monolithic coastal structures and breakwaters subjected to the wave attacks.

This Chapter deals with the analysis of the results of the centrifuge tests. The failure mechanism is studied by examining the effects of the cyclic wave action on the mechanical behaviour of sandy soil foundation. Test results showed that the failure occurred according to a more complex mode than the mechanism expected when the tests were designed, that was a “liquefaction flow failure” involving the structure. Conversely, wave action led to oscillatory motions and residual permanent deformations of the structure, causing a “stepwise” bearing capacity failure in the subsoil. The collapse was induced not as a consequence of a specified wave load but according to a progressive mechanism under repetitive high loads.

The structure was founded on a layer of dense sand with dilative behaviour. Liquefaction flow failure did not occur but phenomena of “instantaneous liquefaction” and “cyclic mobility” have been supposed responsible of failure.

As follows, the performed centrifuge tests and the observed results are presented. The deformation mechanism until failure is analysed and the mechanical response of sandy soils under cyclic loading is briefly studied, with regard to liquefaction and cyclic mobility phenomena.

4.2 General considerations and scaling for dynamic problems

Centrifuge modelling represents one of the most valuable tools in geotechnical engineering in analysing mechanism of deformation and collapse. It is known, in fact, that the stress-strain behaviour of geotechnical materials is non-linear and it is a function of stress level and stress history. Subsequently 1g model experiments cannot correctly model the behaviour of full-scale prototype. Conversely, in a centrifuge experiment a small-scale physical model is subjected to an appropriate gravitational acceleration, many times larger than Earth’s gravity, that provides identical model and prototype stress and strain field. By means of this method, centrifuge test can correctly replicate the prototype reproducing the self-weight stress distribution within the model. The soil behaviour is hence properly reproduced in terms of strength and stiffness. To be representative, scaled model experiments must be based on similarity laws derived from fundamental equations governing the phenomena to be investigated.

In this project, special considerations were made with respect to the centrifuge physical modelling for dynamic problem to ensure conformity between the model and the prototype. The fundamental scale relations were based on the general equation of continuum mechanics that enabled to obtain the scale factor for stress, strain, length, acceleration, velocity, dynamic time and force. Since the cyclic loading of the structure induces pore pressures gradients and then pore pressure dissipation, the flow regime in the soil was taken into account, based on the flow Darcy’s law. From this law it has been derived that the seepage velocity through a model subjected to an increased self-weight of N times is N times greater in the model

than that in the prototype if identical soil and pore fluid are used and identical gradients applied. Then the time scale factor (dissipative or consolidation time), ratio of length over velocity, will be scaled as $t_s = N^2$. On the other hand, the dynamic time obtained from the equation of continuum mechanics is scaled as $t_d = N$. This apparent inconsistency does not mean that two different time scales exist, but that the materials used in the model do not allow for simultaneous similitude of time scale in the dynamic event and the diffusion phenomena. This can be expressed by the fact that the scale factor for the weight and inertia forces is different from the scale factor for seepage forces, when the same soil and porous fluid are used in the model and prototype. Hence, the proportionality of forces is not preserved. In order to equalise the two time scales and to model the inertial effects and the seepage flow effects simultaneously, the dynamic time scale for the loading was followed and the pore fluid was chosen so that the saturated model soil and prototype soil had the same Darcy hydraulic conductivity. Several alternatives were investigated. In order to do not have negative influence on the soil constitutive behaviour, the same soil was used and a model pore fluid with higher viscosity but similar density as the prototype fluid was adopted (Rowe and Craig, 1978). Hence, change of hydraulic conductivity was obtained by altering the viscosity of the pore fluid. A model pore fluid 1000 times more viscous than water at 20 °C was developed, offering similar physical and chemical properties of water.

The scale ratios applied for the centrifuge dynamic test program are reported in Table 4-1. The respect of several geotechnical, geometric and loading conditions resulted in a scale choice of 1:60 (acceleration level $N = 60$ g).

<i>Parameter</i>	<i>Prototype</i>	<i>Centrifuge model</i>
Length	N	1
Acceleration	1	N
Stress	1	1
Strain	1	1
Time	N	1
Force	N ²	1
Soil density	1	1
Pore fluid density	1 (water)	1 (model pore fluid)
Pore fluid viscosity	1 (water)	N (model pore fluid)
Soil hydraulic	1 (water)	1 (model pore fluid)

Table 4-1. Centrifuge dynamic test scaling relations

4.3 Scope of the centrifuge tests

Dynamic centrifuge tests were performed on a model caisson breakwater, founded on medium-dense sand, without a bedding layer. The absence of a bedding layer makes the modelled structure especially representative for offshore gravity platform. The dimensions (caisson width of 13.5 m and water depth of 11.4 m in prototype scale) are however representative for a caisson breakwater rather than for an offshore platform. Thus, the model simulates the behaviour of breakwaters where the thickness of the rubble layer is small. The structure was subjected to cyclic horizontal loading simulating regular and irregular wave loading, until failure occurred. Different aspects were attempted: find a critical failure mechanism; investigate the influence of the loading scheme; analyse the development of instantaneous pore pressures and residual pore pressures in the sandy subsoil.

As discussed in Chapter 2, instantaneous pore pressure is pore pressure fluctuating during each wave cycle, caused by wave-induced fluctuations of the water pressures along the seabed and by the movements of the structure. It is induced by an elastic compression of the skeleton (positive instantaneous pore pressure) and by an instantaneous decompression (negative instantaneous pore pressure) in combination with a limited drainage. Residual pore pressure is caused by gradual contraction

related to gradual change of the strength and stiffness of the soil due to repetitive loading or consolidation. Boundary drainage conditions influence the development of residual pore pressures. Both pressures strongly depend on the mechanical behaviour of the soil under cyclic wave action and, generally, they are not considered by the traditional design approaches.

4.4 Model structure and model set-up

Three adjacent caissons, one central and two edge involving three-dimensional effects, constituted the modelled breakwater. In this thesis, only the central caisson behaviour has been considered, representative of a continuous breakwater wall. The base area of the central caisson was 0.225 m by 0.225 m that means 13.5 m by 13.5 m in the prototype structure. The effective weight of the caisson was 40.5 kN/m (2430 kN/m in prototype). The resulting effective stress at the bottom of caisson was 179.5 kPa. The breakwater was founded on a saturated sand layer with thickness 0.240 m (14.4 m in prototype). The Eastern Scheldt Sand, fine offshore coastal sand from Netherlands, was used for the soil layer. A loose layer of gravel of 0.03 m was added around the structure (1.8 m in prototype). The water around the caisson was not modelled and the absolute pressure corresponding to the water depth was obtained by applying a given air pressure on the saturated soil. As explained in the previous section, the pore water was replaced with a high viscosity fluid to prevent pore flow scale effects. A layer of fluid covered the model soil, in order to ensure the saturation of the soil during the test. A plunger (actuator) provided the horizontal force simulating wave action to the breakwater. A special frame to support the hydraulic actuator was built, fixed to the side of the model soil container. The actuator was attached on this frame with a hinged connection which permits free rotation along the horizontal axis perpendicular to the loading axis. This permits the actuator to follow the structure motion without perturbing the loading. No rotation around the vertical axis was allowed. On the actuator a counter weight was connected to compensate the weight of the loading frame. The actuator was connected rigidly to the loading frame of the caissons. Its point of application was located at 0.19 m from the caisson bottom (11.4 m in prototype, the simulated still water level).

Since the water around the caisson was not modelled the direct wave load on the seabed could not be considered. The effect of the wave action on the seabed has been accurately studied in the past (Prevost et al., 1975; Madsen, 1978; Yamamoto et al., 1978; Mei and Foda, 1980; Gatmiri, 1990). In this tests only the foundation behaviour due to the wave-induced action transmitted by the structure to the sand underneath the caisson could have been modelled.

The caisson movements were monitored using one horizontal displacement transducer (located in line with the point of application of load, at 190 mm above the caisson base) and two vertical displacement transducers. Also these transducers were located along the horizontal line of the actuator at 190 mm above the caisson base, at 70 mm from the centre line of the caisson, with mutual distance of 140 mm.

Pore pressures were investigated at two different depths, by means of two sets of five transducers, distributed along the central axis of the caisson: the first one (series *UM*) was placed at the interface between the structure bottom and the soil layer; the second one (series *US*) was located in the sand layer at 45 mm of depth (2.7 m in prototype).

In Figures 4.1 and 4.2 the test model and a simplified scheme of the structure have been reported.

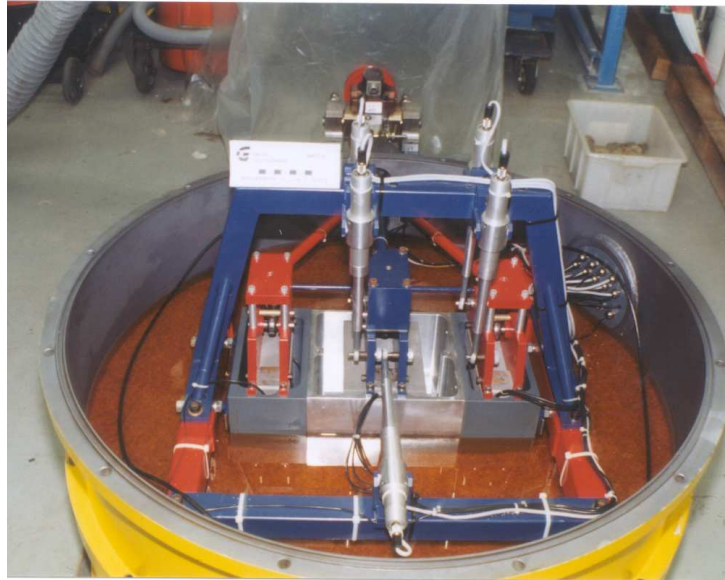


Figure 4.1 - Test model

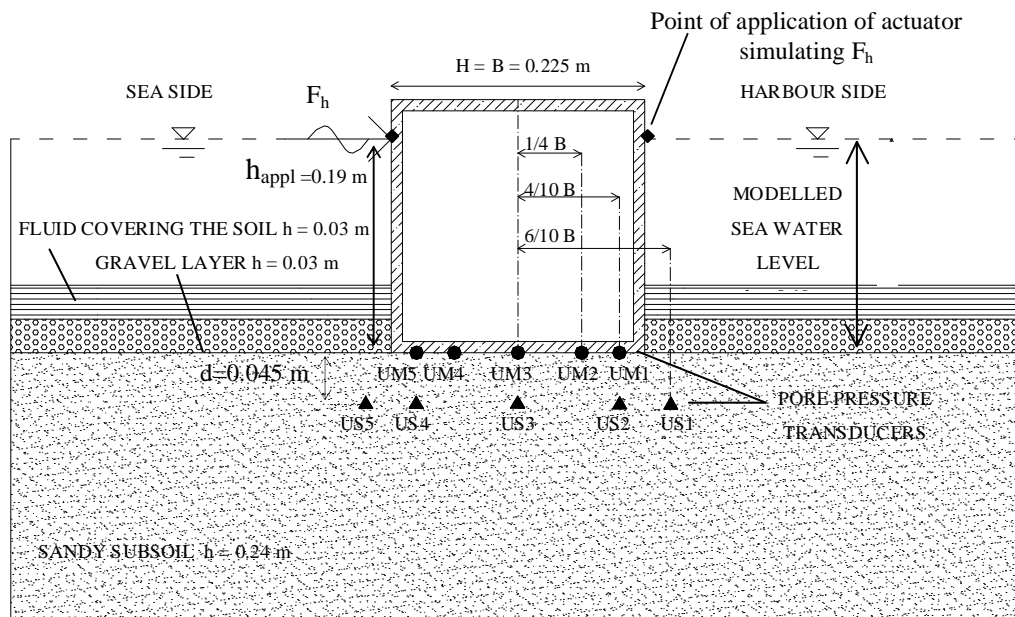


Figure 4.2 - Scheme of model structure (side view)

4.5 Loading scheme

Two different tests were performed in which several storms were simulated until failure.

In *Test 1* two storms with irregular wave loading were simulated, a small storm of short duration and a large one. Between the first and the second storm, a drainage period of 300 s was applied (5 hours in prototype).

In *Test 2* a combination of irregular and regular wave loading was simulated. It also consisted of two storms, separated by a drainage period of 180 s (3 hours in prototype). In the first storm a sequence of 8 "storm parts", each with a duration of ca. 90 s (1.5 hrs prototype) was applied, some storm parts with regular wave loading and others with irregular wave loading. In the second storm a sequence of regular 12 storm parts, also each with duration of 90 s, was adopted until complete failure. More specifically, the second test contained the following parts:

- *1th storm part* of regular waves, applied with a load equal to about 60% of the maximum peak load observed in the first test;
- *sequence of 6 storm parts (2nd-7th)* all with irregular wave loading, applied until to obtain an additional horizontal deformation equal to the deformation reached during the 1th storm part (1.7 mm in the model scale);
- *8th storm part* of regular waves concluding the first storm;
- drainage time of 180 s;
- *sequence of 12 storms parts (9th-20th)*, all with regular wave loading, making up the second storm and applied until failure occurred.

In both of the tests "failure" was declared as:

$$\max (U_{vert}, U_{hor}) \approx 20 \text{ mm (1,2 m in prototype)}$$

where U_{vert} and U_{hor} are respectively vertical and horizontal caisson displacements.

The value of 20 mm (1.2 m in prototype) was considered as a "threshold" in which the caisson loses its function.

Figures 4.3 and 4.4 show, in model scale, the loading scheme applied during the two tests. In the graphs, because of the model facility, positive peak load corresponds to the wave trough while negative peak load represents the wave crest. So, tension forces have been considered positive.

Both in the first and in the second test the irregular wave model was based on the results of some hydraulic tests performed in HR Wallingford (Allsop et al., 1996) and consisted of load parcel with duration of 9.62 s (9.62 minutes in prototype). In each parcel 48 waves were represent with wave period $T = 0,2$ s (12 s in prototype). Figure 4.5 shows the irregular wave load. Each regular storm part was constituted of eight blocks of regular wave loads with amplitude 0.125 times the maximum peak load, followed by a final block with duration 60 s (60 minutes in prototype) (Figure 4.6). A number of 25 waves constituted each block, with 5 s of duration (5 minutes in the prototype). Regular wave load had a very asymmetric, non-sinus type, shape and the period was also $T = 0,2$ s, with 33 ms for wave crest and 167 ms for wave trough. Figure 4.7 shows a sequence of regular waves, while a detail of regular wave load is reported in Figure 4.8.

In Table 4-2 details of the loading scheme are summarised.

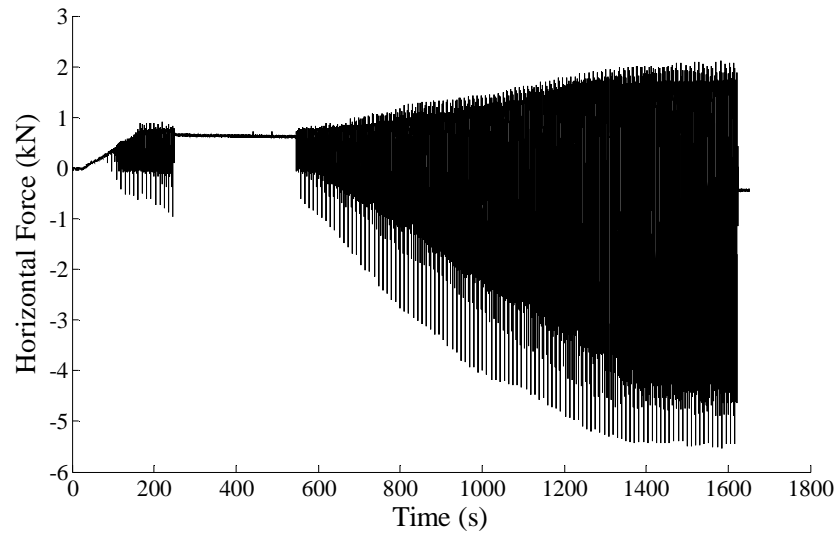


Figure 4.3 - Test I: scheme of total load

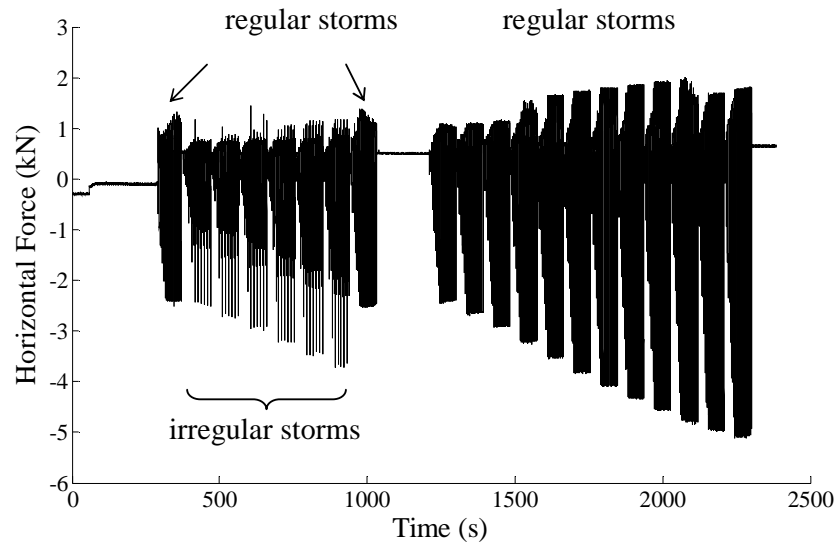


Figure 4.4 - Test II: scheme of total load

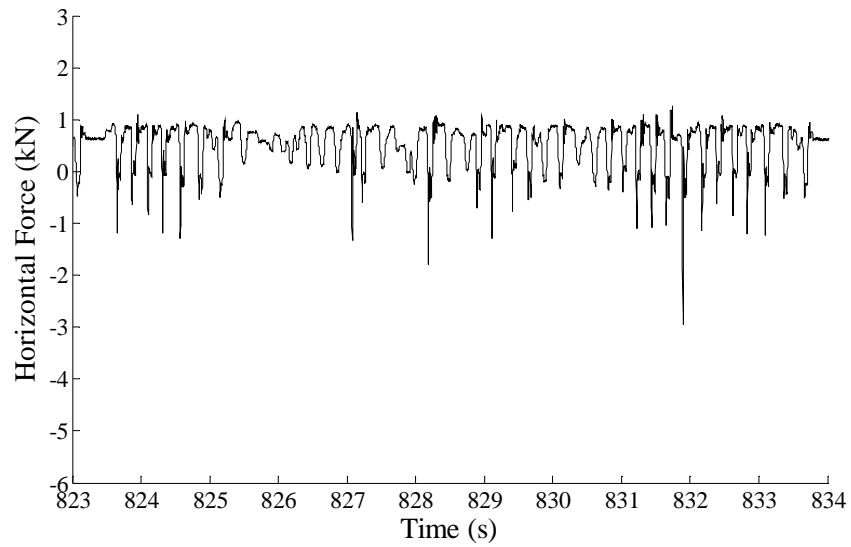


Figure 4.5 - Test I and storm parts 2-7 of Test II: irregular wave load

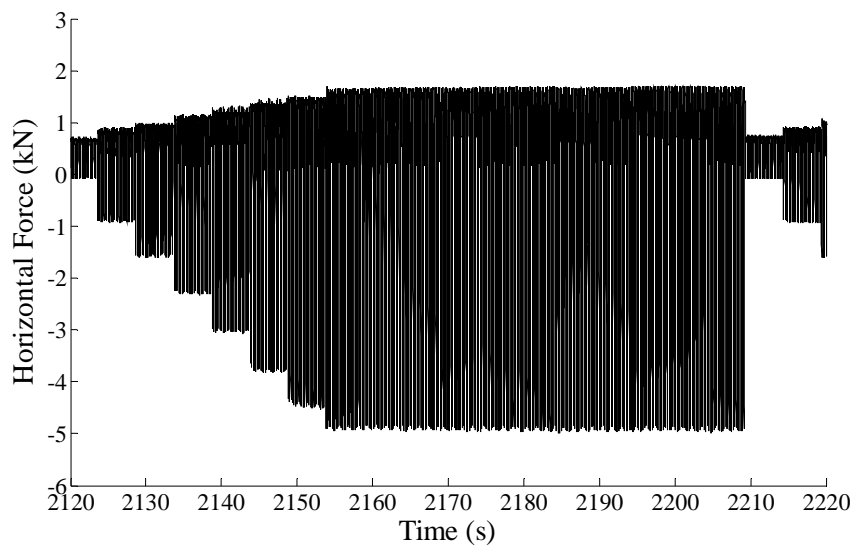


Figure 4.6 - Test II: blocks of regular loads making up one storm part (storm parts 1, 8, 9-20)

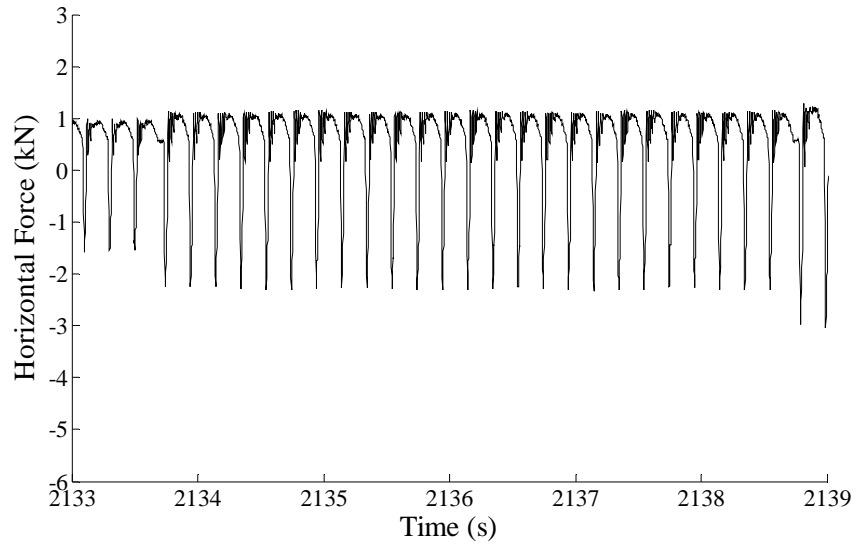


Figure 4.7 - Test II: sequence of regular waves

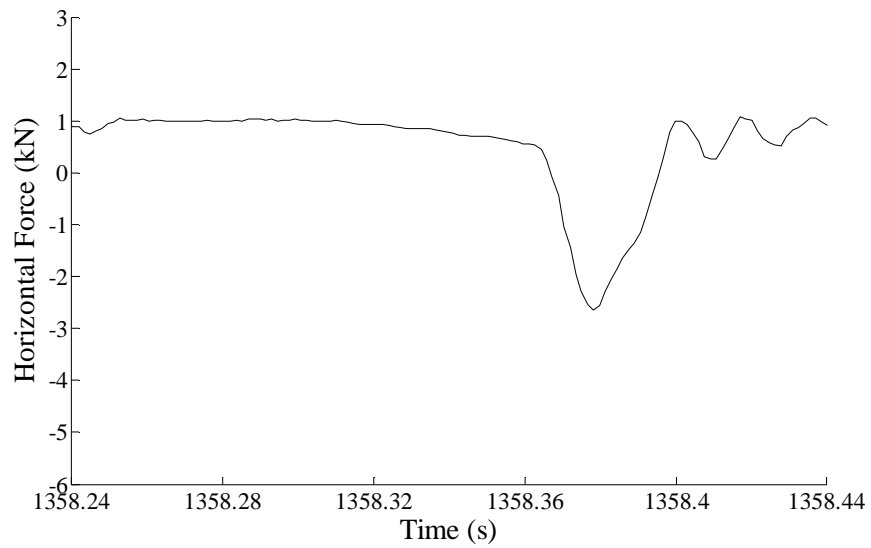


Figure 4.8 - Test II: detail of regular wave load

<u>TEST 1</u>										
	<i>Duration</i>		<i>HPV_i</i>		<i>I/wt</i>		<i>HPV_f</i>			
	m (s)	P (hrs)	m (kN)	p (MN/m)	m (kN)	p (MN/m)	m (kN)	p (MN/m)		
<i>First storm</i>	150	2,5	1,0	0,267	0,05	0,013	2	0,534		
<i>Second storm</i>	1074	18	1,5	0,400	0,10	0,027	5	1,335		
<u>TEST 2</u>										
<i>First storm</i>	<i>Duration</i>		<i>1st and 8th storm parts with regular wave loading</i>				<i>storm parts nrs 2 to 7 with irregular wave loading</i>			
			<i>HPV_i</i>		<i>HPV_f</i>		<i>HPV_i</i>		<i>HPV_f</i>	
	m (s)	P (hrs)	m (kN)	p (MN/m)	m (kN)	p (MN/m)	m (kN)	p (MN/m)	m (kN)	p (MN/m)
	741	13	0,5	0,133	3	0,801	3	0,801	4,5	1,201
<i>Second storm</i>	<i>Duration</i>		<i>storms parts nrs 9-20, with regular wave loading</i>							
			<i>HPV_i</i>		<i>I/wt</i>		<i>HPV_f</i>			
	m (s)	P (hrs)	M (kN)	P (MN/m)	m (kN)	p (MN/m)	m (kN)	p (MN/m)		
	1092	18	3	0,801	0,3	0,080	6,3	1,682		
<p><i>Notation:</i> <i>m</i> = model; <i>p</i> = prototype <i>HPV_i</i> = initial highest peak value of wave load applied <i>I/wt</i> = increment of peak wave load applied for load parcel (irregular wave) or storm part (regular wave) <i>HPV_f</i> = final highest peak value of wave load applied</p>										

Table 4-2. Loading scheme

4.6 Model soil

The physical and mechanical characteristics of the sand used in the model were analysed in the Soil Mechanics Laboratory at Aalborg University (Andersen et al., 1997).

From the grain size distribution curve a well-sorted sand type resulted, with $d_{50} = 0.17$ mm and Uniform Coefficient $U (d_{60}/d_{10}) = 1.52$ (see Figure 4.9). The specific weight is $\gamma = 2.65$ and the maximum and minimum void ratios, determined on the basis of the Danish Standard, are $e_{max} = 0.855$ (porosity $n = 46.1\%$) and $e_{min} = 0.591$ (porosity $n = 37.1\%$). The two centrifuge tests have been executed at a relative density respectively of $ID = 58.1\%$ and $ID = 58.0\%$. The values for the void ratio and porosity were respectively $e = 0.68$ and $n = 40.4\%$. The hydraulic conductivity at $1g$ was $k = 2.0 \cdot 10^{-4}$ m/s.

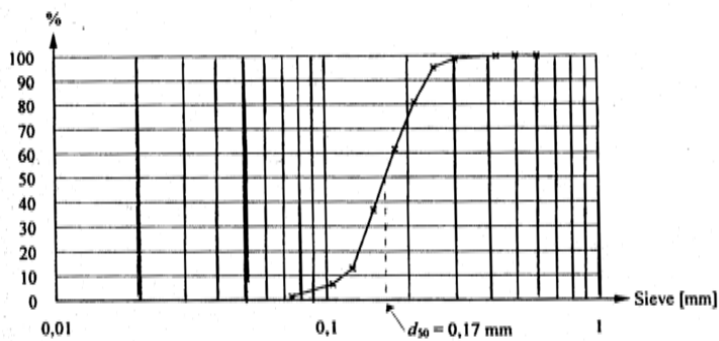


Figure 4.9 – Grain size distribution curve

Several *drained triaxial tests* were carried out with several loading and unloading cycles (Andersen et al., 1997). Specimens with two different void ratios have been tested: $e = 0.59$ and $e = 0.67$. These values correspond, respectively, to relative density of $ID = 99\%$ and $ID = 68\%$. Hence, tested specimens range from very dense to medium dense.

Amongst the performed triaxial tests, in three of them un- and reloading cycles have been executed before failure, during the hydrostatic compression, as well as during the subsequent shearing part of the tests. In these tests the characteristic state values

were not determined. In the remaining tests, the loading and reloading cycles have been executed only after the peak failure. In this case the performed tests enabled to determine stress and strain values corresponding with the peak failure and with the characteristic state (at which the behaviour of the sand changes from contraction to dilation).

In the graphs of Figure 4.10, 4.11 and 4.12 the curves resulting from a triaxial test with loading and reloading cycles executed after failure on a specimen with void ratio $e_0 = 0.67$, have been reported.

The curves show clearly the dilative behaviour. From the stress-strain behaviour observed during cyclic loading and reloading, the hysteresis between the loading and reloading lines appears. This means that plastic deformation occurred during the stress reversals and a change of void ratio was experienced. Moreover, besides the hysteresis experienced during large stress reversals, it is observed that, the current yield point reached, the stress-strain curve does not follow the direction of the curve before unloading, but it continues beyond the current yield point. Hence, probably an additive strengthening of the material was introduced.

For all the tested specimens, the following results, for the two void ratios respectively investigated, were obtained:

a) $e = 0.59$

- slope of the drained failure envelope $M_f = 1.45$
- slope of the characteristic state line $M_{CSL} = 1.22$
- secant friction angle: $\varphi_s' = 38.2^\circ$
- tangent cohesion and tangent friction angle: $c_t' = 54.3$ kPa; $\varphi_t' = 36.3^\circ$

b) $e = 0.67$

- slope of the drained failure envelope $M_f = 1.56$
- slope of the characteristic state line $M_{CSL} = 1.22$
- secant friction angle: $\varphi_s' = 35.5^\circ$
- tangent cohesion and tangent friction angle: $c_t' = 36.7$ kPa; $\varphi_t' = 34.1^\circ$

In Figures 4.13 and 4.14 the slopes of M_f and M_{CSL} for the two void ratios investigated are reported.

We observe that the characteristic state points are located on a straight line, independent of void ratio, that is the characteristic state line.

From the performed tests has been observed that, at the same confining pressure, a different stress-strain behaviour is evident for the two different void ratios. It has been seen that the dilation is more evident for the specimen with the smallest void ratio. In general, dense specimens exhibit a large amount of dilation before the maximum shear stress is reached, which causes a strengthening of the material. Looking at the confining pressure dependency, the strength of the sand increases with the confining pressure.

Stress-strain behaviour observed during the tests with cyclic loading performed after the failure, at the same confining pressure, evidenced that the denser specimen exhibits a stiffer stress-strain response and a larger amount of developed dilation during the test. Dilation development is larger for the test with the lowest confining pressure, meaning that a higher strength is present in this case.

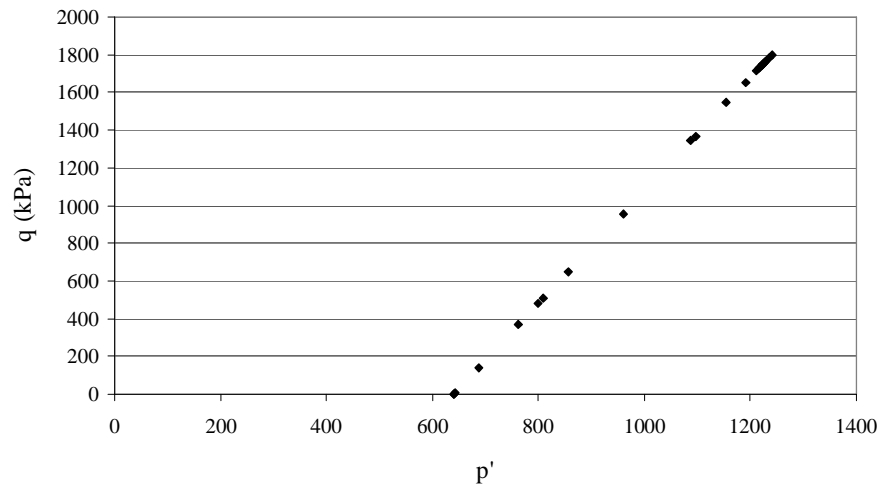


Figure 4.10 – Mean effective normal stress-Deviator stress

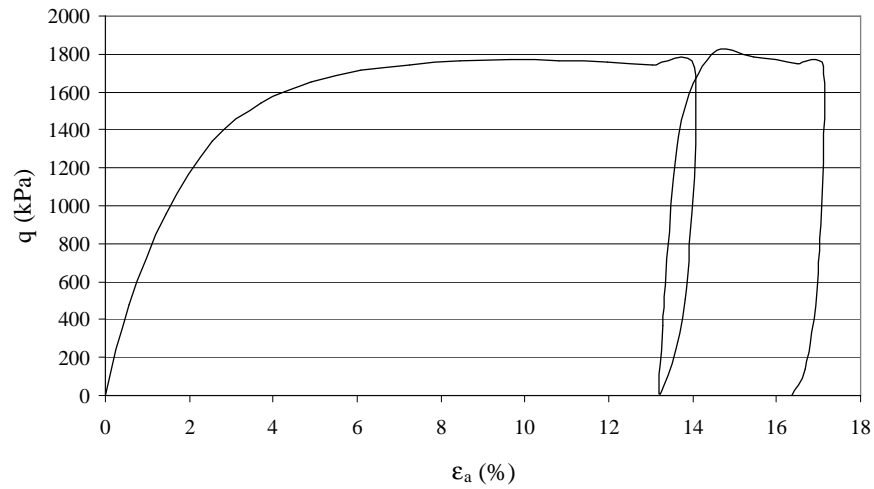


Figure 4.11 – Axial strain-Deviator stress

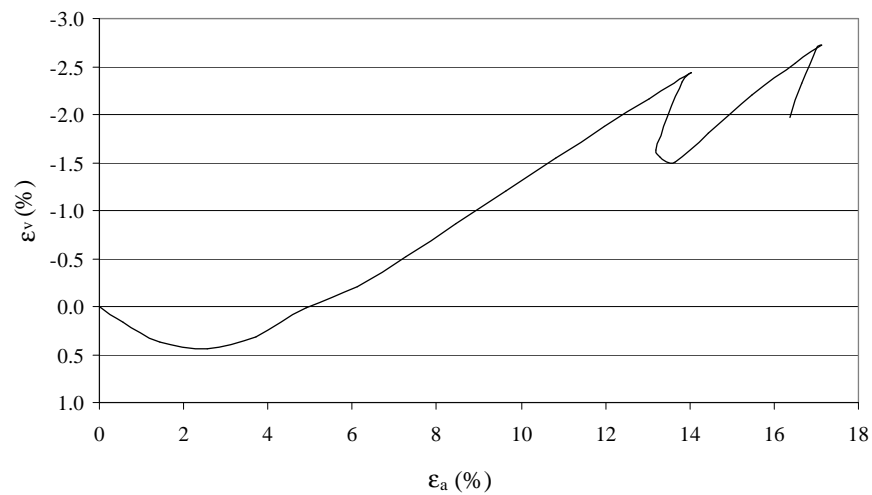
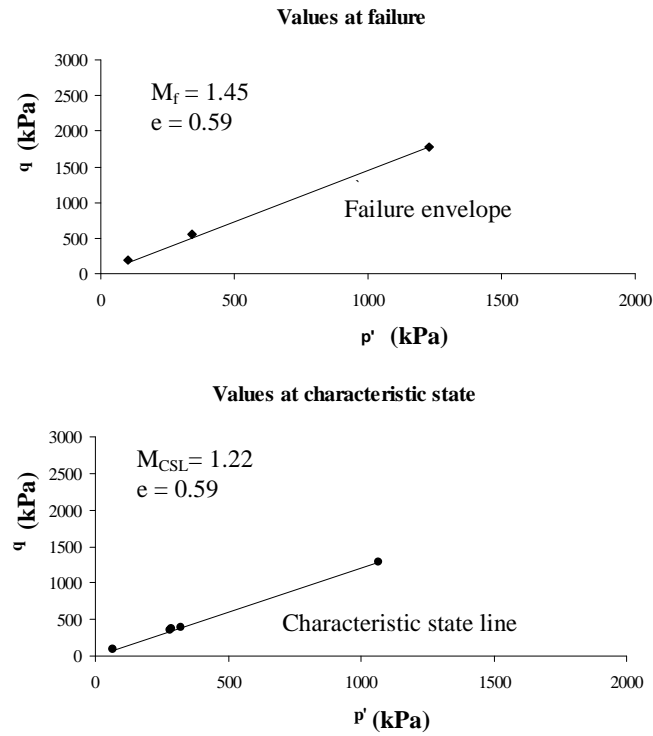
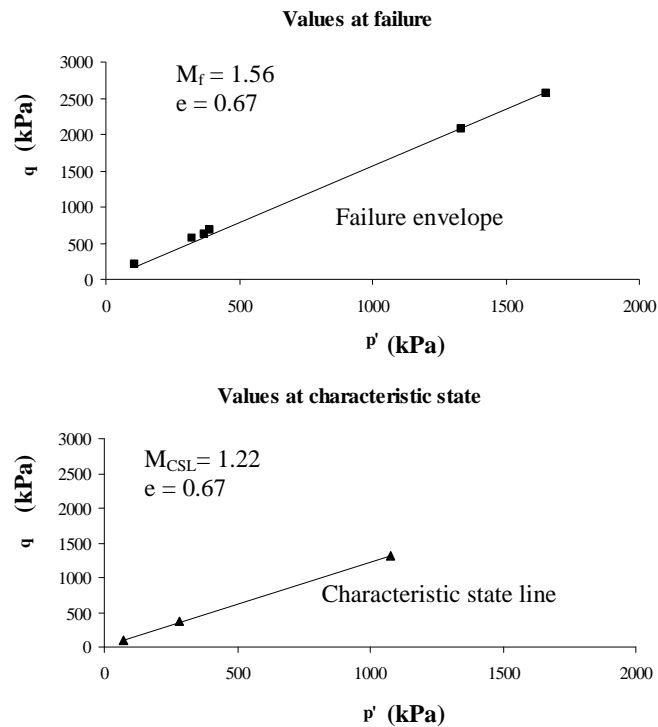


Figure 4.12 – Axial strain-Volumetric strain

Figure 4.13 – Slopes of failure envelope and characteristic state line for specimens with $e = 0.59$ Figure 4.14 – Slopes of failure envelope and characteristic state line for specimens with $e = 0.67$

4.7 Measurements and test results

As follows, the results are separately discussed, in model scale, for both tests and for their loading parts.

Being the caisson a structure with three degrees of freedom, the process leading the caisson to fail is studied by analysing the time history of horizontal displacements (U_h), vertical (U_v) displacements and tilting (M). In the graphs, vertical upward displacements have been considered positive and settlements negative. Horizontal displacements towards the actuator (harbour-side) have been considered positive. Rotations from the actuator direction to the vertical upward direction have been also considered positive.

Then, the measured pore pressures underneath the caisson are studied. In the graphs, pore water pressures are given with respect to the atmospheric pressure. Pore pressures were called respectively “EPP” (excess pore pressures) if positive (higher than the hydrostatic pressures) and “UP” (underpressures) if negative (lower than hydrostatic pressures).

Although all the measured data have been analysed in order to give an interpretation of the failure mode, as follows only a few selected graphs will be shown.

All the graphs of the measured displacements, rotations and pore pressures are reported in Annex I.

4.7.1 Test n. 1: two irregular storms

This test was performed in two steps, simulating two different storms, separated by a drainage period of 300 s.

First storm

a) Deformations

In the first storm, before the drainage period, very small vertical and horizontal displacements were recorded (Figures 4.15 and 4.16 for $100 \text{ s} < t < 250 \text{ s}$). The maximum amplitudes of the horizontal displacements, equal to 0.3 mm (18 mm in prototype), appear larger than the vertical ones, equal to 0.1 mm (6 mm in prototype)

at the harbour side. The values of settlements at the sea-side and the value of rotation are very small (see Annex I, Figures A4 and A5).

b) Pore pressures

Instantaneous pore pressures increased with load and the values in the subsoil were usually larger than the values at the caisson bottom (see Annex I, Figure A6 - Figure A15, for $100 \text{ s} < t < 250 \text{ s}$). This is in contrast to the general analytical pore pressure distribution with depth induced by the rocking motion of the caisson, for which a decrease of pore pressure would be expected. Probably, drainage along the caisson bottom occurred. Below the caisson there may have been a thin zone with a relatively high hydraulic conductivity, especially in the transducers closest to the edges (*UM1* and *UM5*), where the gravel layer could have influenced the drainage conditions. It has also to be considered that the interface between the caisson and the soil constitutes a “discontinuity surface”.

Both below the caisson and in the subsoil the maximum *EPP* was recorded at the harbour-side (equal to 100 kPa below the caisson (*UM1*) and 185 kPa in the subsoil (*US2*)). The *EPP* is very low at the centre and increases at the sea-side, even though it is lower than the values at the harbour-side (maximum values of 25 kPa below the caisson (*UM1*) and 55 kPa in the subsoil (*US4*)).

As concerns the *UP* below the caisson, a minimum value of $UP = -30 \text{ kPa}$ was recorded at the harbour-side (*UM1*), while a value of $UP = -45 \text{ kPa}$ was recorded at the sea-side (*UM5*). Very small values, almost zero, were observed in the middle of the caisson (*UM3*). The minimum values of *UP* in the subsoil were -75 kPa (*US2*) at the harbour-side and -90 kPa at the sea-side (*US4*).

The transducers placed in the subsoil at $\pm 6/10 B$ (*US1*, *US5*) recorded very small values of excess pore pressures and underpressures. This means that, in this phase, the loading has influenced only the area of subsoil limited by the base of the caisson.

No residual pore pressures were recorded.

Second storm

In the *second storm* the load was gradually increased to a maximum value and kept at this level for approximately 150 s (1.5 hours on prototype), until failure occurred.

a) Deformations and failure

A fast increase of both horizontal and vertical deformation was observed during this storm, with horizontal displacements larger than the vertical ones (see Figures 4.15 and 4.16 for $548 \text{ s} < t < 1622 \text{ s}$). Failure occurred after approximately 1080 seconds (about 18 hours in prototype) as an excess of horizontal displacements at the top of the caisson. The maximum load applied at the end of the test was 5 kN (1.33 MN/m in prototype). The failure was a combination of horizontal sliding and rotational failure toward harbour-side (see also Annex I, Figure A5), most likely due to the asymmetry of the load, with a wave crest load much larger than the wave trough load.

The deformations were developed during the highest peak loads of each wave train (Figures 4.17, 4.18 and 4.19). The irregularity and the asymmetry of the applied load induced horizontal displacements larger than settlements. High peaks induce only small additional vertical displacement and the largest part of settlements is due to the lower peaks. Conversely, high peaks of load cause a large increment of horizontal deformation.

At larger loads the velocity of the generation of plastic deformations remains constant and becomes independent of the peak load.

The failure did not occur as a consequence of one extreme load but as a result of several small plastic horizontal displacements, after a sufficient number of cycles.

At failure, horizontal displacements of 18.9 mm (1.13 m in prototype) were measured and settlements of 12.4 mm (0.74 m in prototype) and of 4.5 mm (0.27 m in prototype) were respectively recorded at the harbour-side and at the sea-side (see also Annex I, Figure A4). The rotation of the caisson was equal to 0.056 rad (about 3 degrees) toward the harbour-side (see Annex I, Figure A5).

b) Pore pressures

The analysis of pore pressures revealed no presence of residual pore pressures at the end of the test. It appears that the time needed for drainage was smaller than the total duration of wave train.

On the contrary, extremely high positive and negative instantaneous pore pressures were observed, also in this case usually larger in the subsoil than underneath the caisson bottom (see Annex I, Figure A6-Figure A15).

Both in the subsoil and at the interface, the *EPP* at the harbour-side was larger than the *EPP* at the sea-side.

At the interface, maximum values of *EPP* = 275 kPa and *EPP* = 90 kPa were measured respectively at the harbour-side (UM1) and at the sea-side (UM5). The minimum values of *UP* were respectively equal to *UP* = -170 kPa at the harbour-side (UM1) and *UP* = -185 at the sea-side (UM5).

In the subsoil, at the harbour-side (US2), the maximum *EPP* exceeded the registration limit (550 kPa). Lower values were usually recorded in the middle (US3, *EPP* = 170 kPa) and at the sea-side (US4, *EPP* = 195 kPa).

An opposite distribution is observed for the underpressures, although the differences are not so remarkable in the minimum values (US2, *UP* = -225 kPa; US3, *UP* = -225 kPa; US4, *UP* = -225 kPa).

It is important to observe that the minimum values of *UP* are so low to exceed the absolute minimum pressures, in which cavitation occurs. So, because of values lower than the cavitation values are physically impossible, they were probably caused by the pore pressure transducers and should be disregarded.

The excess pore pressures recorded by the transducers placed in the subsoil at $\pm 6/10 B$ (US1, US5) became significant in this phase. This means that some stress redistribution occurred at large loads.

In both sides, *EPP* and *UP* did not increase linearly with load and the maximum values did not occur at the maximum load applied but at lower loads (see example of Figure 4.20).

Recorded values of *EPP* were so high to exceed the estimated applied weight load of the caisson at rest, being about 180 kPa, leading to think that the effective stresses were likely to be almost zero. Nevertheless, liquefaction flow failure was not triggered and the failure mechanism occurred as previously discussed.

An interpretation of the occurred failure process, based on probable dilation effects of sand, is given in Section 4.8.

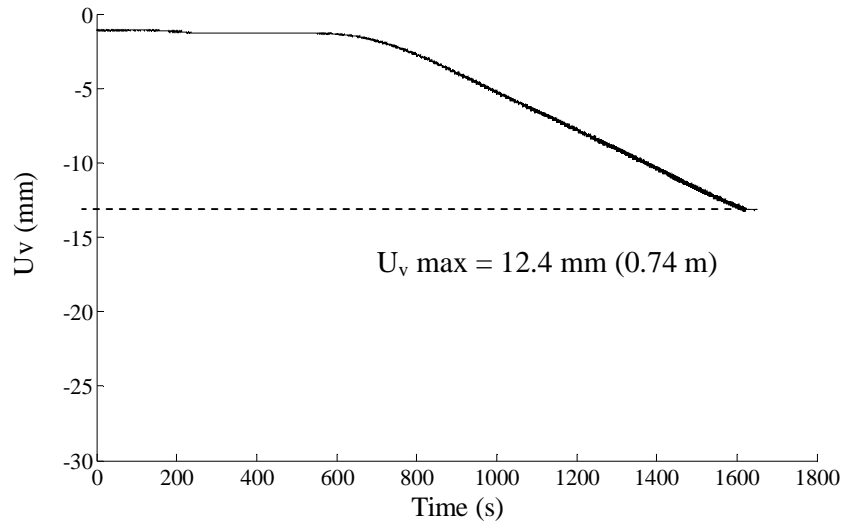


Figure 4.15 – Vertical displacements at the harbour-side

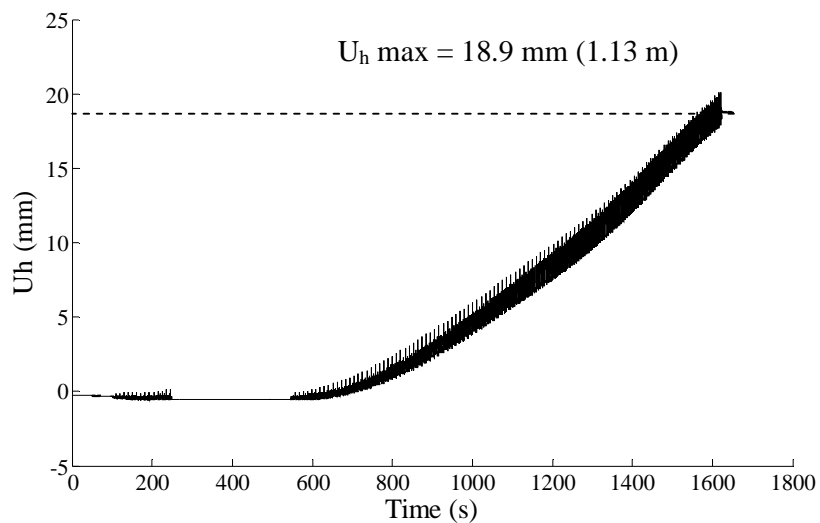


Figure 4.16 – Horizontal displacements

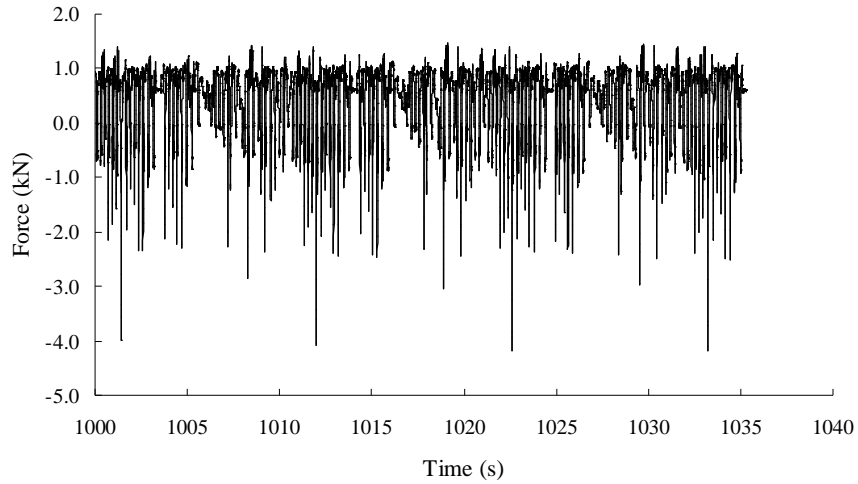


Figure 4.17 – Detail of applied force, between 1000 and 1035 s

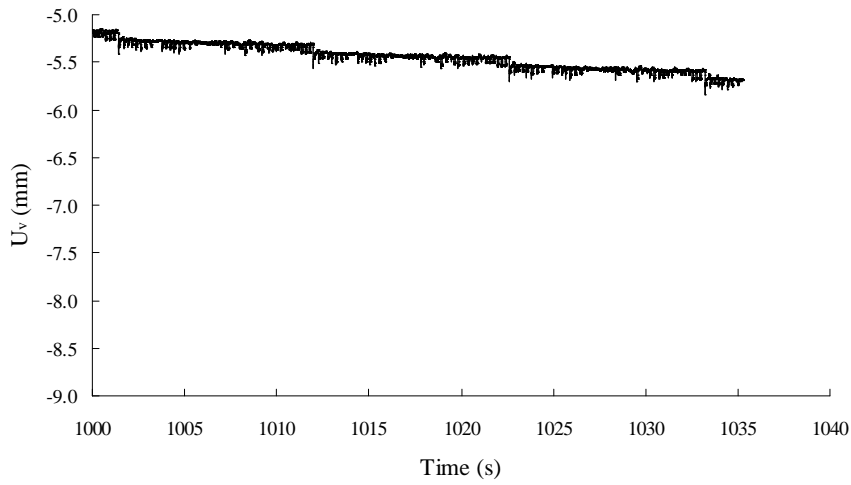


Figure 4.18 – Detail of vertical displacements (harbour-side), between 1000 and 1035 s

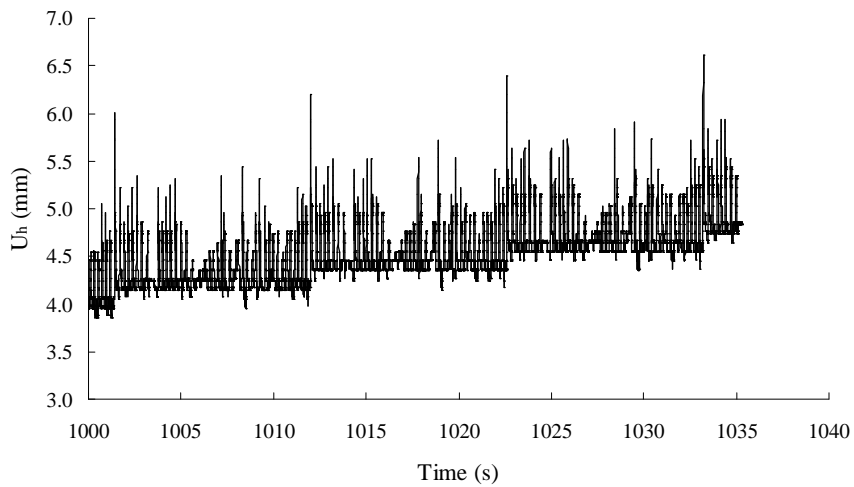


Figure 4.19 – Detail of horizontal displacements, between 1000 and 1035 s

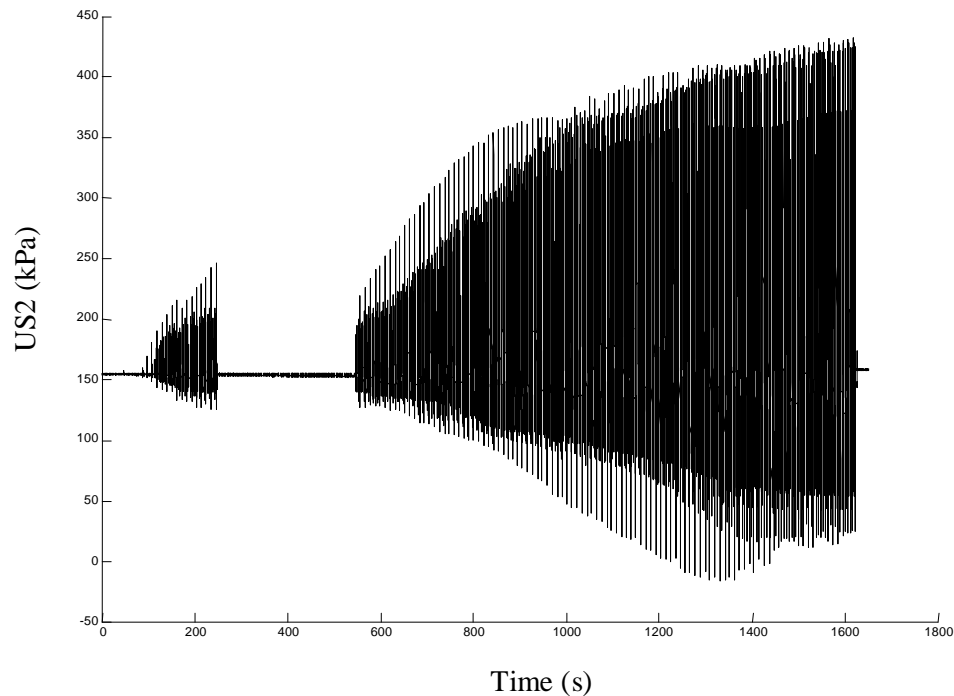


Figure 4.20 – Example of non-linear behaviour of *EPP* and *UP* with load

4.7.2 Test 2: regular/ irregular storms and regular storms

First storm: 1th “storm part” with regular wave loading

a) Deformations

Within the first storm part the caisson was not led to failure but it was loaded with a load approximately equal to 60% of the maximum peak load observed in the first test. This storm part resulted in an horizontal deformation equal to 1.7 mm (0.10 m in prototype). As opposed to the irregular loads, settlements larger than horizontal displacements were recorded during these regular loads, causing an increase of the initial relative density. The regularity of the applied load seems to have significant influence on the deformation mechanism, inducing almost uniform settlements of the structure. Values of settlements of 4 mm (0.24 m in prototype) were recorded at the

harbour-side and values of 3.8 mm (0.23 m in prototype) were measured at the sea-side. Tilting of caisson in harbour-side direction is very small (0.085 rad, equal to about 0.5 degrees).

Most of deformations (about 62% of total horizontal displacements) took place after 40 s (40 minutes in prototype) and they occurred in correspondence of the increase of each stepwise load (Figures 4.21 and 4.22).

b) Pore pressures

Underneath the caisson, for both of depths, the same distribution of instantaneous pore pressures observed during the first test was recorded, with higher values of *EPP* at the harbour side and higher values of *UP* at the sea-side (see Annex I, Figure A21-A30, first storm part).

An important difference with the Test 1 is found for all pore pressure transducers: the development of residual pore pressures. This can be clearly observed in the example of Figure 4.23, between 290 s and 320 s. Every stepwise load increase led to a new generation of residual pore pressures. They were probably developed because of the short time between the highest peaks (0.2 s equal to 0.2 minutes in prototype) that prevented the drainage. Residual pore pressures were not observed in the first test where the time between the highest peaks was longer and equal to 9.62 s. However, they dissipated at the end of the storm part and they did not influence the failure.

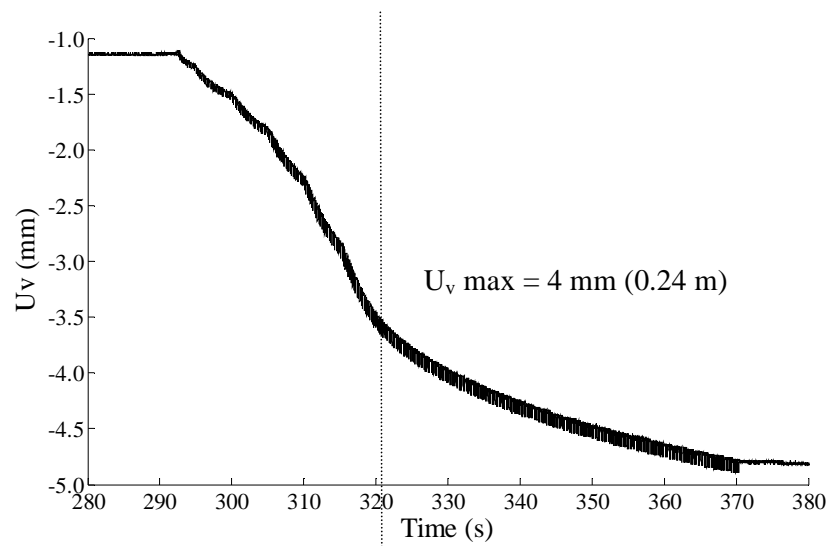


Figure 4.21 - Test II (1th storm part): vertical displacements at the harbour-side

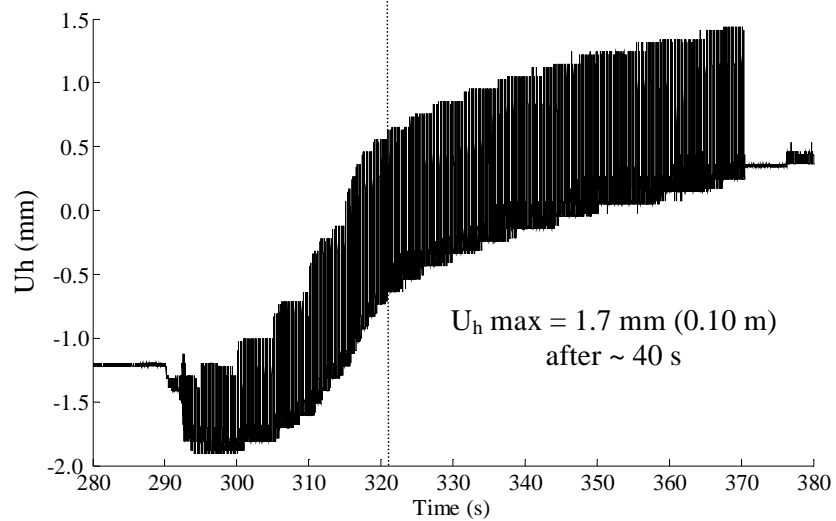


Figure 4.22 - Test II (1th storm part): horizontal displacements

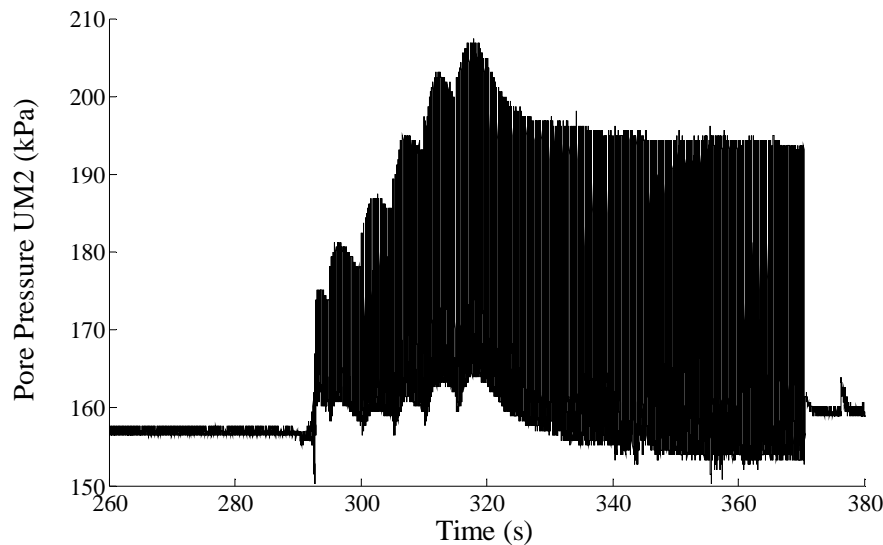


Figure 4.23 - Test II (1th storm part): development of pore pressure, including residual pore pressures at the harbour-side

First storm: 2nd - 7th “storm parts” with irregular wave loading

a) Deformations

By means of this sequence of storm parts an additional horizontal deformation of 1.7 mm was obtained (Figure 4.24). This was achieved with 6 irregular storm parts after 520 s and with a highest peak value of ca. 5 kN (1.33 MN/m in prototype). During the previous regular storm part, the same horizontal deformation was reached faster. This can be explained because the peak load was applied during every wave in the regular storms and just once in 48 waves in the irregular storm.

Vertical displacements were smaller than the horizontal ones and they slowly increased with time at the harbour-side (Figure 4.25), while they remained almost constant at the sea-side (Annex I, Figure A19, 2nd – 7th storm parts, 350s<t<950s).

b) Pore pressures

Very high instantaneous pore pressures were recorded. The maximum values of *EPP* and *UP* were recorded during the last storm of the sequence (see Annex I, Figures A21-A30, 7th storm part). Within this storm, underneath the caisson bottom (UM1), a value of 230 kPa of *EPP* was measured at the harbour-side, while lower values, respectively equal to 45 kPa and 40 kPa, were found at the centre (UM3) and at the sea-side (UM5). In the subsoil, at the harbour-side (US2), the maximum excess pore pressure was significantly high (660 kPa), lower at the centre (US3, *EPP* = 70 kPa) and at the sea-side (US4, *EPP* = 130 kPa).

Also in this case, the maximum values of *EPP* exceeded the estimated applied weight load of the caisson at rest and it can be hence supposed that the effective stresses were likely almost zero. In spite of such a high values of the *EPP* and large strains, the caisson did not fail for liquefaction, as it could be expected.

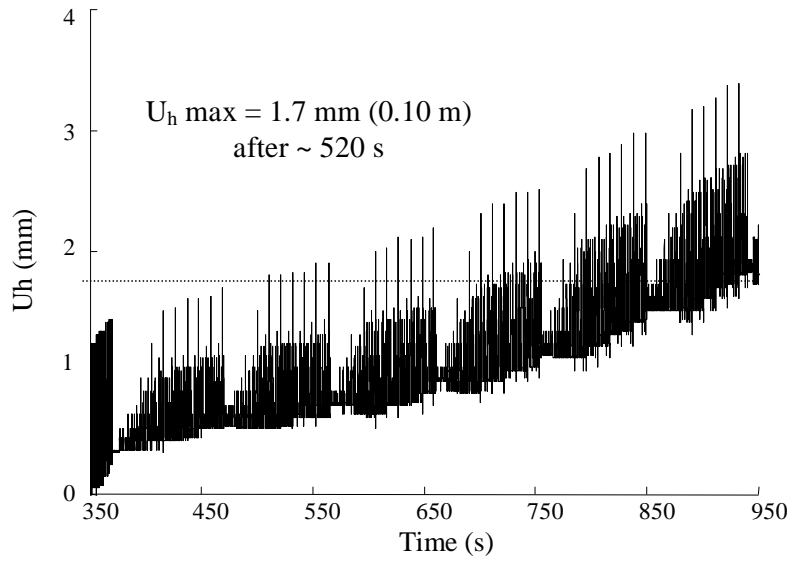
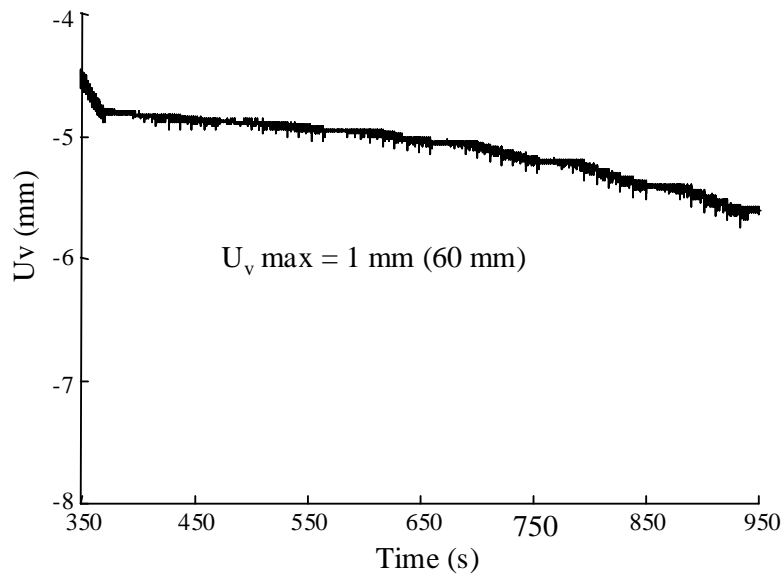
At sea-side very high values of *UP* were induced. Below the caisson, a value of -90 kPa was recorded at the harbour-side (UM1) and a value of -110 kPa was measured at the centre (UM3) and at the sea-side (UM5). The values of the underpressures in the subsoil were very high, respectively equal to -225 kPa at harbour-side (US2), equal to -135 kPa in the middle (US3) and equal to -225 kPa at the sea-side (US4).

Also in this case, the values of underpressures exceeded the absolute minimum (cavitation) pressures and values lower than cavitation should be disregarded.

Larger values of excess pore pressures at the harbour-side and lower values at the sea-side, in combination with an almost opposite distribution for underpressures, may have induced larger settlements at the front side compared to the back. Here, vertical deformations are practically negligible.

Concerning the pore pressures recorded by the transducers sited in the subsoil at $\pm 6/10$ B, at the harbour-side the maximum excess pore pressures was 115 kPa, while at the sea-side was 55 kPa. The underpressures were respectively -155 kPa and -125 kPa.

No residual pore pressures were found.

Figure 4.24 - Test II (2nd -7th storm parts): horizontal displacementsFigure 4.25 - Test II (2nd -7th storm parts): vertical displacements at the harbour-side

First storm: 8th “storm part” with regular wave loading

a) Deformations

Before the drainage period a last storm part of regular wave loading concluded the first part of the Test II. It had the same highest peak value applied in the previous 1st storm part (3kN equal to 0.8 MN/m in prototype). Settlements quickly increased, much more than during the irregular storm parts but much less rapidly than during the first regular storm part. They were approximately equal to 10% of the vertical displacements caused by the first regular storm part (see Figure 4.26).

Such a reduction of settlements can be associated to “precycling” phenomena of sand (Bjerrum, 1973, Andersen et al. 1976, Smits et al., 1978), due to the cyclic action of the previous storm parts, with higher loads applied, which induce compaction of the soil and its increase in stiffness. The same effect is obviously observed on the rocking motion of caisson. The “benefic” effect of precycling is particular interesting from a practical engineering point of view and it has been observed also during the life of real structures (Grisolia and Maccarini, 2004; Maccarini et al., 2005).

b) Pore pressures

As concerns pore pressures distribution along the caisson and with depth, behaviour similar to the previous storm parts is observed. Values similar to the measured values in the first regular storm were recorded (see Annex I, Figures A21-A30, 8th storm part).

No residual pore pressures were found.

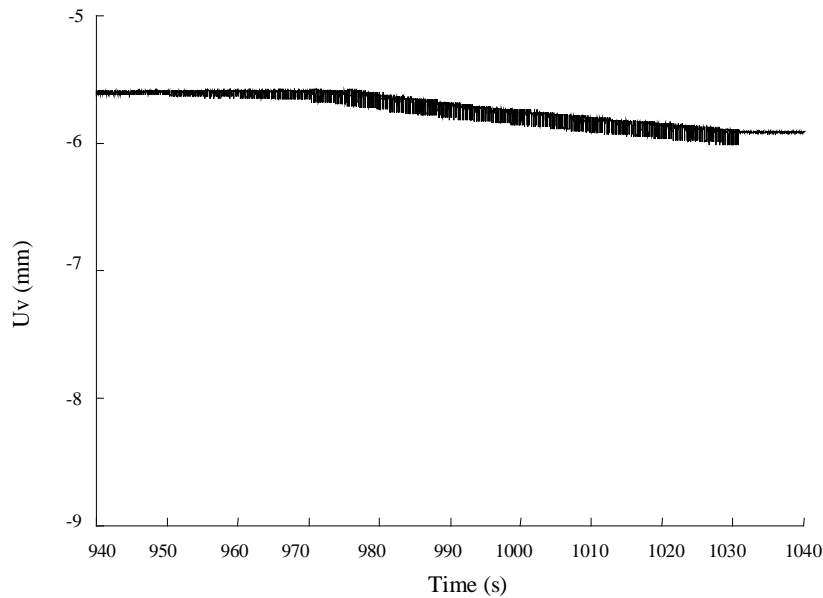


Figure 4.26 - Test II (8th storm part): vertical displacements at the harbour-side

Second storm: 9th-20th “storm parts” with regular wave loading until complete failure

a) Deformations and failure

After the drainage period the test proceeded applying several regular storm parts with increasing amplitudes, until complete failure. Failure occurred after 12 regular storm parts in 1090 s (about 18 hours in prototype) and in 2300 s from the beginning of test (about 38 hours in prototype), inducing a maximum horizontal deformation at the top of the caisson equal to 20.9 mm (1.25 m in prototype). Vertical displacements at failure were lower than the horizontal ones and respectively equal to 14.1 mm (0.85 m in prototype) at the harbour-side and 6.5 mm (0.39 m in prototype) at the sea-side (see Annex I, Figures A17, A18 and A19). Plastic deformation velocity increases with the peak load. The displacement curves become steeper from the 15th storm part and very steep from the 18th storm part until failure, especially in the case of horizontal displacements (see Figures 4.27 and 4.28).

In this case regular wave loading induced, at failure, horizontal displacements larger than settlements. This is apparently in contrast with the behaviour observed during the first storm part, also with regular wave loading. On the other hand, we note that, before the 18th storm part is applied, settlements and horizontal displacements increase almost with a similar trend. From the 18th storm part until failure horizontal displacements increase much faster than settlements. Approaching the maximum load (6.3 kN) the plastic horizontal displacement velocities increased very fast.

The history experienced by the structure during the previous irregular storm parts could have had significant influence on the general caisson's behaviour.

The observed failure mechanism, as in the case of irregular storms, can be regarded as a combination of horizontal sliding and rotation (0.05 rad equal to about 3.1 degrees, see Annex I, Figure A20) and it occurred according to a step-by-step process.

Detailed results (Figure 4.29, 4.30 and 4.31) show the development of irreversible displacements for each peak load.

b) Pore pressures

Once again the highest values of pore pressures were induced in the subsoil and at the edges of the caisson (see Annex I, Figures A21-A30).

Underneath the caisson bottom, at the harbour-side (UM1), the maximum value of *EPP* was 280 kPa and the maximum *UP* was -120 kPa. In the central zone (UM3) the values of *EPP* and *UP* were lower than the values at the edges and a linear increase with load is observed. At the sea-side (UM5) the maximum *UP* was -200 kPa (exceeding cavitation pressure), while the maximum *EPP* was 90 kPa.

Concerning the pore pressures in the subsoil, very high values were measured at the harbour-side (US2, *EPP* = 740 kPa and *UP* = -225 kPa). At the centre (US3) values respectively equal to *EPP* = 130 kPa and *UP* = -220 kPa (exceeding cavitation pressure) were recorded. At the sea-side (US4) the maximum *EPP* was 155 kPa and the maximum underpressure was - 220 kPa (exceeding cavitation pressure).

As in the previous cases, values exceeding the cavitation pressure should be disregarded.

The highest value of *EPP* was measured at harbour-side during the 18th storm part. During the same storm a strong increase of horizontal deformation was also observed.

Also in this case, *EPP* at the harbour side were so high that in this region it may be supposed that the effective stresses become instantaneously zero, with (instantaneous) tendency of sand to partially liquefy. Although high values of *EPP* and large deformations occurred, as observed in the previous storm parts and during the first test, the failure did not occur as a result of flow liquefaction.

The pore pressure transducers in the soil at $\pm 6/10$ B showed respectively 255 kPa (US1) and 40 kPa (US5) of maximum *EPP* and –105 kPa (US1) and –110 kPa of underpressure (US5).

No underpressures were found.

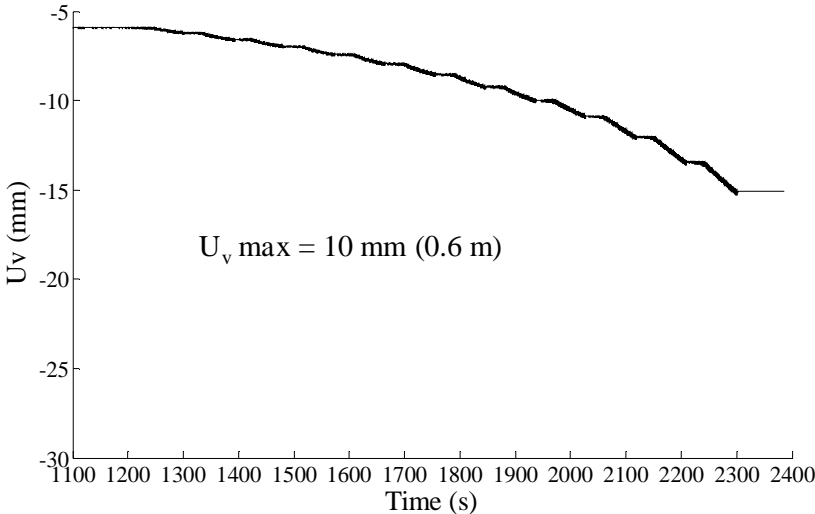


Figure 4.27 - Test II (9th -20th storm parts): vertical displacements at the harbour-side

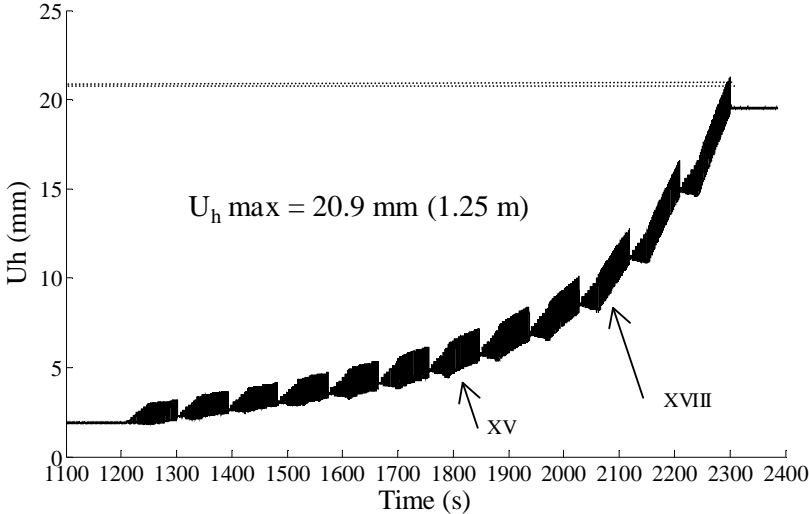
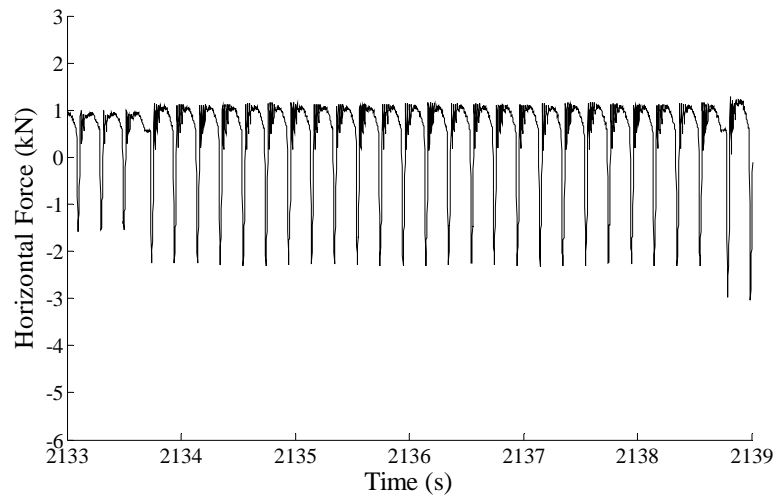
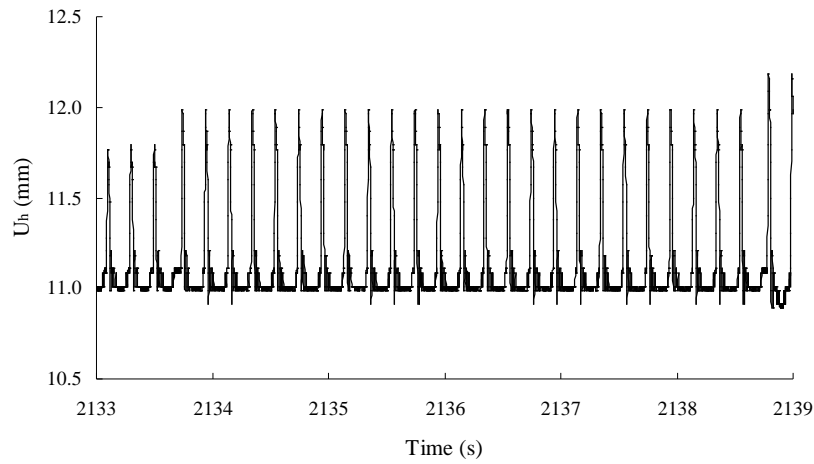
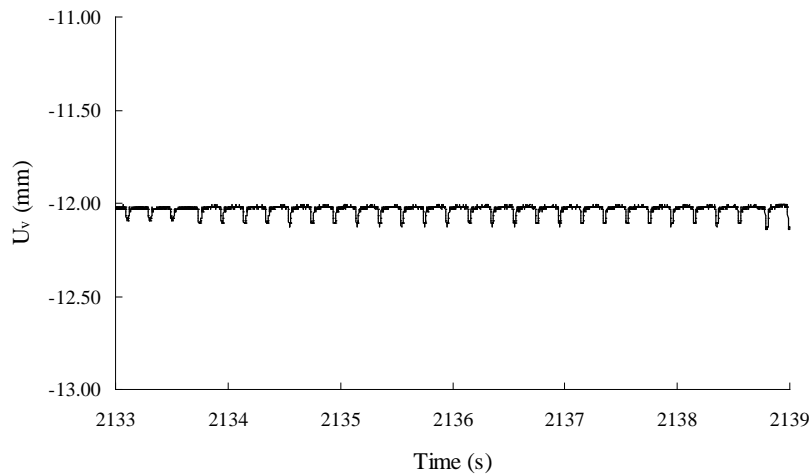


Figure 4.28 - Test II (9th -20th storm parts): horizontal displacements

Figure 4.29 – Test II (18th storm part): detail of applied forceFigure 4.30 – Test II (18th storm part): detail of horizontal displacementFigure 4.31 – Test II (18th storm part): detail of vertical displacement at the harbour-side

4.8 Failure mechanism: role of instantaneous pore pressures and cyclic mobility

In the previous Sections it has been shown that, for both tests, failure occurred according to a mechanism not expected and which is not generally considered by the traditional design approaches.

Failure involved the foundation soils but it did not take place as a consequence of a specified significant wave load. A step-by-step failure's process was observed, with progressive displacements and rocking motion toward the harbour-side direction.

The direction of the sliding and rotation toward harbour-side can be explained by the asymmetry of load, with wave crest much larger than wave trough, both for regular and irregular storms.

The general pore pressure distribution along the base of the caisson, with higher values of *EPP* at the harbour side and higher values of *UP* at the sea-side, can be attributed to compression-decompression phenomena of the sand subsoil, due to the rocking motion of the caisson. Positive excess pore pressures at the harbour-side can be associated with the wave crest, while positive excess pore pressures at the sea-side are induced by the wave trough. Since the wave crest is much larger than the wave trough, the induced values of *EPP* are higher at harbour-side than at the sea-side. As concerns the *UP* they can be associated to the wave trough at the harbour-side and to the wave crest at the sea-side.

Values of *EPP* at harbour-side higher than the estimated applied weight load of the caisson at rest, lead to the assumption that the effective stresses became instantaneously (nearly) zero in a significant part of the potential rupture surface, with possible tendency to liquefaction. On the other hand, even though large deformations are observed, liquefaction flow failure did not occur.

More detailed analyses of the development of pore pressures with load make clear that the *EPP* do not increase continuously with load, but a strong reduction follows during the last part of loading and within the unloading.

In Figure 4.32 an example of this behaviour has been reported. In the graphs are respectively represented the wave cycle applied and the development of instantaneous pore pressures observed in the subsoil, at the harbour side, during the Test II, 16th storm part.

We observe that in correspondence of the first 0.05 s ($2073.80 < t < 2073.85$) and the last 0.05 s ($2073.90 < t < 2073.95$) the load applied is shifted to 1.5 kN, as a consequence of the previous part storms applied, and the measured pore pressure is close to the hydrostatic pore pressure. Here, the value of *EPP* and *UP* is zero.

As long as the wave crest is applied pore pressures starts to increase until a positive peak of *EPP* is reached. Then, meanwhile the wave crest is still increasing, a strong reduction of pore pressures follows. During unloading pore pressures continue to decrease but much slower than the reduction observed during the final loading phase. The peak of *UP* is reached before the occurrence of the wave trough. Then, during the last part of wave crest unloading, pore pressure seems to slowly increase. The behaviour of pore pressures induced by the wave trough is not easy to be examined, because of the small negative peak load applied.

The development of *EPP* at harbour-side during the first part of the wave crest loading can be associated to isotropic compression of the skeleton. The strong reduction of *EPP* during the same loading phase could be explained by the tendency of sand to dilate in undrained condition, mobilised by the shearing, in concomitance of high deformations experienced by the sand. In this hypothesis the tendency to dilate during the final loading phase results in a decrease of pore pressure.

Such phenomenon might have played an important role in the observed progressive failure of the caisson. It follows, in fact, that complete liquefaction could not occur since there was not a continuous and homogenous increase of positive pore pressure, not only at the end of the loading cycles but also within each cycle of loading. Hence, the effective mean pressure did not become completely zero but a sort of local “recovering” of strength is supposed during each cycle. Correspondingly the failure resulted in progressive limited soil deformations without liquid-like flow and the observed failure mechanism can be associated to cyclic mobility failure mechanism, according to the concepts discussed in Chapter 3.

This behaviour could also explain the non-linear development of pore pressures with load, as observed in the example of Figure 4.20.

It is important to observe that two important conditions contribute to suppose the occurrence of phenomenon close to the cyclic mobility.

The first one is a sufficient high relative density of the sand to mobilise dilation with increasing loading. The dilative behaviour of sand has been already discussed in Section 4.6.

The second one is the instantaneous limited drainage conditions that converted the tendency to dilate in increasing of negative pore pressures and consequent increasing in effective stresses.

The drainage conditions depend on the wave period (T) and on the so-called 'characteristic drainage period' of the soil ($T_{CHAR,DRAIN}$). According to De Groot et al. (2004), $T_{CHAR,DRAIN}$ is mainly determined by a combination of two physical phenomena:

- elastic storage of some pore water in the pores, due to the elastic compressibility of the skeleton (α) and the compressibility of the pore water (β);
- flow resistance in subsoil, as determined by the permeability (k) of the soil and by the distance (d) over which the excess pore water flows to the surface.

Analytical modelling of these phenomena yields the following expression of the characteristic drainage period with a homogeneous sandy seabed:

$$T_{CHAR,DRAIN} = d^2/c_v$$

where d is the characteristic drainage distance and $c_v = k/\{\gamma_w(\alpha + n\beta)\}$ is the elastic consolidation coefficient, with k hydraulic conductivity, γ_w fluid unit weight, α and β respectively elastic compressibility of the skeleton and compressibility of pore water, n porosity. In the centrifuge tests $d = 0.1125$ m equal to the half width of the caisson m, $k \cong 2 \cdot 10^{-4}$ m/s, $\alpha \cong 5 \cdot 10^{-5}$ m²/kN and $\beta \ll \alpha$ (high degree of saturation). Hence, values of $c_v \cong 0.0066$ m²/s and $T_{CHAR,DRAIN} \cong 2s \cong 10 T$ are found. This condition occurred during each load and consequently undrained behaviour of a large part of the relevant subsoil can be supposed.

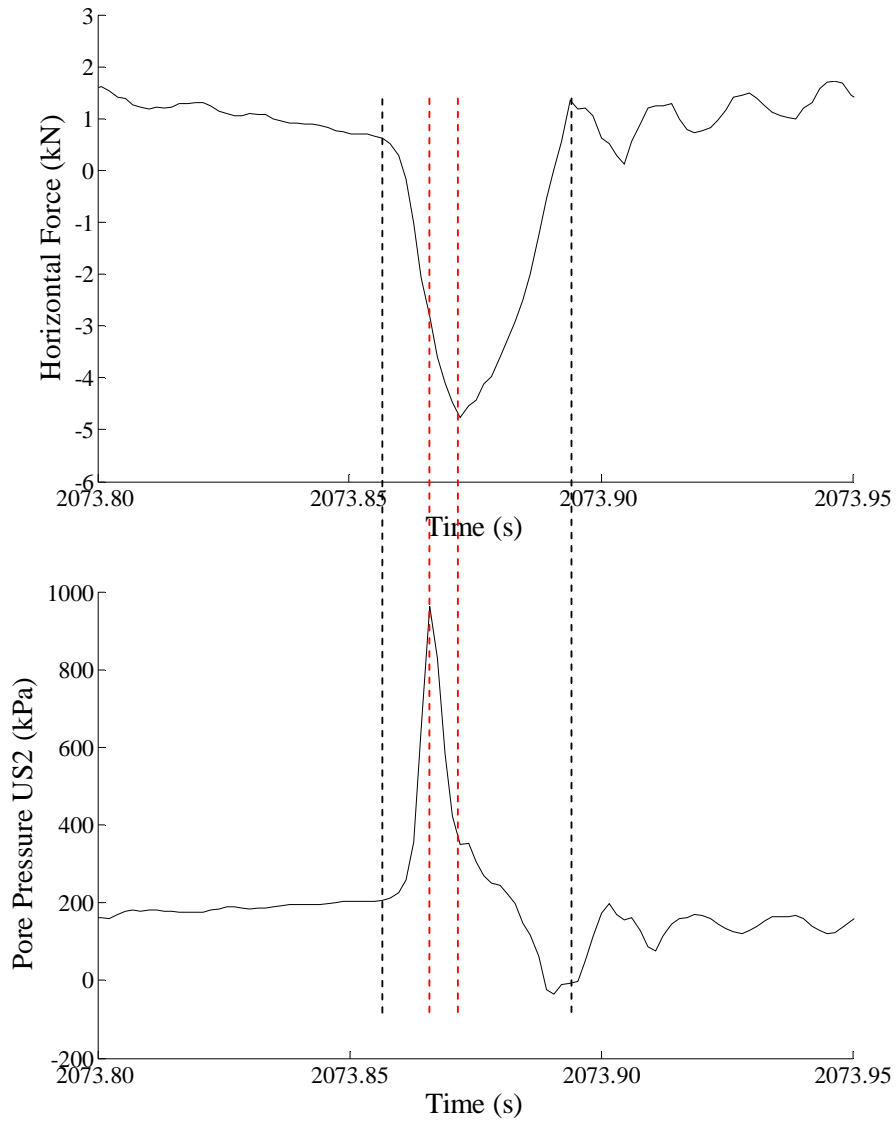


Figure 4.32 - Test II (16th storm part): detail of wave load peak - instantaneous pore pressures
(subsoil, harbour-side)

4.9 General Conclusions

In this Chapter the foundation behaviour of vertical caisson breakwaters placed on sand has been studied by analysing the results of dynamic centrifuge tests.

Both in the first and in the second test, the *failure mechanism* consisted in a combination of horizontal sliding and rotation toward the harbour-side. This can be probably related to the asymmetry of the load, with wave crest much larger than trough wave. The horizontal displacement at failure was equal to about 20 mm (1.2 m in prototype) and the rotation was about 3 degrees in both of the tests. The maximum load applied was approximately equal to 5 kN (1.3 MN/m).

Regular and irregular storms were simulated during the tests, showing that regular loading induced higher plastic deformations and faster lead to failure than an irregular loading, with the same peak load. During the regular storms, significant settlements occurred as a consequence of cyclic compaction of the sand. Settlements of the caisson were determined for large part by the primary load. In the second test the level of the primary load was quite large (half of the failure load) compared to the primary storm load in the first test. This induced larger vertical settlements.

As concerns the mechanism of pore pressures, very high *instantaneous excess pore pressures and underpressures* occurred during wave crest and trough. The instantaneous pore pressures follow the wave action at sea directly and can be distinguished from the reading by the sharp high rise peaks. These fluctuations occurred rapidly in time. All the values were usually higher in the subsoil rather than at the interface between the caisson and the subsoil. In both of the tests, the *EPP* at the harbour-side was usually higher than the *EPP* at the sea-side, where very high values of *UP* were recorded. Low values of *EPP* and *UP* were measured in the middle, so that the central zone can be regarded as a “transition” zone.

A simplified scheme of instantaneous pore pressure distribution in the subsoil is reported in Figure 4.33.

With regard to the *residual pore pressures* due to cyclic compaction they occurred only during the regular loading, as soon as the applied load exceeded the previous loads and only in the first cycles. This can be easily understood remembering that in the irregular storms the time lag between the two highest peaks was 9.62 s, hence enough long for drainage, while in the regular storms it was 0.2 s, insufficient to

allow the drainage. However, because of the residual excess pore pressure occurred only during the first cycles, they dissipated at the end of the storm part and they did not influence the failure.

The short duration loads and the cyclic action induced a complicated mechanical behaviour of sand soil foundations. Compaction of soil and increase in stiffness, due to the cyclic action of the previous storms, is evident if the same storm occurs after different several storms, with higher loads. If medium-dense sand with dilative behaviour features the foundation and if undrained conditions are established, phenomena of cyclic mobility are supposed to develop. This means that, although very high values of positive pore pressures may occur underneath the caisson, they do not accumulate continuously to cause complete liquefaction. A sort of “recovering” of soil strength occurs during each cycle and failure occurs step-by-step, according to a progressive mechanism.

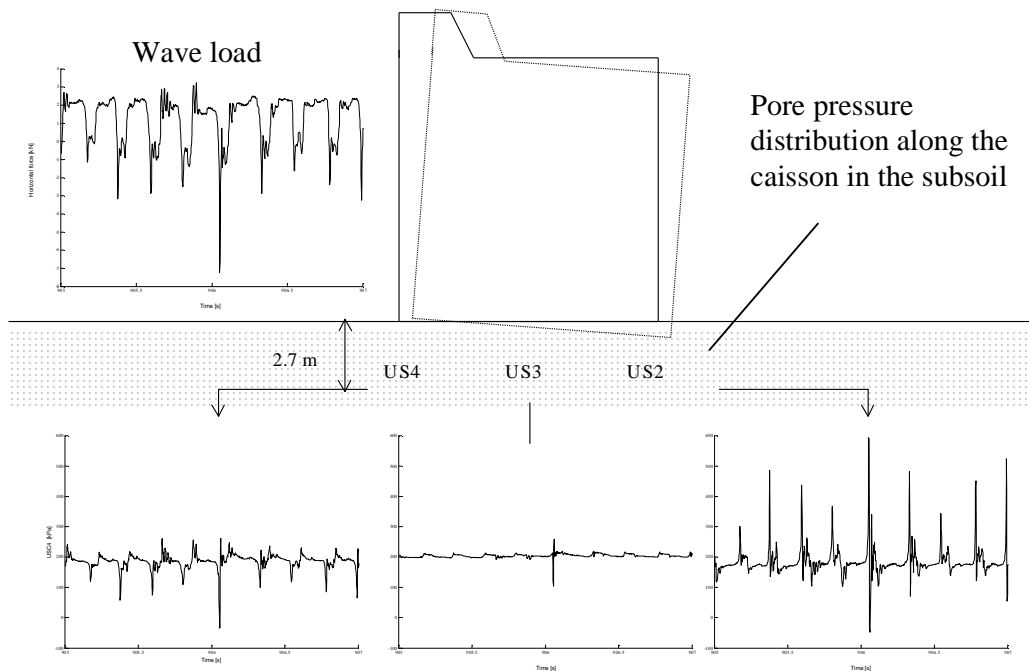


Figure 4.33 – Scheme of instantaneous pore pressure distribution in the subsoil

4.10 Additional research and numerical approach

In the previous Sections an interpretation of the mechanism failure observed during the centrifuge tests has been proposed and the development of instantaneous liquefaction and cyclic mobility phenomena have been supposed.

Although the dilative behaviour characterising the foundation sand and the analysis of the time history of pore pressures compared to the time history of applied forces seem to support such interpretation, on the other hand, it could significantly be important to study the mechanical response of sand underneath the caisson in terms of effective and total stress paths. This could prove that the soil follows the typical path of cyclic mobility. To confirm that, it would particular be important to carefully investigate the cinematic aspects in the structure-foundation interaction, especially as regards the deformation field characterising the subsoil. Another point that should be better analysed is the boundary drainage conditions in the sand underneath the caisson, in order to verify if partial drainage could have been developed, due to the very high hydraulic gradient between the harbour-side and the sea-side.

On the other hand, the research provides the basic tools useful to develop a modelling activity based on experimental results. Numerical analyses aimed at simulating the experimental behaviour observed during the performed experimental tests may constitute a valuable tool to better understand the actual processes involved in foundation soils and the mechanical response of the soil. A good analysis shall adopt a *sophisticated constitutive model of soil*, able to reproduce the behaviour of granular soil under transient and cyclic loading.

Within this research, the implementation of a sophisticated model has been started and only a few simplified tests, useful to verify the correct implementation, have been performed. Furthermore, simplified tests using basic constitutive model for soil, has been started, in order to study the boundary conditions of centrifuge tests and to make a significant selection of the complex simulated loading conditions.

The numerical study is, however, just at the beginning.

Acknowledgements

This text is based on the Report “Results of Centrifuge Tests on Caisson Breakwater”, CO-364820/89, August 1997, authored by GeoDelft (previously Delft Geotechnics). Ir. Frans Koop and Ir. Henk den Adel are gratefully acknowledged for assistance in the acquisition of the presented data.

Notation

B	[mm]	caisson width
c_v	[m ² /s]	elastic consolidation coefficient
d	[m]	characteristic drainage distance
EPP	[kPa]	excess pore pressure
F_h	[kN]	horizontal force
g	[m ² /s]	Earth’s gravity
h	[m]	layer thickness
H	[mm]	caisson length
HPV _i	[kN]	initial highest peak value of wave load applied
HPV _f	[kN]	final highest peak value of wave load applied
I/wt	[kN]	increment of peak wave load applied for load parcel (irregular wave) or storm part (regular wave)
I_D	[%]	relative density
k	[m/s]	hydraulic conductivity
m	[-]	model
n	[%]	porosity
N	[g]	acceleration gravity
p	[-]	prototype
T	[s]	wave period
$T_{CHDRAIN}$	[s]	drainage characteristic period
t_s	[s]	dissipative or consolidation time
t_d	[s]	dynamic time
U_h	[mm]	horizontal caisson displacement
U_v	[mm]	vertical caisson displacement
UM	[-]	series pore pressure transducers at the caisson bottom
UP	[kPa]	underpressure
US	[-]	series pore pressure transducers in the subsoil
α	[m ² /kN]	elastic compressibility of the skeleton
β	[m ² /kN]	compressibility of the pore water
γ	[kN/m ³]	specific particle weight $\gamma= 2.65$
γ_w	[kN/m ³]	water unit weight

Chapter 5

Conclusions and Research Needs

State of the art and research motivations

The geotechnical aspects of vertical breakwaters are not yet well known and the foundation design is mostly based on stationary simplified methods and practical formulae.

A literature survey has revealed that many structures so designed and realised have sometimes experienced important failures or significant damages. Most of failure modes, correctly investigated, have to be associated with the dynamic nature of the wave loads.

Many studies have been carried out on the effect of the direct sea-wave action on the seabed but many uncertainties characterise the dynamic wave-structure-foundation interaction, not yet well investigated.

Particular interesting, from a geotechnical point of view, is the effect of the wave action transmitted by the structure on the mechanical response of soil foundation. This effect will depend on several different aspects as nature of wave load, thickness of the rubble layer, nature of soil foundation, number of cycles, stress history experienced by the soil, boundary drainage conditions, etc..

The understanding of the foundation response to the wave-induced cyclic loading appears useful to explain the reasons for failures in cases apparently properly designed and to improve the design that shall consider the mechanical response of soils.

The research

This research has been referred to vertical breakwaters founded on medium-dense sandy subsoils, without rubble layer.

A preliminary detailed study of mechanical behaviour of sands under monotonic and cyclic loading has shown that the mechanical response of granular soils depends mainly on their granular structure and relative density.

Contractive and dilative behaviour assumes significant importance in relation with the boundary drainage conditions. Concepts of *liquefaction flow failure*, *flow structure*, *steady state condition*, *flow liquefaction surface*, *phase transformation line*, *true cyclic liquefaction* and *cyclic mobility* have been introduced.

On the basis of extensive experimental centrifuge investigations, the failure mechanism of a caisson breakwater model has been studied.

The structure was founded on a layer of medium-dense saturated sandy subsoil. The physical and mechanical characteristics of the sand used in the model have been preliminarily investigated. Triaxial tests with loading and reloading cycles evidenced the dilative behaviour of sand.

The occurrence of regular and irregular storms has been simulated until failure. The critical failure mechanism has been studied by means of measurements of caisson's displacements (vertical and horizontal) and rocking motion. Pore pressure transducers enabled to observe pore pressure distribution along the caisson and in depth.

The influence of the loading scheme on the structure's response has been studied. Regular and irregular loads cause different modes of deformation: regular loads usually induce settlements larger than horizontal displacements, while the opposite occurs during irregular unloading. If the same storm occurs after several events with higher load, the previous cyclic wave action induces compaction of soil and increase in stiffness. Strengthening of the soil structure toward the cyclic wave action and toward the impact of successive bigger storms is observed.

The failure mechanism has shown that, in all loading conditions, the collapse is induced according to a progressive mechanism under repetitive loads. The wave

action led to oscillatory motions and residual permanent deformations of the structure, causing a “stepwise” bearing capacity failure in the subsoil.

The development of pore pressures played a significant role in the failure process.

Residual pore pressures due to cyclic compaction occurred only during the regular loading and only in the first cycles. Drainage conditions influenced their development. However, they dissipated at the end of the storm part and they did not influence the failure.

Very high values of instantaneous excess pore pressure, especially at the harbour-side, has risen the question whether “liquefaction”, at least “pore pressure build-up after each load cycle”, may have played a role in the failure or rather an accumulation of small irreversible strains at repetitive peak stresses.

Although high values of instantaneous pore pressures developed underneath the caisson, they did not accumulate continuously to cause complete liquefaction flow failure, unlike expected.

The dilative nature of sand and the instantaneous undrained conditions, with drainage time larger than time of load application, lead to think that phenomena of “instantaneous liquefaction” and “cyclic mobility” were probable responsible of failure process.

Non-linearity development of pore pressure with load history, decrease of pore pressure during loading and increase of pore pressure during unloading lead to support that hypothesis. This means that, although the high impacts of wave loads caused high values of pore pressures, a recovering of soil strength may have been occurred during each cycle and failure was developed step-by-step, with a progressive mechanism. This could explain the observed failure process.

Research needs

The discussed cyclic mobility phenomena constitute an interesting interpretation of the observed failure mechanism. However, to be scientifically validated, the analysis of the mechanical response of sands, in terms of effective and total stress paths and deformation field experienced by the soil, should be known. Furthermore, partial

drainage, due to the very high hydraulic gradient between the harbour-side and the sea-side, should be excluded.

On the other hand, the research provides the basic tools useful to develop a numerical modelling activity based on experimental results. Numerical analyses may constitute a valuable tool to better understand the actual processes involved in foundation soils and the mechanical response of the soil. A good analysis shall adopt a *sophisticated constitutive model of soil*, able to reproduce the behaviour of granular soil under transient and cyclic loading. In this thesis the generalised plasticity model (Pastor et al. 1990), describing the behaviour of sands under monotonic and cyclic loading, has been presented. It has been studied in order to start its implementation in a finite element code and to perform numerical analyses simulating the experimental program. Within this research, the model has been partly implemented and only a few simplified tests, useful to verify the correct implementation, have been performed.

Furthermore, a program of simplified tests using basic constitutive model for soil, has been started, in order to study the boundary conditions of centrifuge tests and to make a significant selection of the complex simulated loading conditions.

These numerical studies are just at the beginning.

“Practical engineering” aspects

The “Geotechnics of Marine Structures” is still at the beginning and several uncertainties still characterise the design of vertical breakwaters.

The research makes a contribution to better understand the complex mechanisms between caissons wave-induced cyclically loaded and soil foundation. This is of great interest in the practical engineering design.

For a real problem the understanding of failure modes becomes even more complex than in laboratory, due to the great numbers of factors that characterises the “in situ” conditions.

The monitoring of the behaviour of real structures, based on specific field observations and measurements, may constitute a valuable tool to improve the

knowledge of the “in situ conditions”. Within this thesis, the monitoring of a real vertical caisson breakwater, wave-induced cyclically loaded for a long period, constituted an interesting opportunity to better understand the behaviour of the structure founded on a rubble layer and posed on sandy subsoil.

APPENDIX I

Results of centrifuge tests

First Test: pages 135 – 149

Second Test: pages 150 - 164

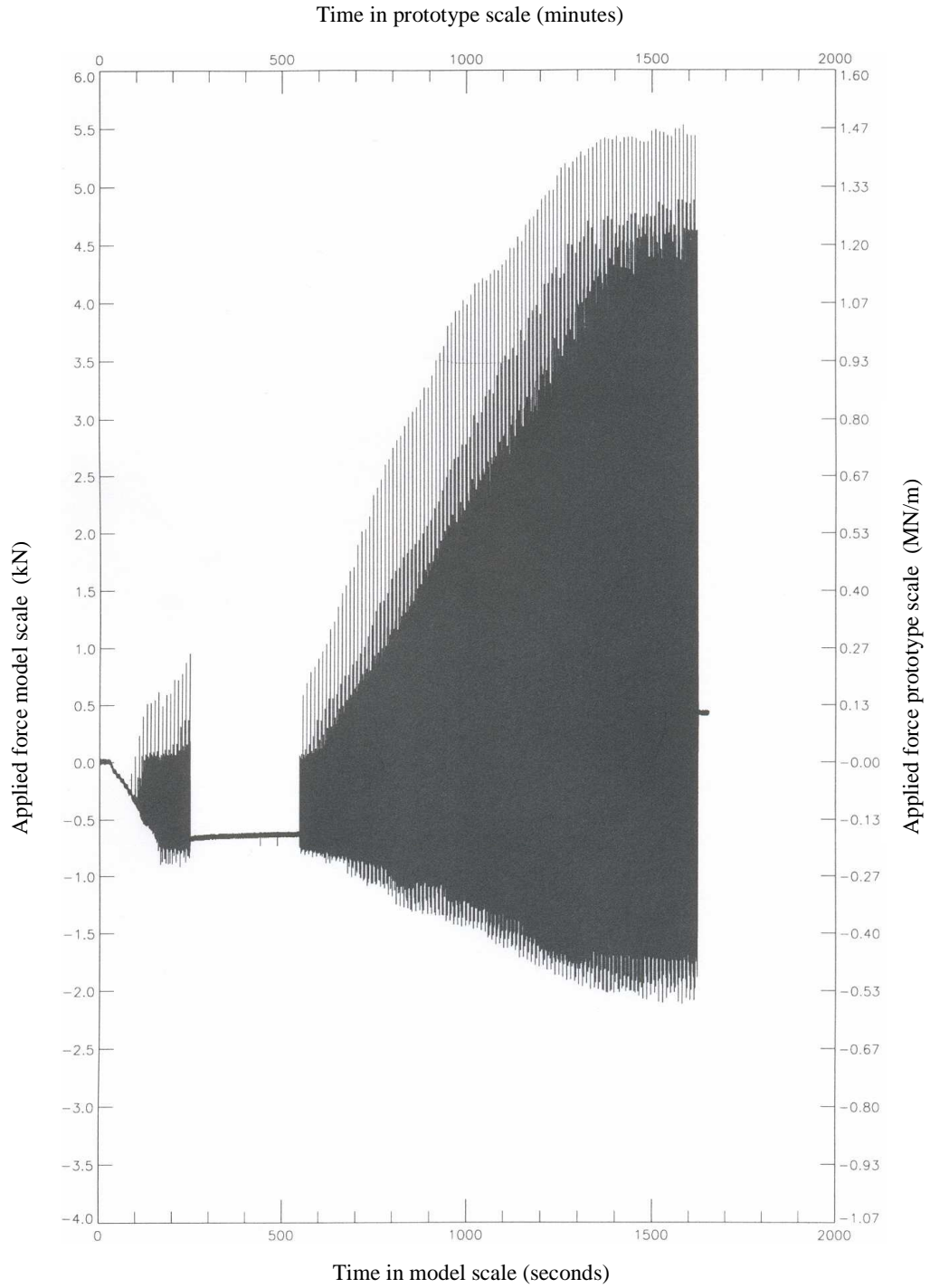


Figure A1 - Applied force versus time

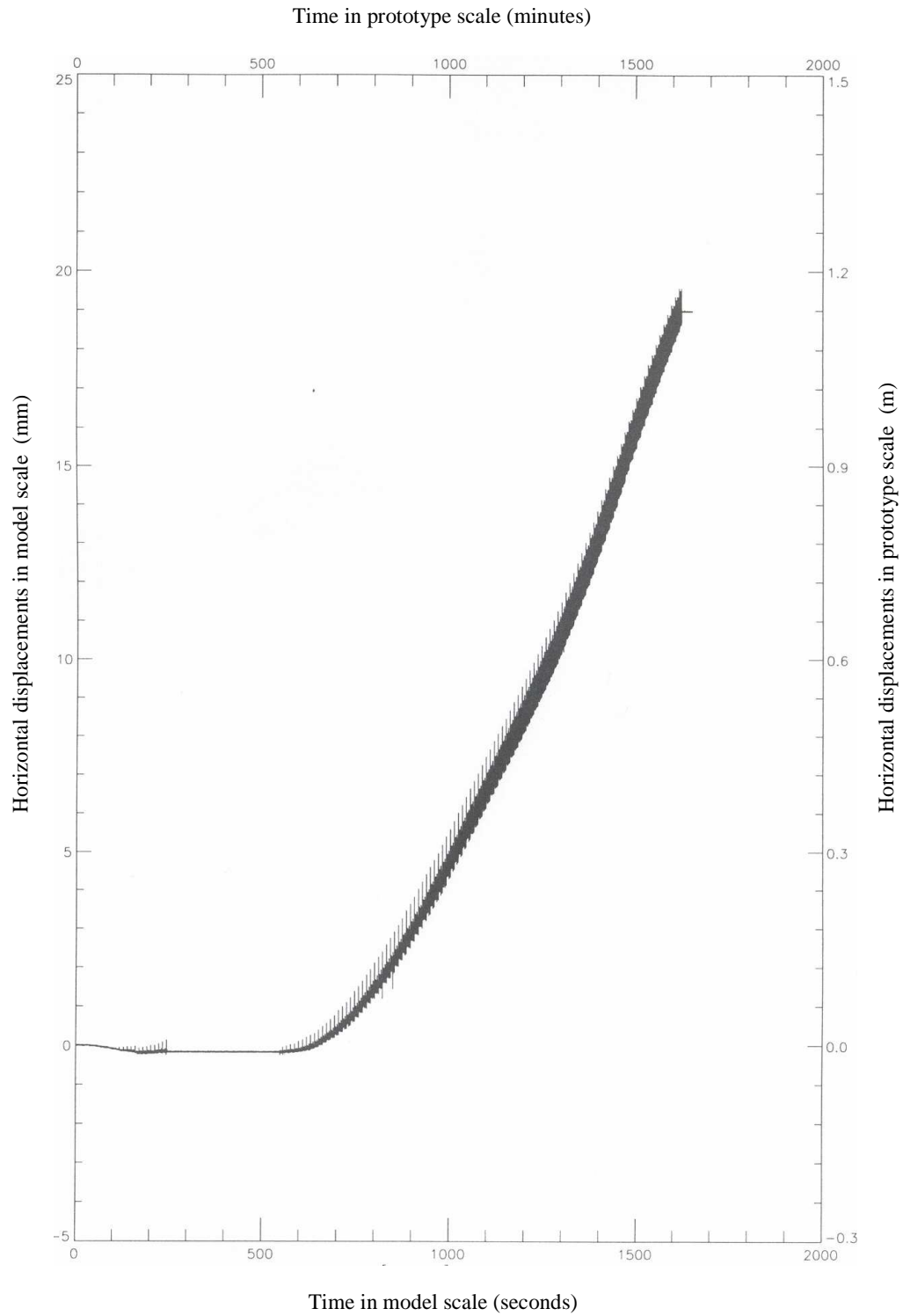


Figure A2 - Horizontal displacements versus time

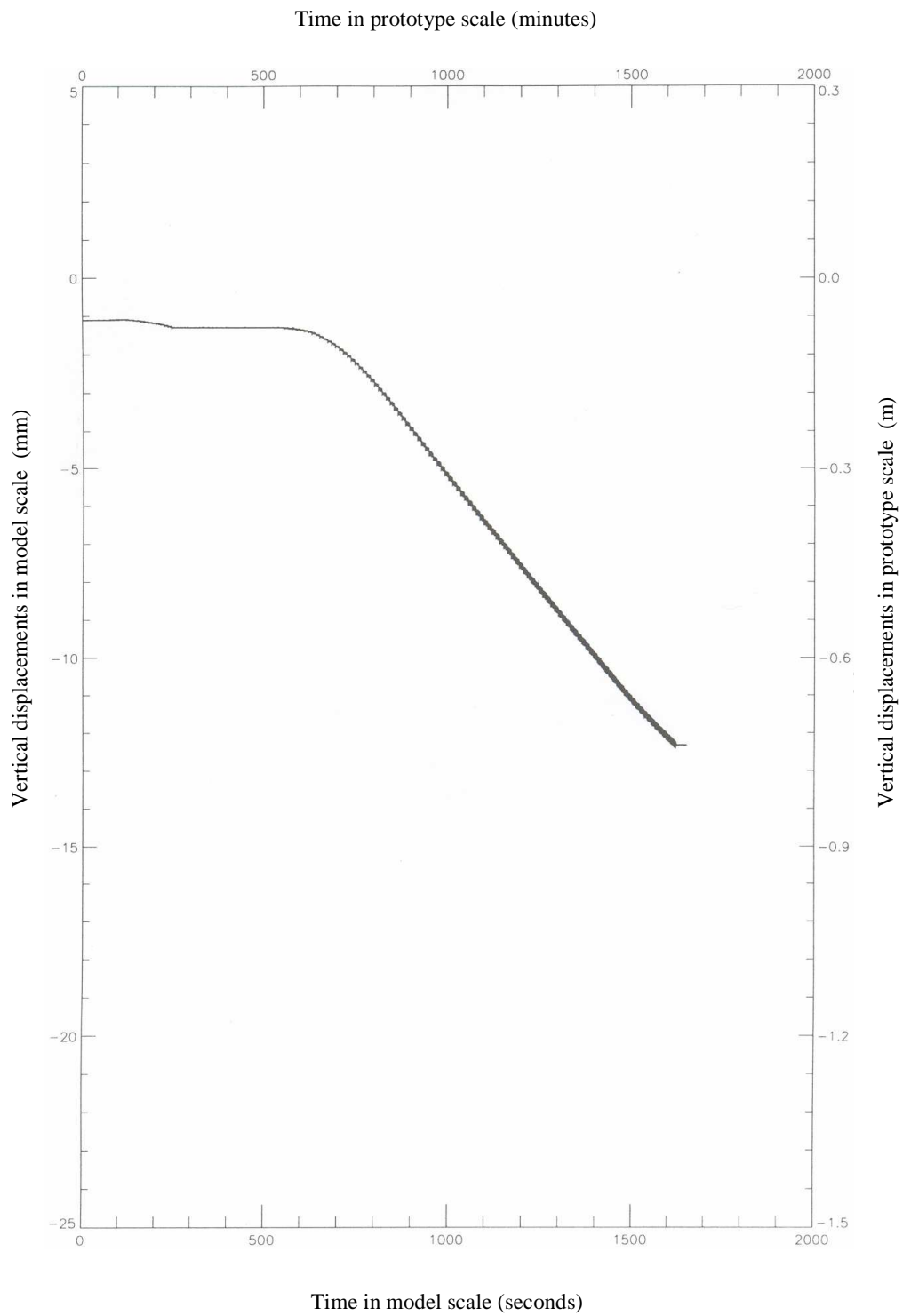


Figure A3 – Vertical displacements (front) versus time

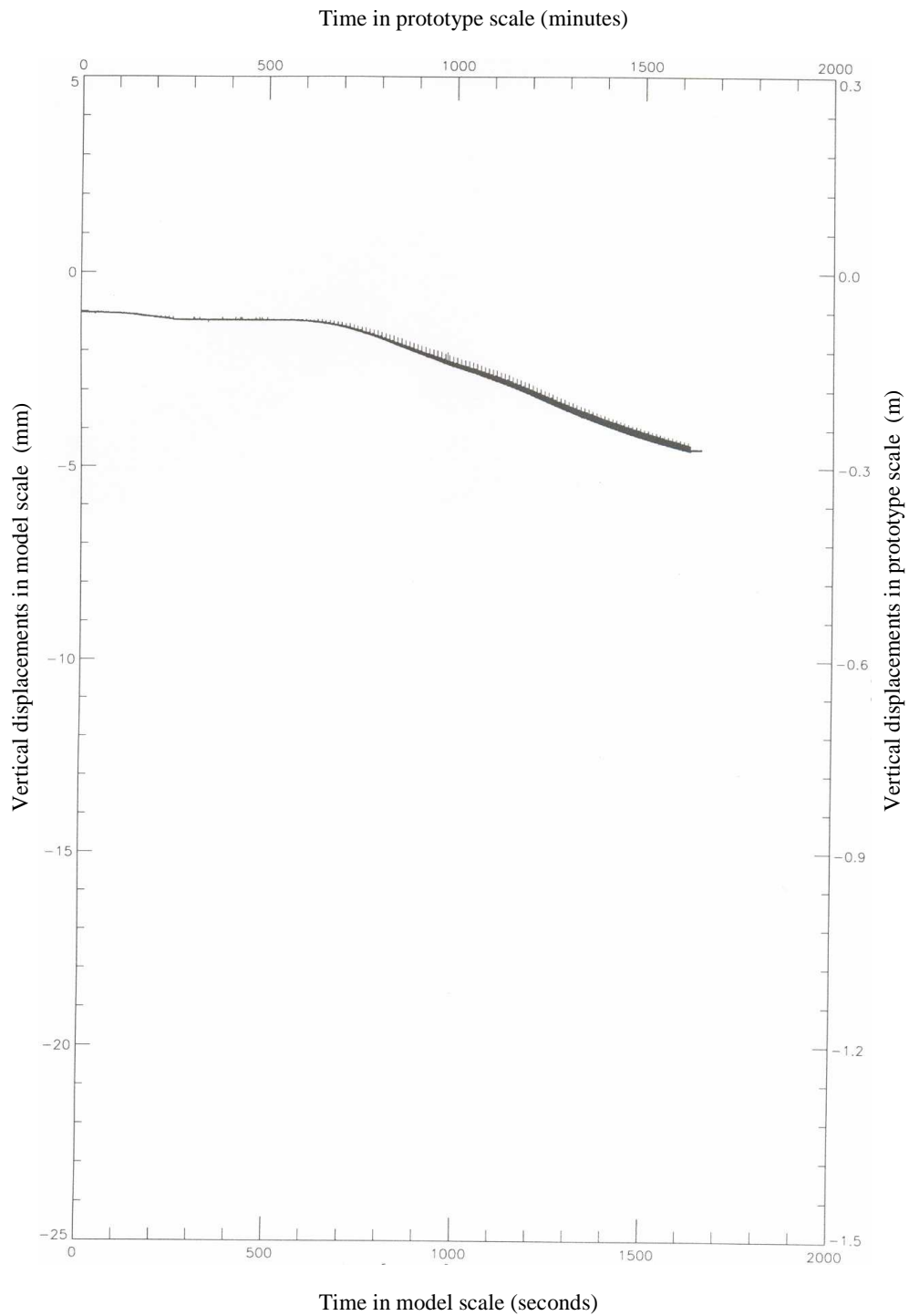


Figure A4 – Vertical displacements (back) versus time

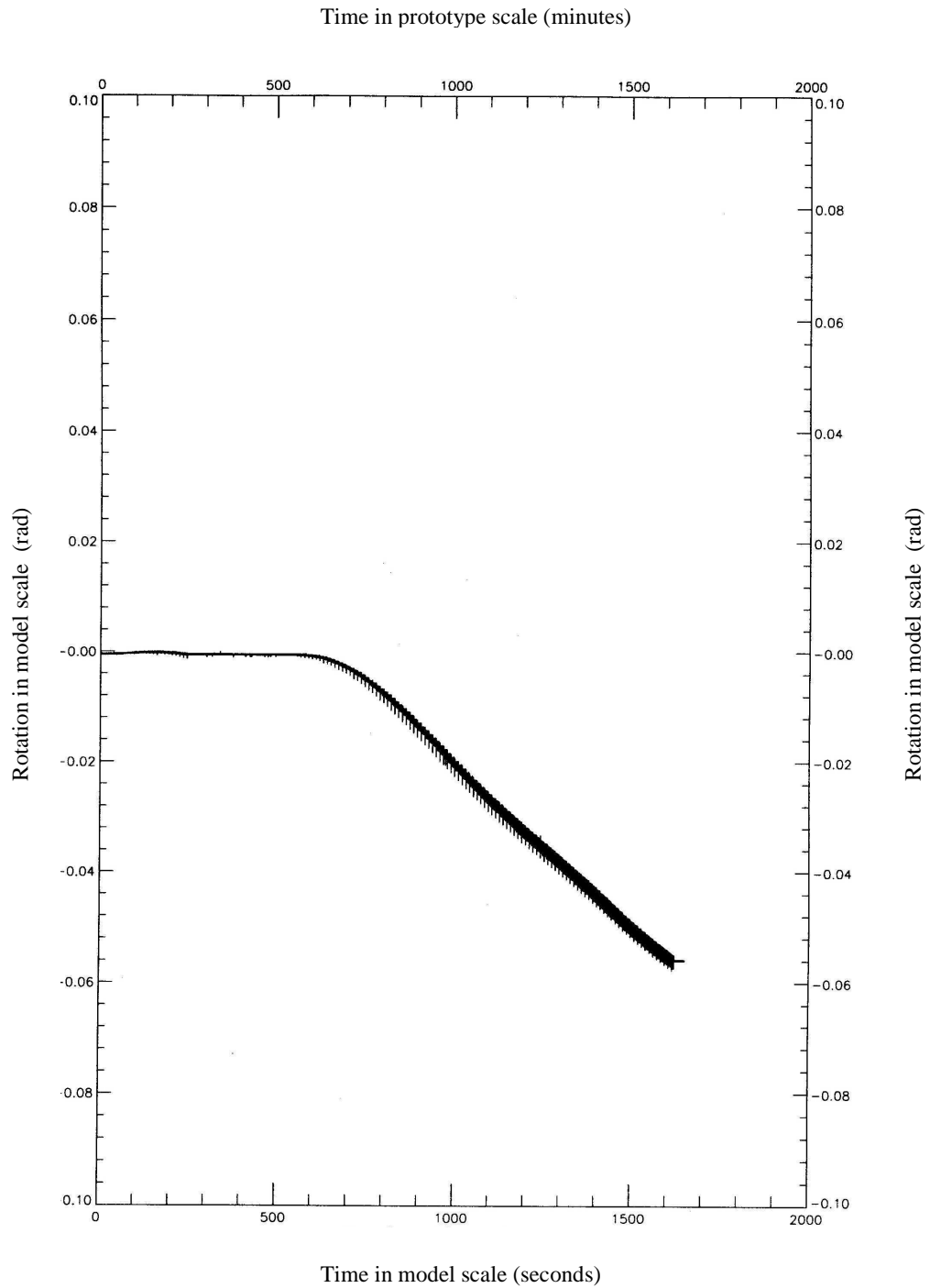


Figure A5 – Rotation versus time

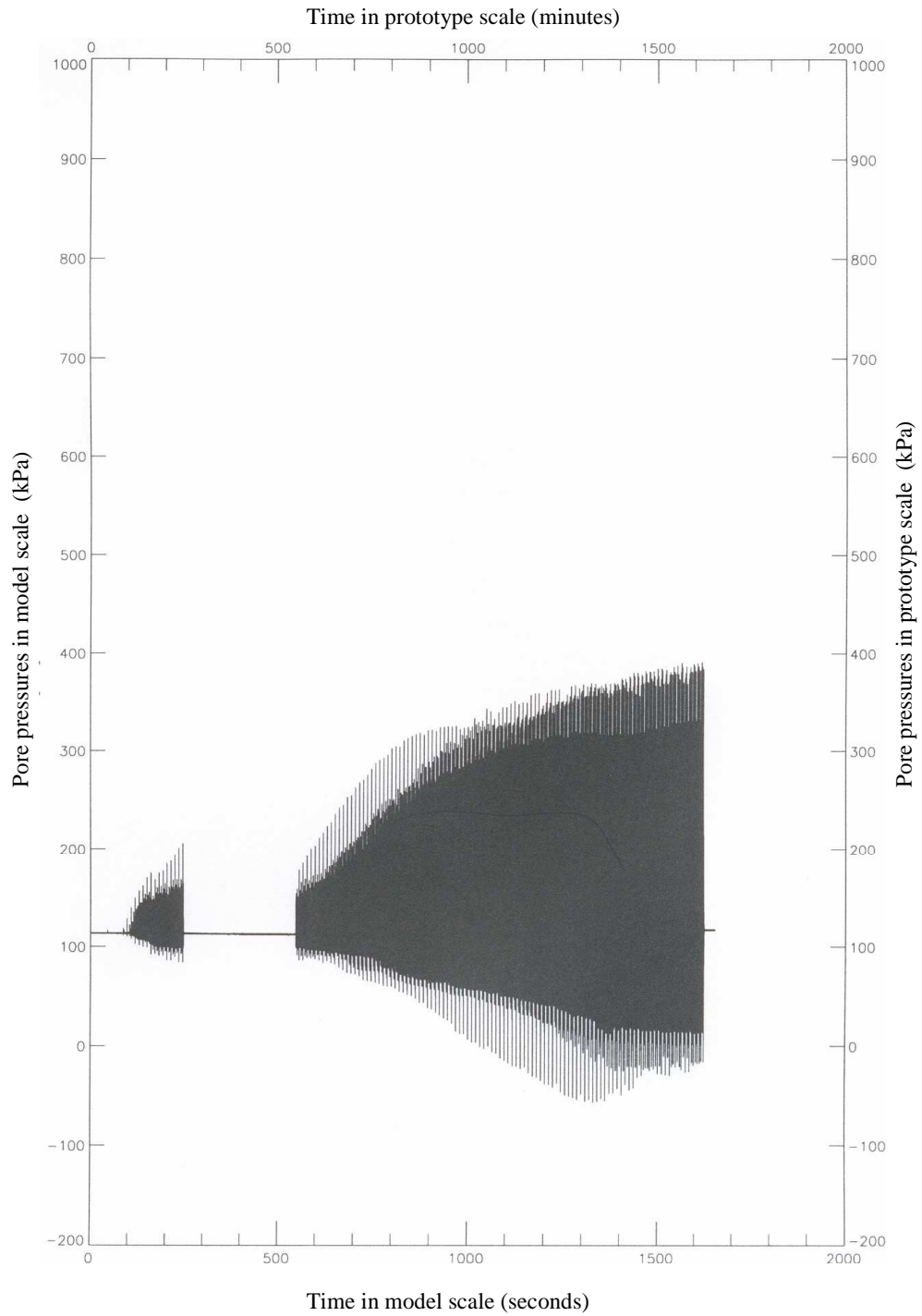


Figure A6 – Pore pressures versus time, transducer UM1

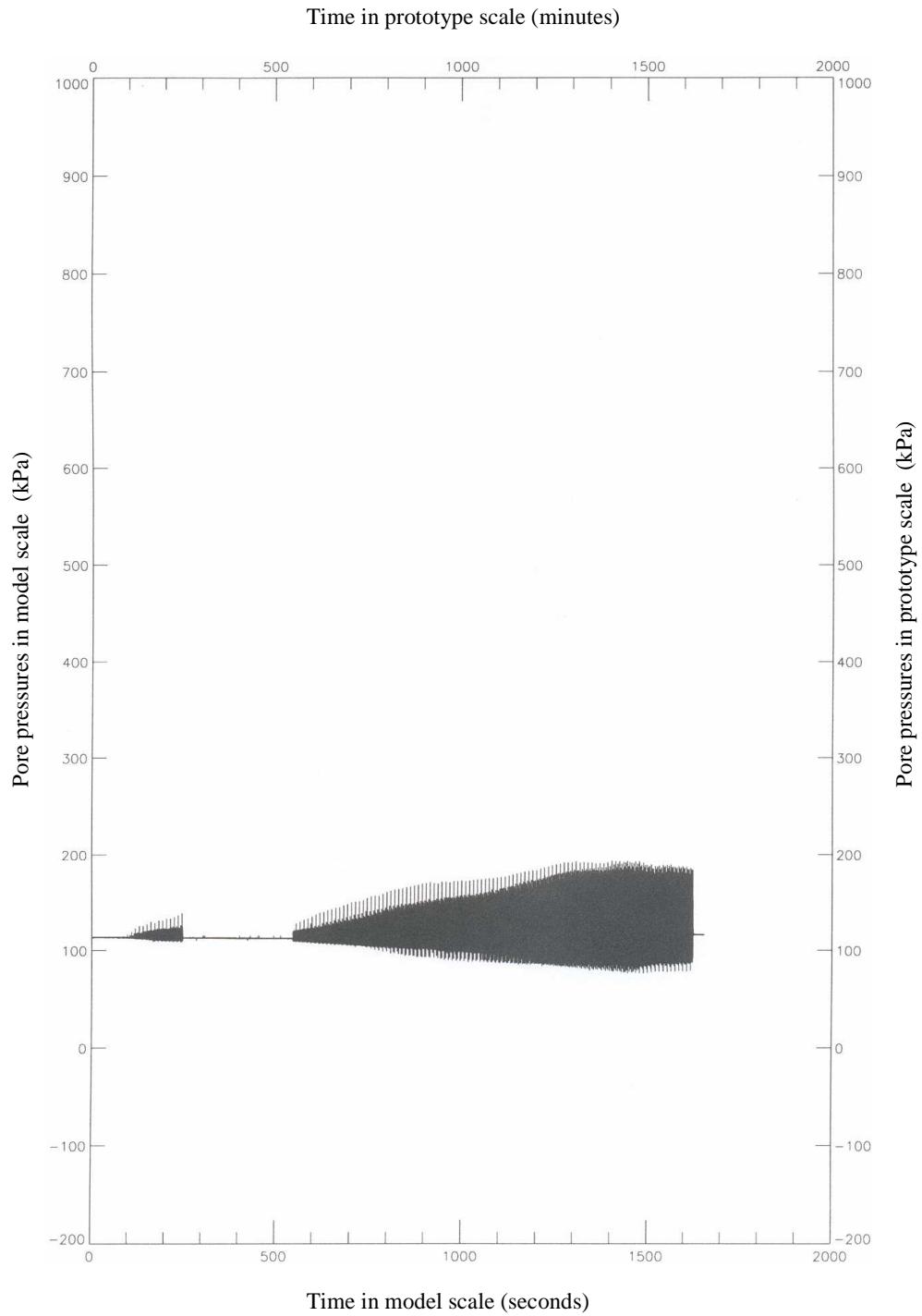


Figure A7 – Pore pressures versus time, transducer UM2

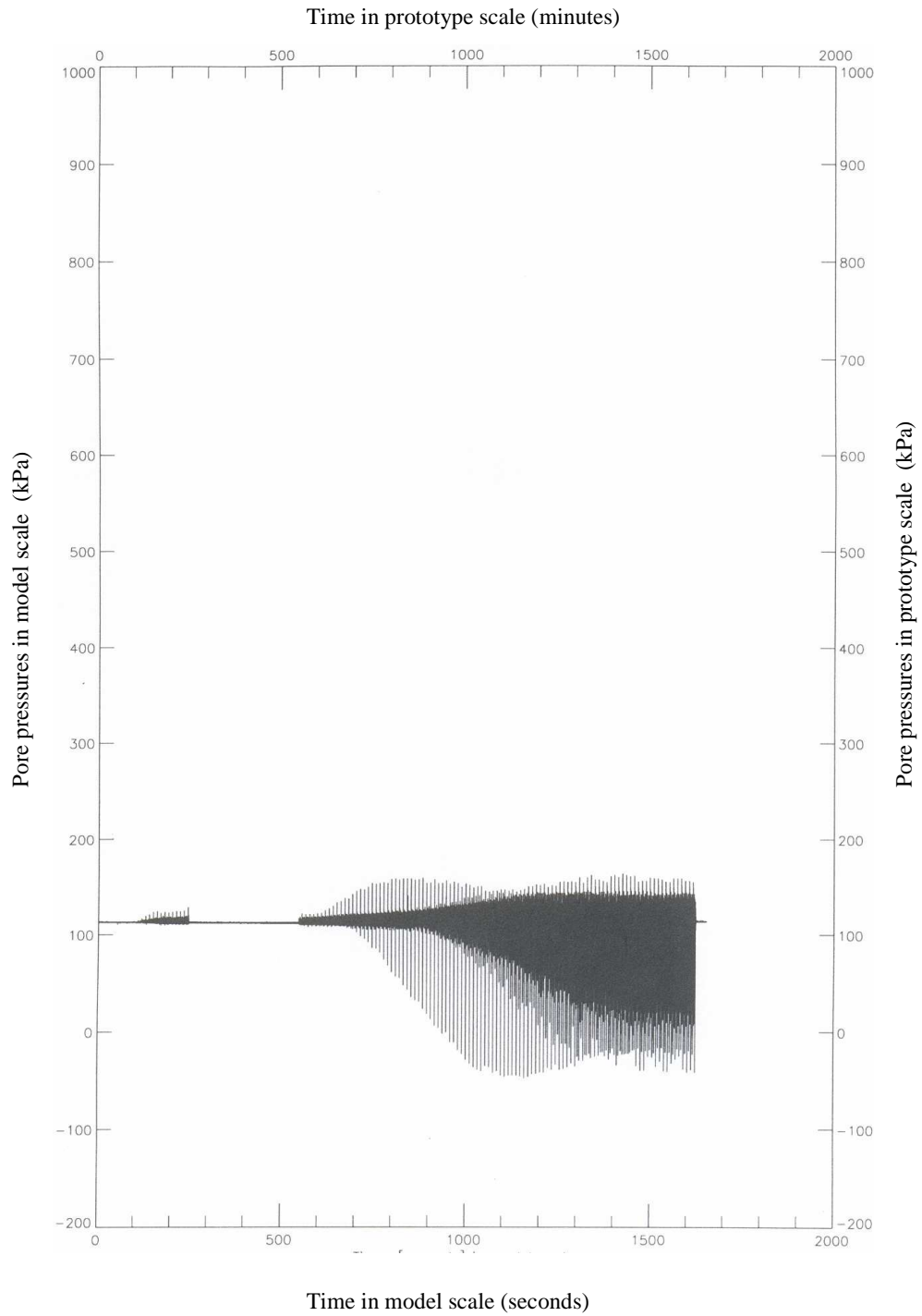


Figure A8 – Pore pressures versus time, transducer UM3

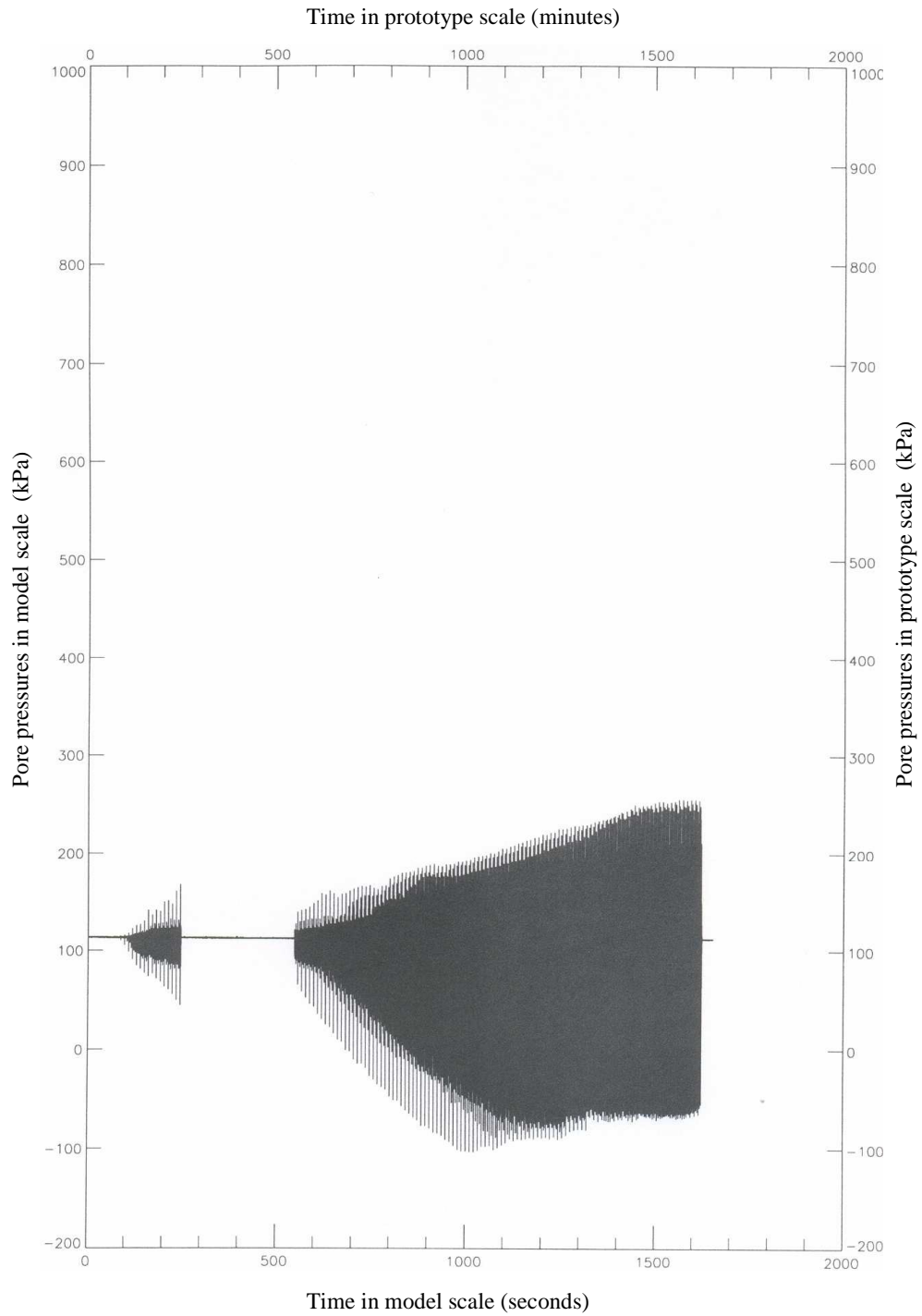


Figure A9 – Pore pressures versus time, transducer UM4

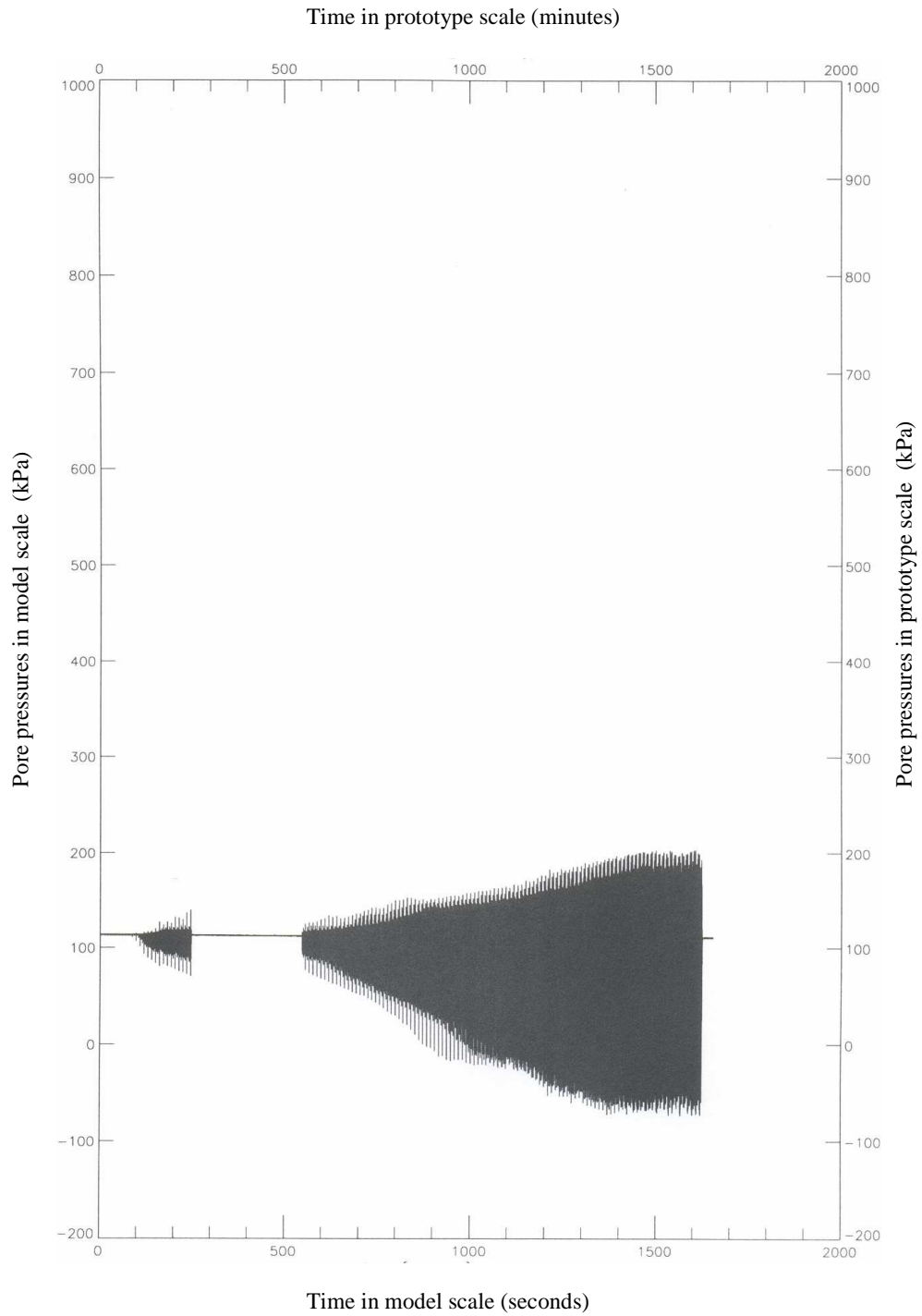


Figure A10 – Pore pressures versus time, transducer UM5

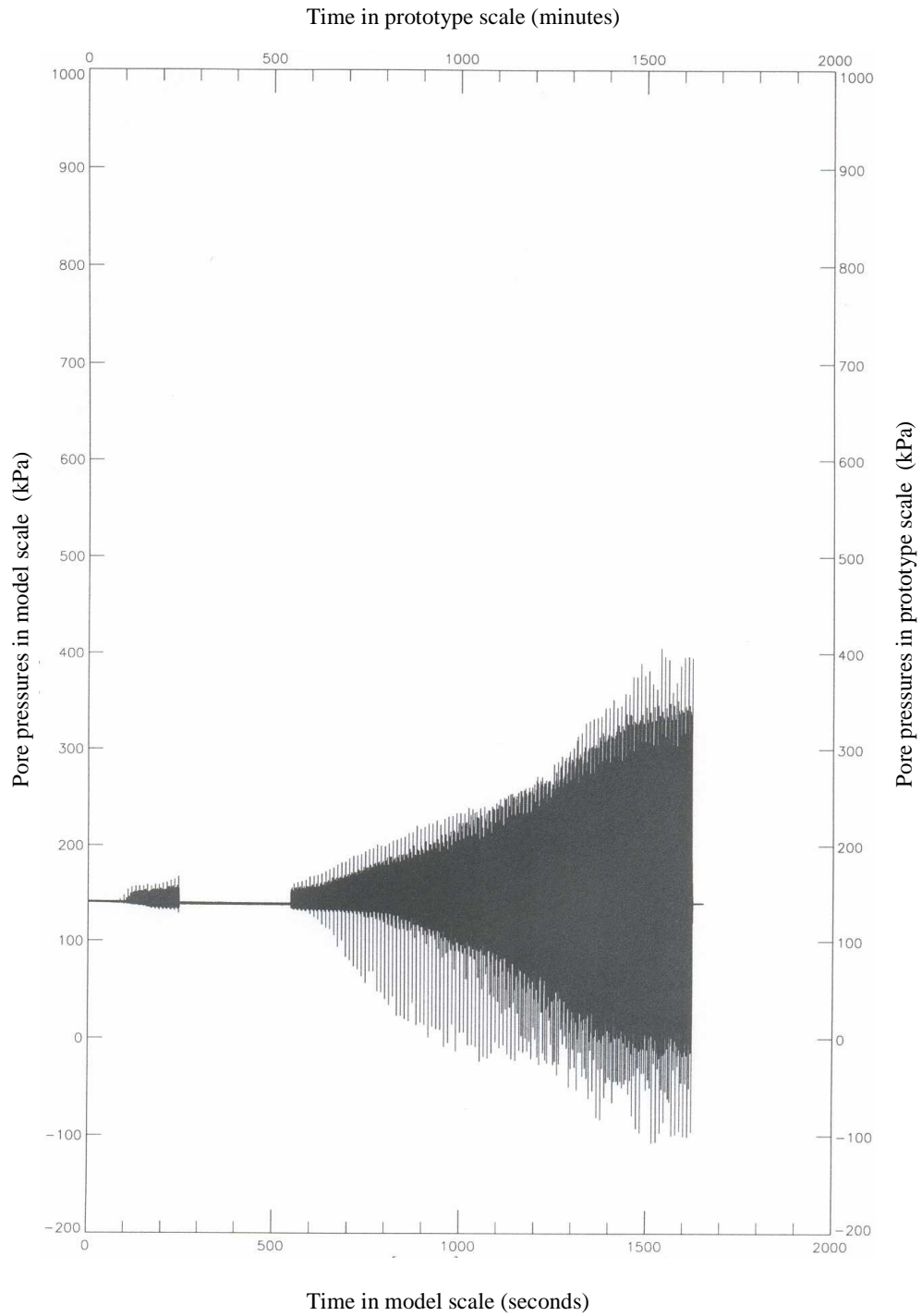


Figure A11 – Pore pressures versus time, transducer US1

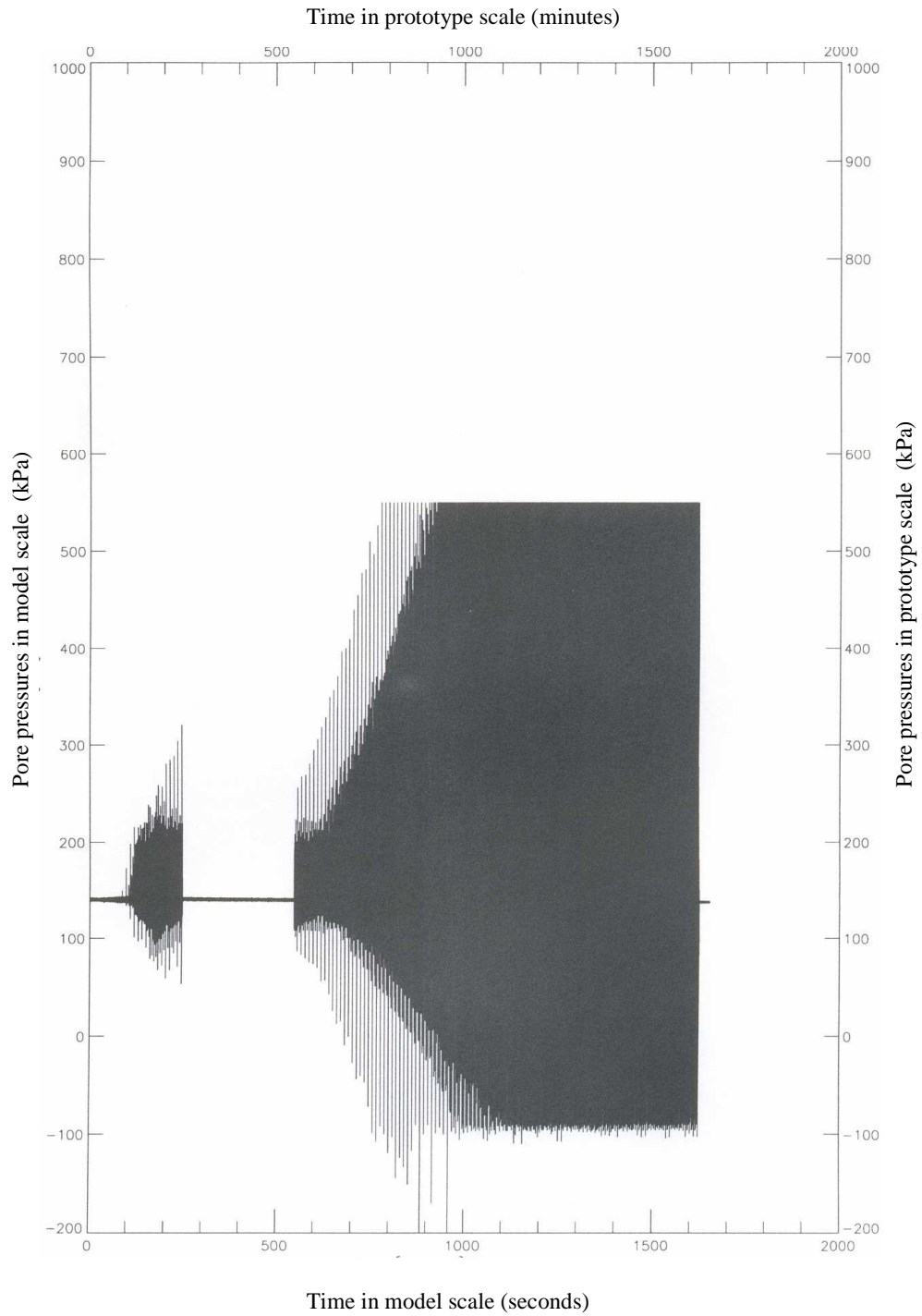


Figure A12 – Pore pressures versus time, transducer US2

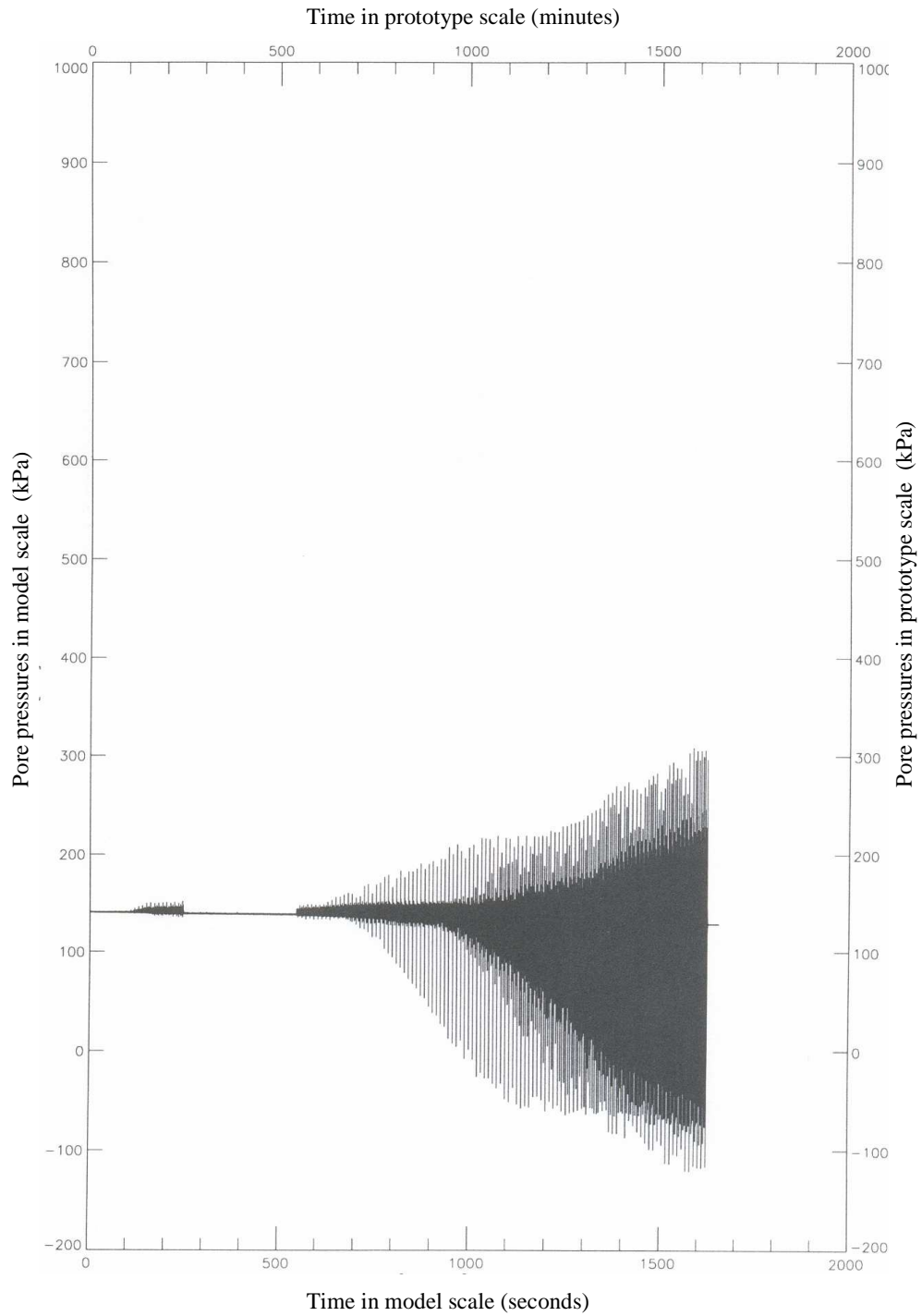


Figure A13 – Pore pressures versus time, transducer US3

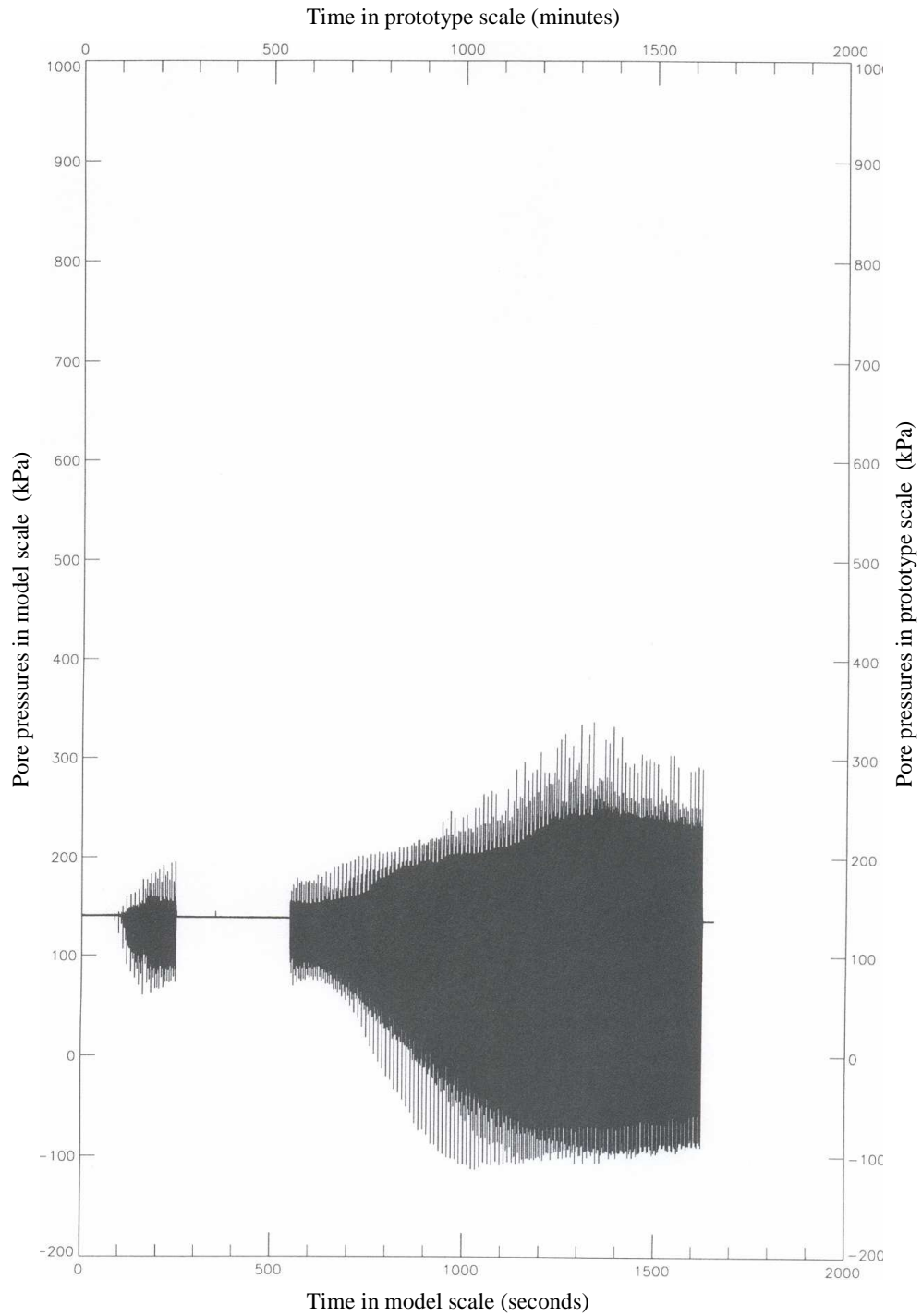


Figure A14 – Pore pressures versus time, transducer US4

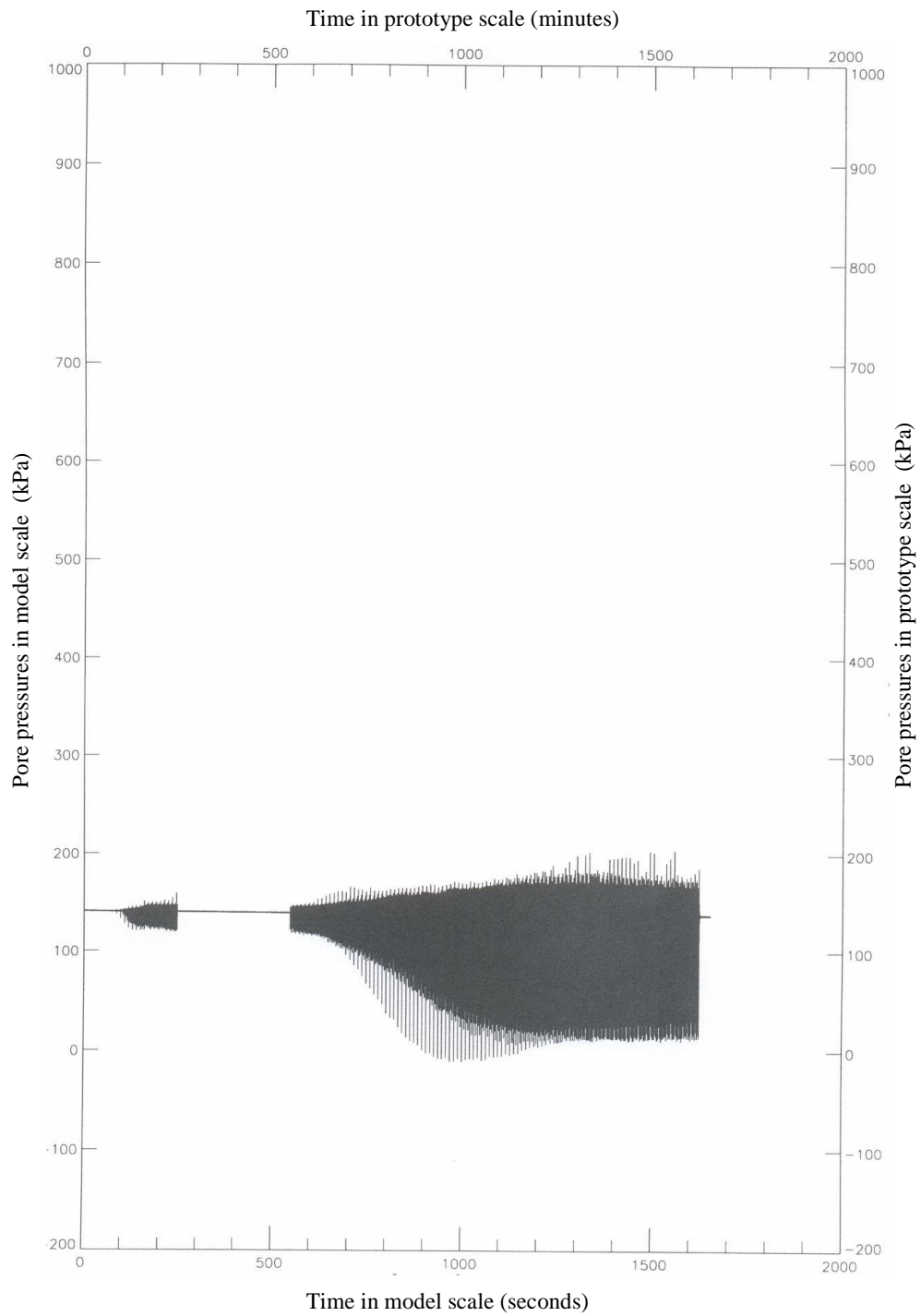


Figure A15 – Pore pressures versus time, transducer US5

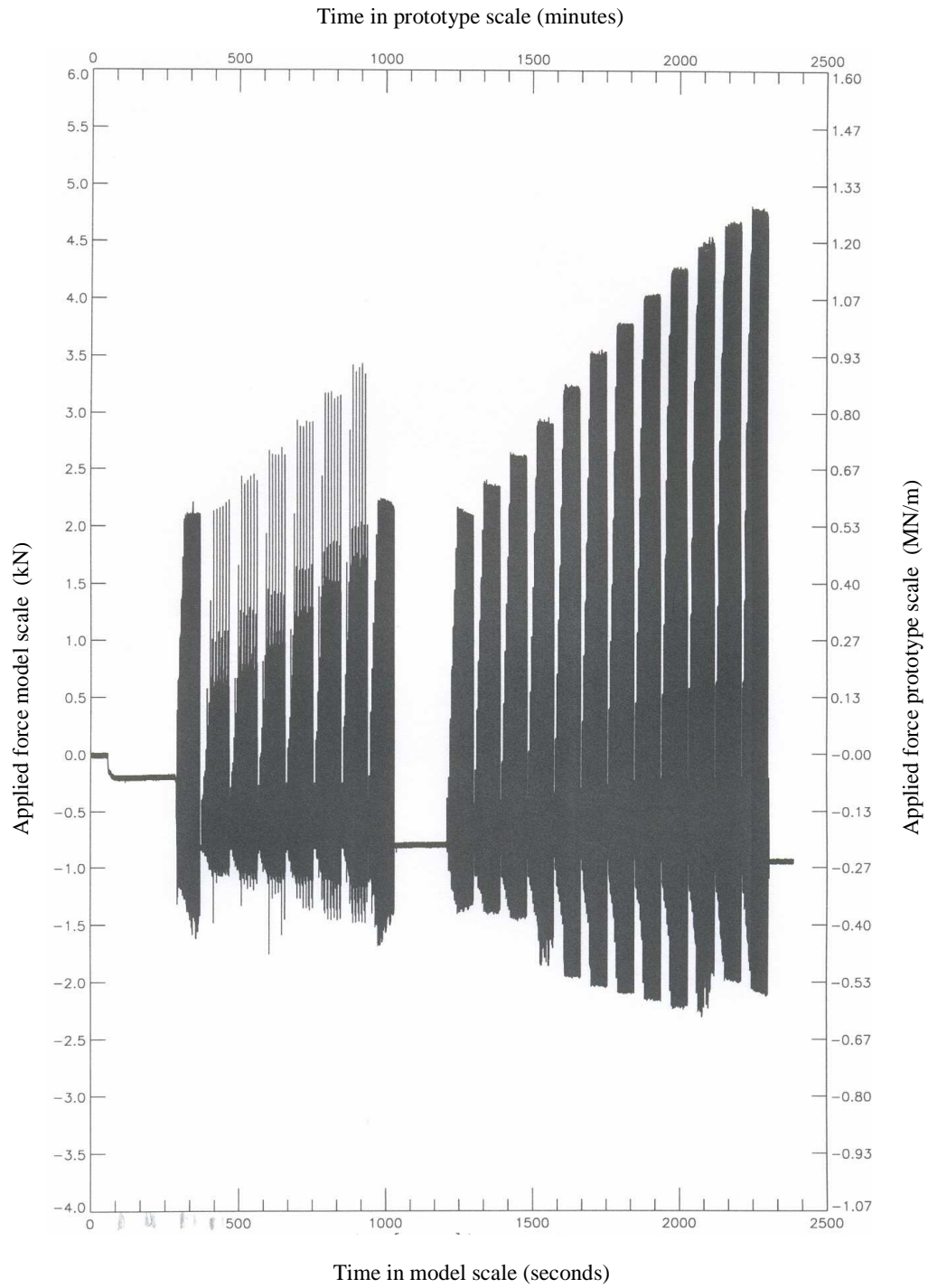


Figure A16 - Applied force versus time

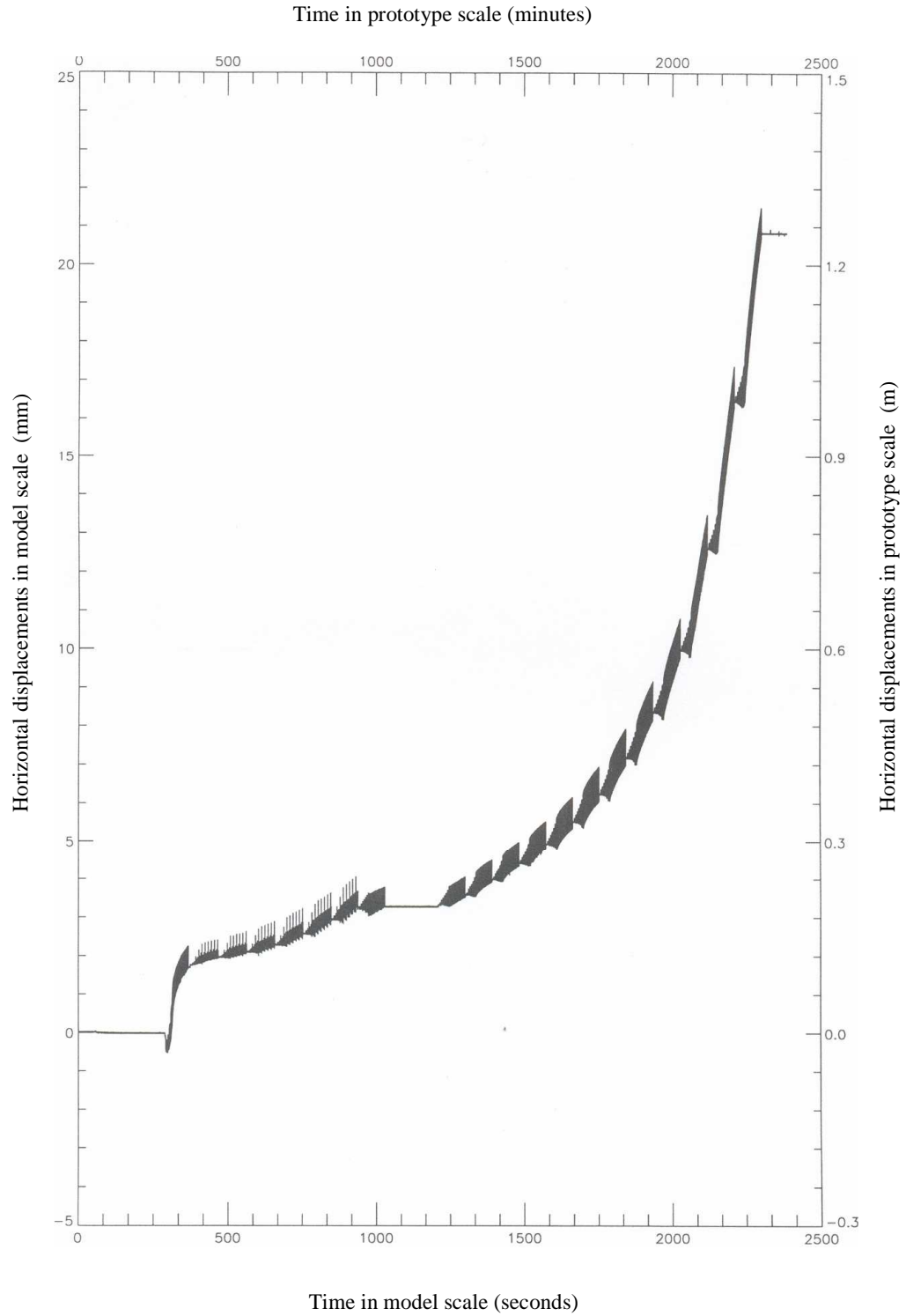


Figure A17 - Horizontal displacements versus time

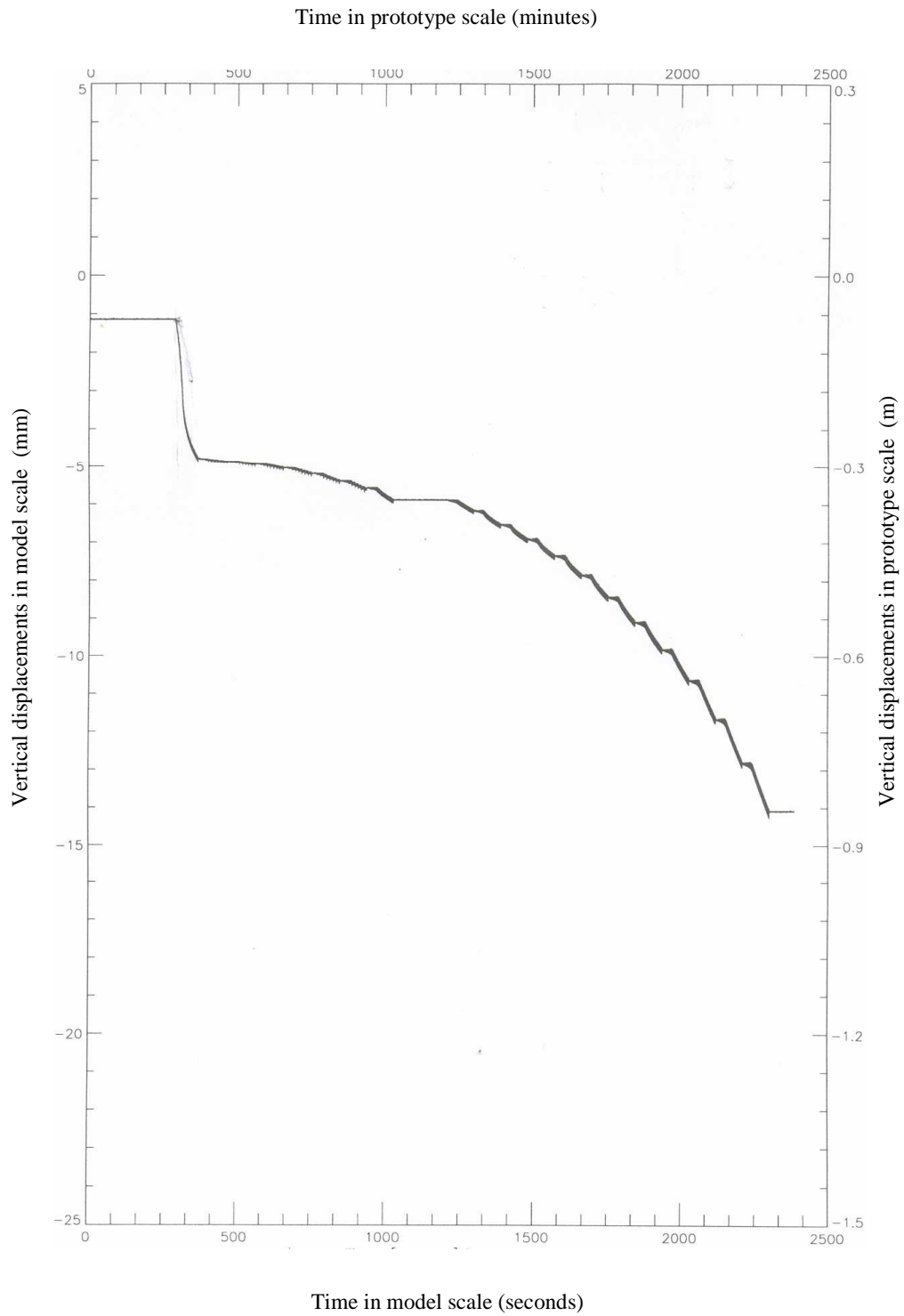


Figure A18 – Vertical displacements (front) versus time

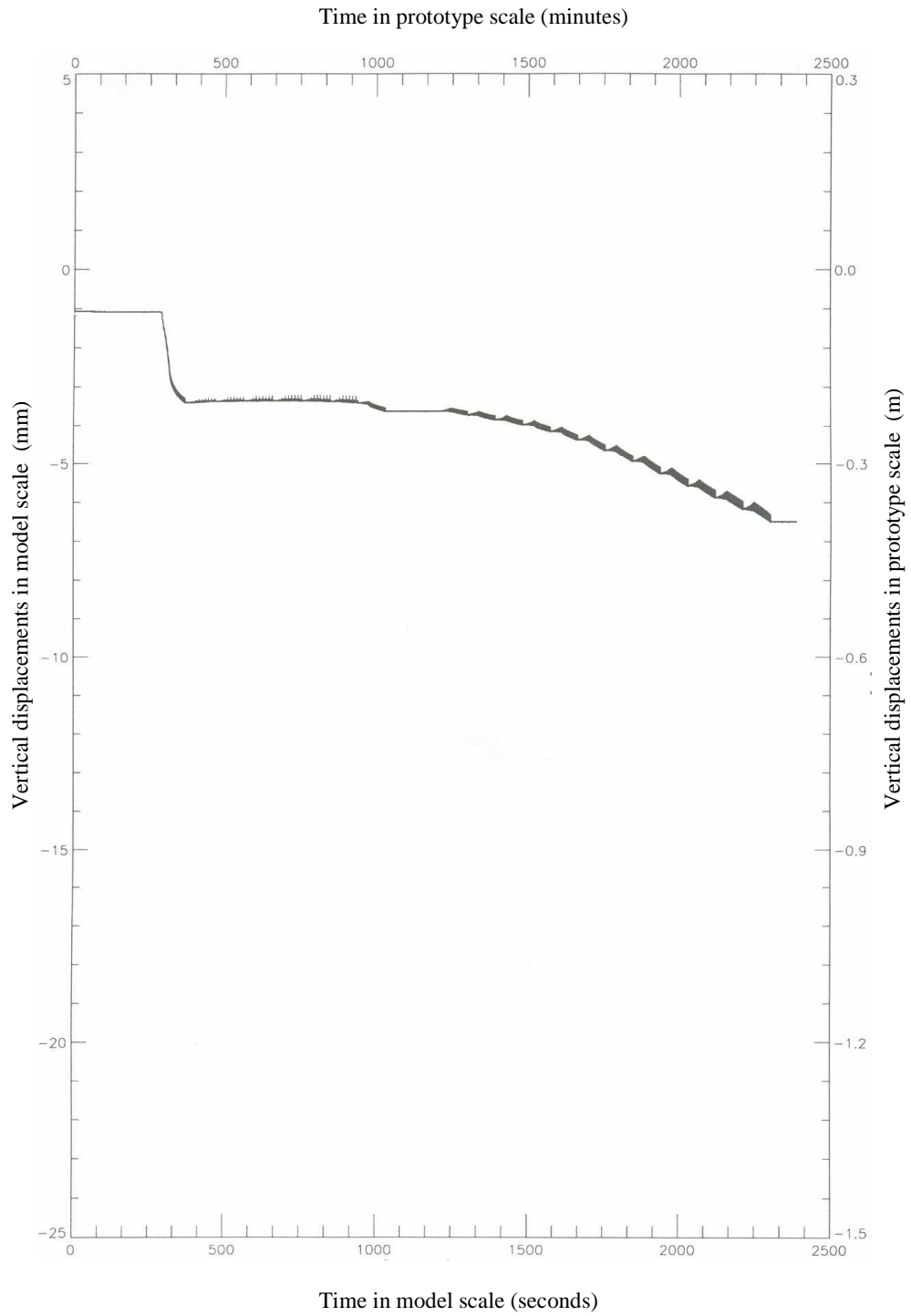


Figure A19 – Vertical displacements (back) versus time

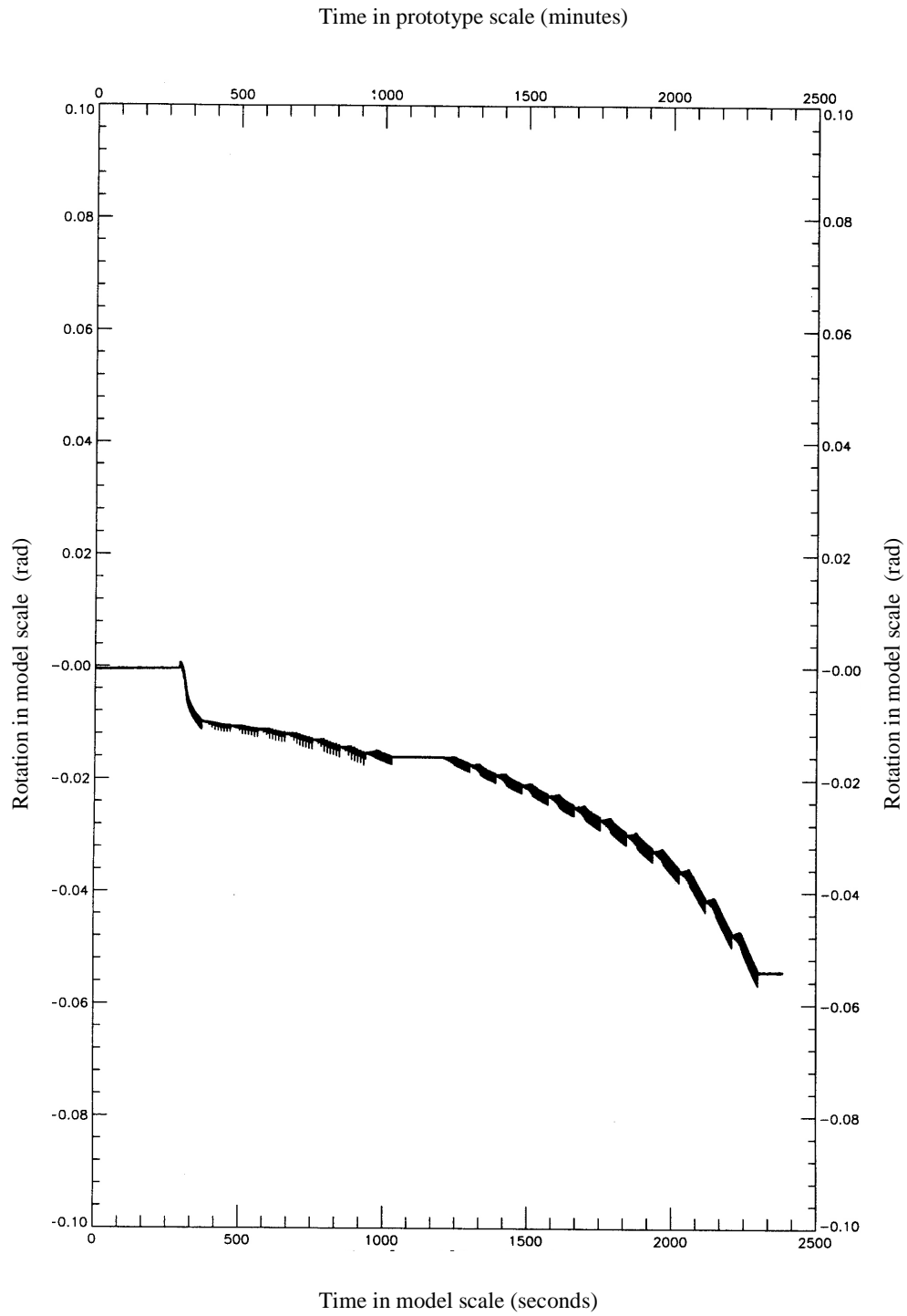


Figure A20 – Rotation versus time

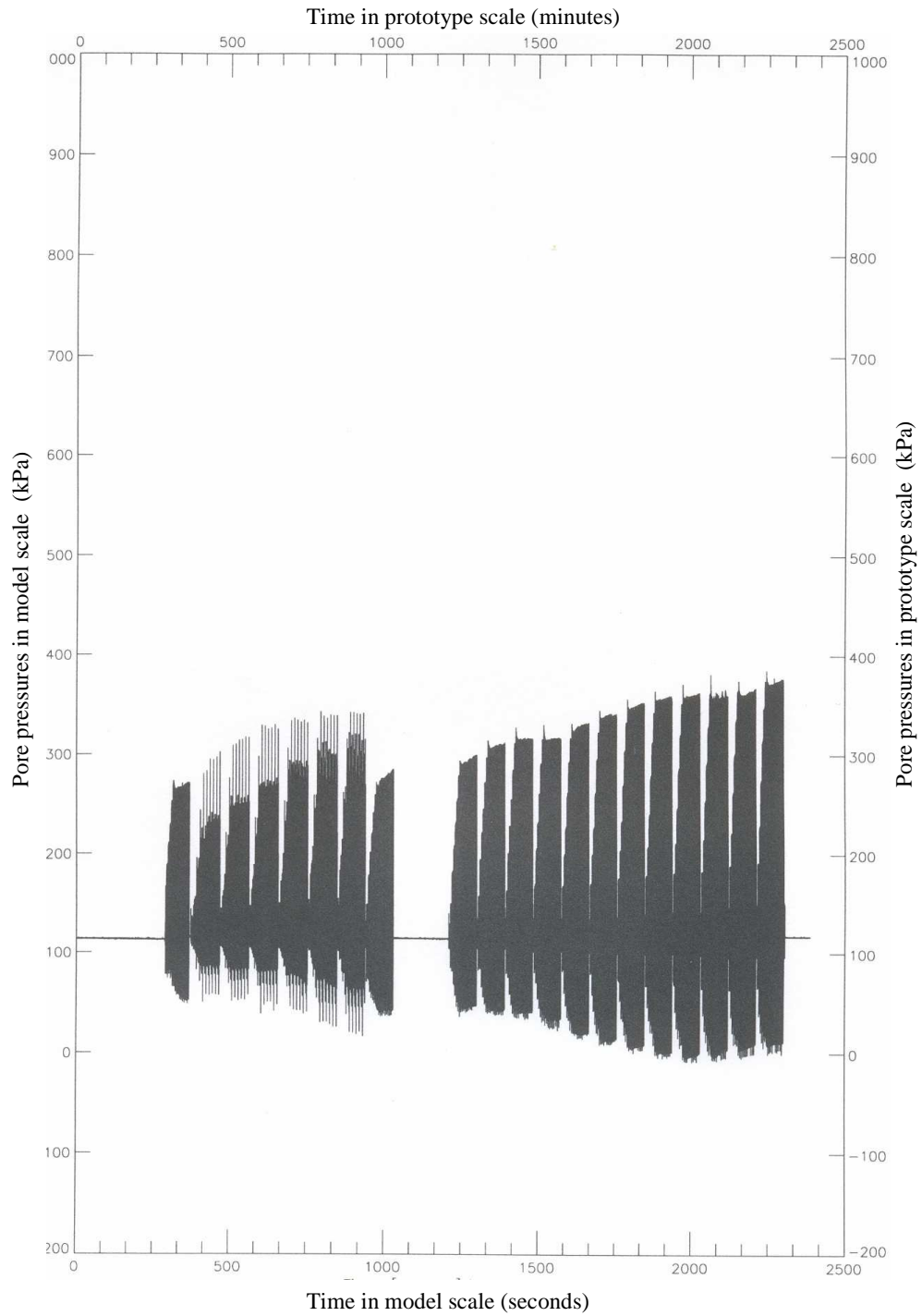


Figure A21 – Pore pressures versus time, transducer UM1

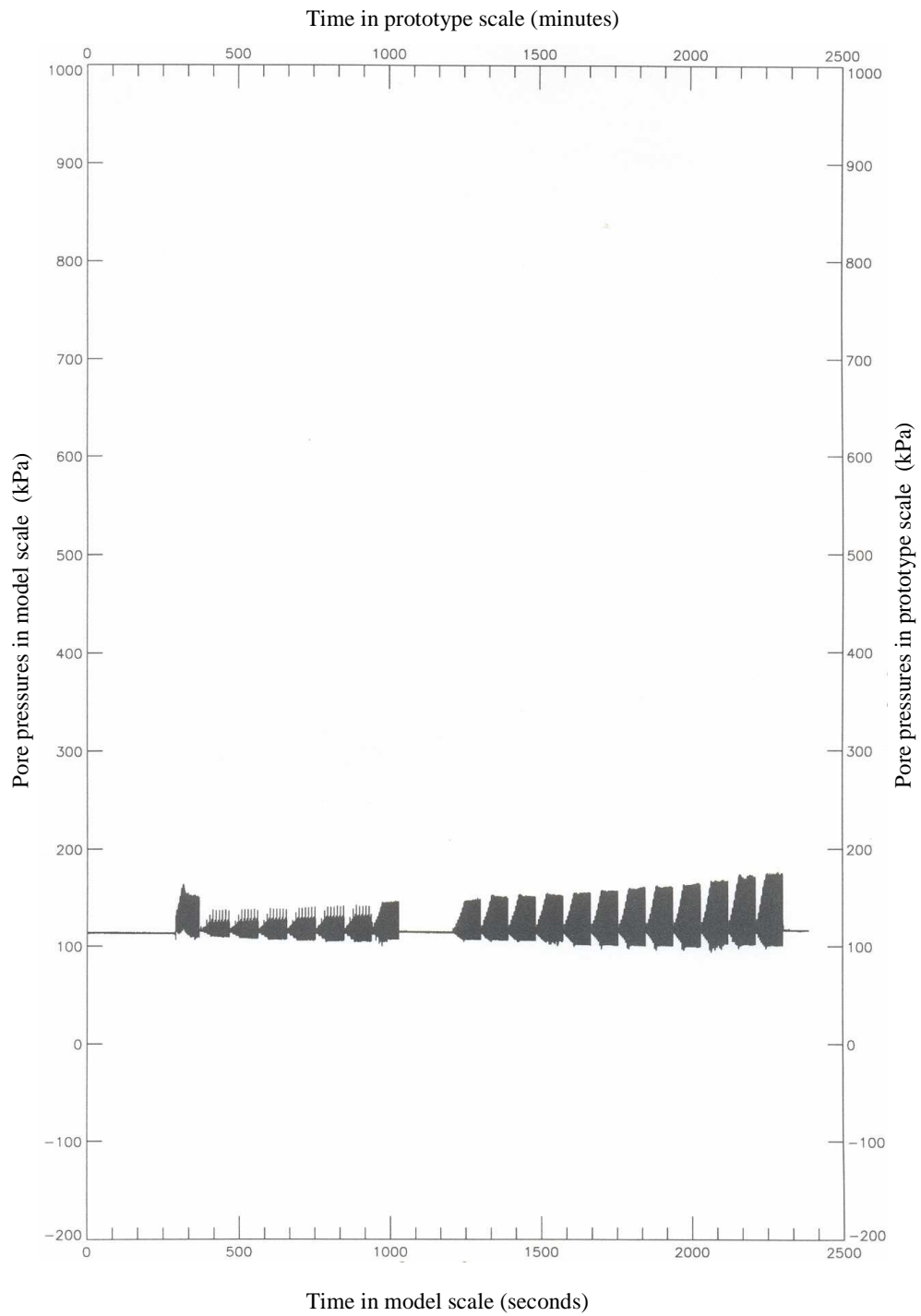


Figure A22 – Pore pressures versus time, transducer UM2

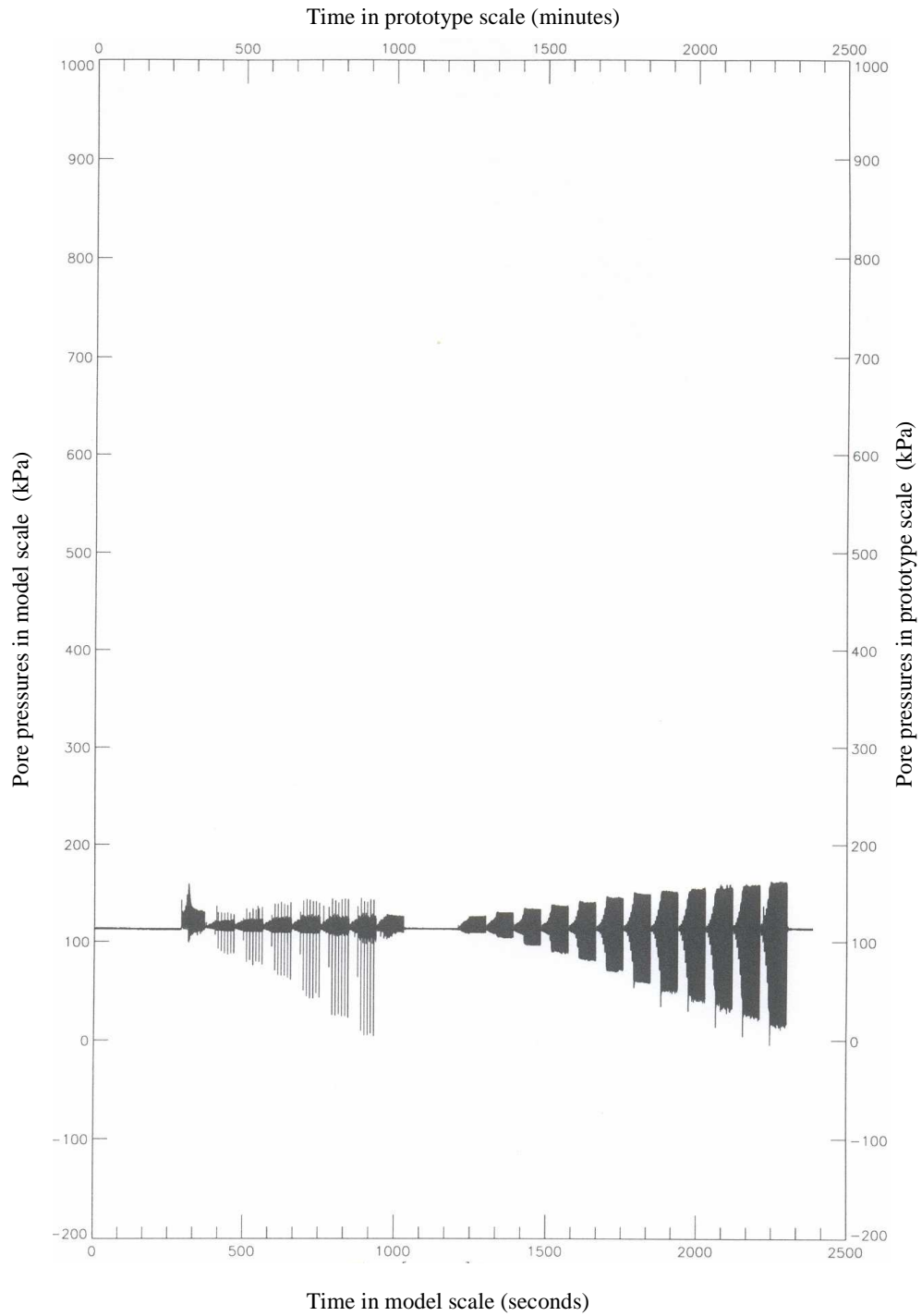


Figure A23 – Pore pressures versus time, transducer UM3

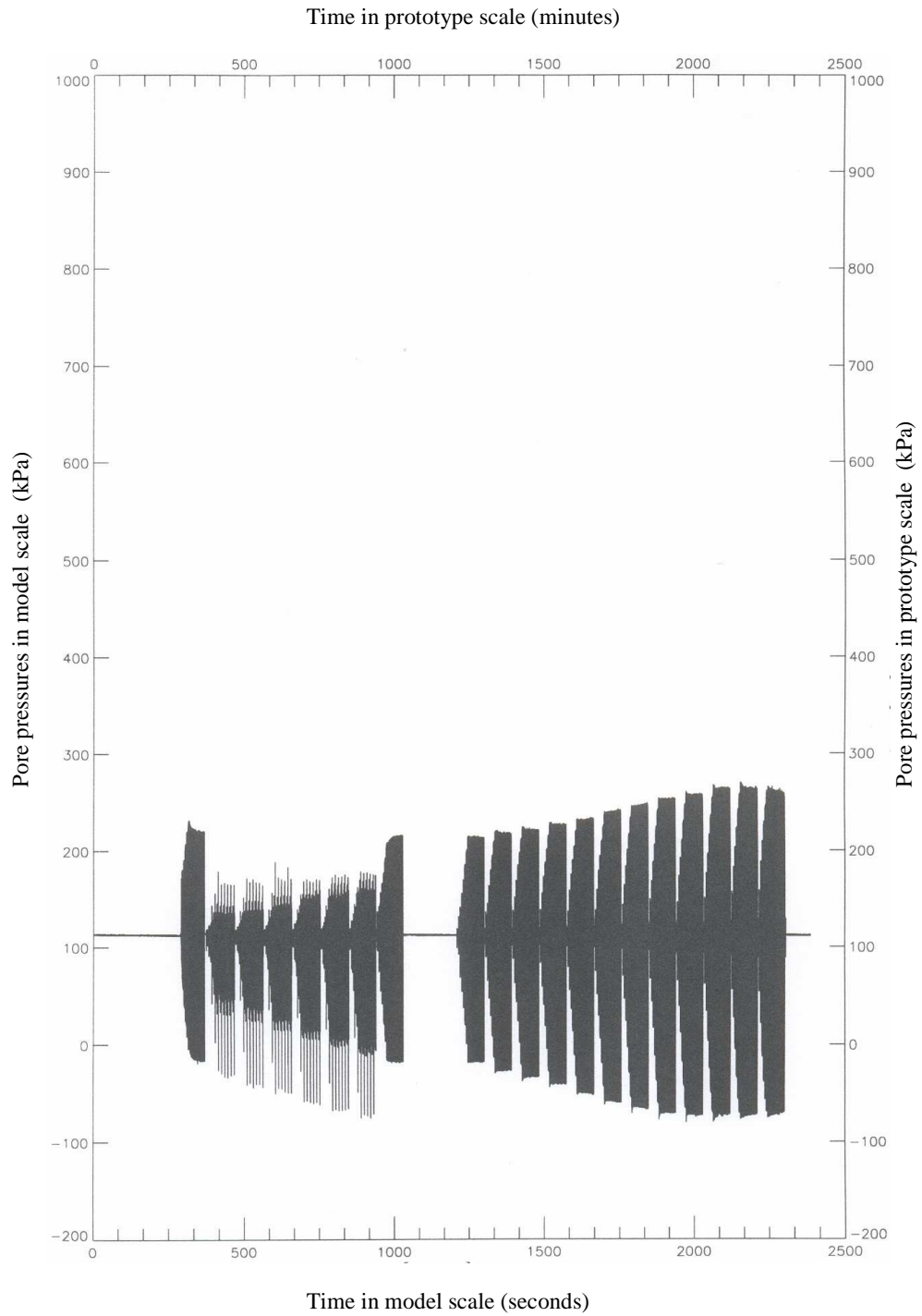


Figure A24 – Pore pressures versus time, transducer UM4

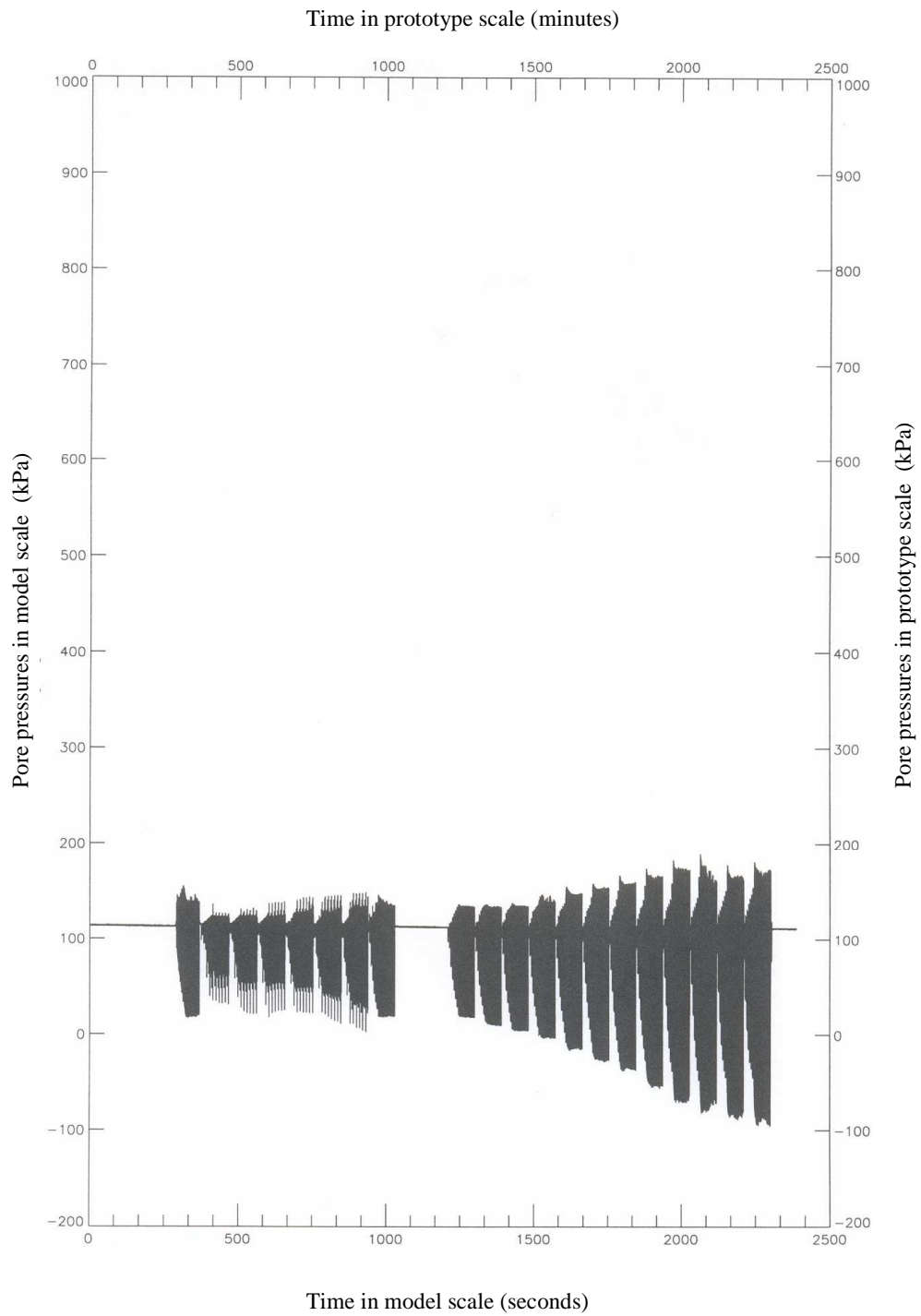


Figure A25 – Pore pressures versus time, transducer UM5

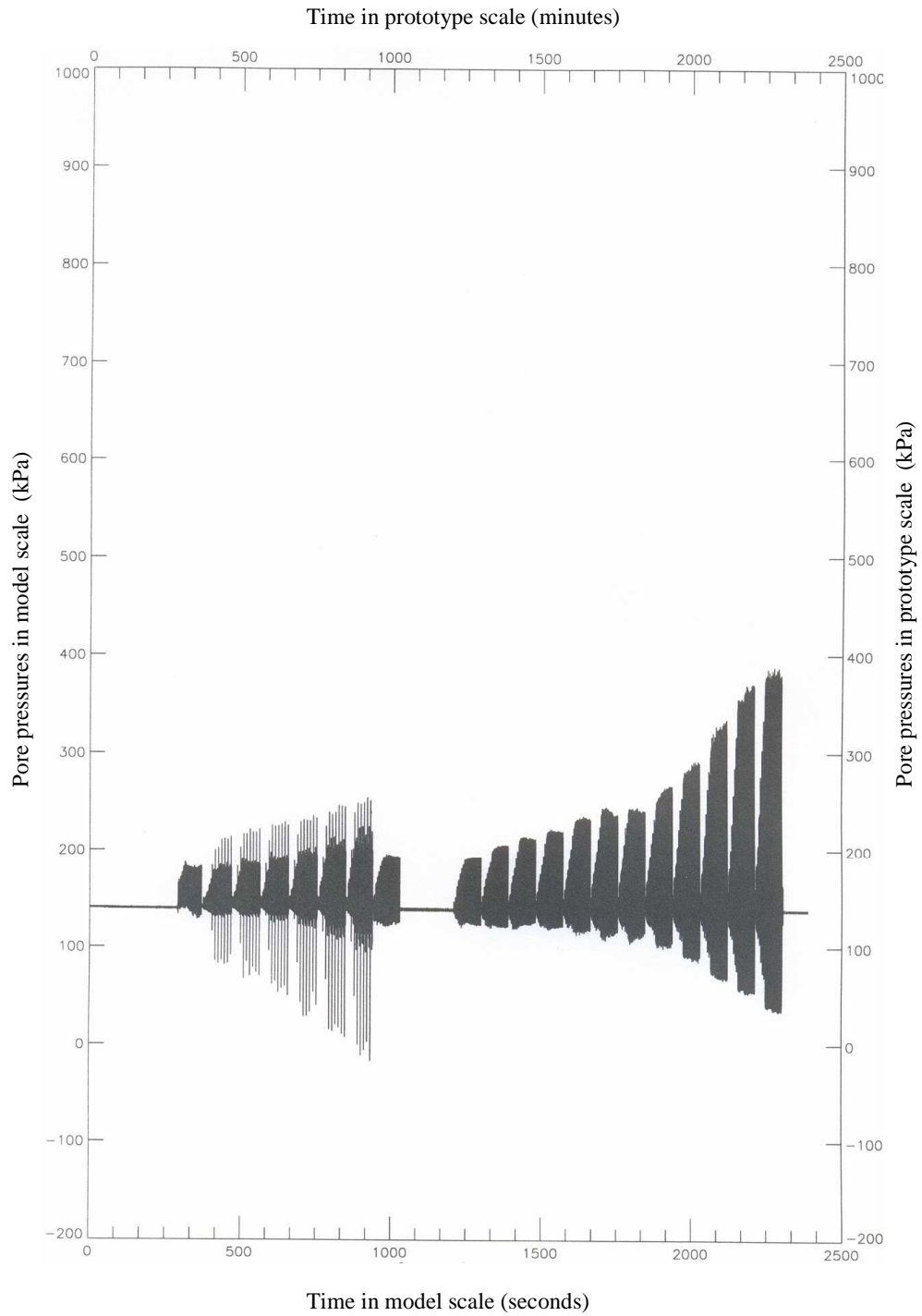


Figure A26 – Pore pressures versus time, transducer US1

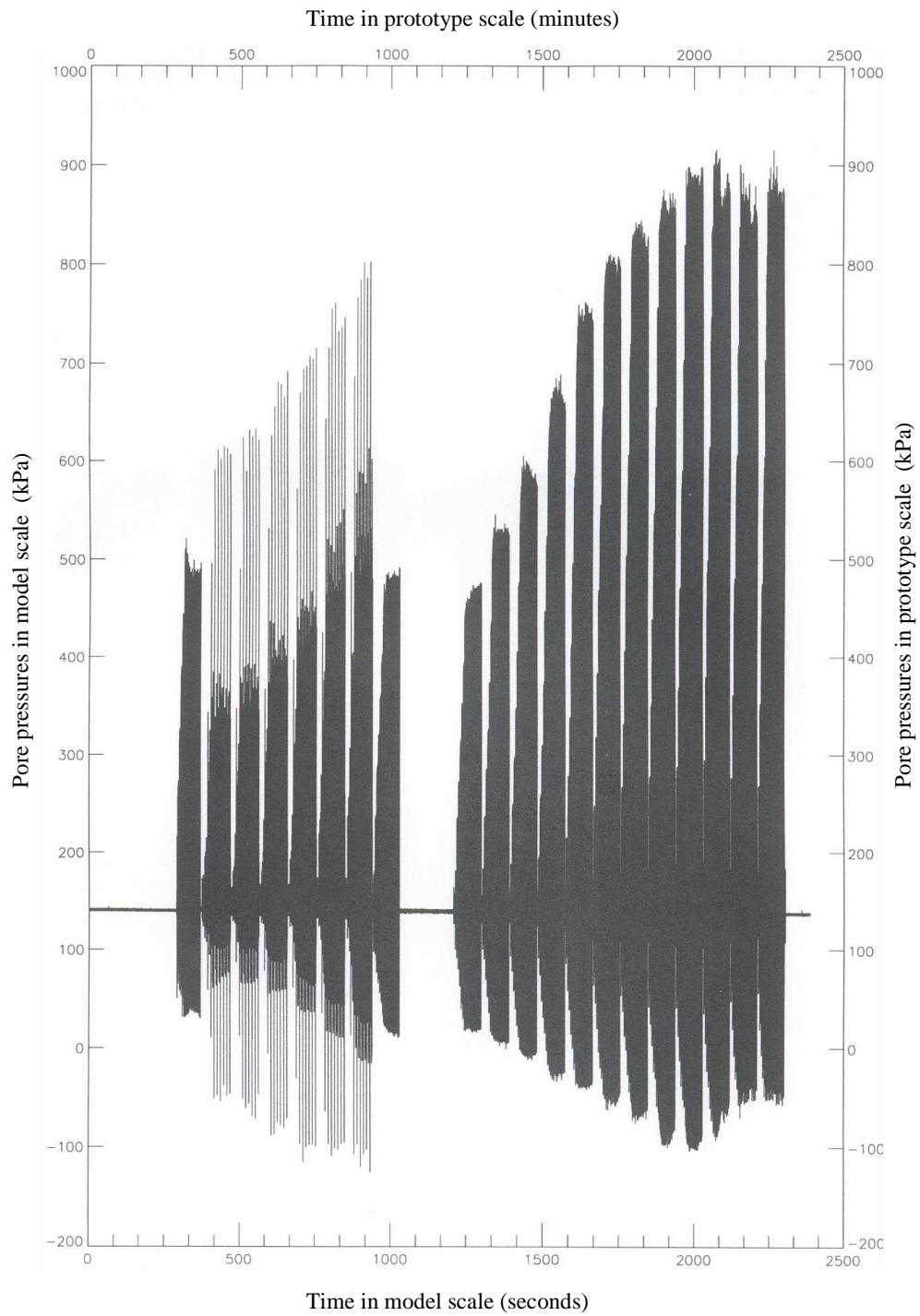


Figure A27 – Pore pressures versus time, transducer US2

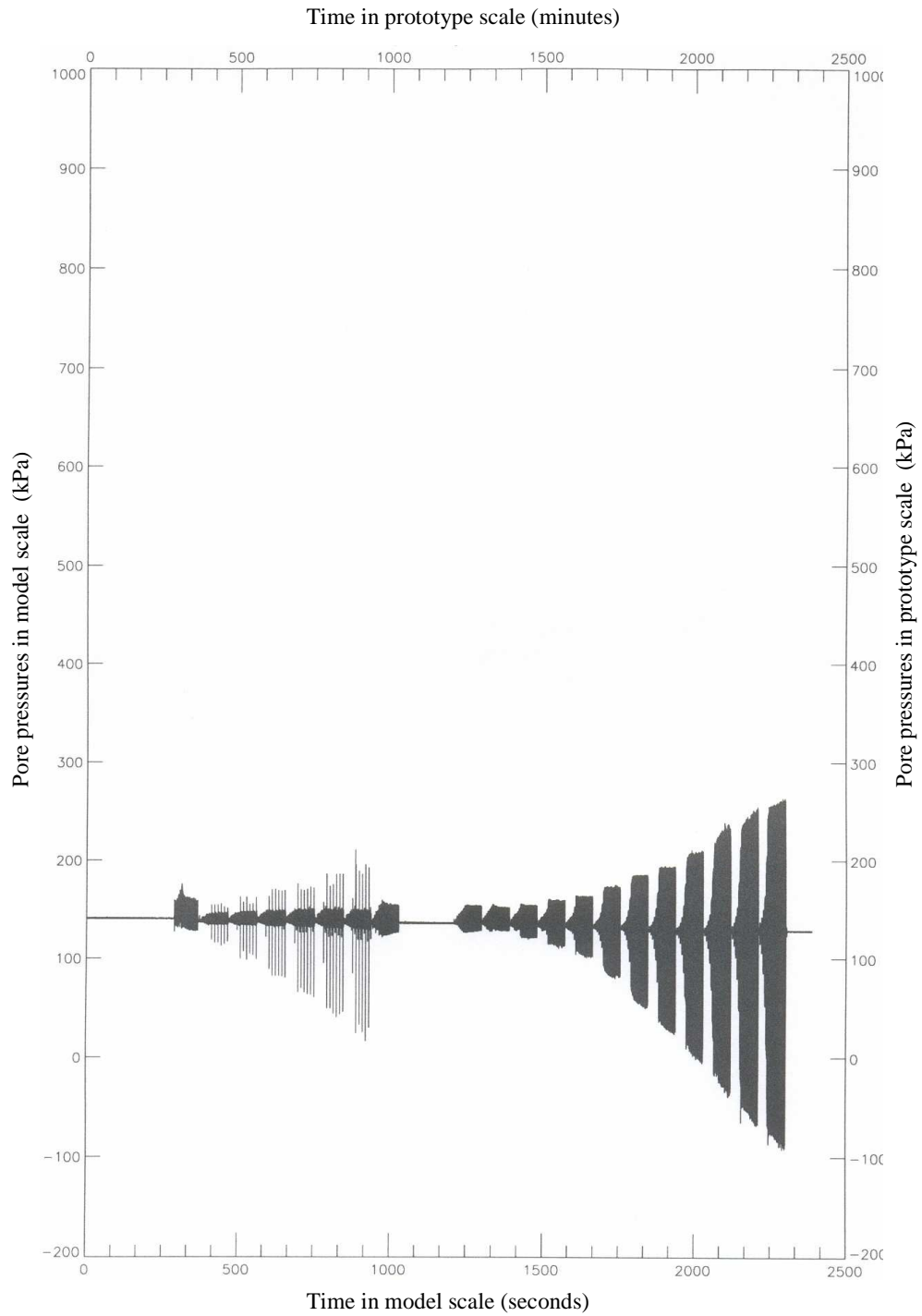


Figure A28 – Pore pressures versus time, transducer US3

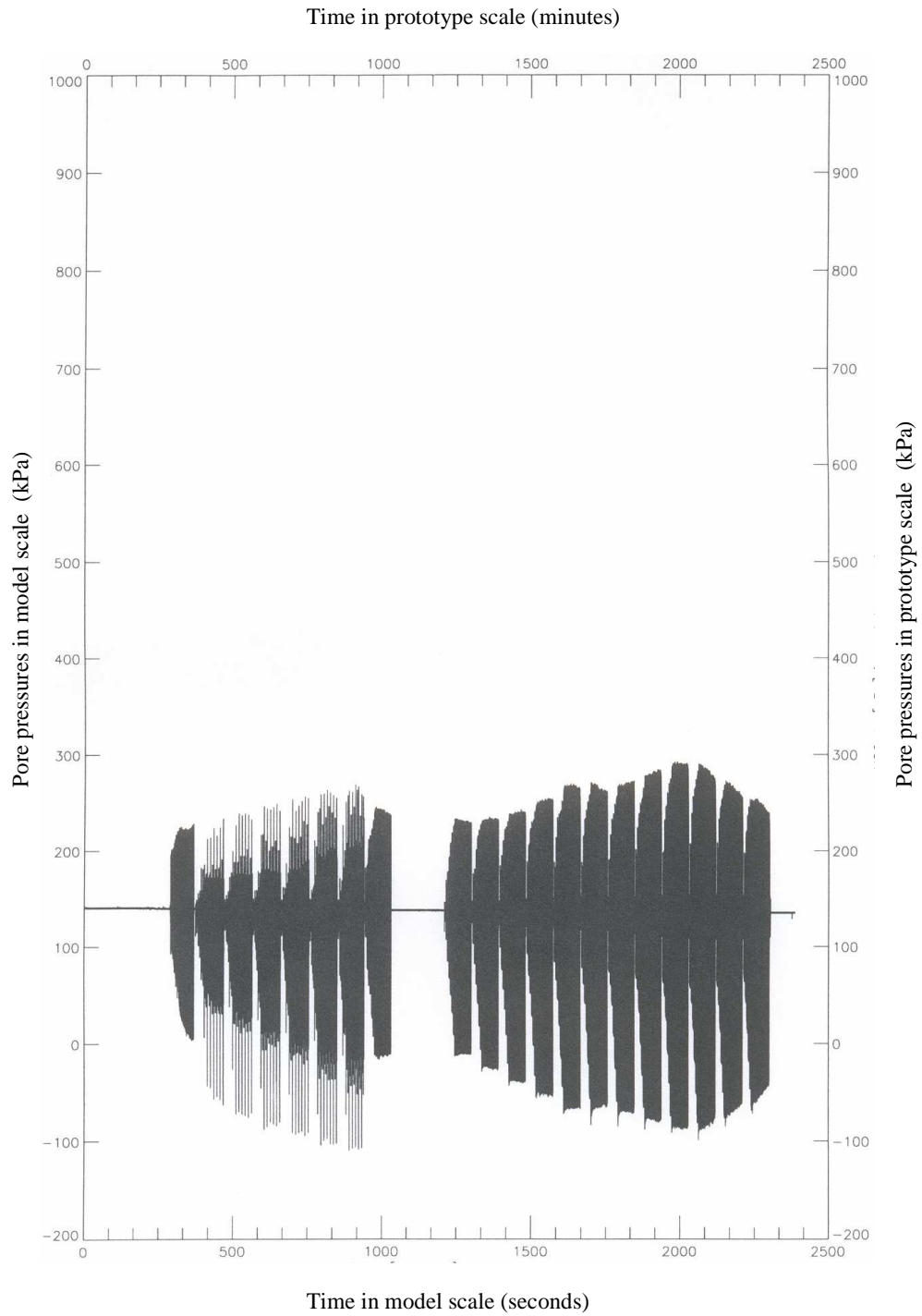


Figure A29 – Pore pressures versus time, transducer US4

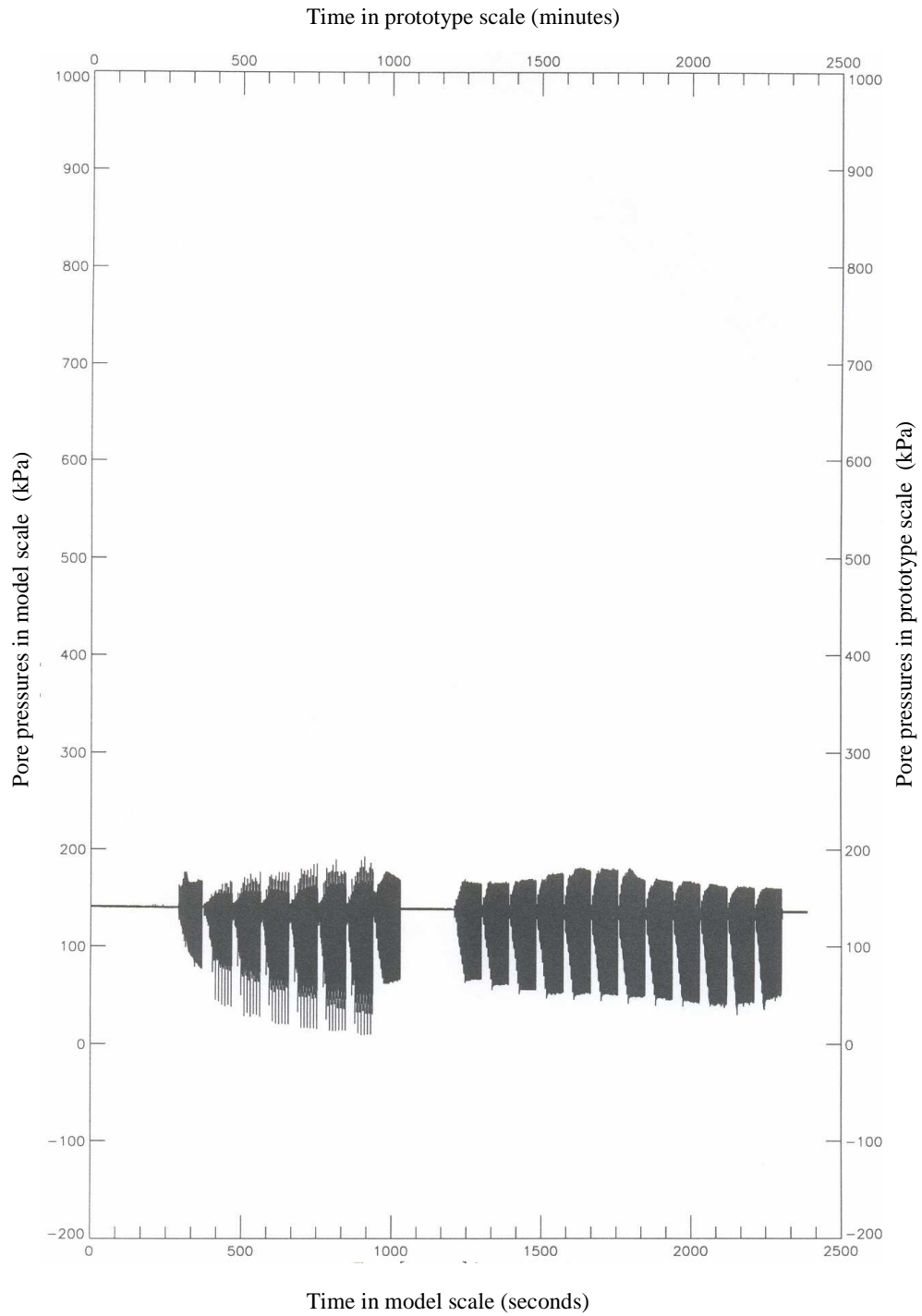


Figure A30 – Pore pressures versus time, transducer US5

Appendix II

Settlements of a real vertical caisson breakwater under wave-induced cyclic loading

1. Introduction

As previously mentioned, this PhD research has been partially supported by “Impresa Pietro Cidonio” S.p.A, specialised Companies for civil and maritime works which promoted the research activity.

Gratefully to this Company, which made the data available, in the framework of this PhD we had the opportunity to follow extensive maritime works carried out in the Port of Civitavecchia (Rome, West Coast of Italy). This port has been recently object of an important renovation and modernisation, in view of a significant expansion of the port itself. Insofar, a breakwater called “Cristoforo Colombo” has been prolonged for a total extension of about 1100 m. A first part of this extension, 510 long, was carried out between 1998-2000. A second part, 570 m long, has been realised between April 2003 and June 2004 and the superstructure is still under construction and it will be completed within June 2005. The breakwater is a monolithic breakwater realised by using seventeen concrete caissons for the first part and nineteen caissons for the second part. Each caisson, with length equal to 30 m, width equal to 20 m and height equal to 20 m, is multi-celled with a granular fill inside each cell. Caissons are placed on an important thickness of rubble layer founded on sandy subsoils. The original seabed is 30÷35 m below the sea level. The structure has been subject to non-breaking waves conditions.

During the construction of the breakwater, monitoring of caissons displacements was carried out. The measurements, collected by means of an accurate geodetic levelling, were performed on the two sides of each caisson so as to monitor the displacements of both sea-side and port-side of the breakwater. At the same time, continuous wave parameters were recorded by a wave-meter sited nearby the breakwater area.

The study has been performed preliminarily for the first extension of the breakwater (Grisolia and Maccarini, 2004), in order to estimate the expected settlements for the second extension and to determine the proper time to place the superstructure.

The monitoring period for the first part is between November 1998 and December 2000 and the recorded measurements include the placement of the first caisson until the complete carrying-out of the superstructure. As far as the second extension is concerned, the measurements of settlements are referred to the period between April 2003 and November 2004.

Collected data enabled to do interesting observations on the breakwater's behaviour under wave-induced cyclic action and to relate the observed settlements to the following aspects:

- a) *placing and filling* of caissons, during which the settlements can be essentially related to the initial compressibility of the seabed and, mainly, of the rubble layer, in "loose" conditions before the placement of the caissons;
- b) *cyclic wave loading* with consequent variation of pore pressure and effective stresses in the rubble layer and in the subsoil;
- c) wave action due to *significant storms* which have different effects on the displacements, depending on the time at which the storm occurs, with respect to the state of construction of the breakwater and to the occurrence of others previous storms.

Figures 1 and 2 show the first extension already completed and the superstructure of the second part, still under construction.

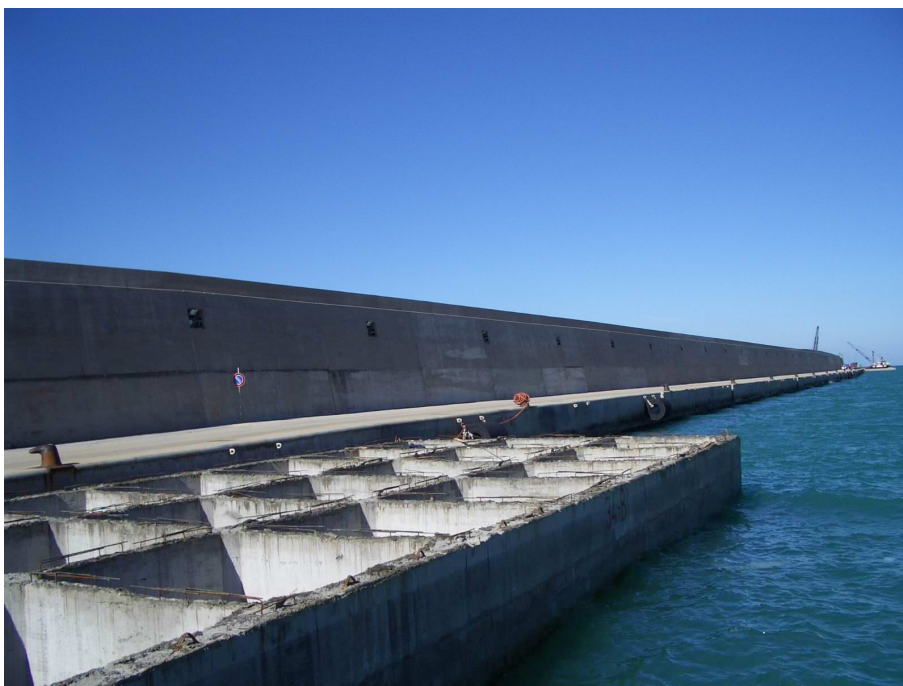


Figure 1

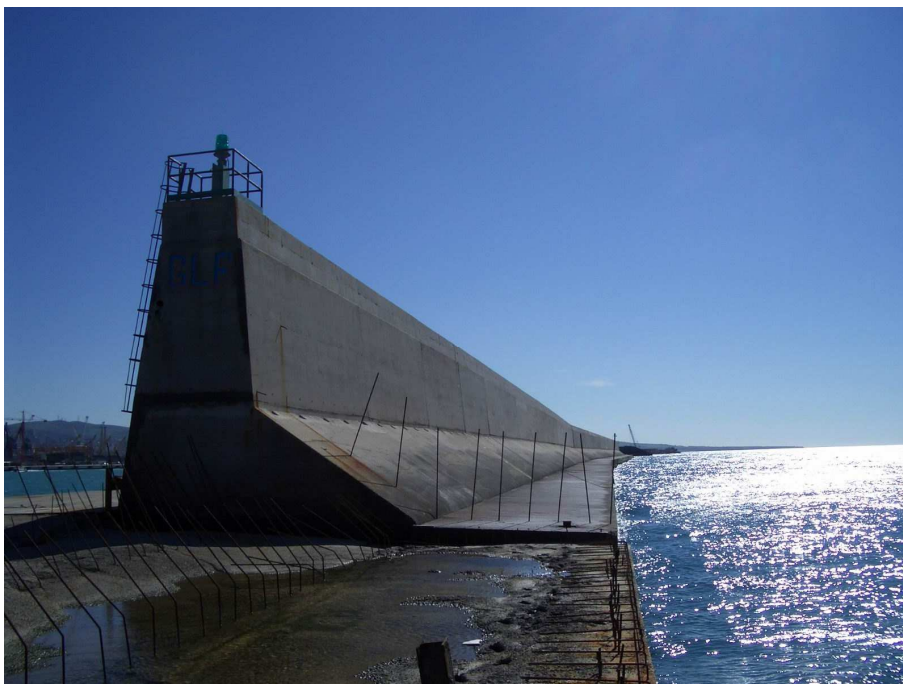


Figure 2

2. Ground profile and geotechnical characterisation

Site soil classification and geotechnical characterisation have been performed by analysing the results of boreholes, in situ and laboratory tests. A topographic survey of the seabed was also carried-out. For the first extension the geotechnical characterisation has been performed on the basis of a previous geotechnical study (Marchetti, 1981), while for the second part a specified geological survey and geotechnical investigations have been carried out. Figures 3 and 4 show the planimetry for the two extensions of the breakwater. In Figures 5 and 6 the longitudinal sections for the first and second part are shown. In the first case (Figure 5) the thickness of the rubble layer ranges between 7 m (below caisson n. 2) and 11 m (below caisson n. 9), due to the seabed depth. Amongst the rubble layer and the original seabed, a layer of “tout-venant” of 2.50 m, realised with dense sand mixed to gravel, has been placed. The original seabed it is characterised by a layer of gravel mixed to sand of about 4.00 m of thickness. Then, a substrate of stiff silty-sand features the subsoil. As far as the second extension is concerned (Figures 6), a different geotechnical situation is present. Below the rubble layer (that ranges between 8 and 12 m) and the constant thickness of tout-venant (equal to 2.5 m), a layer of sandy soil is found. The thickness of this layer is strongly variable, amongst 10 m (boreholes S1, S6) and 2÷3 m (in the remaining investigated zone). The substrate is characterised, in this case, by sand and dense silty-sand mixed to fragments of carbonate rock. In Figures 5 and 6, the geotechnical parameters deduced for all the soils have been reported. It is important to observe that the Young’s modulus for the rubble layer is not always easy to evaluate. In fact, even though the material is usually very stiff, the layer may be greatly compressible because of the highly loose conditions and the high void ratio of the gravel established during the placement of the material. The Young modulus, equal to 10 MPa, has been deduced from a back analysis of the settlements recorded during the placing and filling of the caissons. Figures 7 and 8 show a simplified scheme of the structure and some cross-sections of the subsoils.

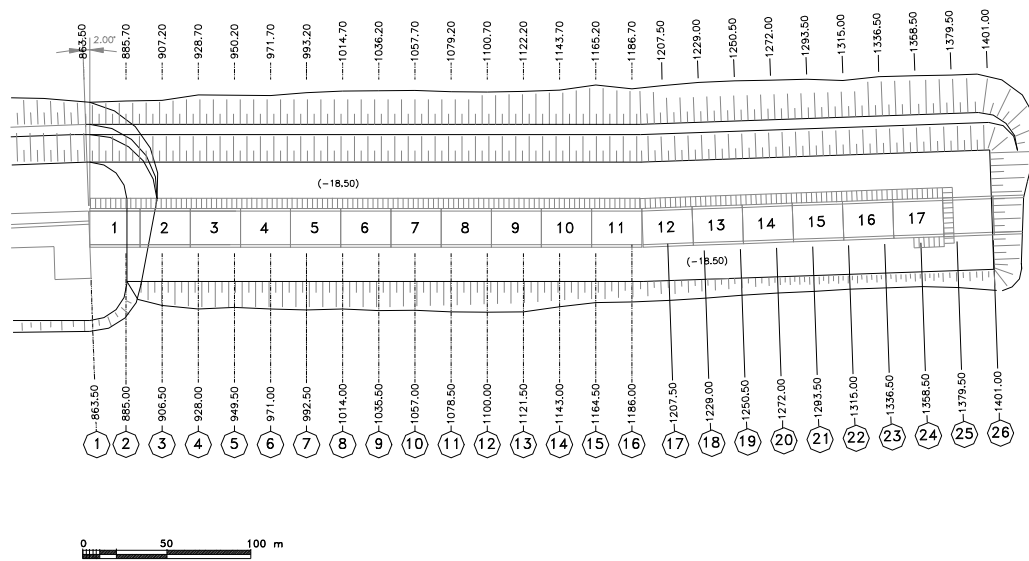


Figure 3. Port of Civitavecchia – “Cristoforo Colombo” Breakwater – Planimetry I extension

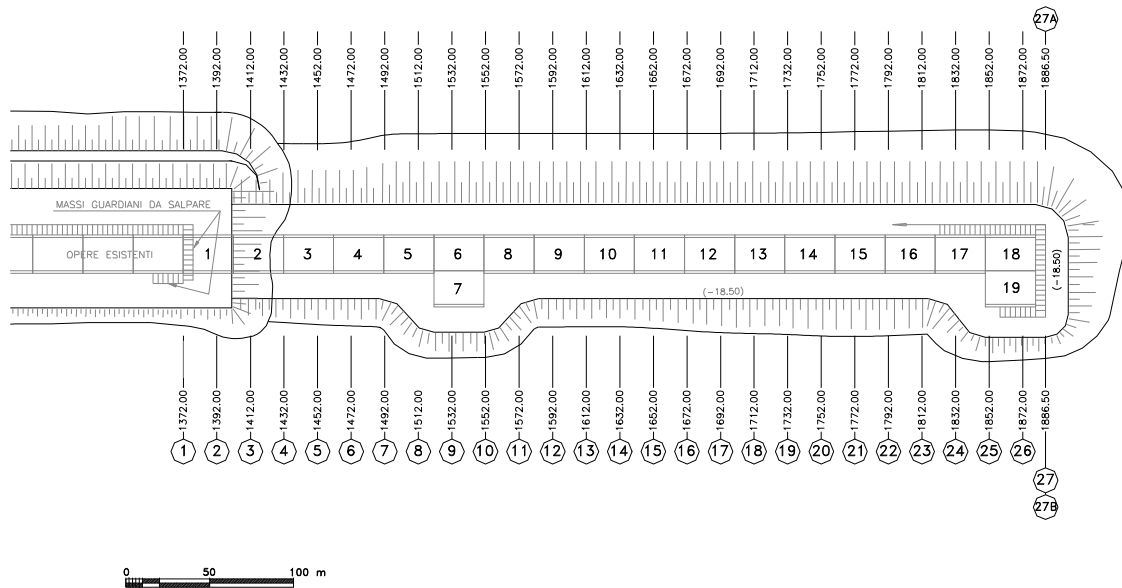
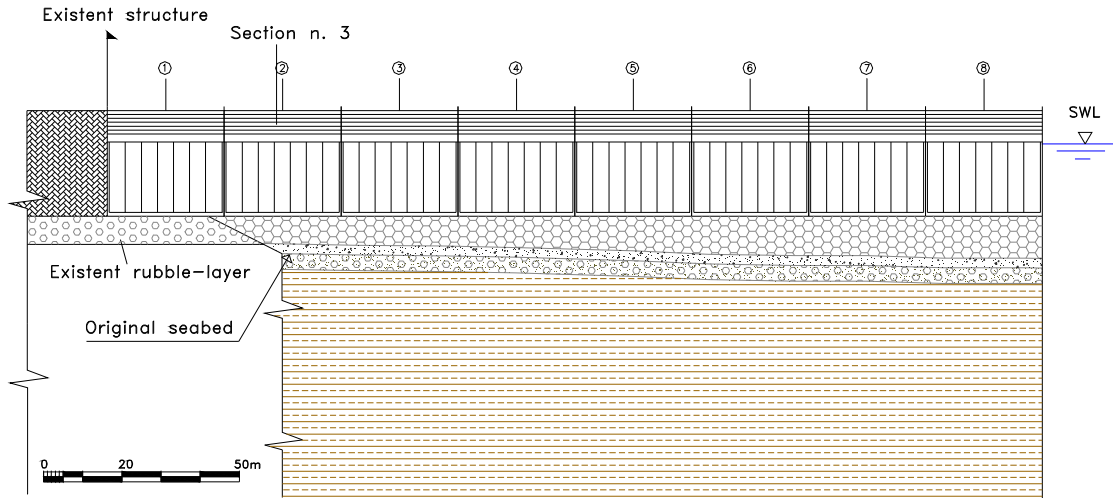


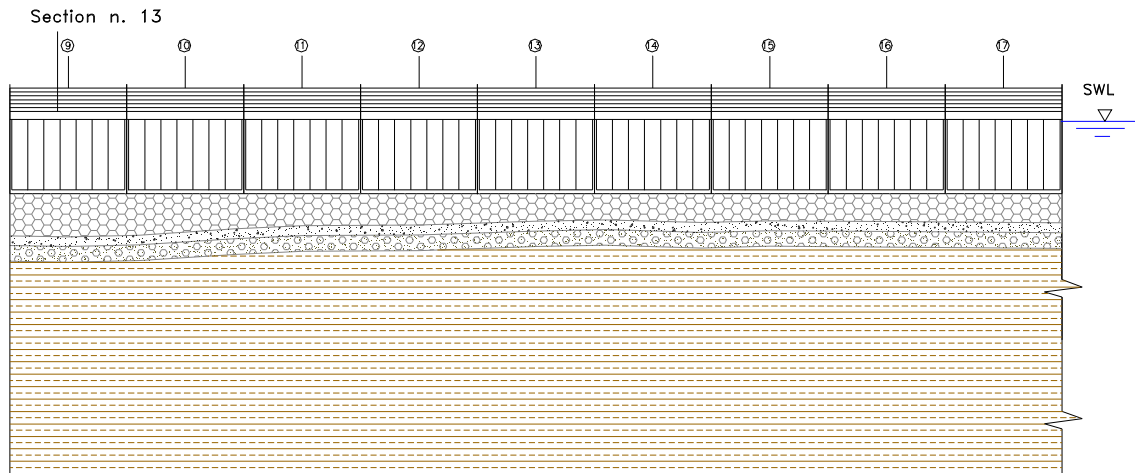
Figure 4. Port of Civitavecchia – “Cristoforo Colombo” Breakwater – Planimetry II extension

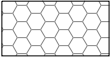
PORT OF CIVITAVECCHIA
Cristoforo Colombo Breakwater

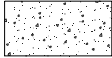
Longitudinal section I Extension (chainage 863.50 – 1100.00)

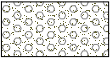


Longitudinal section I Extension (chainage 1100.00 – 1358.00)



 Rubble mound
 $\gamma=20 \text{ kN/mc}$
 $c'=0 \text{ kPa}$ $\phi'=40^\circ$ $E'=10 \text{ MPa}$

 Layer of "tout venant"
 $\gamma=20 \text{ kN/mc}$
 $c'=0 \text{ kPa}$ $\phi'=35^\circ$ $E'=10 \text{ MPa}$

 Gravel and Sand
 $\gamma=20 \text{ kN/mc}$
 $c'=0 \text{ kPa}$ $\phi'=27^\circ$ $E'=20 \text{ MPa}$


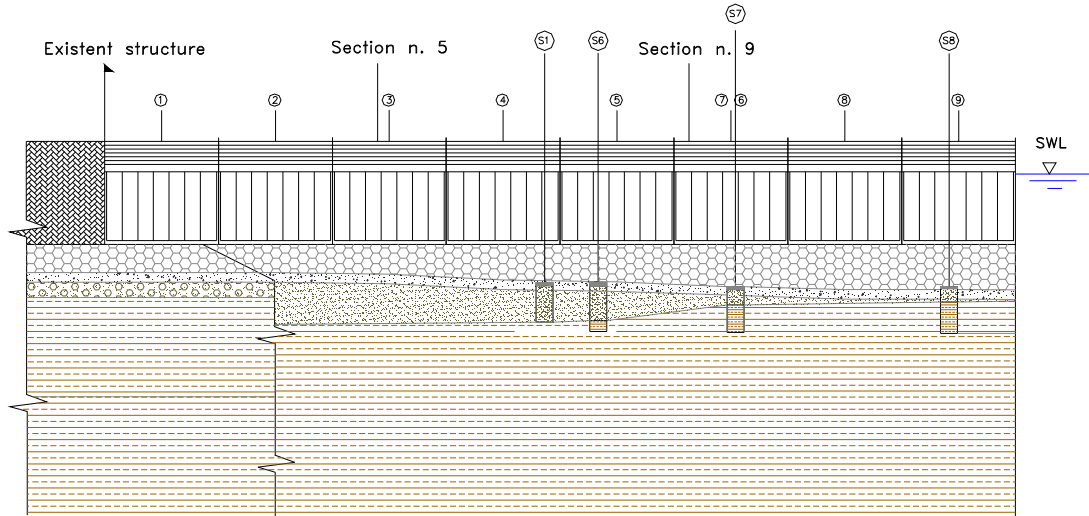
 Silty sand
 $\gamma=20 \text{ kN/mc}$
 $c'=10 \text{ kPa}$ $\phi'=20^\circ$ $E'=50 \text{ MPa}$

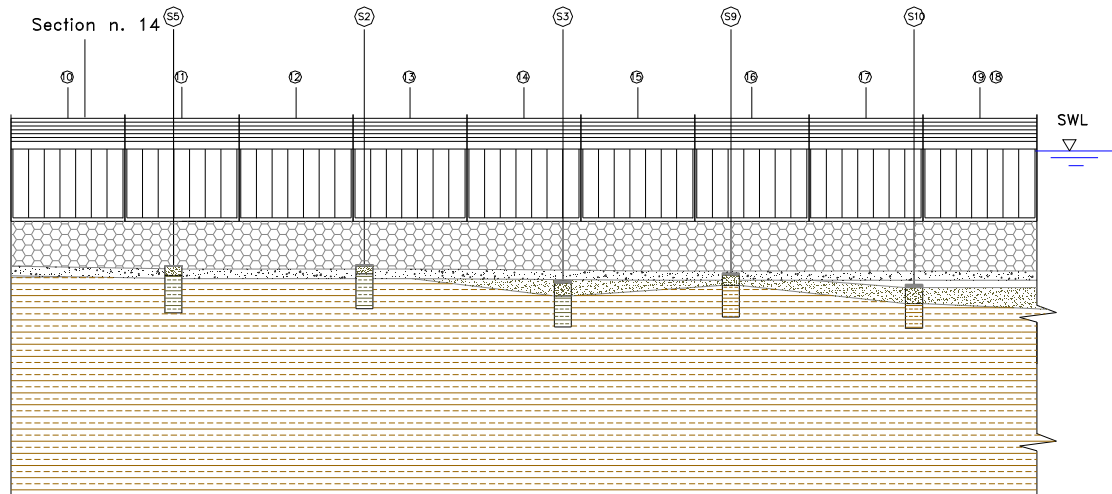
Figure 5. Ground profile and geotechnical scheme – I Extension

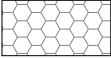
PORT OF CIVITAVECCHIA
Cristoforo Colombo Breakwater

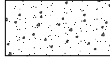
Longitudinal section II Extension (chainage 1372.00 – 1612.00)

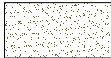


Longitudinal section II Extension (chainage 1612.00 – 1872.00)



 Rubble mound
 $\gamma=20 \text{ kN/mc}$
 $c'=0 \text{ kPa}$ $\phi'=40^\circ$ $E'=10 \text{ MPa}$

 Layer of "tout-venant"
 $\gamma=20 \text{ kN/mc}$
 $c'=0 \text{ kPa}$ $\phi'=35^\circ$ $E'=10 \text{ MPa}$

 Sand medium-dense mixed to gravel
 $\gamma=19 \text{ kN/mc}$
 $c'=0 \text{ kPa}$ $\phi'=30^\circ$ $E'=20 \text{ MPa}$


 Dense sand very stiff
 $\gamma=20 \text{ kN/mc}$
 $c'=5000 \text{ kPa}$ $E'=50 \text{ MPa}$

Figure 6. Ground profile and geotechnical scheme – II Extension

Cross sections I Extension

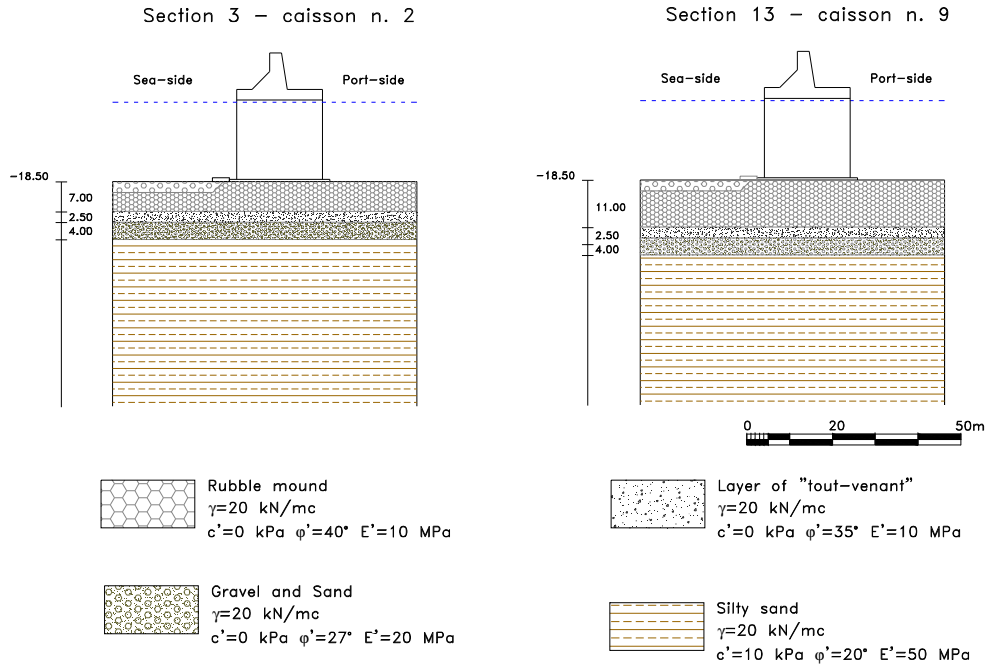


Figure 7. Cross Sections – I Extension

Cross sections II Extension

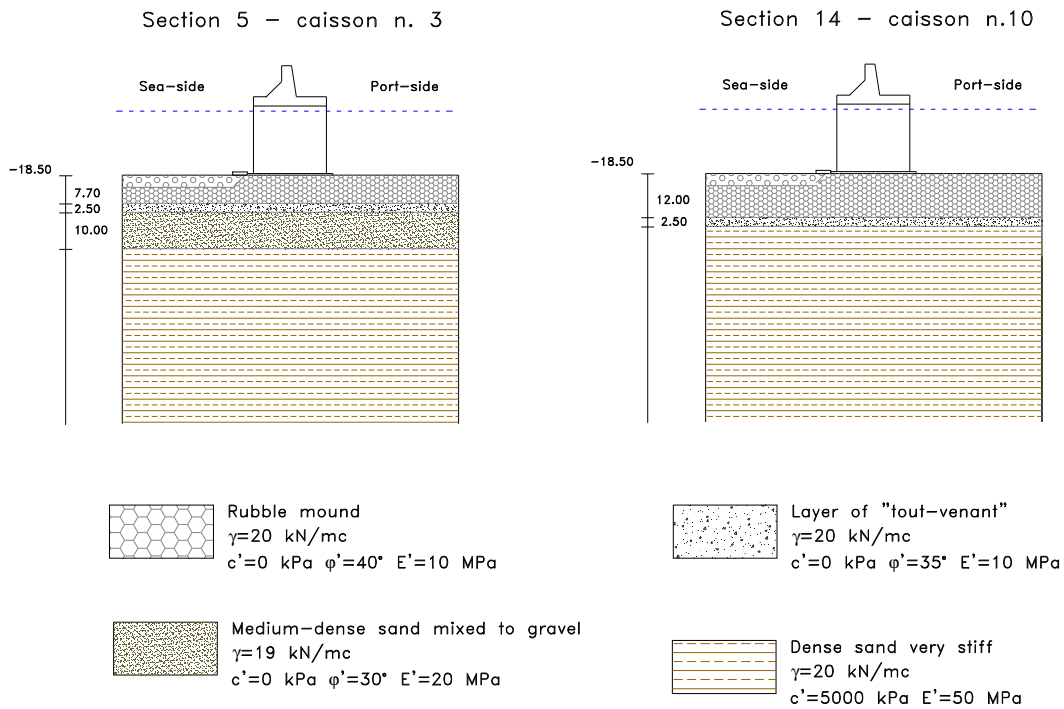


Figure 8. Cross Sections – II Extension

3. Recorded settlements

3.1 Total settlements

Both, in first and second extension of breakwater, settlements were measured by means of topographic levelling of four targets, as shown in Figure 9.

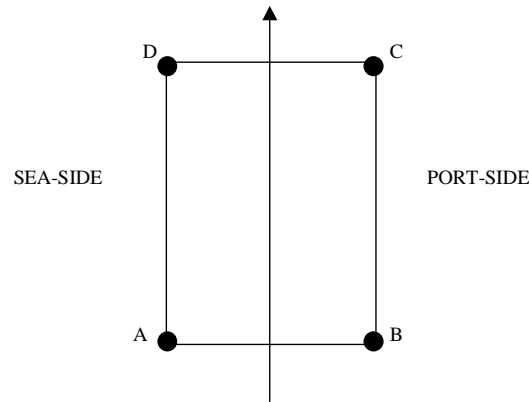


Figure 9. Targets position

The graphs in Figures 10-13 and 14-17 show the total displacements recorded for all the caissons during the whole observation period and the wave characteristics, in terms of significant height, frequency and duration. The Figures 10-13 are referred to the first extension and the Figures 14-17 are referred to the second extension of the breakwater. In both of cases only the storms with significant height higher than 2 meters have been taken into account. From the graphs, settlements due to the filling of the caissons and settlements due to the wave action can be distinguished. In the second extension this is particularly evident for the “oldest” caissons, for which a longer period of observation is available. For the others caissons (caissons 15-19 and caisson 7), nowadays the effect of the filling can be mainly observed. As regards the wave parameters, unfortunately, the data between June 2003 and August 2003 are not available. On the other hand, not significant storms occurred in this period of the year.

The typical curve of settlements of the caissons has been reported for the two extensions in the graphs of Figures 18 and 19. In the next sections the different share of settlements are discussed.

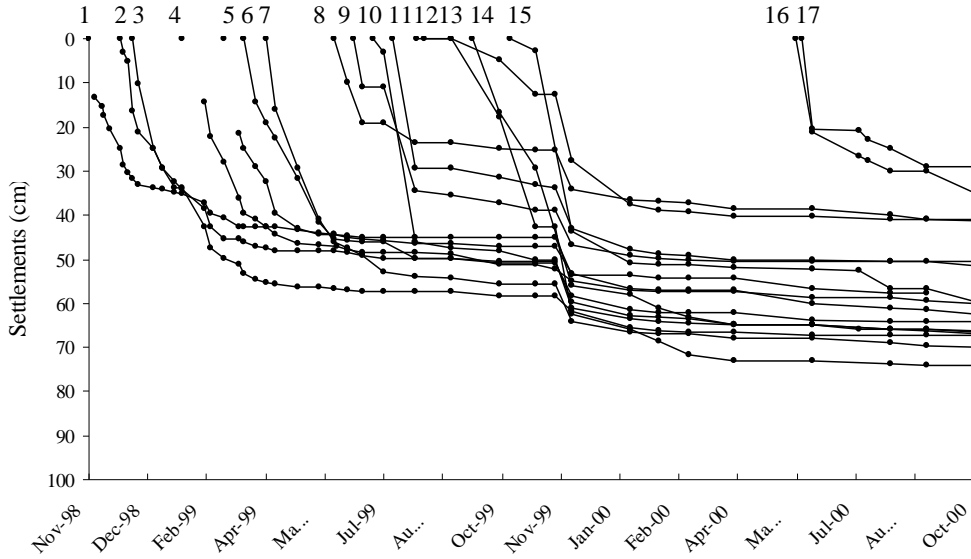


Figure 10. Total settlements of caissons - I Extension

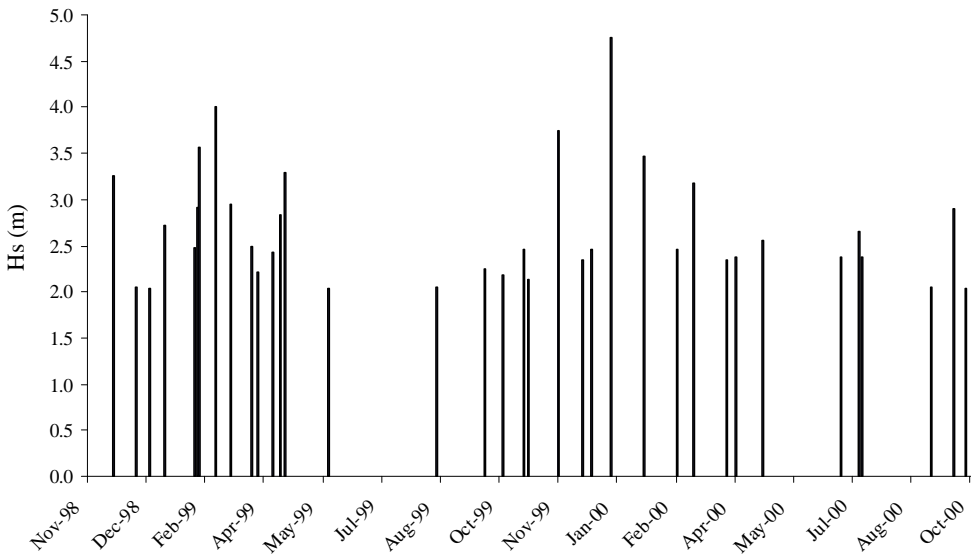


Figure 11. Significant heights of the events recorded during the construction of I Extension

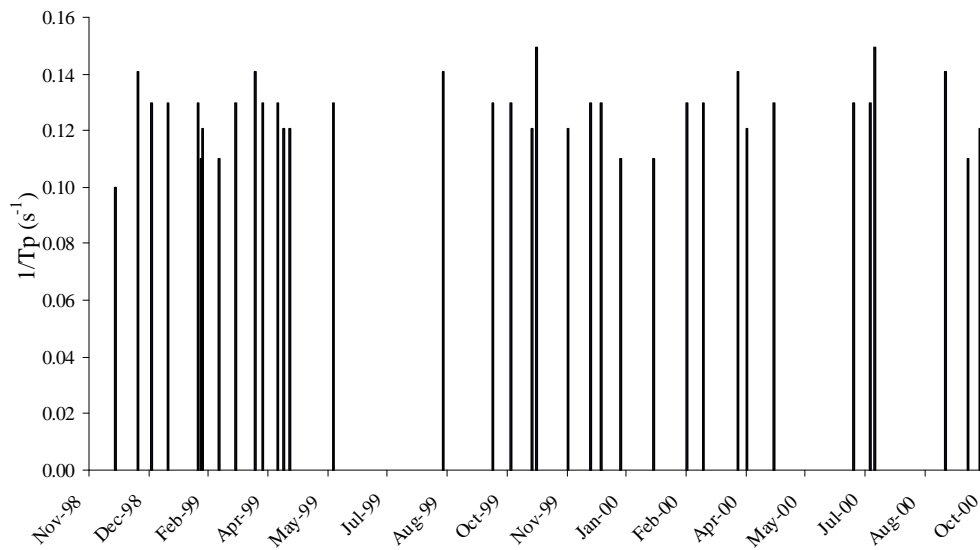


Figure 12. Frequency of the events recorded during the construction of I Extension

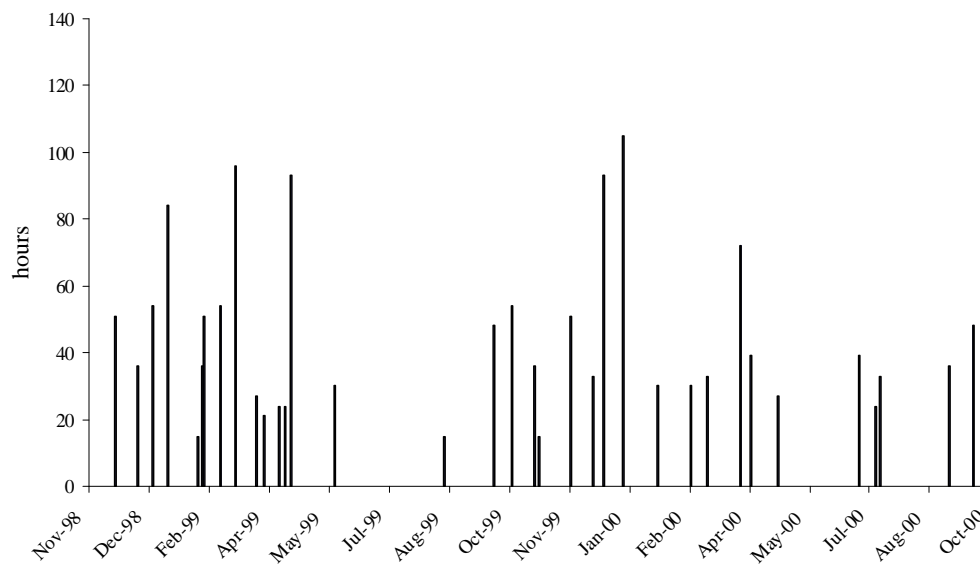


Figure 13. Duration of the events recorded during the construction of I Extension

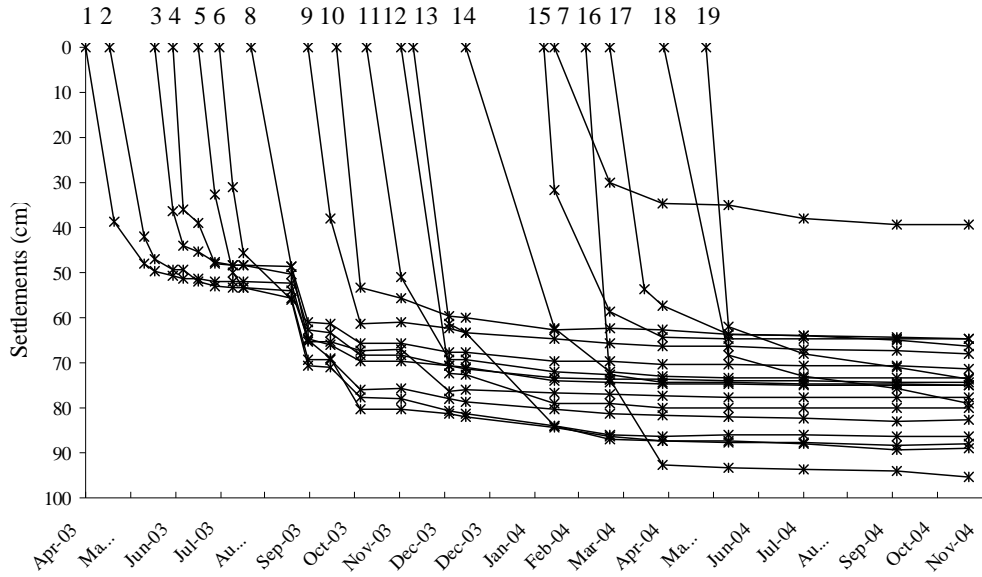


Figure 14. Total settlements of caissons - II Extension

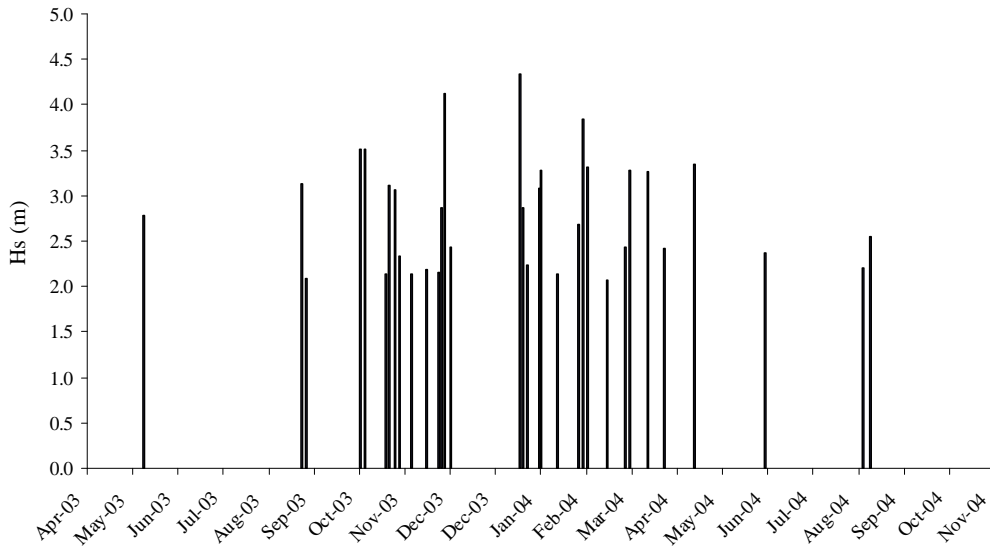


Figure 15. Significant heights of the events recorded during the construction of II Extension

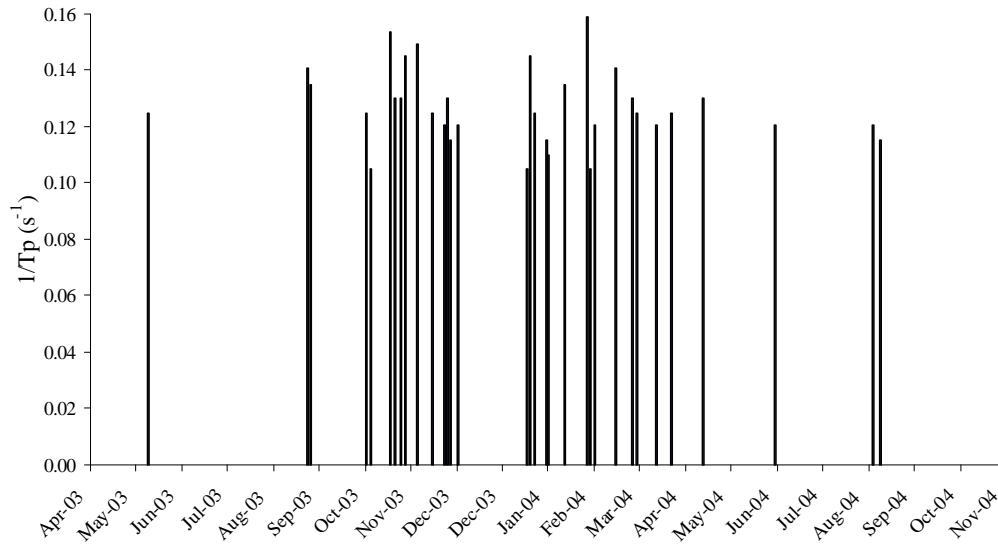


Figure 16. Frequency of the events recorded during the construction of II Extension

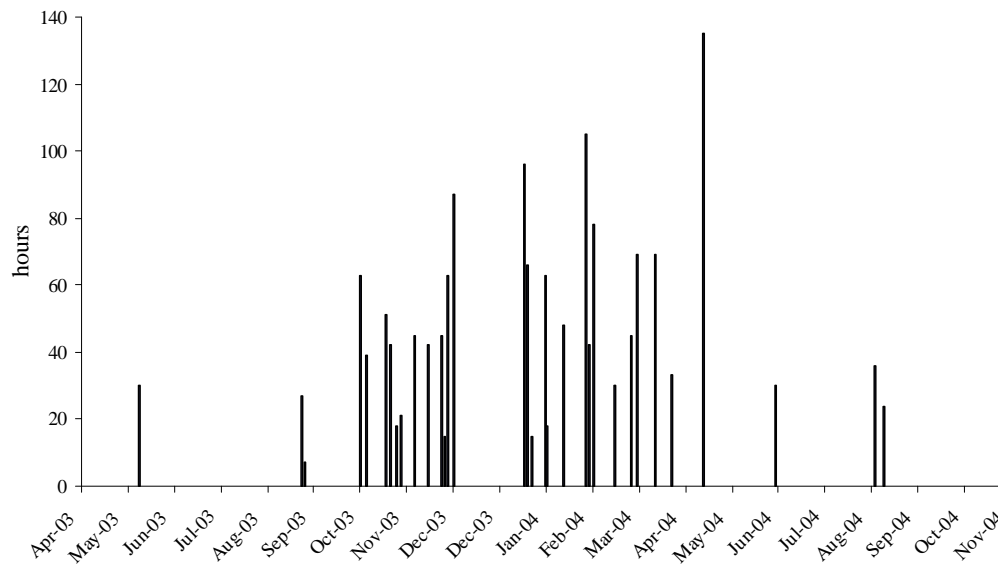


Figure 17. Duration of the events recorded during the construction of II Extension

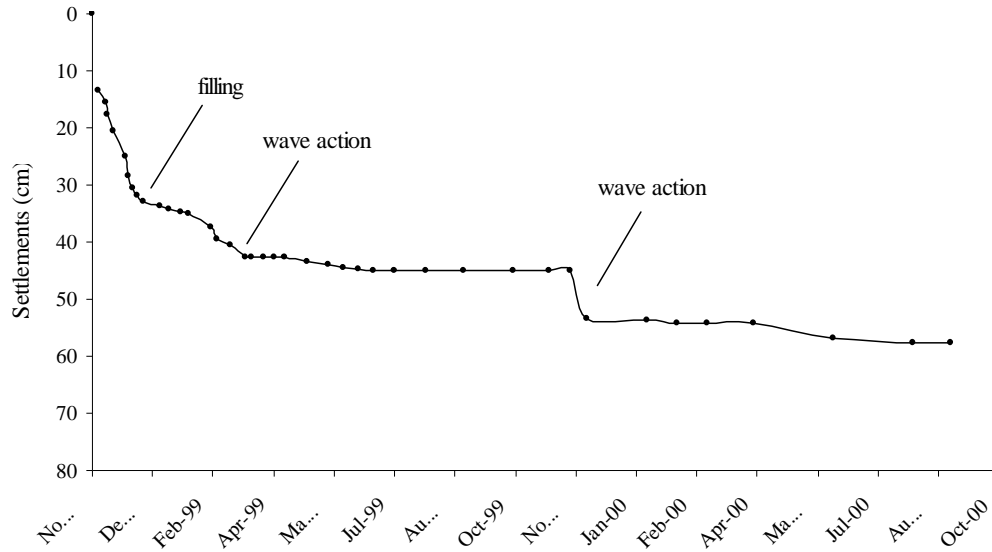


Figure 18. Typical curve of settlements - I Extension

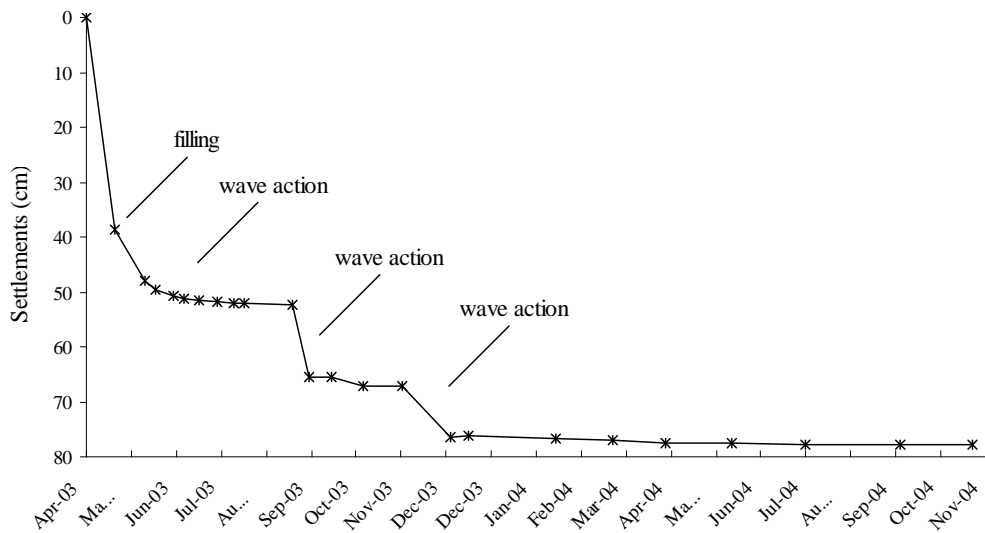


Figure 19. Typical curve of settlements - II Extension

3.2 Settlements due to the filling of the caissons

The average settlements recorded immediately after the filling are reported in Figures 20 and 21 for all the caissons. They can be mainly related to the immediate settlements of the rubble layer, characterised by a considerable thickness (ranging between 7÷11 m in the first extension and between 8÷12 m in the second extension) and by a high void ratio in initial conditions. They range between 25÷45 cm for the first extension and between 40÷50 cm for the second extension. The higher values recorded in the second case can be attributed to the higher thickness of the rubble layer due to the larger depth of the seabed. In both of the cases we observe that larger values are often associated to the simultaneous occurrence of important storms during the filling of the caissons. This has been observed for the caissons 3, 12 and 15 of the first extension, for which settlements respectively of 50 cm and 44 cm have been measured. In the second extension, settlements after the filling increase with the depth of the seabed and they range between 60÷75 cm for caissons 12, 13, 14, 16, 17, 18 and 19. Most of these caissons (12, 13, 14, 17 and 18) were subjected to the action of relevant events during the filling. A different behaviour has been observed for the caissons 7 and 15 for which the recorded values are lower and equal to around 30 cm. The caisson n. 7 is an “edge” caisson that was filled on March 2004 and placed on a rubble layer most likely already made dense by the positioning of the adjacent caissons, filled several months before. Furthermore, although several relevant storms were recorded amongst the positioning and the filling of the caisson, they did not have significant influence since, for its position, the caisson was not directly exposed to the wave action. A singular case is the difference recorded for caisson 15 and 16, for which two quite different values of settlement have been recorded.

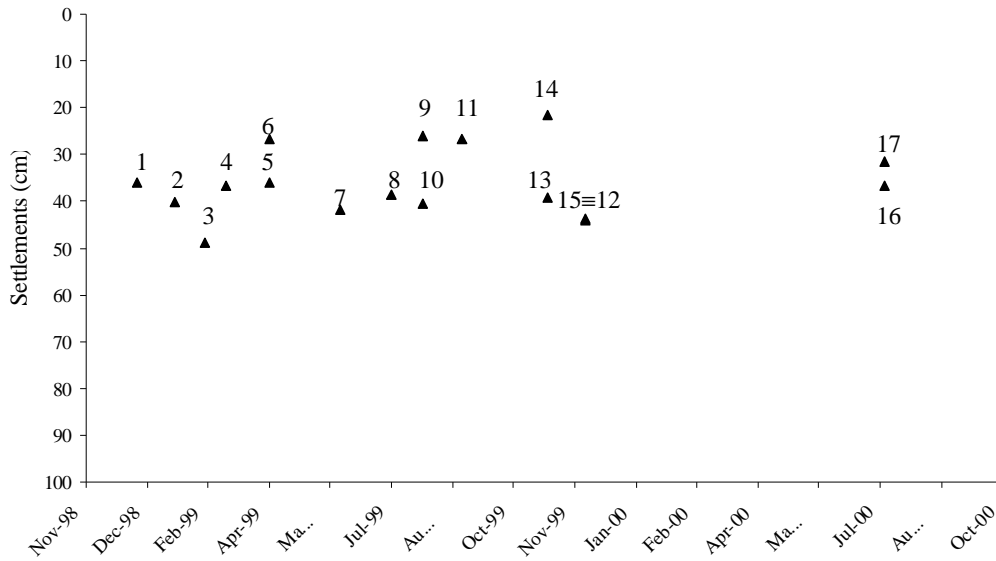


Figure 20. Settlements after the filling of the caissons (I Extension)

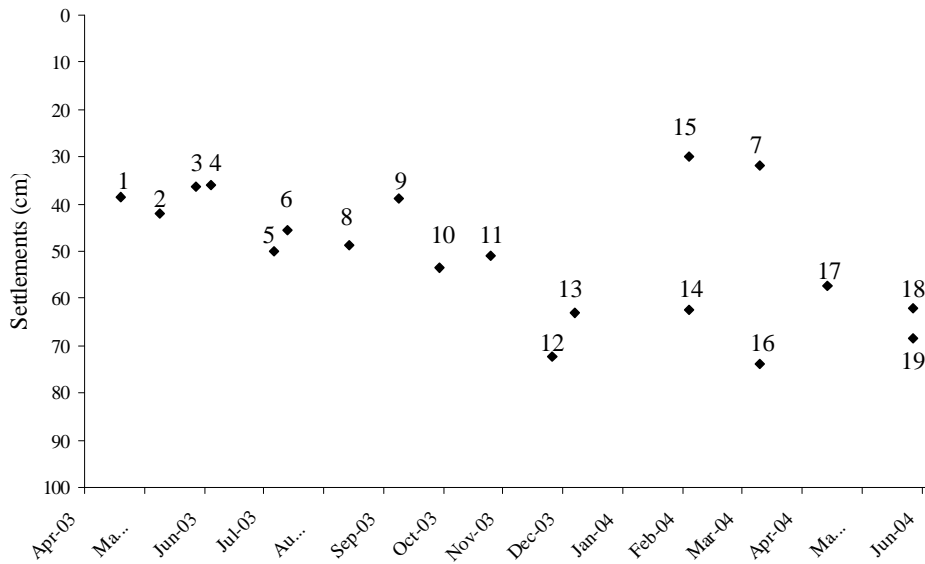


Figure 21. Settlements after the filling of the caissons (II Extension)

3.3 Settlements due to the sea wave action

Transient and cyclic wave loads are transferred to the rubble layer and to the seabed directly by the wave motions and through the movements (rocking and swaying) of the caissons. The effect experienced by the saturated non-cohesive soils under cyclic loads is the tendency of the grains to rearrange. If they are in a loose condition and the drainage is allowed, then sandy soil will be induced to become denser, with consequent deformations and settlements at the surface. The value of the induced settlements will depend on the characteristics of repetitive loads and on the geotechnical parameters of the soils (i.e. relative density, permeability, homogeneity of the layer etc.). During the first period of their life the caissons are subjected to the wave-induced cyclic loading that induces a progressive reduction of the void ratio in the foundation soils and consequent settlements. In order to evaluate this share of settlements, we have considered the behaviour of the caissons where important storms did not occur for a long period after the filling (caissons 7÷11 in the first extension and caissons 2÷6 in the second extension). The measured values range between 4÷10 cm in the first part and between 10÷14 cm in the second part. In both of cases the displacements tend to fade within the first 30÷70 days (Figure 22 and 23), depending on the exposure time to the wave action, after which the settlements remain almost constant until the occurrence of the first significant storm (Figure 24 and 25).

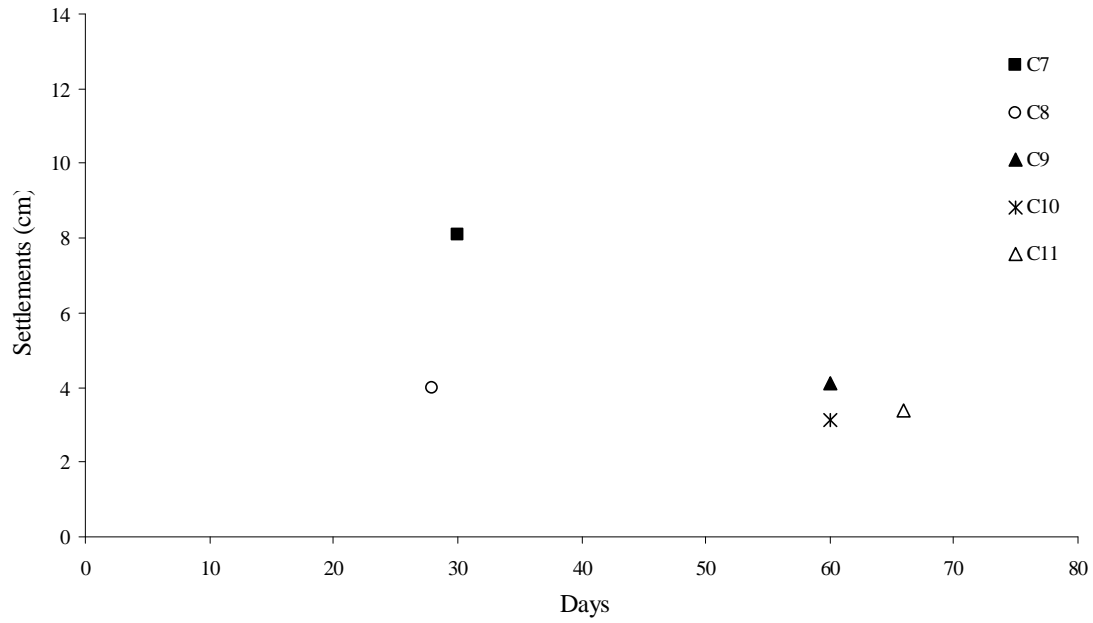


Figure 22. Settlements due to the ordinary wave action (I Extension)

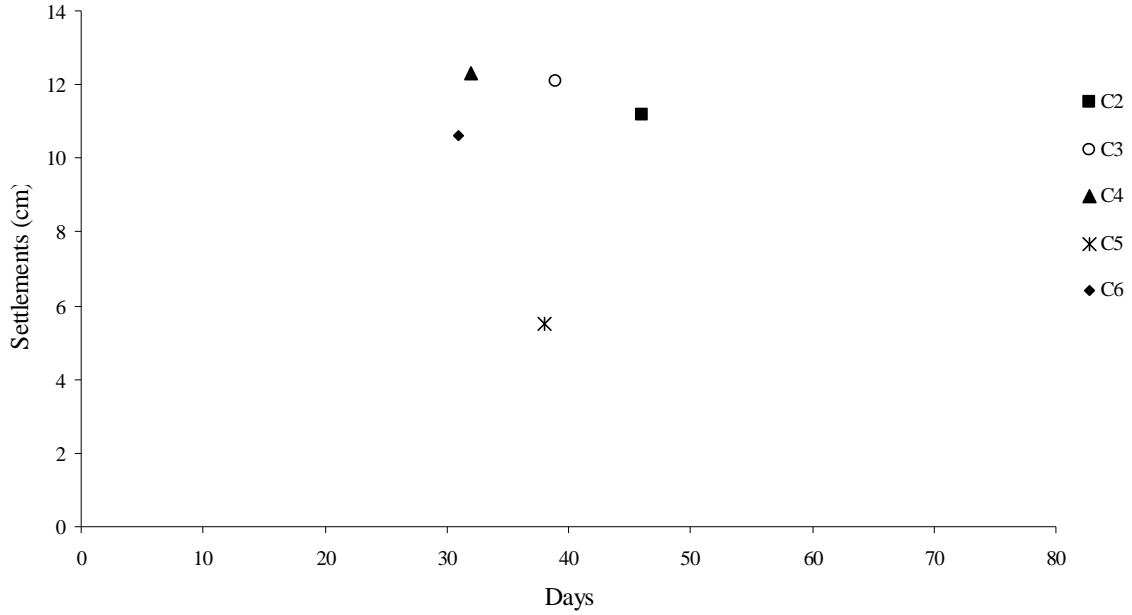


Figure 23. Settlements due to the ordinary wave action (II Extension)

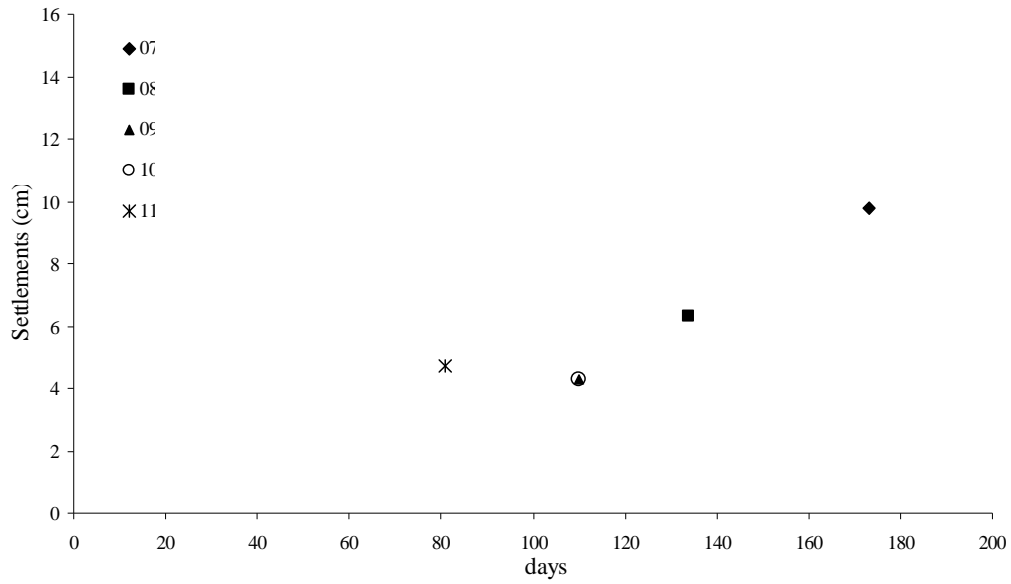


Figure 24. Settlements amongst filling and first significant storm (I Extension)

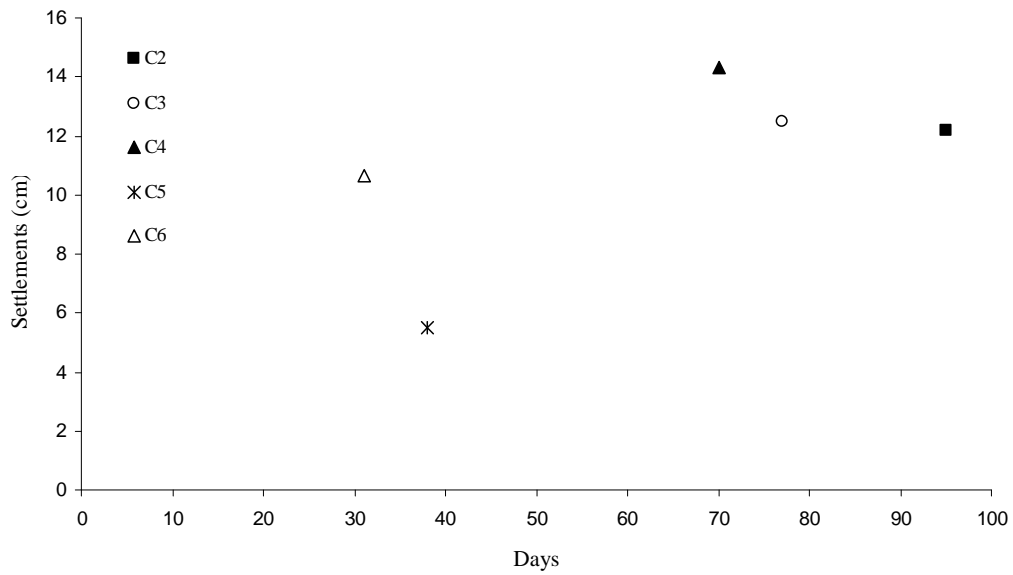


Figure 25. Settlements amongst filling and first significant storm (II Extension)

3.4 Effect of important storms

During the construction and the monitoring of the breakwater, several important storms occurred, causing a significant increase of settlements.

In the graph of Figure 26 the settlements caused on the caissons of the first extension by three significant storms, occurred respectively in November 1999, in December 1999 and in July 2000, have been reported. We chose these events because all the caissons, a part from the 16 and 17 ones, were completely filled at least since one month when these events occurred. Hence, it is possible to relate the settlements only to the storms and the measurements are not influenced by the simultaneous effect due to filling and ordinary wave motion. The occurred event in December 1999 was an exceptional storm with significant height of 4.76 m and return time of 30 years. It caused the sliding of the caissons 16 and 17, not yet filled when the event occurred. In the graph, we note that the storm of November 1999 induced low settlements for the “oldest” caissons (1÷11), ranging between 4 and 11 cm. These caissons were earlier completed and subjected to the wave loading for a longer period. Conversely, the behaviour of the “youngest” caissons (12÷15) is rather different, with settlements ranging between 17 cm (caisson 12) and 36 cm (caisson 15). It is evident that the same storm caused different settlements, depending on the re-arrangement of the grains induced by the former protracted repetitive wave loading. The exceptional storm of December 1999 induced effects considerably lower. The measured settlements for all the caissons are lower than 10 cm and for the “oldest” caissons they are practically negligible.

It is interesting to note that the two storms were similar for frequency, but the second one was more powerful than the first one for significant height and for duration. So, we may conclude that for all the caissons, excepted for the last two ones, the displacements were mainly due to the action of the first storm (November 1999). Such behaviour can be related to the “beneficial” effects of the “precycling” phenomena. As shown from several laboratory tests (Bjerrum, 1973, Andersen et al. 1976, Smits et al., 1978) cyclic loading with consequent pore pressure dissipation may modify the soil structure and the resistance to further pore pressure generation.

Precycling phenomena may happen over small storms prior to the biggest storms and also during the first part of the design storm (de Groot et al., 2001).

Finally, the latter storm of July 2000 induced settlements only on the caissons 16 e 17 and the displacements induced on the others caissons were practically null (not reported in the graph). The low value of the settlements (equal to 2.5 cm), even though the storm occurred immediately after the filling, can be related to the stress history experienced by the soils over the previous exceptional storm. During this storm the caissons 16 and 17, not yet filled, were seriously damaged. These caissons were replaced and filled on May 2000, during the final stages of the breakwater construction (first extension). It is evident that the soil over which the caissons were placed was made dense and strengthened by the previous storm.

As regards the second extension similar behaviour has been observed. In the graph of Figure 27 we note that the first event was the most significant for settlements. All the caissons, in fact, experienced an immediate increase of settlements ranging between 10 cm (caisson 2) and 16 cm (caisson 8). It is interesting to note that all the events later occurred, even though characterised by higher values of H_s and longer duration, caused settlements ever more smaller. From the graph we also observe that the caissons that did not follow this “law” and, conversely, experienced important settlements, were the ones lately filled and for which the event occurred immediately after the filling. These higher values of settlements can be hence justified since the storm occurred before the complete stabilisation of settlements due to the static loading.

Also in this case precycling phenomena induced by the storms firstly occurred, in spite of their lower power, strengthened the soil structure and increased the resistance to further settlements.

In the pictures of Figure 28 the breakwater subjected to the action of storms is represented.

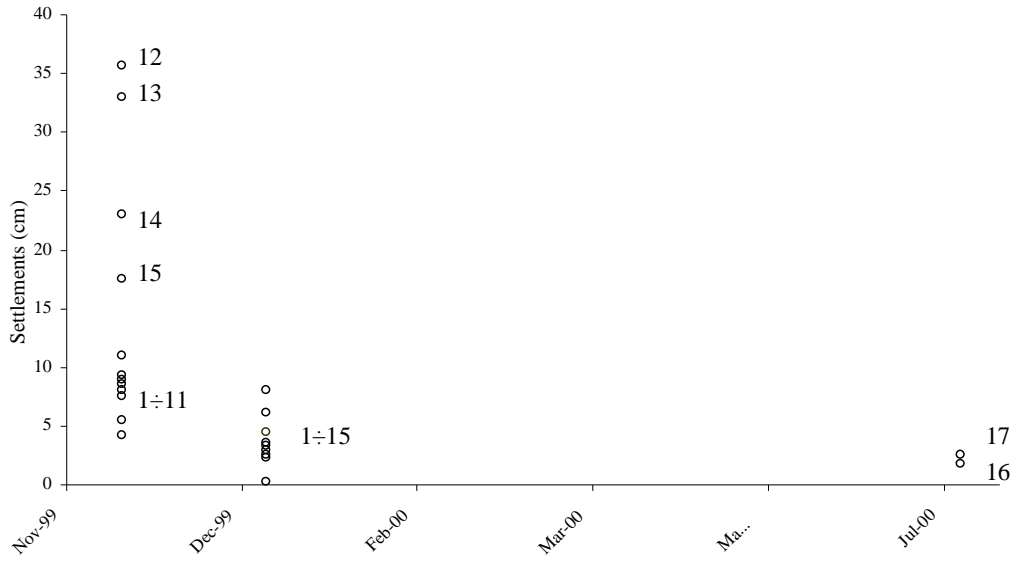


Figure 26. Effect of important storms (I Extension)

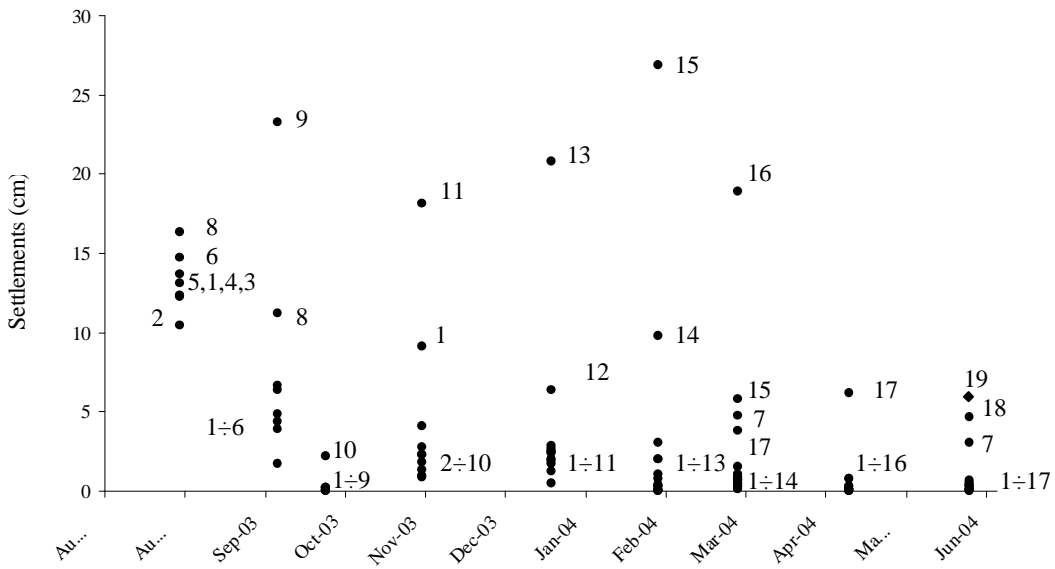


Figure 27. Effect of important storms (II Extension)



Figure 28. Construction of superstructure (II Extension) under the storm of 23rd February 2004
(photo's Pietro Cidonio S.p.A)

4. Final remarks

The monitoring of a real vertical caisson breakwater has been valuable to better understand the behaviour of the structure founded on a rubble layer and posed on sandy subsoil.

Settlements can be mainly associated to the behaviour of the rubble layer, characterised by important thickness.

Great part of the displacements is systematically induced by the static loading due to the *placing* and *filling* of the caissons. At the end of the filling, settlements between 25 and 50 cm have been recorded, depending on the depth of the seabed and, consequently, on the thickness of the rubble layer. If the depth of the seabed increases, larger settlements are recorded. Furthermore, the occurrence of the storm during the filling or immediately after the filling, induces significant increase of initial settlements.

A further increase of displacements is caused by the “ordinary” *cyclic wave loading* that accelerates the dissipation of pore pressures. The wave action induces settlements in the order of 10÷15 cm, that occur within the first 1÷3 months and would tend to fade within 6 months in absence of important storms. If in the first period *significant storms* occur, the process may be faster without any effect on the final values of settlements.

During the “normal life” of the caissons, the occurrence of significant storms induce an increase of settlements that are higher as the storm is the “first” occurred. The highest values of settlements (ranging between 10÷15 cm) have been recorded in concomitance of the event earliest occurred, in spite of lower values of H_s and duration of the events. This means that after the first significant storm, the next storms cause ever more small settlements until to do not have any effect at all.

From a geotechnical point of view, on the basis of the observed behaviour, it is evident that the superstructure, which cannot tolerate significant settlements, has to be realised not only when the settlements appear to be stabilised but at least after the occurrence of the first significant storms. Only in this case, in fact, the process of reduction of the void ratio can be considered almost completed and the soil structure

strengthened toward the cyclic wave action and toward the impact of following possible storms.

References

- Allsop, N.W.H.P.; Vicinanza, D. and Mc Kenna, J. E., 1996. Wave forces on Vertical and Composite Breakwaters, HR Wallingford, *Report SR 443*, 1996.
- Andersen Anders T.; Madsen Erik B.; Schaarup-Jensen A. Louise; Ibsen Lars Bo, 1997. Constitutive modelling of Baskarp sand, *Research Report by Aalborg University, Geotechnical Engineering Group*, 120 pp.
- Andersen, K.H.; Brown, S.F.; Foss, I.; Pool, J.H.; Rosenbrand, W.F., 1976. Effect of cyclic loading on clay behaviour. *Proc. Conf. Design and Construction of Offshore Structures*, London.
- Andresen, A.; Lunne, T. 1986. Soil investigation for strait crossing. *Proceeding International Conference on Strait Crossings*, Stavanger, Norway, October 1986, Vol. 2, pp. 783-798.
- Barton, N., Kjaernsli, B., 1981. *Shear strenght of rockfill. Journal of Geotechnical Engineering Division*, ASCE, vol. 107, no. GT7, pp. 873-891.
- Been K. and Jeffries, M.G., 1985. A state parameter for sands. *Geotechnique*, Vol. 35, No. 2, pp. 99-112.
- Benahmed, N., 2001. Comportement mécanique d'un sable sous cisaillement monotone et cyclique: application aux phénomènes de liquéfaction et de mobilité cyclique. *Thèse de doctorat de L'ENPC*, 2001, 351 pp.
- Bjerrum, L., 1973. Geotechnical problems involved in foundations of structures in the North Sea. *Geotechnique*, Vol.23-3, pp.319-358.
- Blackman, D.J., 1982. Ancient harbours in the Mediterranean, *International Journal of Nautical Archaeology and Underwater Exploration*, part 1 in 11.2 pp. 97-104; part 2 in 11.3 pp. 185-211
- Blondeau, F., 1986. Incidence de l'anisotropie de consolidation sur le potentiel de liquéfaction statique; application au glissement sous-marine du port de Dunkerque. *Review française de géotechnique*, n.37, 1986, pp. 72-80.

- Bouchet, R.; Cellario, P.; Isnard, J.L., 1994. New types of breakwater: two projects in Monaco. *Proceeding International Conference on Hydro-Technical Engineering for Port and Harbour Construction (Hydro-Port)*, Yokosuka, Japan, vol. 1, Part 1, pp. 581-592.
- Brinch Hansen, J., 1968: A Revised and Extended Formula for Bearing Capacity. *Reprint of Lecture in Japan*, October 1968.
- Canou, J., 1987. Liquéfaction statique des sables effondrables. *Conférence au Comité française de mécanique des sols*, Octobre, Paris, 1987.
- Canou, J., 1989. Contribution à l'étude et à l'évaluation des propriétés de liquéfaction d'un sable. *Mémoire de thèse de doctorat de l'ENPC*, 1989, 337 pp.
- Canou, J., Benhamed, N., Dupla, J.-C., De Gennaro, V., 2002. Instabilités de liquéfaction et phénomène de mobilité cyclique dans les sables. *Revue Française de Géotechnique*, no. 98, 2002, p. 29-45.
- Casagrande, A., 1936. Characteristics of Cohesionless Soils Affecting the Stability of Slopes and Earth Fills. *Journal of the Boston Society of Civil Engineers*, Jan. 1936, pp. 257-276.
- Casagrande, A., 1969. *Memorandum* titled "Terminology concerning Cyclic Tests", June, 11, 1969.
- Casagrande, A., 1976. Liquefaction and cyclic mobility of sands: a critical review. *Harvard Soil Mechanics Series 87*, Harvard University, Cambridge, Massachusetts.
- Castro, G., 1975. Liquefaction and Cyclic Mobility of Saturated Sand, *Journal Geotechnical Engineering*, Div. ASCE 101 (GT6), pp.551-569.
- Castro, G., and Poulos S.J., 1977. Factors Affecting Liquefaction and Cyclic Mobility. *Journal of Geotechnical Engineering, Div. ASCE*, Vol. 103, No. GT6, June, pp. 501-516.
- CIRIA/CUR 1991. Manual on the use of rock in coastal and shoreline engineering. Rotterdam, The Netherlands / Brookfield, USA: A.A. Balkema, 607 pp.

- De Groot, M.B.; Kudella M.; Meijers P.; Oumeraci H., 2004. Liquefaction underneath wave loaded gravity structures, *Journal Waterway Port Coastal & Ocean Engineering* (submitted).
- De Groot, M.B.; Oumeraci, H.; Kortenhaus, O.; Allsop, N.W.H; Crouch, R.S.; Vrijling, J.K., Voortman, H.G., 2001. Probabilistic Design Tools for Vertical Breakwaters. Rotterdam: Balkema, Lisse, The Netherlands, 373 pp.
- De la Pena, J.M., Prada, E.J.M., Redondo M.C., 1994. *Mediterranean Ports in Ancient Times*, PIANC Bulletin No. 83/84, Brussels, Belgium.
- Dobry, R., Ladd, R.S., Yokel, F.Y., Chung, R.M. and Powell, D., 1982. Prediction of pore water pressure buildup and liquefaction of sands during earthquakes by the cyclic strain method. *NBS Building Science Series 138*, National Bureau of Standards, Gaithersburg, Maryland, 150 pp.
- Elgamal, A; lai, T.; Yang, Z.; He, L., 2001. Dynamic soil properties, seismic downhole arrays and applications in practice (CD-ROM). State-of-the-art paper. In: Prakash S. editor. *Proceedings of the Fourth International Conference on Recent Advances in Geotechnical Earthquake Engineering and Soil Dynamics*, March 26-31, San Diego, CA 2001.
- Franco, L., 1996. History of Coastal Engineering in Italy, in *History and heritage of coastal engineering*, ASCE, New York, USA.
- Gatmiri, B., 1990. A simplified finite element analysis of wave-induced effective stresses and pore pressures in permeable sea beds. *Géotechnique*, 40, no. 1, 15-30.
- Goda, Y., 1985. Random seas and design of marine structures. Tokyo: University of Tokyo Press, 323 pp.
- Goda, Y., 1992. The design of upright breakwaters. *Proceedings of the Short Course on Design and Reliability of Coastal Structures*, Venice, Istituto di Idraulica, Università di Bologna, Bologna, Italy.
- Grisolia, M.; Maccarini, F., 2004. Settlements of Vertical Caissons Breakwater. *International Conference on Cyclic Behaviour of Soils and Liquefaction Phenomena*, 31 March – 02 April 2004, Bochum, Germany.

- Hanzawa, H., Itoh, Y. and Suzuki, K., 1979. Shear characteristics of a quick sand in the Arabian Gulf. *Soils and Foundations*, Vol., 19, No. 4, pp. 1-15.
- Heeres, O. M., 2001. Modern Strategies for the Numerical Modelling of the Cyclic and Transient Behaviour of Soils. *Ph.D. Thesis*, Delft University of Technology, The Netherlands
- Hölscher, P.; Zwanenburg, C.; De Groot M.B. 1998. Hindcast Hannover breakwater, *Research Report, GeoDelft (formerly "Delft Geotechnics"*, CO-364920/127, Delft, The Netherlands, ca. 500 pp.
- Ishihara, K., 1985. Stability of natural deposits during earthquake. *Proceedings 11th International Conference on Soil Mechanics and Foundation Engineering*, San Francisco, vol. 1, pp. 321-376.
- Ishihara, K.; Tatsuoka, F., and Yasuda, S., 1975. Undrained deformation and liquefaction of sand under cyclic stresses. *Soils and Foundations*, Vol. 15, No. 1, pp. 29-44.
- Kortenhaus, A. 1996. Pore pressure in rubble foundation underneath a caisson breakwater – results of large-scale model tests. *Research Report. MAST III, PROVERBS-Project: Probabilistic Design Tools for Vertical Breakwaters*, Braunschweig, Germany, 25 pp., 3 Annexes.
- Kortenhaus, A.; Oumeraci, H., 1997a. First results of spring-dashpot model applied to representative structures. *Proceedings 1st Overall Project Workshop, MAST III, PROVERBS-Project: Probabilistic Design Tools for Vertical Breakwaters*, Las Palmas, Gran Canaria, Annex 2A.
- Kramer, S.L., 1996. *Geotechnical Earthquake Engineering*. Edited by Prentice Hall, International Series in Civil Engineering and Engineering Mechanics, Upper Saddle River, New Jersey 07458.
- Lamberti, A.; Martinelli, L. 1998a. Interpretation of dynamic tests of Brindisi and Genoa Voltri breakwaters. *Proceedings 2nd Overall Project Workshop, MAST III, PROVERBS-Project: Probabilistic Design Tools for Vertical Breakwaters*, Naples, Italy, Class 2 Report, Chapter 2.3a).

- Lamberti, A.; Martinelli, L. 1998b. Prototype measurements of the dynamic response of caisson breakwaters. *Proceedings International Conference Coastal Engineering (ICCE)*, ASCE, Copenhagen, Denmark, no. 26, 14 pp.
- Lee, D.S.; Hong, G.P., 1994. Korean experience on composite breakwaters. *Proceedings International Workshop Wave Barriers in Deepwaters*, PHRI, Yokosuka, Japan, pp. 172-183.
- Lee, K.L. and Seed, H.B., 1967. Cyclic stress conditions causing liquefaction of sand. *Journal of the Soil Mechanics and Foundations Division*, ASCE, Vol. 93, no. SM1, pp. 47-70, Proc. Paper 5058, Jan. 1967.
- Lunne, T.; Powell, H.P., 1992. Recent development in in-situ testing in offshore soil investigations. *Proceedings SUT Conference on Offshore Soil Investigations and Foundation Engineering*, London, U.K., September 1992, pp. 147-180.
- Maccarini F., Grisolia M., Fincosit S.p.A. (2005). Geotechnical aspects of a vertical caisson breakwater under wave-induced cyclic loading, submitted to *ICECOAST 2005, Second International Coastal Symposium*, 5-8 June 2005, Hornafjordur, Iceland.
- Madsen, O.S., 1978. Wave-induced pore pressures and effective stresses in a porous bed. *Géotechnique* 28, No. 4, 377-393.
- Marchetti, S., 1981. Personal communications.
- Mei, C.C. and Foda, M.A., 1980. Boundary layer theory of waves in a poro-elastic sea bed, *Proc. Int. Symposium on Soils under Cyclic and Transient Loadings*, Edited by G.N. Pande and O.C. Zienkiewicz, 609-18, Balkema, Rotterdam, 1980.
- Mohamad, R. and Dobry, R., 1986. Undrained monotonic and cyclic triaxial strength of sand. *Journal of Geotechnical Engineering*, ASCE, Vol. 112, No. 10, pp. 941-958.
- Norwegian Geotechnical Institute, 1998. Data base of laboratory test results on selected sands and silts. *NGI Report. MAST III, PROVERBS-Project: Probabilistic Design Tools for Vertical Breakwaters*, no. 524094-1, Oslo, Norway, 39 pp., 22 Annexes.

- Oumeraci, H., 1994. Review and analysis of vertical breakwater failures – lessons learned. *Coastal Engineering*, 22 (1994), 3-29.
- Oumeraci, H., Kortenhaus, O., 1994. Analysis of dynamic response of caisson breakwaters. *Coastal Engineering*, Special Issue on ‘Vertical Breakwaters’, Eds.: Oumeraci H. et al., Amsterdam, The Netherlands: Elsevier Science Publishers B.V., vol. 22, nos. ½, pp. 159-183.
- Oumeraci, H.; Kortenhaus, A.; Klammer, P., 1994. Caisson breakwaters: integrated design and wave load specifications. *Proceedings International Conference on Hydro-Technical Engineering for Port and Harbour Construction (Hydro-Port)*, Yokosuka, Japan, vol. 1, Part 1, pp. 453-472.
- Oumeraci, H.; Kortenhaus, A.; Klammer, P., 1995. Displacements of caisson breakwaters induced by breaking wave impacts. *Proceedings of the International Conference of the Institution of Civil Engineers – Advances in coastal structures and breakwaters*, Clifford, J.E., London, U.K.: Thomas Telford Ltd., Paper 3, pp. 50-63.
- Oumeraci, H.; Kortenhaus, O.; Allsop, N.W.H; De Groot, M.B.; Crouch, R.S.; Vrijling, J.K., Voortman, H.G., 2001. Probabilistic Design Tools for Vertical Breakwaters. Rotterdam: Balkema, Lisse, The Netherlands, 373 pp.
- Oumeraci, H.; Partenscky, H.-W.; Tautenhain, E.; Nickels, H., 1991. Large scale-model investigations: a contribution to the revival of vertical breakwaters. *Proceedings of the Conference on Coastal Structures and Breakwaters*, ICE, London, U.K.: Thomas Telford Ltd., pp. 207-220.
- Pastor, M., Zienkiewicz, O.C. and Chan, A.H.C., 1990. Generalised plasticity and the modelling of soil behaviour. *International Journal for Numerical and Analytical Methods in Geomechanics*, vol. 14, 151-190.
- Peacock, W.H., and Seed H.B., 1968. Sand Liquefaction Under Cyclic Loading Simple Shear Conditions. *Journal of the Soil Mechanics and Foundation Division*, ASCE, Vol. 94, No. SM3, pp. 689-708, Proc. Paper 5957, May, 1968.
- Poulos, S.J. (1981). The steady state of deformation. *Journal of the Geotechnical Engineering Division*, ASCE, Vol. 107, No. GT5, pp. 553-562.

- Prévost, J.-H., Eide, O., Andersen, K., 1975. Wave induced pressures in permeable seabeds. (Discussion). *J. Watways Harb. Coastal Engineering, Am. Soc. Civ. Engrs.* 101, no. WW4,464-465.
- Roscoe, K.H. and Pooroshasb, H.B. 1963. A fundamental principle of similarity in model tests for earth pressure problems. *Proceedings, 2nd Asian Regional Conference on Soil Mechanics*, Tokyo, Vol. 1, pp. 134-140.
- Rowe, P.W. and Craig, W.H., 1978. Prediction of caisson and pier performance by dynamically loaded centrifugal models. *Int. Symp. Soil Mech. Res. And Found. Design for the Oosterschelde Storm Surge Barrier*, Vol.2.
- Rundgren, L., 1958. Water Wave Forces. *Bulletin no. 54*, Royal Institute of Technology, Division of Hydraulics, Stockholm, Sweden.
- Sainflou, G. 1928. Essai sur les diques maritimes verticales. *Annales des Ponts and Chaussées*, vol. 98, no. 4, pp. 5-48. In French.
- Schlosser, F., 1985. Liquéfaction de veines de sable lâche dans des talus sous-marins. C.R. 11th International Conference on Soil Mechanics and Foundation Engineering, San Francisco, 1985.
- Seed, H.B., and Idriss, I.M. Analysis of Soil Liquefaction: Nigata Earthquake. *Journal of the Soil Mechanics and Foundation Division*, ASCE, Vol. 93, No. SM3, pp. 83-108, May, 1967.
- Seed, H.B., and Lee, K.L. Liquefaction of Saturated Sands during Cyclic Loading. *Journal of the Soil Mechanics and Foundation Division*, ASCE, Vol. 92, No. SM6, pp. 105-134, November, 1966.
- Shaw, J., 1974, Greek and Roman Harbour Works, *from Navi e Civiltà*, Milan
- Sladen J.A., d'Hollander, R.D., Krahn, J., 1985. The liquefaction of sands, a collapse surface approach. *Canadian Geotechnical Journal*, vol. 22, 1985, pp. 564-578.
- Smits, F.P.; Andersen, K.H.; Gudehus, G. 1978. Pore pressure generation. *Proc. Int. Symp. On Soil Mech. Research and Found. Design for the Oosterschelde Barrier*, Delft, The Netherlands, Vol. 1-II 3. 16 pp.

- Takahashi, S., 1996. Design of Vertical Breakwaters. *Reference Document no. 34*, Port and Harbour Research Institute, Ministry of Transport, Yokosuka, Japan.
- Takahashi, S.; Tanimoto, K.; Shimosaka, K., 1994. A Proposal of Impulsive Pressure Coefficient for Design of Composite Breakwaters. *Proceedings of International Conference on Hydro-technical Engineering for Port and Harbour Construction*, Port and Harbour Research Institute.
- Tanimoto, K.; Takahashi, S., 1994. Japanese experience on composite breakwaters. *Proceedings International Workshop Wave Barriers in Deepwaters*, PHRI, Yokosuka, Japan, pp. 1-24.
- Vaid, Y.P., and Chern, J.C., 1983. Effect of static shear on resistance of liquefaction. *Soils and Foundations*, Vol. 23, No. 1, pp.47-60.
- Vaid, Y.P., and Chern, J.C., 1985. Cyclic and monotonic undrained response of saturated sands. *Advances in the Art of Testing Soils under Cyclic Conditions*, ASCE, New York, pp. 120-147, ed. V. Khosla.
- Van der Meer, J.W.; d'Angremond, K.; Juhl, J., 1994. Probabilistic calculations of wave forces on vertical structures. *Proceedings 23rd International Conference Coastal Engineering (ICCE)*, ASCE, Kobe, Japan.
- Van der Poel, J.T. and De Groot, M.B., 1998. Cyclic load tests on a caisson breakwater placed on sand. *Proc. Int. Conf. Centrifuge 98*, Tokyo. Balkema, Rotterdam, Vol. 1, pp. 403-408.
- Van Gent, M.R.A. 1993. Stationary and oscillatory flow through coarse porous media. *Communications on Hydraulic and Geotechnical Engineering*, TU Delft, Delft, The Netherlands, Report No. 93-9, 62 pp.; 4 Appendices.
- Van Gent, M.R.A; Van den Boogaard, H.F.P., 1998. Neural network modelling of forces on vertical structures. *Proceedings 26th International Conference Coastal Engineering (ICCE)*, ASCE, Copenhagen.
- Verdugo, R.L., 1992. Characterization of sandy soil behaviour under large deformation. *Ph.D. dissertation*, University of Tokyo, 1992, 455 pp.

-
- Vitruvius, M. L., 27 B.C., *De Architectura*, vol. II-6; vol. V-13 (in Latin). English translation by Morgan, M.H., 1914, in Cambridge or Loeb Classical Library, London, United Kingdom.
- Vrijling, J. K.; Van Gelder, P.H.A.J.M., 1998. The effect of inherent uncertainty in time and space on the reliability of flood protection. Lydersen, S.; Hansen, G.K.; Sandtorv, H. (eds): Safety and Reliability, *Proceedings of the ESREL'98 Conference*, Vol. 1, Trondheim, Norway, A.A. Balkema, Rotterdam, pp. 451-458.
- Wolf, J.P. 1994. Foundation vibration analysis using simple physical models. *Englewood Cliffs/N.J.*, USA: Prentice-Hall, 423 pp.
- Yamamoto, T., Koning, H.L., Sellmeyer, H., and van Hijum, E., 1978. On the response of a poro-elastic bed to water waves, *J. Fluid Mech.*, 87, 193-206.

Acknowledgements

Writing these pages represents for me a mix of happiness (to have finished the thesis!) and great emotion in remembering all the persons that helped me in my research and contributed to make these three years a wonderful experience.

First of all I would like to thank “Pietro Cidonio S.p.A.” that supported this Research. More specifically, Ing. Alessandro Mazzi, Ing. Osvaldo Mazzola and Ing. Giuseppe Grondona are gratefully acknowledged.

For an uncommon and lucky situation, due to the topic of this thesis and to the time spent abroad, during the development of this PhD I had several Supervisors, geotechnical and hydraulic, Italian and Dutch.

Amongst the Italians, I want to thank Prof. Giovanni Calabresi who gave me the possibility to spend one year of my PhD abroad, trusting me and in the fact that in Delft I was not only enjoying channels, herrings and tulips! Then, many thanks to Prof. Alberto Noli and Prof. Leopoldo Franco, who actually “invented” the topic of my research and, most important, introduced me to GeoDelft and TU Delft. Thanks to Prof. Renato Ribacchi and Prof. Giuseppe Scarpelli, my tutors, for their valuable suggestions and advices. Finally, I want to thank Prof. Massimo Grisolia, my professor since 10 years, for having induced me to *love* the Geotechnics.

When I arrived in Delft, in July 2003, I was really terrified, because I was going to live and work in a new country (a colder country!), with new colleagues, new supervisors and speaking a terrible English! At that time I could not imagine that, one year later, it would have been the most beautiful experience of my life. For that, I want to thank Prof. Marcel Stive and Prof. Han J.K. Vrijling, for having kindly hosted me at Delft University of Technology. Then, many thanks to Dr. Stefan van Baars, for his precious suggestions, patience with my English (!) and for having stopped me to work every day after six o'clock and during the weekends!

A very special thank is for Maarten de Groot, who gave me the possibility to work with him, patiently helping me for 12 months and offering me his valuable

experience and knowledge. It is not an exaggeration if I say that without him this research would not have been possible. So, many thanks Maarten!

Finally, in Delft I had the lucky opportunity to meet Ir. Henk den Adel and Ir. Frans Koop, that kindly helped me in the acquisition and elaboration of centrifuge data.

Then, many thanks to all my Dutch colleagues, for having made me feel me at home and for having appreciated my “pizza frita”! Thanks to Wim, my room mate, for all the moka-coffees and thanks to Anneke, Marije, Saskia (I still remember your barbecue in front of the old Church!), Sonja, Xijing, François, Mark Klein, Mark Voorendt, Nobu, Wilfred, Elmar and all the others members and guests of the Hydraulics Section. Finally, many thanks to the secretaries, Adeeba and Chantal, for all that they did for my accommodation and during my staying.

During the year spent in Holland I had the opportunity to meet special persons, now my *special friends* that, in one only word, constituted my family in Delft and made unforgettable this experience: Federico, Claudia, Anja and Norbert, Stan, Andrea, Cecilia, Stella, Beatriz and Stefan, Gerardo, Beatrice, Emanuele. I will never forget you!

When I came back to Italy and to my “old” Department in Monte d’Oro I was really sad to have left Delft but, fortunately, there were others special persons in Rome.

First of all I want to thank Daniela Boldini, my “old” friend and colleague, who induced me to start my PhD (it’s your fault!) and who always sustained me, helping and encouraging. Thanks Daniela, for our special friendship since more than 10 years.

A special thanks is for another colleague and friend, ing. Giuseppe Solinas, for his precious suggestions and support, since the beginning of my PhD.

Thanks to all my colleagues of Monte d’Oro, Paola Caporaletti (for having shared this long experience together), Roberto Tamagnini (who helped me in the numerical part), Gioacchino Altamura (who encouraged me before each oral presentation!), Tatiana Rotonda and Alessandro Graziani (for having promoted me at the course of “Meccanica delle Rocce”!). Many thanks to Luigi Callisto, Sebastiano Rampello and Paolo Tommasi for useful discussions and advices. Thanks to all the others members

of the Department and other friends, Francesca Casini, Sonia Fortuna, Luigi Credendino, Marco D'Elia, Enzo Fontanella, Salvatore Miliziano, Fabio Soccodato, who essentially contributed to the pleasure of working at University!

Finally, I want to thank the secretaries of Monte d'Oro, Dunja Juric (who had a key role in my financial support in Delft!), Maria Leoni (especially for Christmas and Easter breakfasts!) and Daniela Menozzi (who patiently reminded us all the PhD's deadlines, included this final submission of the thesis!). A special thank is also for all the technicians, Franco Brogi, Dino Irti and, in particular Maurizio Di Biase, my affectionate "neighbour"!

My last word is for my family, always present in my life.

Rome, 10th May 2005.

About the author

Fabiana Maccarini was born in Civitavecchia (Rome, Italy) on December 10th 1973.

She graduated in 1999 at the University of Rome "La Sapienza", Faculty of Environmental Engineering - Soil Defence (5-year University Course), with a thesis on Geotechnics regarding the geotechnical characterisation of light expanded clay aggregate.

Between 1999-2002 she was assistant in the teaching course for the Chair of "Fundamentals of Geotechnics" under the leadership of Prof. M. Grisolia, Dept. of Hydraulic, Transportation and Roads, University of Rome "La Sapienza".

Since 1999 she is participating to several research activities performed at the University of Rome "La Sapienza" (Dept. of Hydraulics, Transportation and Roads, Dept. of Structural and Geotechnical Engineering, Dept. of Earth Sciences).

In October 2001 she started her PhD-Research in geotechnical engineering, at the Department of Structural and Geotechnical Engineering, University of Rome "La Sapienza". The research has been titled "Behaviour of Vertical Caisson Breakwaters Under Wave-Induced Cyclic-Loading". From 2003 to 2004 she performed part of the PhD research in Delft (The Netherlands), under the leadership of Prof. Han J.K.Vrijling (Delft University of Technology, Hydraulic Section), Dr. Stefan van Baars (Delft University of Technology, Geotechnical Department) and M. B. De Groot (GeoDelft).

Since 2000 she has been employed as geotechnical consultant on various projects, involving several fields as Hydraulics and Soil Defence, Harbour Structures and Coastal Protection, Management in polluted sites.

Publications

Journal articles

1. Maccarini F., De Groot M.B., Van Baars S., (2004). Vertical Caisson Breakwaters Cyclically Loaded: Centrifuge Tests Results. Submitted to *Geotechnique*.

Conference proceedings

1. Grisolia M., Napoleoni Q., Bocci P., Maccarini F., Braschi R. (2002). Consolidation of urban area caves through preventive filling with expanded clay (in Italian). *XXI Geotechnical National Conference*, 11-14 September 2002, L'Aquila, Italy.
2. Grisolia M., Maccarini F., Napoleoni Q., (2004). Shear Strength of Expanded Clay Aggregates. *The 9th Australian New Zealand, Conference on Geomechanics*, 8-11 February 2004, Auckland, New Zealand.
3. Grisolia M., Maccarini F., (2004). Settlements of Vertical Caissons Breakwater. *International Conference on Cyclic Behaviour of Soils and Liquefaction Phenomena*, 31 March – 02 April 2004, Bochum, Germany.
4. Maccarini F., De Groot M.B. (2004). Cyclic behaviour of vertical breakwaters founded on sandy subsoils: liquefaction and cyclic mobility (in Italian). *Annual Meeting of Geotechnical Researchers*, 7-9 luglio 2004, Trento, Italy.
5. Maccarini F., Grisolia M., Mazzola O. (2005). Geotechnical aspects of a vertical breakwater under wave-induced cyclic loading, submitted to *ICECOAST 2005, Second International Coastal Symposium*, 5-8 June 2005, Hornafjordur, Iceland.

Miscellanea

1. Maccarini, F., Grisolia M. (1999). Geotechnical characterisation of LECA, light expanded clay aggregate. Laboratory tests in conventional triaxial apparatus on large size samples (in Italian). Degree thesis, Department of Hydraulic, Transportation and Roads, University of Rome "La Sapienza".
2. Prestininzi A. et Al. (2000). Location and Characterisation of Landslides in Italian Sites. Hazard and Risk Assessment (in Italian), Dept. of Earth Sciences, University of Rome "La Sapienza", 55 pp., Rome, 2000.

3. Grisolia M., Maccarini F., Napoleoni Q. (2003). Compression triaxial tests on large size samples of expanded clay aggregates (in Italian) – Geotechnical applications”, *Edited by Laterlite S.p.A., 2003.*
4. Bocci P., Grisolia M., Maccarini F., Napoleoni Q. (2003). Laboratory tests on conglomerate of cement and expanded clay for consolidation of urban caves through preventive filling (in Italian) - Geotechnical applications ” *Edited by Laterite S.p.A., 2003.*